The Development of the Neural Crest-Derived Intrinsic Innervation of the Lung

Lucy Jessica Freem

PhD Thesis submitted for the degree of Doctor of Philosophy at University College London

October 2011

Neural Development Unit,
UCL Institute of Child Health
30 Guilford Street
London WC1N 1EH

Declaration of Authenticity

I, Lucy Jessica Freem confirm that the work presented in this thesis is my own. Where information has been derived from other sources, I confirm that this has been indicated in the thesis.

Signed……

Abstract

The autonomic airway ganglia that comprise the intrinsic lung innervation are derived from vagal neural crest cells (NCC) that migrate tangentially from the foregut into the embryonic lung buds. The aim of this PhD thesis was to investigate the mechanisms that direct NCC from the foregut into the lungs and that subsequently influence their development. A novel combination of cell labelling, using *Wnt1Cre:Rosa26YFP* double transgenic reporter mice, and Optical Projection Tomography (OPT) imaging was employed to visualize lung innervation. Results showed that NCC migrated into the lungs from the esophagus early in development, accumulated around the epithelial tubules and differentiated into an extensive network of neurons and glial cells. Next, chick intraspecies grafting was used to test the developmental potential of lung and gut NCC. Results showed that when NCC from the gut were back-grafted into the early migration pathway these cells colonised both the lungs and gut, indicating that vagal NCC are not prespecified to colonise either organ and are thus likely to respond to common signalling cues. When potential cues were tested in organotypic lung culture, NCC migrated towards sources of the RET (Rearranged during Transfection) ligand GDNF (Glial-cell-line-derived neurotrophic factor), suggesting that the RET signalling pathway is involved in NCC colonisation of the lung. However, examination of RET mutants indicated that this pathway is not necessary for NCC colonisation of the lung, since lung innervation in *Ret-/-* mouse embryos was similar to controls. Lung innervation was further examined in several mouse mutants with known NCC defects. Intrinsic ganglia formation was altered in *Sox10Dom* and *Tbx1* mutant mouse lungs, implicating a role for vagal nerve projections in guiding NCC within the lung. Together these studies have described the development of intrinsic lung innervation in the avian and mammal and examined multiple mechanisms underlying NCC development within the lung.

Table of contents

List of Figures

List of Tables

List of Graphs

List of Abbreviations

Abbreviation	Term
°C	Degrees centigrade
APG(s)	Airway parasympathetic ganglion (ganglia)
ASM	Airway smooth muscle
BABB	Benzyl alcohol benzyl benzoate
BDNF	Brain-derived neurotrophic factor
BMP	Bone morphogenic protein
CCHS	Congenital central hypoventilation syndrome
CDH	Congenital diaphragmatic hernia
CGRP	Calcitonin gene-related peptide
ChAT	Choline acetyltransferase
Chd7	Chromatin helicase DNA binding domain 7
CO_2	Carbon dioxide
DBH	Dopamine beta hydroxylase
DCC	Deleted in colorectal cancer
DEPC	Diethyl pyrocarbonate
DMEM	Dulbecco's Modified Eagle Medium
DRG	Dorsal root ganglia
Ednrb	Endothelin receptor-b
EDTA	Ethylenediaminetetracetic acid
EMT	Epithelial-mesenchymal transition
ENS	Enteric nervous system
FACS	Fluorescence-activated cell sorting
FGF	Fibroblast growth factor
GDNF	Glial-derived neurotrophic factor
GFP	Green fluorescent protein
Gfra1	GDNF family receptor alpha 1
ISH	In situ hybridisation
K	One thousand
LMP	Low melting point
M	Molar
MABT	Maleic acid buffer pH7.5 with1% Tween
ml	Millilitre
mM	Millimolar
NANC	Non-adrenergic-non-cholinergic
NCC(s)	Neural crest cells
NEB	Neuroepithelial body
Nrp1	Neuropilin-1
NT	Neural tube
OPT	Optical projection tomography
PBS	Phosphate buffered saline
PFA	Paraformaldehyde
PHOX2B	Paired homeobox transcription factor 2b
PNEC	Pulmonary neuroendocrine cell
PNS	Peripheral nervous system
RET	REarranged during Transfection

RT	Room temperature
SDS	Sodium dodecyl sulphate
Sema	Semaphorin
Shh	Sonic hedgehog
SIDS	Sudden infant death syndrome
SG	Sympathetic ganglia
SMA	Smooth muscle actin
SPRY	Sprouty
SSC	Sodium salts citrate
SUDI	Sudden unexplained death in infants
TBST	Tris buffered saline with Triton
Tbx1	T-box containing transcription factor 1
TH	Tyrosine hydroxylase
Tuj1	Beta tubulin III
VAChT	Vesicular acetylcholine transporter
YFP	Yellow fluorescent protein
μm	Micrometre
μg	Microgram
μl	Microlitre

Gene and Protein nomenclature

Human gene	**Mouse gene**	**Protein name**
CHD7	*Chd7*	Chd7
DCC	*Dcc*	DCC
GFRA1	*Gfra1*	GFRa1
NRP1	*Nrp1*	Nrp1
PHOX2B	*Phox2b*	Phox2b
RET	*Ret*	RET
SOX10	*Sox10*	Sox10
TBX1	*Tbx1*	Tbx1

1. Introduction

1.1 The Lungs

In air-breathing vertebrates the lungs are the organs of gaseous exchange, where red blood cells, brought into close contact with the air, take up oxygen that is carried throughout the rest of the body by the circulatory system. In order to efficiently conduct gaseous exchange, the lungs have a large internal surface area in contact with both inhaled air and blood vessels. In the mammalian lungs this surface area is produced through successive branching of the respiratory tubules, which terminate in alveoli. The terminal branches and alveoli, where respiratory exchange takes place, have a rich blood supply. Carbon dioxide (CO_2), produced by respiration, diffuses out of the blood and oxygen diffuses from the air into the blood along their respective gradients. Chemosensors monitor levels of carbon dioxide and oxygen both in the airways of the lung and in blood circulating in the brain and feed back to respiratory pattern generators in the brainstem that control the rapidity and depth of breathing. Lung chemosensors also monitor inhaled air for irritant or noxious chemicals and feed back to the brain and local effectors to prevent damage (West, 2008).

1.2 Comparative lung anatomy

In mammals, including mice and humans, the lungs have a respiratory tree of successively branching respiratory tubules (Figure 1.1). Gaseous exchange takes place in the distal tubules and terminal alveoli, while the proximal airways conduct air into the lungs, warming and cleaning it before it reaches the alveoli. Mammalian lungs are asymmetric, with different numbers of lobes on each side of the body in different species. Mouse lungs have one left and four right lobes (the apical, azygous, cardiac and diaphragmic lobes) (Ten Have-Opbroek, 1991) while human lungs (Figure 1.1) have two left (superior and inferior) and three right (superior, middle and inferior) lobes. The airflow in mammalian lungs is bidirectional. Air moves tidally in and out along the same conducting airways during breathing. Air is moved in and out of the lung primarily by the alteration of pressure in the thoracic cavity through the movements of the diaphragm and intercostal muscles. By moving downwards and outwards, these muscles increase the volume and hence decrease the

pressure inside the thoracic cavity, causing air to move into the lungs. A corresponding decrease in volume produces exhalation (Kliegman and Nelson, 2007).

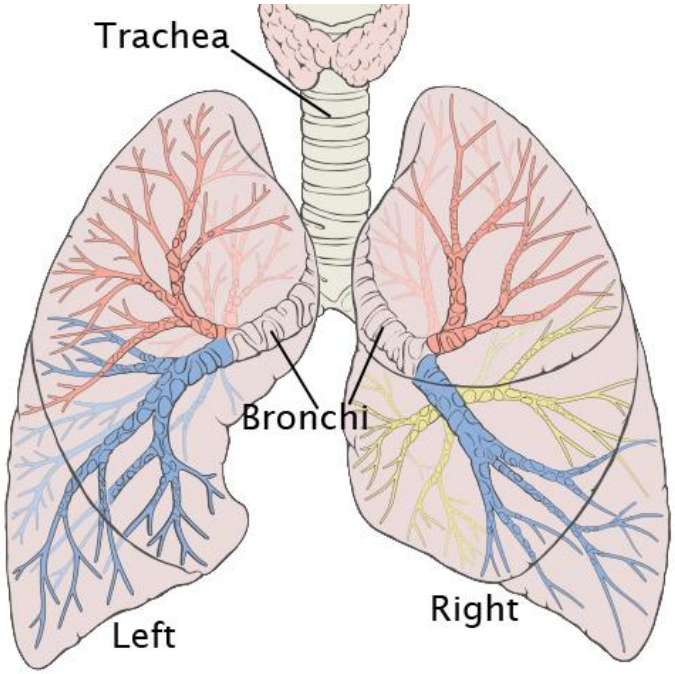

Figure 1.1 The structure of the human lung. Other mammalian lungs have a similar pattern of branching airways but have varying numbers of lobes in the left and right lungs. There are different branches of the respiratory tree (red, blue, yellow) in different lobes of the lung. The branching airways terminate in alveoli (not shown). (Creative Commons licence, Patrick J Lynch 2006).

The avian lungs have significant structural and functional differences to the mammalian lungs (Figure 1.2). The avian lungs are proportionally smaller than mammalian lungs, are symmetric and are both unilobar, not divided into lobes. Each lung has several air sacs, usually nine, which bud off from the secondary bronchi. These air sacs do not play a direct role in gaseous exchange but instead act to ventilate the lung (Duncker, 1974). Due to the arrangement of the air sacs and bronchi, the flow of air through the avian lung is largely unidirectional (Heard, 1997), promoting efficient gaseous exchange. The increased ventilation in avian lungs means that the gradient of oxygen and CO_2 concentration between the air and the blood is more favourable to gas exchange (Duncker, 2004).

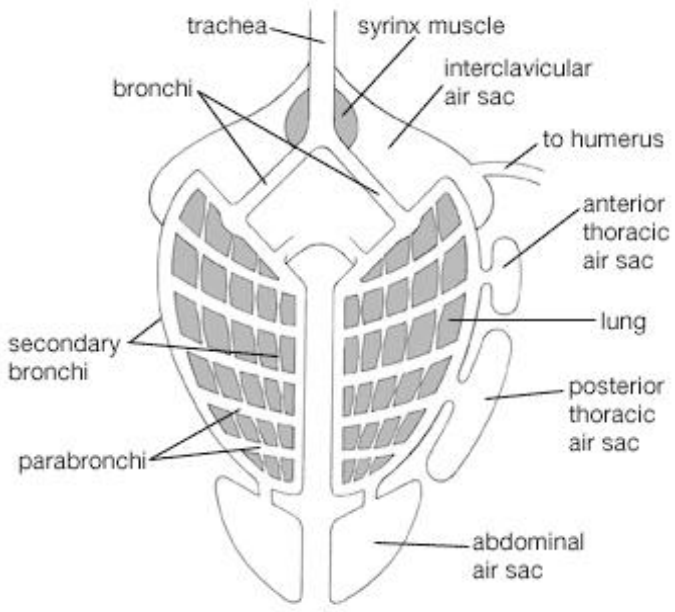

Figure 1.2 The structure of the avian lung. Air enters through the trachea and flows along the primary bronchi into the secondary and parabronchi. The arrangement of the airways and air sacs allows the linear flow of air through the distal bronchi so that tidal flow only occurs in the primary bronchi. Reproduced from the Encyclopedia Britannica, 2008.

1.3 Lung Development

1.3.1 Patterning of lung territory in the foregut

The trachea and lungs are endoderm-derived organs that develop as outgrowths of the foregut, (Grapin-Botton and Melton (2000). Early in development the foregut is patterned into regions with different fates (Figure 1.3), as reviewed in Sherwood et al. (2009). This patterning occurs along anterior-posterior and dorso-ventral gradients and uses several morphogenetic signals to set up overlapping regions of transcription factor expression. The morphogen retinoic acid is present in a posterior to anterior gradient in the developing embryo and is a determinant of Hox gene expression domains (Bayha et al., 2009). Hox (homeobox) transcription factors are encoded by a set of genes expressed in distinct compartments along the anterior-posterior axis and are determinants of anterior to posterior patterning along the entire body axis (Hueber and Lohmann, 2008). Hox transcription factors specify axial regions in which other downstream transcription factors are expressed. In the mouse, Hoxb3, 4 and 5 are expressed in the presumptive lung endoderm (Bogue et al., 1996). Transcription factors downstream of Hox transcription factors including lung domain transcription factors such as Nkx2.1, Forkhead box transcription factors and others (Costa et al., 2001) are necessary for the correct positioning of the lung endodermal domain along the anterior-posterior axis.

Different combinations of transcription factors characterise different organ domains, controlled by multiple upstream morphogens. Acting as a morphogen, the growth factor Fibroblast Growth Factor 4 (FGF4) is expressed in the mesoderm adjacent to the posterior endoderm and represses the anterior endoderm transcription factors Hex1 and Nkx2.1, thus repressing anterior foregut morphogenesis. FGF4 signalling therefore promotes a posterior endoderm fate in the future midgut (Dessimoz et al., 2006). However, the closely related FGF2 is released by the cardiac mesoderm that is adjacent to the ventral foregut and in later development to the lungs, and it induces the expression of Nkx2.1 in the ventral endoderm (Serls et al., 2005). These two morphogens, in addition to others, position Nkx2.1 expression in the future lung domain (Kumar et al., 2005). Nkx2.1 is a transcription factor expressed in the ventral endoderm and is necessary for lung endoderm specification (Pera and Kessel, 1998). The Nkx2.1 domain of expression overlaps with that of the rostrally expressed transcription factor Sox2 and with that of the caudally expressed transcription factor Hex1 (Grapin-Botton and Melton, 2000), so this combination of transcription factors, with others, characterises the region that will become the lungs.

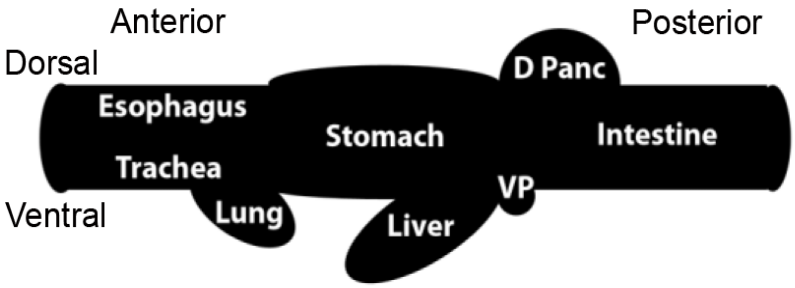

Figure 1.3 Organ domains in the developing foregut. The lung forms from the anterior ventral foregut, immediately posterior to the trachea. D Panc: dorsal pancreas, VP: ventral pancreas. From Sherwood et al. (2009).

Several morphogenetic signals ensure correct patterning of lung development during organogenesis (Warburton et al., 2005), including retinoic acid and Sonic hedgehog. The morphogen Sonic hedgehog (Shh), its receptor Patched and the downstream zinc-finger transcription factors Gli1, 2 and 3 are all members of a pathway necessary for the correct dorso-ventral patterning of the trachea and lung buds. Shh signalling is required for the partitioning of the esophagus from the trachea and bronchi (Litingtung et al., 1998) and for normal lung mesenchyme proliferation (Bellusci et al., 1997a). The transcription factors Gli2 and 3 have a degree of

redundancy in their function. Gli3 mutant mouse lungs are reduced in size (Grindley et al., 1997) while Gli2 mouse mutant lungs show no separation of the lobes of the lung, showing that Shh signalling through Gli2 is necessary for lung lobe separation (Motoyama et al., 1998). However, double Gli2/3 mutants do not form lung buds and have no separation between the trachea and esophagus (Motoyama et al., 1998).

1.3.2 Lung morphogenesis

During embryogenesis the ventral region of the anterior foregut fated to form the respiratory system evaginates to form the tubules of the respiratory system, starting at embryonic day 9 (E9) in mice, E2.5 in chick (Burns and Delalande, 2005) and week 5 in human development (Burns et al., 2008) (Figure 1.4i).

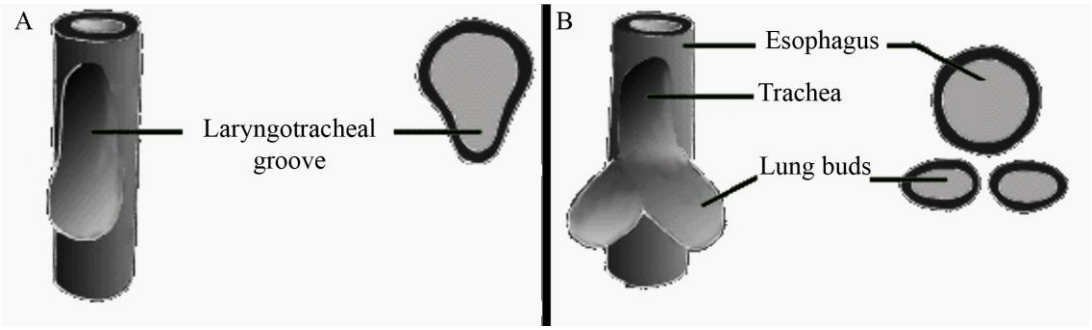

Figure 1.4i Formation of the laryngotracheal groove (A) trachea and lung buds (B), showing 3-dimensional schematic and corresponding sections.

The initial laryngotracheal groove (Figure 1.4ii, A and F) in the ventral anterior foregut deepens to form the trachea (Figure 1.4ii, K). Two swellings in the gut wall develop, forming the early lung buds (Figure 1.4ii, D). The lumen of the trachea then separates from that of the esophagus by the narrowing and pinching together of the two sides of the groove. This process occurs in a caudal to rostral direction. The bronchi are formed as the epithelial tubules extend out into the lung buds (Figure 1.4ii, M, N).

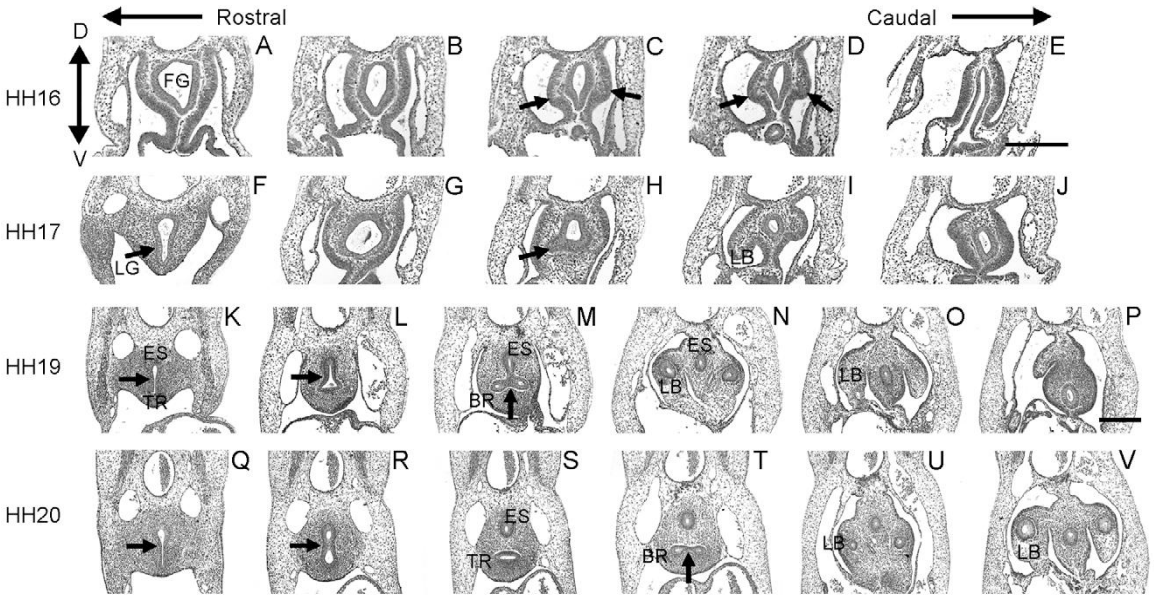

Figure 1.4ii Development of the lung buds in the early chick embryo. At HH stage 17 (day 2.5) the laryngotracheal groove forms in the ventral foregut (F) and deepens over time (K), eventually separating from the gut to form the trachea (S). The trachea bifurcates caudally to produce the bronchi (M, T). The lung buds initially form as swellings in the wall of the foregut (D), which grow outwards over time (I, N, V). BR-bronchi, FG-foregut, ES-esophagus, LB-lung buds, LG-Laryngotracheal groove. From Burns and Delalande (2005).

After separation of the trachea and bronchi from the gut, the epithelial tubules within the mammalian lung that will form the airways undergo successive branching events to generate the respiratory tree. These epithelial tubules are surrounded by a network of capillaries, the early vascular plexus. The larger, anterior, conducting airways branch successively to give rise to smaller airways and eventually join with the mesenchyme at the alveoli, the site of respiratory exchange (Table 1.1). The lung mesenchyme that makes up the lung buds grows and divides into lobes as the lung develops. Left-right asymmetry is seen in mammalian lung lobe formation.

In human lung development, airway branching produces a respiratory tree of 23 generations with a stereotyped structure of upper airways as reviewed in Merkus et al. (1996); Warburton et al. (2003). Airway branching events are highly stereotyped in their orientation and position, producing a respiratory tree that is highly similar between different individuals (Metzger et al., 2008).

Lung stage	**Description**	**Age in human (weeks post conception)**	**Age in mouse (days post conception)**
Embryonic	Initial budding and branching of the lung buds from the primitive foregut.	3-7	Embryonic day 8-10
Pseudoglandular	Further branching of the duct system up to the level of the terminal bronchioles.	7-16	E10-16
Canicular	The terminal bronchioles branch to form several orders of respiratory bronchioles.	16-24	E16-18
Terminal Sac	Branching and growth of the terminal sacs or primitive alveolar ducts.	24-36	E18 - Postnatal day 5
Alveolar	Maturation of the lung indicated by the appearance of fully mature alveoli. Growth continues into adulthood.	36 - postnatal	P5- adult

Table 1.1 The five stages of mammalian lung development. A significant amount of development through alveolar maturation occurs postnatally, more so in mice than humans. The timing and relative duration of different stages of maturation differs between species. Modified from Ten Have-Opbroek (1991).

The mammalian airway branching process has been characterised by categorising the types of branching morphogenesis that occur in the growing lung. Branching events may be characterised as domain, planar or orthogonal depending on the orientation and number of branch points formed (Metzger et al., 2008). Different types of branching predominate in different aspects of mammalian lung formation. For example, domain branching, where multiple buds form in rows along a parent tubule, is important in the development of the primary 'scaffold' tubules of the early respiratory tree, while the later development of the peripheral, smaller tubules at the lung edges occurs through planar branching, bifurcation of the airways in a single plane. The molecular mechanisms behind the generation of stereotyped respiratory tree anatomy are incompletely described (Andrew and Ewald, 2010; Warburton et al., 2005), but some of the key signalling molecules in lung epithelial tubule

branching and their signalling network have been investigated (Figure 1.5) (Affolter et al., 2009).

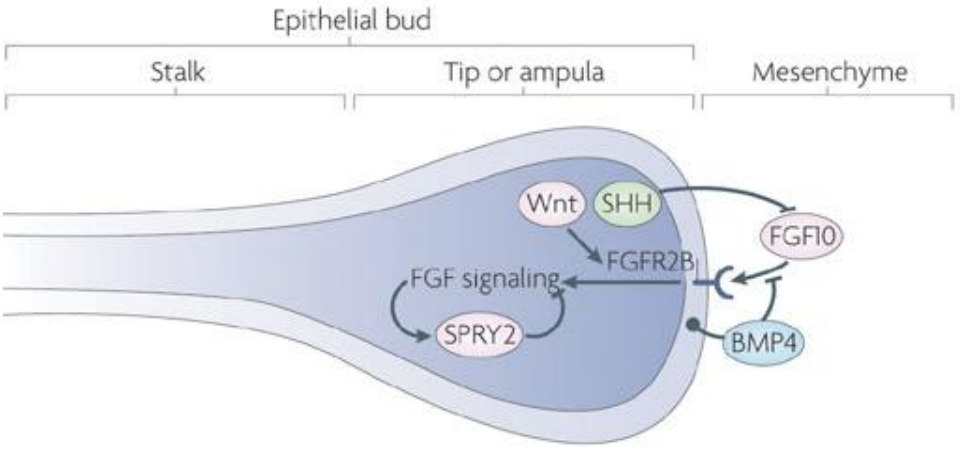

Figure 1.5 Lung bud growth. Mesenchymal FGF10 signals to FGF receptor 2B (FGFR2B) in the distal epithelium. Signalling through this pathway is promoted by Wnt signalling and increases SPRY2 expression. This cascade is negatively regulated by Shh and BMP4. From Affolter et al. (2009).

The interaction between tubule growth and branching is regulated by several factors (Figure 1.5), including Shh (Bellusci et al., 1997b), Bone Morphogenetic Protein 4 (BMP4) (Bellusci et al., 1996) and FGF10 (Abler and Sun, 2009). Branching is more subtly affected by signalling from Wnt family members (De Langhe et al., 2005) and TGF-beta (Zhou et al., 1996). Shh is expressed at the tip of the growing epithelial tubule while its receptor Patched is expressed in the surrounding lung mesenchyme. Shh acts through Patched to regulate FGF10 expression in the mesenchyme (Bellusci et al., 1997b). FGF10 promotes epithelial branching and helps drive epithelial tubule growth into the mesenchyme. It also activates the expression of Sprouty2 (SPRY2), a transcription factor that negatively regulates branching (Mailleux et al., 2001) by limiting the proliferation and migration of cells in the distal tip of the epithelial tubule. Branch point selection and spacing require signalling molecules to regulate the periodicity of branching. FGF10 and SPRY2 appear to be important in the regulation of branching events to ensure normal spacing of airway branches. Bone morphogenetic protein 4 (BMP4) has multiple roles in respiratory tubule branching morphogenesis. BMP4 signalling in the tubule tip epithelium restricts FGF signal transduction and branching, while mesenchymal BMP4 enhances local branching (Affolter et al., 2009). These different autocrine and paracrine functions of BMP4 signalling may also help to regulate branch point

selection. BMP4 has also been shown to be important in the proximal-distal patterning of the lung, promoting distal epithelial characteristics at the tip of the growing epithelial tubule (Weaver et al., 1999).

In parallel with the growth of the respiratory tree, a network of blood vessels also grows and branches. Recent work suggests that the parallel branching of blood vessels and airways in the lung is linked, due to airway dependency on blood vessels to guide the orientation of 3-dimensional airway branching and repress ectopic branch formation. Ablating lung vasculature prevents orthogonal airway bifurcation and leads to a reduction in branching and ectopic branch formation (Lazarus et al., 2011). The major pulmonary vessels were thought to grow into the lung along the airways from external vasculature but it has been observed that new vessels in the lung appear to form by vasculogenesis and condensation of existing capillaries, as reviewed in Hislop (2002). Recent work using clonal analysis to trace tissue lineages within the lung suggests that pulmonary vessels may form initially from condensation of the early vascular plexus, when initial lung bud branching occurs (Prof. Mark Krasnow, unpublished communication). Lung mesothelial cells from the lung surface contribute to pulmonary vascular smooth muscle formation (Que et al., 2008).

FGF signalling has a conserved role in branching morphogenesis in many organ systems as reviewed in Metzger and Krasnow (1999). FGF9 (Yin et al., 2011) and 10 (Abler and Sun, 2009) mouse mutants have severely disrupted lung epithelial tubule branching and lung hypoplasia while exogenous application of FGF10 to cultured lungs increases the rate of epithelial tubule branching (Acosta et al., 2001). In the developing mammalian lung, positive intraluminal pressure of the fluid in the developing lung is believed to increase FGF10 expression and hence epithelial tubule branching via mechanotransduction. Unbekandt et al demonstrated this by using tracheal occlusion to increase intraluminal pressure in cultured embryonic mouse lung (Unbekandt et al., 2008). This increased intraluminal pressure was shown to cause increased epithelial tubule branching. Intraluminal pressure is also thought to stimulate lung growth *in vivo*, where more nutrients are available to fuel tissue expansion (Moessinger et al., 1990). Peristaltic contractions of ASM may

contribute to positive intraluminal pressure during development, as discussed later in section 1.5.1.

Airway branching in the avian lung is very different to that in mammals. Sequential bifurcation is not a key structural feature of the avian respiratory tree; instead multiple airways bud off from primary and secondary bronchi (Maina, 2003). Secondary bronchi bud off laterally from the intrapulmonary primary bronchus in a process similar to domain branching. Parabronchi then bud laterally and non-sequentially from the secondary bronchi and form a connecting network between the secondary bronchi. The respiratory tree forms a parallel system of continuous airways that do not terminate in alveoli, as in mammals. The signalling events behind avian lung morphogenesis have not been investigated in depth (Maina, 2003).

The embryonic and fetal lung has considerable differences in function and alveolar structure from that of the adult, as the lungs undergo significant postnatal modification triggered by the onset of breathing for respiratory exchange. Upon birth, blood flow is redirected into the lungs and oxygen uptake through the lungs begins. The lung continues growing until body size has stabilised, as the lung alveolar surface area must be proportional to the size of the body for sufficient oxygen uptake. This thesis deals primarily with the development of the neural crest-derived innervation in the embryonic lung, and so postnatal lung development will not be addressed in detail.

1.4. Lung innervation and its development

The lungs have both extrinsic and intrinsic innervation with both sensory and effector functions. Extrinsic vagal and sympathetic nerve branches innervate the lung. Bronchial branches of the vagal nerve join nerve fibres from the sympathetic trunk before entering the lung, forming mixed nerve fibres. Extrinsic projections can innervate intrinsic pulmonary neurons or directly innervate sensory or effector structures. Extrinsic and intrinsic neuronal fibres form a network of nerves around the airways, called the pulmonary plexus. Efferent nerves regulate airway smooth muscle tone and mucus secretion from submucosal glands, goblet cells, and Clara cells in the airway epithelium. Vascular permeability and blood flow in pulmonary blood vessels is also regulated by pulmonary innervation. Sensory nerves provide

homeostatic feedback on lung inflation, and detect irritant chemicals and oxygen concentration within the lung either directly or through sensory cells.

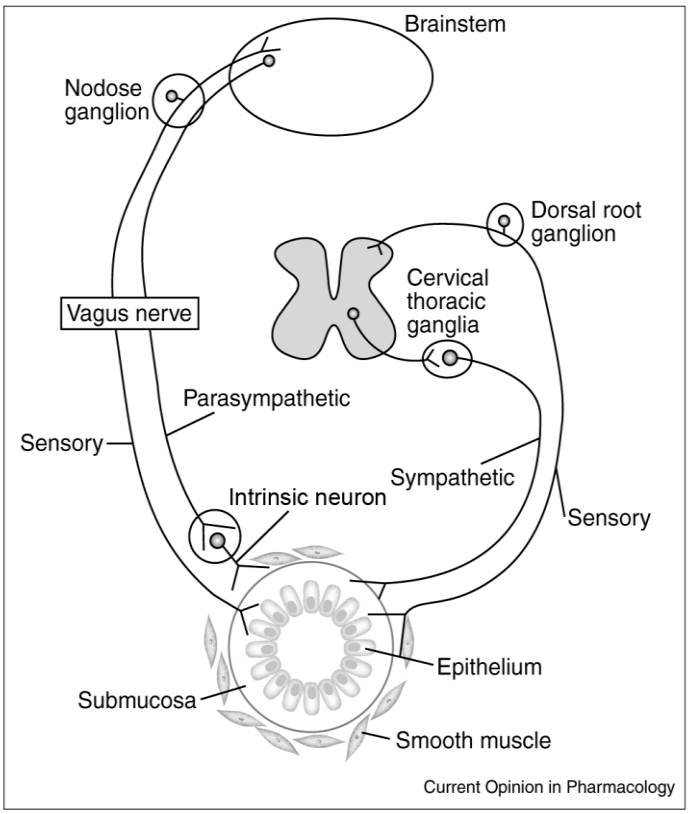

Figure 1.6 Summary of pulmonary innervation. Efferent parasympathetic innervation from the brainstem travels along the vagal nerve and synapses with intrinsic pulmonary neurons, which then innervate ASM. Efferent extrinsic sympathetic neurons from the cervical and thoracic ganglia synapse directly onto targets of lung innervation such as airway smooth muscle. Afferent sensory nerve terminals from the nodose and jugular ganglia and DRGs can synapse onto sensory structures such as neuroepithelial bodies(shown in Figure 1.10) or innervate the lung directly. From Belvisi (2002).

1.4.1 Extrinsic sensory innervation of the lung

The vagal nerve, also called cranial nerve X, contains a mix of afferent fibres that transmit sensory information to circuits in the brainstem, and efferent fibres that transmit effector impulses to targets within the lung (Monkhouse, 2005). The nodose and jugular ganglia receive a variety of types of sensory information from the lung through sensory afferent fibres in the vagal nerve, and transmit this information to the brainstem. Somatosensory information from the lung is also carried to the central nervous system by afferent pulmonary sensory fibres from the cervical and thoracic dorsal root ganglia. Input from pulmonary sensory nerves modulates respiratory and cardiac activity in the central pattern generator in the brainstem.

Pulmonary sensory nerve terminals may be stretch receptors or chemosensory terminals. Slowly-adapting stretch receptors in the wall of the trachea and rapidly-adapting stretch receptors in the walls of the lower airways respond to lung inflation (Widdicombe, 2001) and to pathological stimuli (Belvisi, 2003). Chemosensitive C-

fibres can also sense lung inflation, but their primary function appears to be chemosensation. They signal in response to irritant chemicals including capsaicin (Bevan and Szolcsinyi, 1990) and cigarette smoke and inflammatory agents including bradykinin, eliciting homeostatic cardiopulmonary responses. Despite their primary function as afferent sensory nerves, chemosensitive C-fibres can also affect local processes in the lung such as bronchoconstriction, vasodilation, bronchial edema and mucus hypersecretion locally by releasing neuropeptides from sensory terminals in the parenchyma and bronchi. For example, release of the neurotransmitter neurokinin A from sensory C-fibre terminals promotes inflammation (Belvisi, 2003). Sensory input to afferent nerves from sensory neuroepithelial bodies within the lung is discussed in section 1.5.2, below.

1.4.2 Extrinsic effector nerves and non-neuronal signalling

Vagal nerve efferent fibres provide motor innervation to a number of target organs, including the gut and lung. They originate from brainstem nuclei: the nucleus ambiguus and the dorsal motor nucleus (Chang et al., 2003). Parasympathetic projections from the dorsal motor nucleus pass through, and are augmented by afferent fibres from the jugular and nodose ganglia (the superior and inferior ganglia of the vagal nerve; Monkhouse, 2005). The pulmonary or bronchial branches of the vagal nerve provide extrinsic motor innervation to the lung (Figure 1.6). Cholinergic parasympathetic nerves from the vagal nerve innervate airway parasympathetic autonomic ganglia (APGs), which relay their signals to downstream targets. Acetylcholine is the main neurotransmitter in the lung, but 5-HT, neurokinin, nitric oxide and noradrenaline are also released from nerve terminals in the lung (Barnes, 1988). Acetylcholine release causes airway smooth muscle (ASM) contraction and bronchoconstriction. ASM and its functions are discussed in more detail in section 1.5.1 below.

Parasympathetic Non-Adrenergic-Non-Cholinergic (NANC) projections extend from neurons in the brainstem along the vagal nerve into the lungs (Stretton, 1991). The role and extent of these nerves varies between mammalian species (Andersson and Grundstrom, 1987; Canning and Fischer, 2001; Gu et al., 2006). Inhibitory NANC neurons cause bronchodilation and are thought to use nitric oxide (NO) and vasoactive intestinal peptide (VIP), though this is disputed (Watson et al., 1993),

while excitatory NANC nerves using tachykinins as neurotransmitters cause bronchoconstriction (Widdicombe, 1998).

Not all extrinsic innervation is part of the vagal nerve bundle. Postganglionic noradrenergic fibres from the cervical and thoracic sympathetic ganglia innervate pulmonary blood vessels, submucosal glands and airway smooth muscle (Figure 1.6) (Belvisi, 2002). Signalling through these nerves produces a sympathetic bronchodilation response, decreasing the basal tone of the airway smooth muscle.

The physiological functions of lung innervation in mature lungs are diverse and depend on the type, source and target of innervation. Many of the neurotransmitters that are released by or affect nerve terminals in the lung also have non-neuronal effects – for example, acetylcholine is released from both neurons and non-neuronal tissue and as well as transmitting neuronal signals to the muscles functions as a paracrine regulator of inflammation (Racke and Matthiesen, 2004), causing histamine release from mast cells. Airway inflammation is a key feature of asthma and other reactive airway diseases, and so the interaction of airway inflammation with ASM contraction and sensory cells in the lung has been much studied, as reviewed in Barnes (2011); Verhein et al. (2009). Some tissues in the lung, including ASM, can release signalling molecules that can have neuronal and non-neuronal effects. For example, inflammatory mediators such as nitric oxide are released by ASM and macrophages, affecting acetylcholine release by APGs (Figure 1.7, below). The hormone adrenaline, diffusing into lung tissue from the blood, affects both non-neuronal ASM and APG neurons.

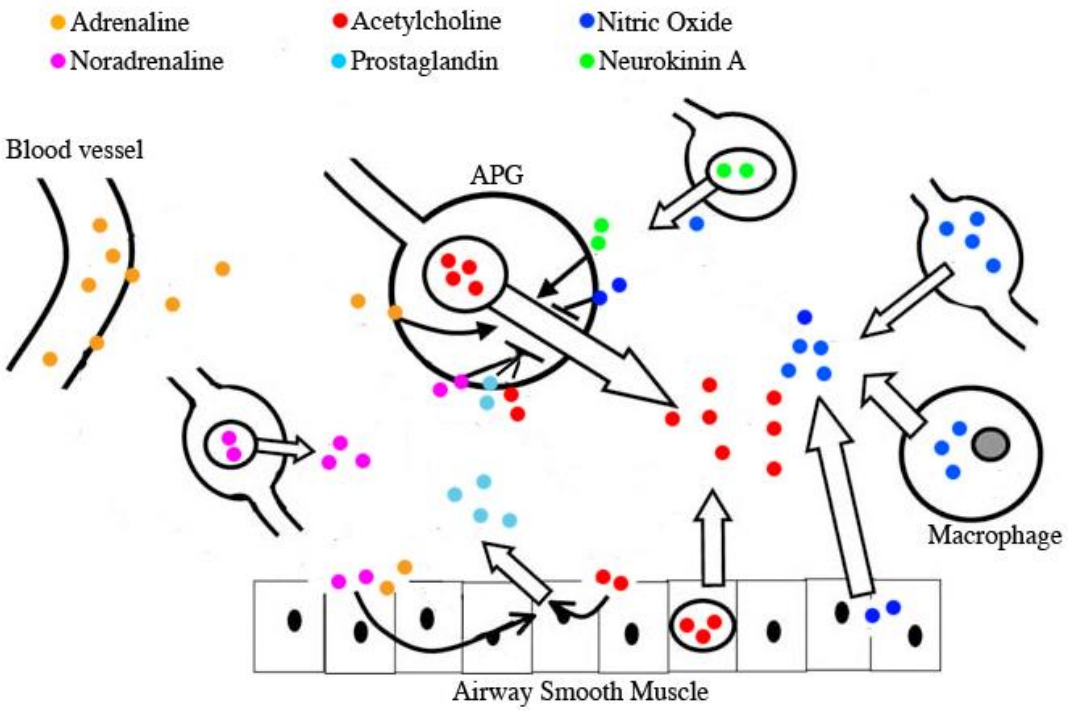

Figure 1.7 Mechanisms controlling acetylcholine (red) release from a cholinergic airway parasympathetic ganglion (APG). Both nerve terminals and non-neuronal tissues in the lung release signalling molecules or neurotransmitters that affect acetylcholine release. Modified from Racke and Matthiesen (2004).

1.4.3 Intrinsic lung neurons

Intrinsic pulmonary neurons form parasympathetic ganglia that are located next to the airways. Their postganglionic projections form an autonomic plexus around the airways that innervates ASM (Brouns et al., 2003). Intrinsic airway ganglia are often found at conducting airway branching points and act as sites of convergence for several different classes of pulmonary innervation (Brouns et al., 2009) (Figure 1.8). They receive input from extrinsic and other intrinsic neurons, and may act as sites of signal integration before signalling to downstream targets of innervation in the ASM (Myers, 2001).

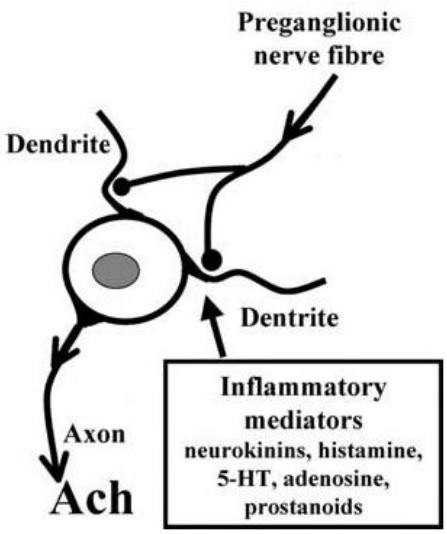

Figure 1.8
Acetylcholinergic airway parasympathetic neurons have multiple inputs. Airway parasympathetic ganglion neurons receive and process input from extrinsic neurons and local inflammatory mediators, before signalling to airway smooth muscle. Modified from Racke and Matthiesen (2004).

Intrinsic cholinergic neurons in the mouse lung express the acetylcholine-processing enzyme choline acetyltransferase (ChAT) at embryonic stages and in adulthood (Tallini et al., 2006). In some species, a portion of intrinsic airway parasympathetic ganglia may be NANC, expressing nitric oxide, vasoactive intestinal peptide, or sometimes substance P. However, this component of parasympathetic innervation varies in position and role between species. For example, in the guinea pig, NANC ganglia are situated in the myenteric plexus around the foregut and project from there into the lung (Pan et al., 2010). The release of acetylcholine from intrinsic lung neurons in APGs stimulates the contraction of airway smooth muscle, causing bronchoconstriction (Gabella, 1987). Cholinergic signalling appears, from examination of the roles of muscarinic receptors in ASM, to be the major input for ASM contraction (Undem and Larry, 2009). The majority of efferent fibers innervating airway smooth muscle in the trachea and bronchi originate from the tracheal and bronchial airway parasympathetic ganglia.

Acetylcholine is released from the APG nerve terminals that innervate the ASM in response to a number of upstream signalling pathways (Figure 1.8). This acetylcholine release may be promoted or suppressed by extrinsic neuronal input through preganglionic nerve terminals. Cholinergic APG activation can be influenced by the action of local non-neuronal inflammatory mediators, as in the suppression of acetylcholine release by nitric oxide (Figure 1.7) on APG neurons (Racke et al., 2006; Racke and Matthiesen, 2004). The release of acetylcholine from airway parasympathic nerve terminals is inhibited by muscarinic autoreceptors

present on cholinergic APG neurons (Myers et al., 1996) allowing local control of acetylcholine release by negative feedback. Acetylcholine is found at both neuronal and non-neuronal sites in lung tissue (Wessler et al., 1999), so acetylcholine and its synthetic enzyme ChAT cannot be used as neuronal markers. However, vesicular acetylcholine transporter (VAChT), which marks cholinergic vesicles, is specific to cholinergic neurons (Wessler and Kirkpatrick, 2001). Acetylcholine from APGs and non-neuronal sources can act as a paracrine regulator of processes in the lung, including inflammation and wound healing (Racke and Matthiesen, 2004), allowing acetylcholine from APGs to affect tissues at a distance from APG synapses. APGs can also influence mucus secretion from epithelial cells and vasodilation of pulmonary blood vessels via acetylcholine release (Myers, 2001).

1.4.4 Development of lung innervation

Intrinsic lung neurons are derived from the neural crest. The development of the intrinsic innervation of the lung begins with the migration of undifferentiated neural crest cells (NCC) into the embryonic foregut. These NCCs arise in the vagal (hindbrain) region, adjacent to somites 1-7, and subsequently colonise the entire length of the gut to form the enteric nervous system (ENS), the intrinsic innervation of the gastrointestinal tract (Le Douarin and Teillet, 1973), as reviewed in Anderson et al. (2006a); Burns and Thapar (2006). From the vagal NCCs migrating in the foregut, a subpopulation moves tangentially from the foregut to colonise the adjacent lung buds, a process demonstrated by NCC tracing in chick (Burns and Delalande, 2005), human (Burns et al., 2008) and shown recently in work from this thesis in mouse embryonic development (see chapter 3) (Freem et al., 2010). This subpopulation of NCCs thus undergoes a two-step migration, first migrating from the vagal neural crest to the gut and then tangentially from the gut into the lungs. At the time of vagal NCC migration, the trachea and lung buds are in the process of separating from the foregut (Figure 1.4), so the lung bud and gut endoderm are connected and NCCs can migrate to the lung buds. NCCs within the chick lung express the RET receptor (Burns and Delalande, 2005) and have been shown to migrate towards the RET ligand GDNF in mouse lung culture (Freem et al., 2010; Tollet et al., 2002). Within the chick lung, vagal NCCs have been shown to differentiate to form neurons that are present adjacent to the future airways and are associated with ASM (Burns and Delalande, 2005). These intrinsic lung neurons

appear to aggregate and form the airway parasympathetic ganglia. Lung innervation studied in human (Burns et al., 2008; Sparrow et al., 1999), pig (Sparrow et al., 1995) and mouse (Tollet et al., 2001) embryos demonstrates that intrinsic lung innervation is closely associated with ASM in the distal lung. Surrounding the future airways, a neuronal plexus lies on top of a layer of airway smooth muscle and extends into the distal lung over time along the growing airways (Tollet et al., 2001). Lung NCCs are closely associated with the vagal nerve throughout their migration into the lung (Tollet et al., 2001).

Extrinsic pulmonary innervation develops at the same time as intrinsic lung innervation. The extrinsic efferent innervation of the lung arises from the vagal and sympathetic nerve trunks of the autonomic nervous system. A proportion of extrinsic lung innervation, the afferent vagal nerve fibres from the vagal nodose ganglia, is derived from the nodose epibranchial placode (Baker and Bronner-Fraser, 2001). Other sensory innervation, including that from the dorsal root ganglia and vagal jugular ganglia, is neural crest-derived (Kwong et al., 2008). The vagal fibres that innervate the mouse lungs have been shown to contain a mix of placode-derived and neural crest-derived fibres (Nassenstein et al., 2010). Parasympathetic innervation from the brainstem enters the lung via the vagal nerve, while sympathetic pulmonary innervation comes from the cervical and thoracic ganglia (Kummer et al., 1992). Although it is unknown which cues guide the bronchial branches of the vagus into the lungs a potential parallel exists in the gut, where vagal sensory axons respond to chemoattractive netrin signalling through the receptor Deleted in Colon Cancer (DCC) in *in vitro* experiments. Vagal gut axons terminate their response to netrin in the presence of laminin, found in the gut ECM, a possible mechanism for vagal nerve terminal positioning (Ratcliffe, 2011).

1.5 Targets of Pulmonary Innervation

The principal targets of lung innervation include airway smooth muscle, innervated by efferent postganglionic fibres from intrinsic airway parasympathetic ganglia and sympathetic cervical and thoracic ganglia, and neuroepithelial bodies (NEBs) which are innervated by afferent fibres from nodose ganglion neurons and dorsal root ganglia (DRG). NEBs are innervated by both sensory and effector nerves. These two targets of innervation have been hypothesised to be involved in lung development and in early lung disorders. Airway submucosal glands also receive innervation from intrinsic and extrinsic neurons that regulate their mucus secretion (Wine, 2007), but this target of lung innervation will not be addressed in detail as the involvement of these glands in lung development is less well described than that of airway smooth muscle.

1.5.1 Airway Smooth Muscle

Airway smooth muscle (ASM) is found beneath the lung epithelium and extends from the trachea into the lower respiratory tree but does not extend to the alveoli. ASM develops *in situ* with the growth of the airways that it surrounds and so is present early in lung development. It is first seen at around E11 in the mouse (Mitzner, 2004) and is present by week 6 of human development (Burns et al., 2008). The prevailing theory is that ASM develops from mesenchyme-derived precursor cells found close to growing epithelial tubules. At the tip of the growing epithelial tubule, BMP4 and Shh are expressed at high levels and induce myogenic differentiation in mesenchymal progenitor cells (Weaver et al., 2003). As the epithelial tubule tip extends distally into the mesenchyme, the source of BMP4 and Shh moves away from the smooth muscle cells around the epithelial tubule. A layer of smooth muscle is formed around the airway as the airway grows (Mailleux et al., 2005).

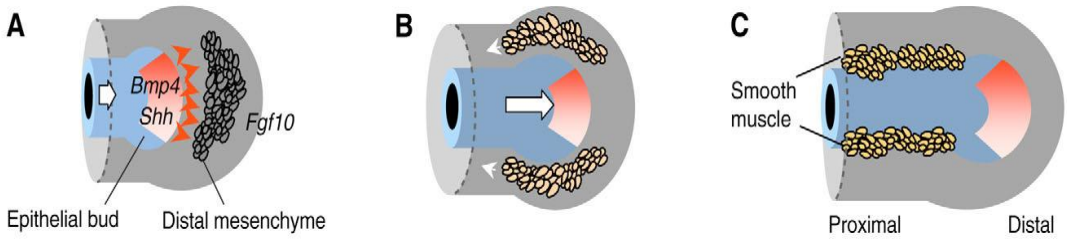

Figure 1.9 Airway smooth muscle development. A: The tip of the growing epithelial tubule secretes BMP4 and Shh. These signals are received by mesenchymal progenitor cells (MPCs) in the distal mesenchyme. B: MPCs undergo myogenic differentiation. C: as the epithelial bud moves distally, it leaves behind a layer of muscle cells surrounding the tubule that forms the ASM. From Cardoso and Lu (2006).

Recent research using progenitor cell tracing (Prof. Mark Krasnow, unpublished communication) suggests that ASM may have a different origin, a putative pool of self-renewing precursors at the tip of the growing tubule that give rise to differentiated ASM cells. These cells form a layer of ASM around the tubule, laid down as the airway extends. This idea is supported by reports of stem cell niches in the epithelium of terminal bronchioles in the mature lung (Giangreco et al., 2002) that are known to contain epithelial progenitors but might also harbour ASM progenitors during development.

ASM has a potential role in the antenatal development and growth of the lung (Jesudason, 2009). It has been suggested that the peristaltic contraction of ASM moves fluid through the developing lung (Schittny et al., 2000) and that this promotes lung growth. The pressure of the fluid against the lung tissue may provide a mechanical stimulus for growth (Sparrow et al., 1994). Increasing intraluminal pressure within the lung stimulates epithelial branching in culture and may increase lung growth *in vivo* (Unbekandt et al., 2008). In the absence of positive internal pressure, lung growth is decreased (Sparrow et al., 1999). In further support of the possible link between embryonic ASM peristalsis and lung growth, ASM dysfunction has been linked to hypoplastic lung growth (Jesudason et al., 2006). Also, ASM dysfunction occurs in, and may cause, lung hypoplasia in a congenital diaphragmatic hernia (CDH) rat model, where lung hypoplasia precedes CDH (Featherstone et al., 2006).

This peristaltic movement of airway smooth muscle appears to be initiated and maintained independently of neuronal input (Sanderson et al., 2008). Intrinsic calcium channel activity is important in maintaining ASM contractility prenatally (Bai et al., 2007) and tone postnatally (Sanderson et al., 2008), but the role of lung innervation in patterning ASM peristalsis has not been investigated. ASM contraction is mediated by intrinsic calcium currents and appears to be modulated by neuronal input (Berridge, 2008).

After birth, the role of ASM in the healthy lung is less clear (Mitzner, 2004). In postnatal lung, airway smooth muscle shows no peristaltic contractions but instead contracts tonically. This tonic contraction has been posited to provide structural support for the airways. ASM may also contribute to mucus clearance and coughing through occasional spasmic contractions in response to chemical stimuli. The effect of neuronal inputs on ASM contractility has been well studied in pathogenic contexts such as asthma (Belmonte, 2005; Canning and Spina, 2009), but their role in ASM development and normal function has been less researched.

1.5.2 Neuroepithelial Bodies

Pulmonary neuroendocrine cells (PNECs), also called neuroepithelial endocrine cells, are hypoxia-sensitive chemoreceptors found in lung airway epithelium next to the lumen of the airway, as reviewed in Cutz and Jackson (1999); Van Lommel (2001) (Figure 1.10). They express the calcitonin neurotransmitter marker CGRP (Keith, 1991) and unlike intrinsic pulmonary neurons are not derived from the neural crest, instead arising from the endoderm that forms the airway epithelium (Sorokin et al., 1997). Some, but not all, PNECs aggregate with other PNECs to form specialised structures innervated by multiple extrinsic nerves, the neuroepithelial bodies (NEBs) (Van Lommel, 2001). NEBs are also sites of airway epithelial stem cell reservoirs (Reynolds et al., 2000) as well as afferent and efferent nerve terminals (Brouns et al., 2006) (Figure 1.10).

Intrinsic neural crest-derived pulmonary neurons in airway ganglia are often found near NEBs (Garcia-Suarez et al., 2009) but have not to date been shown to directly innervate NEBs (Brouns et al., 2009). However, NEBs have been shown to receive

innervation from extrinsic efferent and afferent brainstem neurons in the nucleus ambiguous, dorsal motor nucleus and solitary tract (Adriaensen and Scheuermann, 1993; Brouns et al., 2003). Also, PNECs either with NEBs or as isolated cells are responsive to acetylcholine via nicotinic receptors. This is a mechanism by which acetylcholine release from APGs can affect PNEC activity, despite the lack of direct innervation from APGs. Acetylcholine signalling both increases PNEC secretion of 5-HT (Freitag et al., 1996) and, interestingly, promotes PNEC proliferation in adulthood (Schuller et al., 2003). Whether this proliferative response also exists during development is unknown.

It is likely that extrinsic neurons relay sensory information from NEBs to the central respiratory circuits in the brain. An increase in the density of NEBs has been reported in lungs from cases of Sudden Infant Death Syndrome (SIDS) (Cutz et al., 2007a; Gillan et al., 1989). One of the possible consequences of this reported increased density of NEBs is increased sensitivity to hypoxia. The control of proliferation of NEBs and PNECs is thus potentially important in early respiratory function.

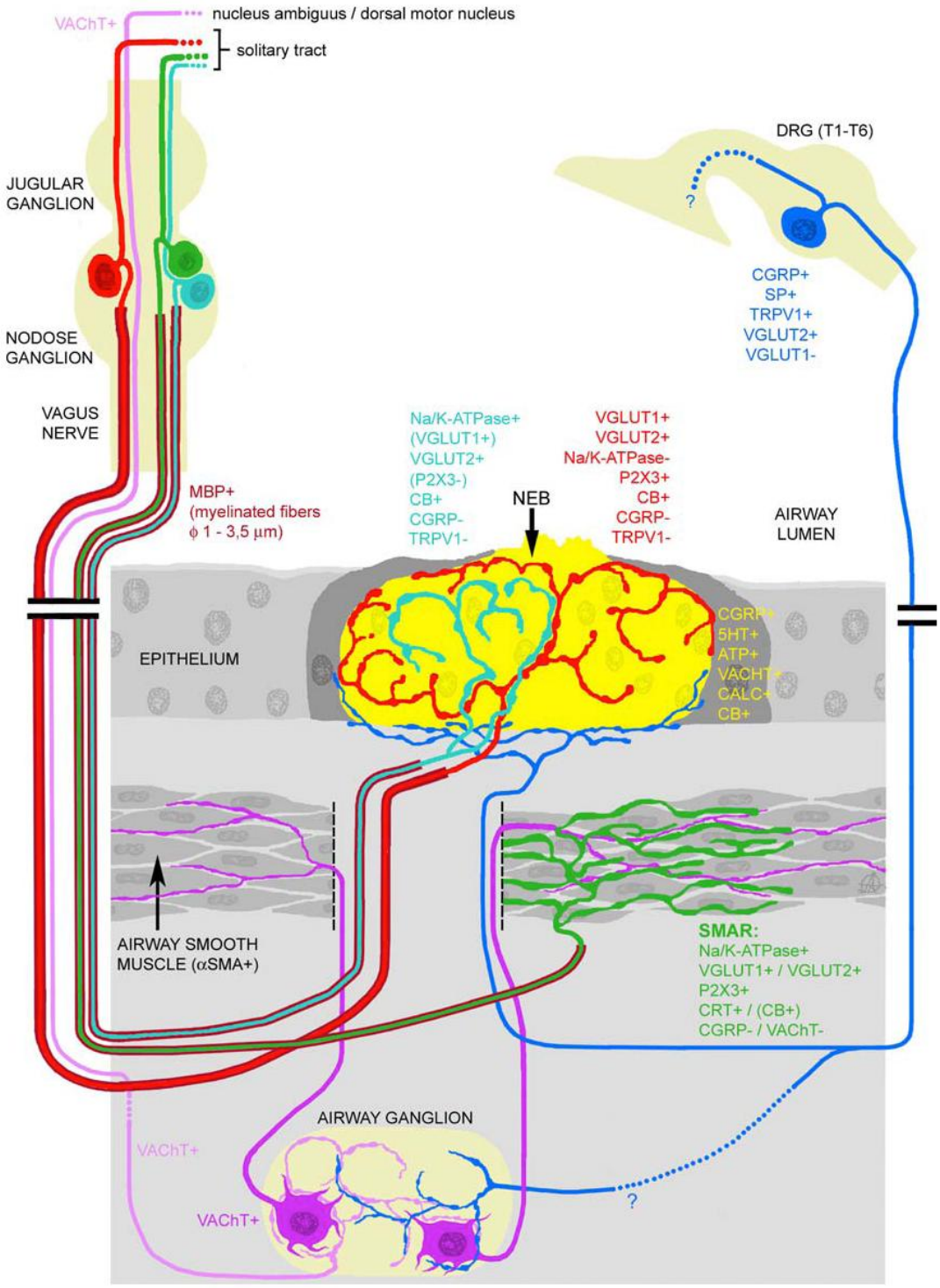

Figure 1.10 Interrelationship of lung innervation, NEBs and airway ganglia. Intrinsic lung neurons (purple) innervate airway smooth muscle and relay information from the brain and other signal sources. From Brouns et al. (2006).

1.6 Neural crest cell development and migration

Neural crest cells (NCC) are highly migratory, multipotent cells that arise during vertebrate neurulation and give rise to multiple distinct cell types in a range of embryonic regions (Kalcheim and Le Douarin, 1999). In order to carry out their role, NCCs are induced and undergo specification to delaminate from the neural epithelium and assume migratory mesenchymal characteristics, including responsiveness to a range of signalling cues. They then migrate under the influence of diverse cues to locations throughout the developing embryo, where they differentiate to give rise to a range of cell and tissue types including neural and glial cells of the autonomic nervous system, melanocytes, and bone and cartilage components of the head (Baker, 2008; Bronner-Fraser, 1993). Along the anterior to posterior axis, different regions of the neural crest give rise to NCCs with different fates.

1.6.1 NCC induction

NCC formation begins with the development of the neural plate boundary, a region between the dorsal neural tissue that will invaginate to form the neural tube and the surrounding epithelial tissue. During neurulation, a region of the dorsal ectoderm called the neural plate invaginates from anterior to posterior to form the neural tube. The cells at the neural plate boundary, between the neural ectoderm and epithelial non-neural ectoderm, are induced to form NCCs by external diffusible signalling molecules including BMPs (Liem et al., 1995), FGFs (Mayor et al., 1997) and Wnts (Saint-Jeannet et al., 1997), as reviewed in Basch and Bronner-Fraser (2006); Steventon et al. (2005). These neural crest inductive signals are also involved in neural and epidermal induction, which occur at the same time. For example, in *Xenopus* BMP is present along a diffusion gradient and induces epidermis at high levels, neural crest at intermediate levels and neural plate at low levels (Marchant et al., 1998). The combination of diffusible morphogenetic signals sufficient to induce neural crest both supplies redundancy in NCC specification and spatially restricts NCCs to the plate border, as do other non-diffusible organising signals. Cell-cell signalling through the Delta-Notch signalling pathway is also important in spatially restricting development of the neural crest to the neural plate boundary (Cornell and Eisen, 2005; Endo et al., 2002). The specific BMP, FGF and Wnt proteins involved in NCC development may vary between species: for example, Wnt6 from the non-

neural ectoderm induces NCCs in chick (Garcıia-Castro et al., 2002) while in zebrafish Wnt8 (LaBonne and Bronner-Fraser, 1998), Wnt1 and Wnt3a (Saint-Jeannet et al., 1997) induce NCCs. The organising tissue also varies between species. In chick the non-neural ectoderm is the major source of canonical Wnt signalling (Garcia-Castro et al., 2002) while in mice the source is unknown. The neural and non-neural ectoderm and the paraxial mesoderm are all sources of morphogenetic signals in most vertebrates (Garcia-Castro and Bronner-Fraser, 1999), but their precise roles vary between species. Other specialised tissues, including preplacodal ectoderm, arise from regions near or adjacent to the neural plate border (Baker and Bronner-Fraser, 2001; Schlosser, 2006; Schlosser, 2010; Streit, 2007). Several morphogenetic signals inducing a precise combination of transcription factors are needed to delineate neural crest territory within the neural plate.

1.6.2 Early NCC specification

Due to differences in NCC characteristics and fate along the rostro-caudal axis, one gene regulatory network cannot account for the process of NCC formation along the entire length of the embryo, even in a single species (Sauka-Spengler and Bronner-Fraser, 2008). There are however several genes that appear to be evolutionarily conserved in neural crest formation and are important in the neural crest gene regulatory network.

NCCs arise from the dorsal lip of the neural folds, a process that begins at the time of neural tube closure (Figure 1.11). Future NCCs at the neural plate boundary are marked by their expression of a combination of transcription factors, including Pax7 (Basch et al., 2006), Pax3, Zic1 (Sato et al., 2005), Msx1 and Msx2 (Khadka, 2006), known as the neural plate border specifiers. Some regions of the neural crest need particular transcription factors for their specification, as with the requirement for Dlx1-5 in cranial NCCs as reviewed in Panganiban and Rubenstein (2002). Dlx also has downstream roles in other NCC populations. Many neural plate border specifiers control the expression of suites of neural crest specifier genes that grant NCCs their migratory phenotype, signal response competency and potency, and are evolutionarily conserved (Baker, 2008). These include the transcription factors Snail1 and 2, Twist, Sox9 and 10, which are important in driving the changes in gene expression that allow NCCs to undergo epithelial to mesenchymal transition

(EMT) and become migratory. After EMT, NCCs have a highly migratory, mesenchymal phenotype and are characterised by the expression of transcription factors including the anti-apoptotic Snail1, Snail2, Wnt1 (Barembaum and Bronner-Fraser, 2005), Sox10, Sox9 (Hong and Saint-Jeannet, 2005) and FoxD3. The overlapping functions of the combination of transcription factors that specify NCCs allows some genes to compensate for related genes when their function is impaired. For example, Sox9 is capable of replacing the early requirement for Sox10 in *Xenopus* when Sox10 function is impaired (Taylor and LaBonne, 2005) but not the later requirement for Sox10 in PNS formation. Sox10 is the major SoxE transcription factor expressed in autonomic nervous system precursor cells and is required to specify that precursor population (Haldin and LaBonne, 2010).

1.6.3 Epithelial-mesenchymal transition

Once the neural tube has formed, NCCs delaminate from the epithelium in an anterior to posterior wave in a process called epithelial to mesenchymal transition (EMT), as reviewed in Saint-Jeannet and Duband (2006); Sauka-Spengler and Bronner-Fraser (2008). Morphogens involved in NCC induction and early specification can also initiate EMT. BMP4 and its antagonist noggin interact in chick to control the onset of NCC delamination (Sela-Donenfeld and Kalcheim, 1999). The transcription factors outlined above (section 1.6.2) control the expression of molecules that directly affect NCC migratory behaviour. These include cadherins, which mediate cell-cell adhesion by adhering to each other (Maschhoff and Baldwin, 2000). Snail2 expression in NCCs downregulates Cadherin6B (Taneyhill et al., 2007), which helps maintain the contact between cells in the epithelium, allowing NCCs to break contact with neighbouring cells in the neuroectoderm and delaminate. N-Cadherin, a cell-cell adhesion molecule expressed on NCCs before EMT, is also downregulated at EMT. Contributing to the switch in NCC behaviour, Cadherin7 mediates adhesion between NCCs and is upregulated at EMT (Kuriyama and Mayor, 2008), facilitating the migration of NCCs in cohesive groups. The Sox-E family of transcription factors (Sox8, Sox9 and Sox10), among others including Snail and FoxD3, help to control the changes in NCC gene expression necessary for EMT. The switch in the types of cells that NCCs adhere to, from neuroepithelial cells to mesenchymal cells, allows them to move out of the epithelium and become mesenchymal.

After EMT, NCCs begin to migrate away from the neural tube. NCC transcription factors described above, including the Sox-E family, control the expression of signalling receptors such as RET and neuropilin in NCCs. These receptors enable NCCs to respond to externally expressed guidance cues including the chemoattractive RET ligand GDNF, and chemorepulsive Sema3A and Sema3F (Sauka-Spengler and Bronner-Fraser, 2008). The expression of cytoskeletal regulators, such as the actin-regulating Rho GTPases (Hall, 1998), is also upregulated in NCCs. This confers increased cell motility, as in the induction of the GTPase RhoB in NCCs by BMP (Liu and Jessell, 1998). When GTPases are inhibited, NCC motility is decreased (Stewart et al., 2007). The regulation of the actin cytoskeleton through RhoA and other cystoskeletal regulators controls the formation of polarised membrane protrusions, which are needed for directional NCC migration (Matthews et al., 2008).

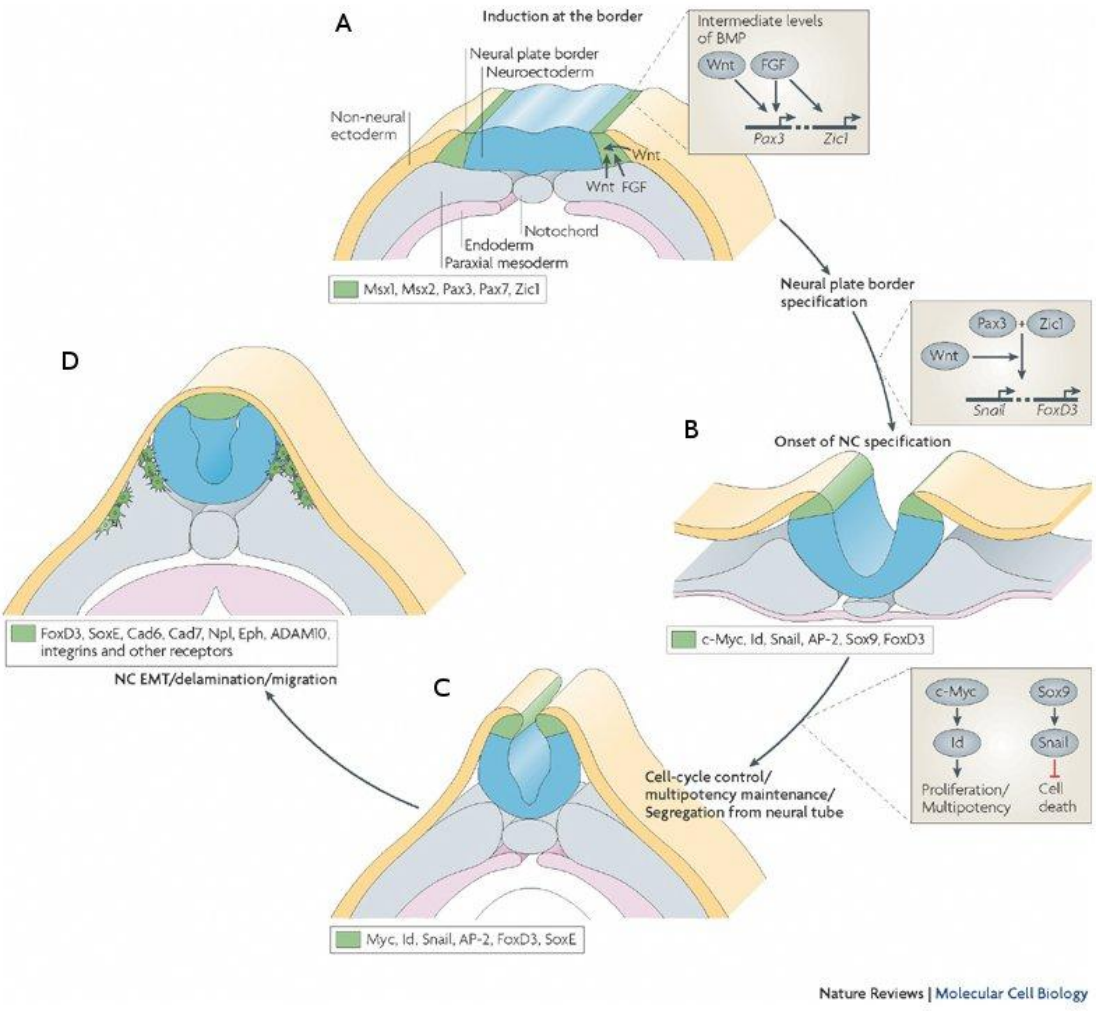

Figure 1.11 Neural crest development. A: Pax7 and other signals are induced at the neural plate border. B and C: Sox9, c-myc and others control the induction of the multipotent NCC phenotype. D: FoxD3, SoxE and other later stage transcription factors control the expression of effector genes such as cadherins and cell-surface receptors that enable NCCs to migrate away from the endoderm. From Sauka-Spengler and Bronner-Fraser (2008).

1.6.4 NCC migration

The early migration pathway of NCCs is complex and constrained by multiple factors. Neural crest cells are guided by interactions with repulsive and attractive signalling cues. Their migration pathways are also shaped by interactions with permissive and non-permissive components of the extracellular matrix (ECM) (Kulesa and Gammill, 2010).

On delaminating, NCCs migrate through pathways of permissive extracellular matrix in which cells can move rapidly. These NCC migration pathways are flanked by nonpermissive or repulsive tissues that block NCC migration. The presence of

both permissive and nonpermissive substrate components in defined positions and quantities seems to be necessary for normal NCC migration. Thus, the NCC migration pathway is dependent on the extra-neural tissues through which these cells migrate.

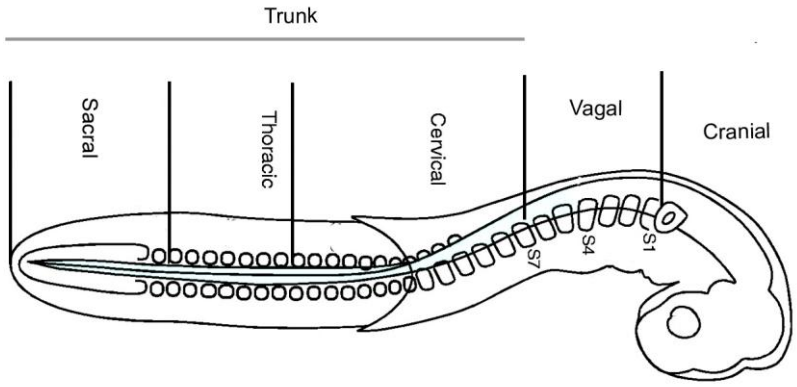

Figure 1.12 Different NCC populations arise from different axial regions of the neural tube. NCC populations from different axial levels, such as vagal NCCs, cranial NCCs and trunk NCCs, show differences in fate. Modified from Le Douarin et al. (2004).

NCCs from different regions (Figure 1.12) migrate in differing environments and may have different fates. For example, cranial NCCs do not migrate in segmented streams through the pre-somitic sclerotome as trunk NCCs do, as sclerotome is not present at the cranial level. Vagal and sacral NCCs contribute to the intrinsic enteric nervous system, but cervical and thoracic NCCs do not.

Early trunk NCC migration is partly driven by surrounding repulsion from the posterior sclerotome, driving NCCs and neuronal projections into streams through the anterior sclerotome, as reviewed in Bronner-Fraser (1993); Gammill and Roffers-Agarwal (2010); Kuan et al. (2004). This confinement of trunk NCC migration into streams contributes to the concerted development of the spinal cord and peripheral nervous system, as a sub-population of NCCs remain close to the neural tube and form dorsal root ganglia in the position of the NCC streams. Neuropilin-mediated repulsion from semaphorins in the posterior sclerotome is important in organising trunk NCCs into streams (Gammill et al., 2006) and in the segmentation of neural crest-derived sensory ganglia (Schwarz et al., 2009a). Repulsive ephrins (Krull et al., 1997) and F-spondin (Debby-Brafman et al., 1999) are also present in the tissues surrounding the NCC migration pathway and are

necessary for correct NCC migration stream segmentation. Long-distance chemoattractive forces guide NCC migration in later migratory pathways, for example in the guidance of vagal NCC in the gut, but are not considered key in early NCC migration. It is however possible that migration away from the neural tube cannot be initiated under the influence of repulsive cues alone. One theory is that NCCs migrate away from the neural tube in response to an attractive signalling cue. Many molecules have been suggested to act as early NCC attractants, but none are conclusively linked to NCC migration *in vivo* at all NCC axial levels. One such molecule is stromal cell derived factor 1 (Sdf1), which is important in cranial NCC migration.

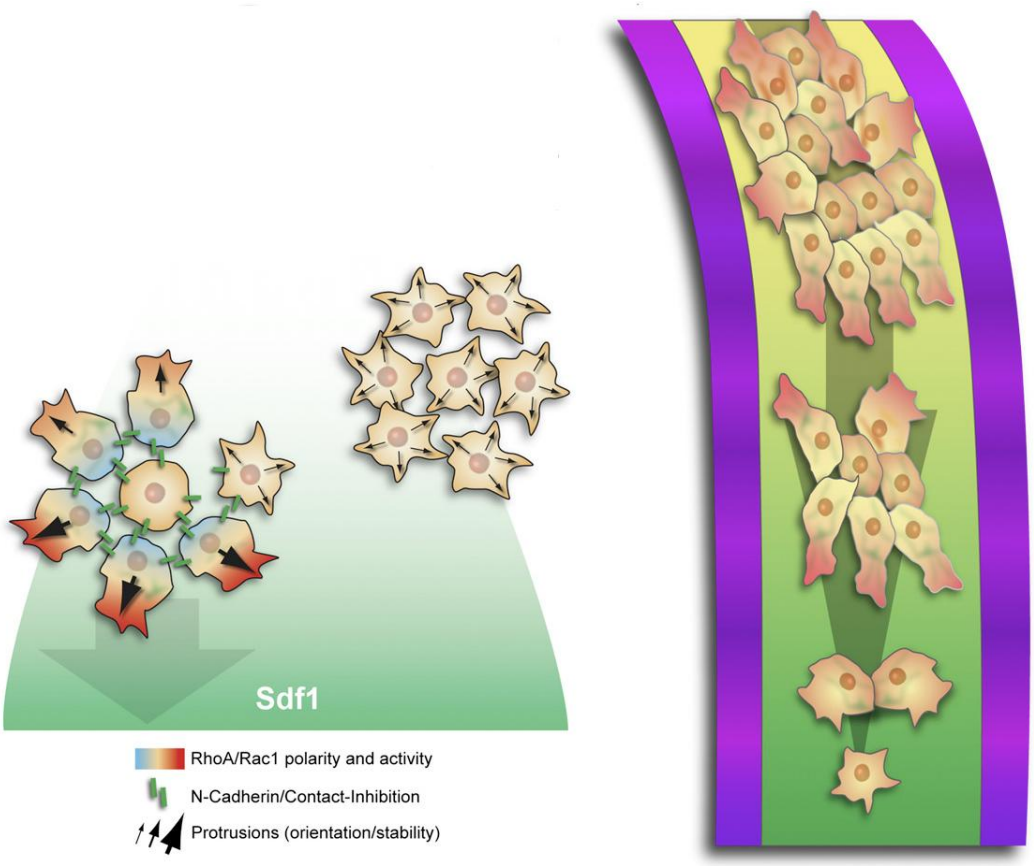

Figure 1.13 Contact repulsion and chemoattraction in NCC migration. Contact repulsion prevents NCCs producing cell protusions towards each other, directing NCCs away from the main NCC mass. Sdf1 expressed in a gradient polarises NCC protusions away from the neural tube and hence induces chemotaxis away from the neural tube. From Theveneau et al. (2010).

Sdf1, a chemoattractive cytokine, is expressed in the head during cranial neural crest migration in zebrafish, and appears to attract NCCs away from the neural tube along their migration streams in the branchial arches (Olesnicky Killian et al., 2009; Theveneau et al., 2010) (Figure 1.13). When Sdf1 signalling is blocked, NCC migration away from the neural tube does not initiate (Theveneau et al., 2010). The Sdf1 receptor CXCR4 is necessary for normal cranial NCC migration (Olesnicky Killian et al., 2009) and for ventral NCC migration to the sympathetic ganglia (Kasemeier-Kulesa et al., 2010). Although Sdf1 may initiate NCC migration out of the neural tube, research into the mechanics of early NCC migration dynamics is ongoing.

Repulsive cell-cell contacts are also important in shaping the pathway of NCC migration. Observation of fibroblast behaviour gave rise to the idea of contact inhibition of cell movement (Abercrombie and Heaysman, 1953). This contact inhibition or contact repulsion model could explain the partial dispersion of NCCs following their delamination from the neural tube. Work from the Mayor group (Carmona-Fontaine et al., 2008) has recently added to the contact repulsion model of early neural crest migration. In this model, repulsion between migrating NCCs drives them away from the neural tube, where they are high in number, towards peripheral tissues where they are sparser (Figure 1.13). Surrounding repulsion from adjacent tissues helps to enforce directed NCC migration in early neural crest migratory streams.

1.6.5 Migration of NCCs along permissive pathways

NCCs may be guided by diffusible guidance cues, but they may also undertake directed migration along a previously laid-down permissive pathway that constrains their migration. The extracellular matrix (ECM) has an established role in NCC guidance along these pathways, as reviewed in Henderson and Copp (1997); Perris and Perissinotto (2000). NCC migration occurs along pathways expressing permissive ECM components including fibronectin (Newgreen and Thiery, 1980), laminins (Perris et al., 1996), tenascin (also called cytotaxin) (Halfter et al., 1989) and heparan sulfate proteoglycans (Bronner-Fraser, 1993). Migrating NCCs are less able to progress in ECM containing nonpermissive aggrecan (Perissinotto et al., 2000), versican (Dutt et al., 2006), or Collagen IX (Ring et al., 1996). Tenascin is

permissive but in contrast to fibronectin promotes NCC detachment from the ECM, increasing the speed of NCC migration (Halfter et al., 1989). NCCs bind to fibronectin and laminin via cell surface receptors including integrins and laminin binding protein. Integrins are transmembrane glycoproteins that bind a range of ligands including fibronectin and laminin, and numerous integrin subtypes are expressed on NCC (Previtali et al., 2001). Permissive fibronectin, laminin and Collagen I and IV isoforms (Perris et al., 1993) are expressed in ECM that forms the NCC migration pathways and are suggested to be permissive for NCC migration (Perris and Perissinotto, 2000). Since fibronectin and laminin are also expressed outside the NCC migratory pathway (Rickmann et al., 1985), nonpermissive ECM components and repulsive cues are thought to be most instrumental in shaping NCC migration pathways. Fibronectin (Lefcort et al., 1992) and laminin (Ratcliffe et al., 2008) can also guide peripheral nerve axons during development. Directed migration of NCCs along fibronectin is enabled by syndecan-4 signalling (Matthews et al., 2008) and non-canonical Wnt signalling (De Calisto et al., 2005), which act on the cytoskeletal regulators Rac and RhoA, respectively, to polarise migrating NCC.

The use of developing blood vessels as a scaffold for vagal NCC migration has been suggested in the formation of the enteric nervous system (Nagy et al., 2009). Blood vessel formation and early trunk neural crest migration to the site of sympathetic ganglia are both guided by semaphorin signalling through neuropilin1 (Nrp1) (Fantin et al., 2009).This raises the possibility that NCC migration can be guided by spatially restricted ‘tracks’ of a pre-existing migratory substrate on an already patterned structure such as a blood vessel or endothelial tubule.

Non-permissive ECM components include the chondroitin sulphate proteoglycans, aggrecan and versican. Chondroitin sulphate proteoglycans are expressed in the posterior sclerotome and are necessary for NCC migration stream segmentation in the mouse (Kubota et al., 1999). Versican isoforms are expressed in barrier tissues that impede NCC migration during embryonic trunk development (Landolt et al., 1995) and versican overexpression in the *Pax3* mouse mutant *Splotch* prevents neural crest migration (Henderson et al., 1997). NCC interactions with the ECM are important in late as well as early NCC migration, for example in the enteric ECM (Rauch and Schafer, 2003) as shown by the necessity for integrins in NCC migration

in the gut (Breau et al., 2006). Integrins are cell surface molecules which mediate NCC adhesion to fibronectin in the extracellular matrix (Maschhoff and Baldwin, 2000). A deficiency in extracellular adhesion prevents NCC migration along the ECM, as the cells cannot gain traction without adhesion, and causes similar problems in gut colonisation to a deficiency in NCC guidance signalling molecules in the gut. When beta1 integrins are removed from NCCs, NCCs cannot colonise the distal gut (Breau et al., 2006).

There is some evidence that the various pathways that control NCC migration, including cell adhesion, ECM components and attractive and repulsive signalling molecules, interact. Prevention of NCC migration by blocking integrin binding to fibronectin causes rapid N-cadherin–mediated NCC clustering (Monier-Gavelle and Duband, 1997). Ongoing modulation of NCC behaviour by external signalling also occurs. For example, BMP signalling increases cell adhesion in migrating enteric NCCs by promoting polysialic acid addition to neural cell adhesion molecule (Ncam1) on the NCC surface (Fu et al., 2006). Although secretion of serine protease by NCCs has been proposed to alter the ECM and thus NCC migration along the ECM (Henderson and Copp, 1997), it seems likely that the secreted protease is acting as a growth factor rather than affecting the ECM (Agrawal and Brauer, 1996).

Migration requires a delicate balance of cell adhesion and cell motility, and coordinated interplay between cell–cell and cell–substratum adhesion. Cell processes must adhere to the ECM and surrounding cells in order to generate traction, but they also need to detach in order for the cell to move forward. At the end of migration, upregulation of cell-cell adhesion molecules such as cadherins is a common mechanism by which NCCs cease migrating, and they can play a role in neural crest-derived ganglion formation (Newgreen and Tan, 1993) by slowing cell migration and linking neural crest-derived neurons into ganglia (Fu et al., 2006).

There are numerous guidance cues involved in NCC migration in different regions of the embryo, some of which are discussed in the following section. As mentioned in section 1.4.4 above, vagal NCCs give rise to neurons and glia that comprise the enteric nervous system in the gut as well as intrinsic neurons within the lung (Burns and Delalande, 2005). Although the guidance cues that attract NCCs from the gut

into the lung are unknown, the guidance cues that attract NCCs into and along the gut to form the ENS have been well studied in recent years (Amiel et al., 2008; Burns and Thapar, 2006) (see section 1.7). It is reasonable to hypothesise that some of the signalling molecules involved in formation of the ENS may also be involved in the formation of the intrinsic pulmonary innervation, considering that their precursor cells have the same vagal neural crest origin.

1.7 Genetics of neural crest cells and neurocristopathies

In this section a number of key genes in neural crest development are described, looking at their roles in normal migration and the NCC defects caused when they are mutated (Table 1.2). Many genes are involved in different roles in NCC development, migration and survival. Mutations in genes coding for NCC signalling molecules or receptors, or transcription factors, can cause neurocristopathies through their effect on NCC migration, survival or differentiation. Non-NCC-autonomous mutations can also cause neurocristopathies if they occur in genes necessary for the development of NCC migratory scaffolding, as in *Tbx1* mutation, discussed below. Neurocristopathies are a heterogeneous group of disorders which all result from deficiencies in neural crest development (Bolande, 1997). Neurocristopathies may affect many different tissues or be restricted to a single organ depending upon the nature and localisation of the NCC defect. A disorder in a local guidance cue will cause a local defect in NCC migration, while a disorder in NCC formation may affect many different neural crest-derived tissues.

As the NCCs that migrate into the lung are a subset of those that migrate into the gut, this section outlines genes and neurocristopathies that are linked to the neural crest-derived intrinsic nervous system of the gut, or that are implicated in potential lung innervation disorders. In the neurocristopathy Hirschsprung's disease, disruption of NCC signalling pathways or early NCC death mean that NCCs fail to colonise part of the distal gut. The length of the aganglionic region varies depending on the causative mutation and genetic background. Mutations in any of several genes, including *RET*, *EDNRB* and *SOX10* can cause Hirschsprung's disease of varying degrees of severity.

Molecule	Role	Role in NCC development	Chosen for investigation because:
RET	Receptor	NCC guidance along gut	Enteric NCC guidance molecule. Mutated in gut innervation disorder Hirschsprung's disease and related respiratory disorder Haddad syndrome.
GFRa1	Co-receptor	NCC guidance along gut	Enteric NCC guidance molecule.
GDNF	Ligand	NCC guidance along gut	Enteric NCC guidance molecule.
Phox2b	Transcription factor	Necessary for the development of neural crest-derived peripheral autonomic innervation	Mutations cause central congenital hypoventilation syndrome (CCHS).
Sox10	Transcription factor	Necessary for early NCC specification and survival	Mutations cause cell-autonomous NCC defects including gut aganglionosis.
Tbx1	Transcription factor	Necessary for development of pharyngeal arch structures and NCC migration within them	Mutations cause non-autonomous NCC defects and vagal nerve hypoplasia.
DCC	Receptor	Guides lateral migration of NCC from gut into pancreas	Lateral NCC migration into pancreas is analogous to lateral NCC migration into lung.
Neogenin	Receptor	Receptor for netrin	Expressed in the embryonic mouse lung.
Netrin	Ligand	Guides lateral migration of NCC from gut into pancreas	Lateral NCC migration into pancreas is analogous to lateral NCC migration into lung.
Nrp1	Receptor	Receptor for repulsive semaphorin, which guides NCC into the posterior sclerotome.	NCC guidance molecule.
Chd7	Chromatin remodelling protein	Involved in early NCC specification	Mutations cause non-autonomous NCC defects.

Table 1.2 Signalling molecules involved in NCC migration. The role of candidate molecules in NCC migration into the lung and intrinsic pulmonary neuron differentiation can be investigated using mouse mutants and chemoattractant assays in cultured lungs. Signalling molecules in **bold** are in the RET signalling pathway and those underlined are in the DCC pathway.

1.7.1 The RET signalling pathway, Hirschsprung's disease and Haddad Syndrome

One of the most important signalling pathways in enteric NCC guidance is the RET signalling pathway (Manie et al., 2001). The tyrosine kinase transmembrane receptor REarranged during Transfection (RET) and co-receptor GDNF family receptor alpha 1 (GFRa1) are expressed in foregut NCCs and in lung NCCs in the chick (Burns and Delalande, 2005). The RET ligand Glial cell line-Derived Neurotrophic Factor (GDNF) is expressed in the gut mesenchyme and is thought to attract enteric NCC from the foregut towards the stomach, guiding NCCs along the gut in a rostral to caudal direction. GDNF is expressed in the gut mesentery in a dynamic pattern consistent with enteric NCC migration patterns (Natarajan et al., 2002) and attracts enteric NCCs in organotypic gut culture (Yan et al., 2004; Young et al., 2001). RET is required for the directed migration of NCC along the gut, as *Ret* mutant mice have NCC migration defects in the gut (Natarajan et al., 2002; Yan et al., 2004). RET can act as a receptor for the ligands artemin (ART), persephin (PSP), and nurturin (NTN) as well as GDNF (Figure 1.14). Ligand binding specificity is conferred by the presence of different GDNF family receptor alpha co-receptors which act in concert with RET. GDNF preferentially binds to GFRa1 forming a complex that can bind with RET and promote its dimerisation (Jing et al., 1996).

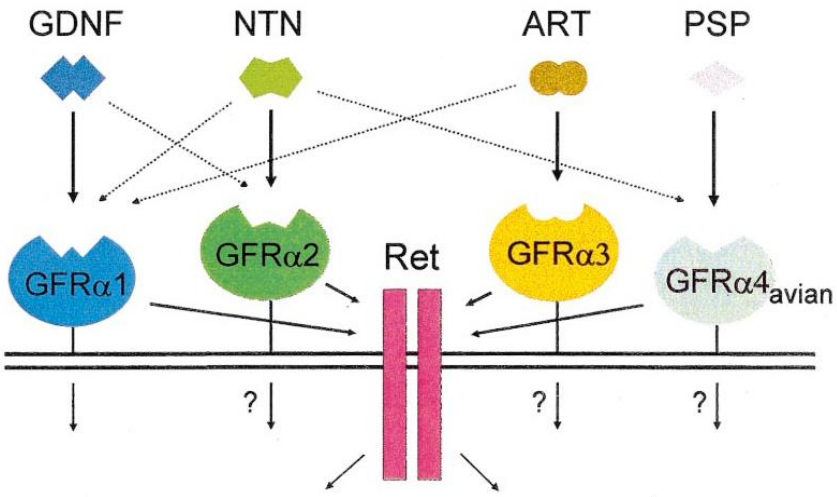

Figure 1.14 The RET receptor and GFRa family of co-receptors. All the GDNF family ligands (GDNF, NTN, ART, and PSP) activate the transmembrane RET receptor via different glycosyl phosphatidylinositol-linked GFRa receptors. Thick lines represent preferred ligand binding, but some cross-reactivity occurs *in vitro*, shown by dotted lines. GFRa4 has been found in avians only. From Airaksinen et al. (1999).

RET and GFRa1 are both found in cholesterol-rich rafts within the cell membrane (Tansey et al., 2000). In the classical model of GDNF signalling, GDNF binds GFRa1, forming a complex before recruiting RET receptors to the cholesterol-rich rafts (Figure 1.15, a). The RET receptors dimerise around the GDNF-GFRa1 complex and their intracellular terminals are autophosphorylated (Jing et al., 1996). This phosphorylation of the RET intracellular tyrosine kinase domain activates intracellular signalling pathways, including the PI3 kinase, Ras/MAP kinase, PLC-gamma/Calcium ion and JNK pathways, as previously reviewed (Manie et al., 2001). In an alternative model for RET signalling, RET and GFRa1 may form a complex before binding GDNF (Eketjall et al., 1999) (Figure 1.15, b). Co-localisation in the lipid rafts may promote GDNF signalling by facilitating GFRa1 and RET binding. Soluble GFRa1 is present in some systems (Paratcha et al., 2001) and can bind GDNF and RET (Figure 1.15, c).

GFRa1 may also be capable of transducing GDNF signalling when RET is not present. This might be through interaction with NCAM, a transmembrane receptor that can transduce GDNF signals (Paratcha and Ledda, 2008), or through a RET and NCAM-independent mechanism (Pozas and Ibanez, 2005), which may be due to cooperation with another, undescribed receptor. It may also occur through GFRa1 clustering in the cell membrane under the influence of GDNF, as GDNF can bind to multiple GFRa1 molecules simultaneously. GFRa1 promotes the phosphorylation of Src kinase, which activates intracellular calcium signalling via IP3.

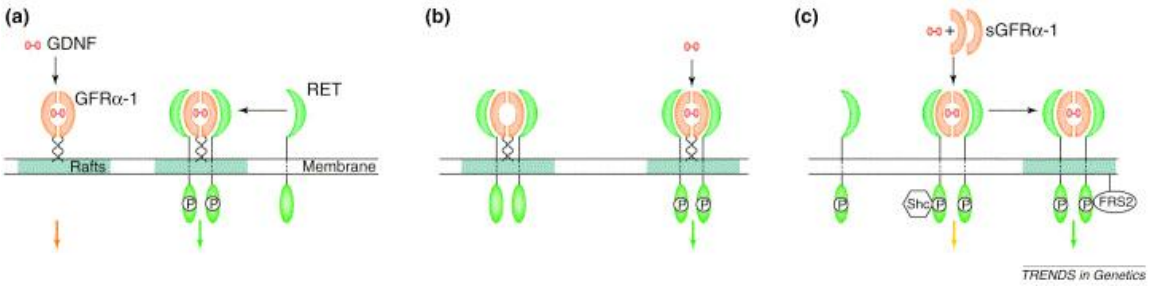

Figure 1.15 Models of GDNF signalling through RET and GFRa1 receptors. Soluble GDNF binds GFRa1, and the GDNF-GFRa1 complex can then activate RET signalling. (a) Dimerised GFRA1 in the membrane may first bind soluble GDNF, and then recruit 2 RET monomers. (b)The RET-GFRa1 complex may form before GDNF binds GFRa1. (c) Alternatively, if soluble GFRa1 is present, GFRa1 and GDNF may bind and only then, as a complex, bind to the transmembrane RET. From Manie et al. (2001).

RET mutations in humans are a strong risk factor for long segment Hirschsprung's disease (Parisi and Kapur, 2000), where NCC colonisation of the distal gut is severely affected and a long segment of distal bowel is aganglionic. In Hirschsprung's disease, enteric ganglia fail to form in a variably sized terminal gut region, due to failure of enteric NCCs to colonise the distal gut as reviewed in Burns and Thapar (2006). *Ret* mutant mice are used as an animal model for the processes underlying RET-associated Hirschsprung's disease, as they display a more severe form of the long segment intestinal aganglionosis seen in the human disease (Schuchardt et al., 1994). *Gfra1* mutant mice also lack enteric neurons in the gut distal to the stomach (Enomoto et al., 1998), although *GFRa1* mutations have not been linked to human disease as conclusively as mutations in *RET* (Angrist et al., 1998). These gut innervation defects are due to deficits in the RET pathway, probably due to its role in transducing guidance signals in enteric NCC, but possibly related to its role in promoting cell survival (Taraviras et al., 1999) or non-autonomously promoting NCC migration (Bogni et al., 2008).

In the human congenital disease Haddad syndrome, intestinal aganglionosis similar to that seen in Hirschsprung's disease is accompanied by respiratory problems similar to central congenital hypoventilation syndrome (CCHS) (Haddad et al., 1978; Verloes et al., 1993). Haddad syndrome is associated with mutations in *RET* (Amiel et al., 1998). RET is also important for the development of respiratory

carbon dioxide sensitivity (Burton et al., 1997), likely through a role in the development of brainstem or peripheral autonomic neurons.

1.7.2 Central congenital hypoventilation syndrome and Phox2b

In CCHS, respiration slows dramatically during sleep and does not speed up in response to hypoxia, causing suffocation. CCHS is primarily considered a disorder of central respiratory pattern generation and can cause death before the age of two years. Congenital abnormalities that impair lung function to a significant extent have high early mortality rates. Mutations in *PHOX2B* are strongly associated with CCHS in humans (Berry-Kravis et al., 2006; Weese-Mayer et al., 2009) and have a similar effect on respiration in mouse models (Amiel et al., 2003). There also exists a weaker association between CCHS and *RET* mutations, in which *RET* mutations increase the risk of intestinal aganglionosis when accompanying *PHOX2B* mutations (de Pontual et al., 2006). Phox2b regulates the downstream expression of *Ret* and *Gdnf* (Pattyn et al., 1999). Phox2b is a paired homeobox transcription factor present in neurons in the central and peripheral nervous system (Pattyn et al., 1997) and is necessary for the development of much of the autonomic nervous system, including neural crest-derived peripheral autonomic innervation and neural crest-derived intrinsic enteric neurons (Dauger et al., 2003; Pattyn et al., 1999). Phox2b is also important in the development of neurons in the brainstem that regulate ventilation in response to carbon dioxide levels (Onimaru et al., 2008).

In CCHS brainstem control of ventilation exhibits a reduced response to hypoxia. It is possible that a defect in oxygen sensing by NEBs or in transmission of information by airway ganglia could contribute to deficient brainstem control of ventilation. As well as defects in breathing control CCHS patients have deficiencies in autonomic function (Ogren et al., 2010), which may be central or peripheral. Although the non-neural crest-derived brainstem neurons involved in respiratory control that are affected by *PHOX2B* mutation have been studied in the context of CCHS, the role of neural crest-derived intrinsic lung innervation in CCHS has not been investigated to date.

1.7.3 Sox10 and Waardenburg Syndrome Type 1V

Sox10 is a member of the SoxE transcription factor gene family, expressed in delaminating and migrating NCC (Haldin and LaBonne, 2010). It regulates neural crest development, along with its earlier expressed relatives *Sox8* and *Sox9*, and maintains NCC pluripotency and survival (Stolt and Wegner, 2010). Sox10 promotes neurogenesis in autonomic lineages by switching on Mash1 (Kim et al., 2003). It also controls the transcription of a number of downstream PNS markers, including RET, which are important in the development of the neural crest-derived ENS, as reviewed in Sauka-Spengler and Bronner-Fraser (2008). Later in development it is involved in specification of neural crest-derived glia (Mollaaghababa and Pavan, 2003). *Sox10* loss-of-function mutation in a single allele produces defects in intrinsic ENS formation and skin pigmentation in mice (Southard-Smith et al., 1998). The decrease in numbers of neural crest-derived neurons in DRGs and ENS seen in many *Sox10* mutations has a number of possible causes, including early differentiation of proliferating precursors and cell death. The loss of one allele of *Sox10* leads to a smaller pool of ENS progenitors and hence a deficit in NCC-derived cell populations (Paratore et al., 2002). Sox10 has a role in maintaining the progenitor state of migrating NCC, allowing them to produce more progeny before differentiating (Kim et al., 2003). When it cannot fulfill this role, progenitor cells differentiate early.

Cell death is a consequence of some *Sox10* mutations. Loss of Sox10 function as a survival factor can be a direct cause of death of NCC, for example when Sox10 is necessary for NCCs to respond to the extrinsic diffusible ligand and survival factor neuregulin during migration (Paratore et al., 2001). Sox10 is also required for the maintenance of neural crest-derived ENS precursor cells (Bondurand et al., 2006). Indirect death of neural crest-derived neurons can also occur through loss of accompanying neural crest-derived glial cells (Stolt and Wegner, 2010), as Sox10 is required for glial fate acquisition in neural crest-derived glial lineages (Britsch et al., 2001).

There are several *Sox10* mutant mouse models, as reviewed in Kelsh (2006). In this investigation the Sox10 Dominant Megacolon (*Sox10Dom*) mouse was studied, as it has well-characterised defects in enteric nervous system development (Kapur, 1999;

Southard-Smith et al., 1998) (Figure 1.15). In the *Sox10Dom* mutation a single base pair is inserted into the *Sox10* open-reading frame, causing a frame shift. This leads to the generation of a mutant Sox10 protein. The *Sox10Dom* mutation is autosomal dominant with incomplete penetrance.

The *Sox10Dom* mutation affects skin pigmentation, and PNS and enteric ganglia formation. The *Sox10Dom* heterozygous mutant mouse has deficient NCC migration along the gut (Southard-Smith et al., 1998), producing a variable-length aganglionic distal bowel phenotype. This variation occurs because the *Sox10Dom* allele has a variably penetrant phenotype in heterozygotes, depending on the genetic background of the mutation (Hakami et al., 2006; Walters et al., 2010). Embryos homozygous for the mutation die before birth, usually before E15, and have complete intestinal aganglionosis. In the *Sox10Dom* mutant mouse strain, the loss of enteric innervation may be due to the role of Sox10 as a survival factor, as the *Sox10Dom* homozygous mutant mice have increased levels of early NCC death near the neural tube, preventing NCCs from reaching and colonising the gut (Kapur, 1999)(Figure 1.16). However, other studies have described the *Sox10Dom* mutation as decreasing apoptosis and preventing NCCs from undergoing EMT (Cossais et al., 2010). In both models, the decreased numbers of NCCs are thought to mean that the NCC-derived intrinsic innervation of the gut is reduced.

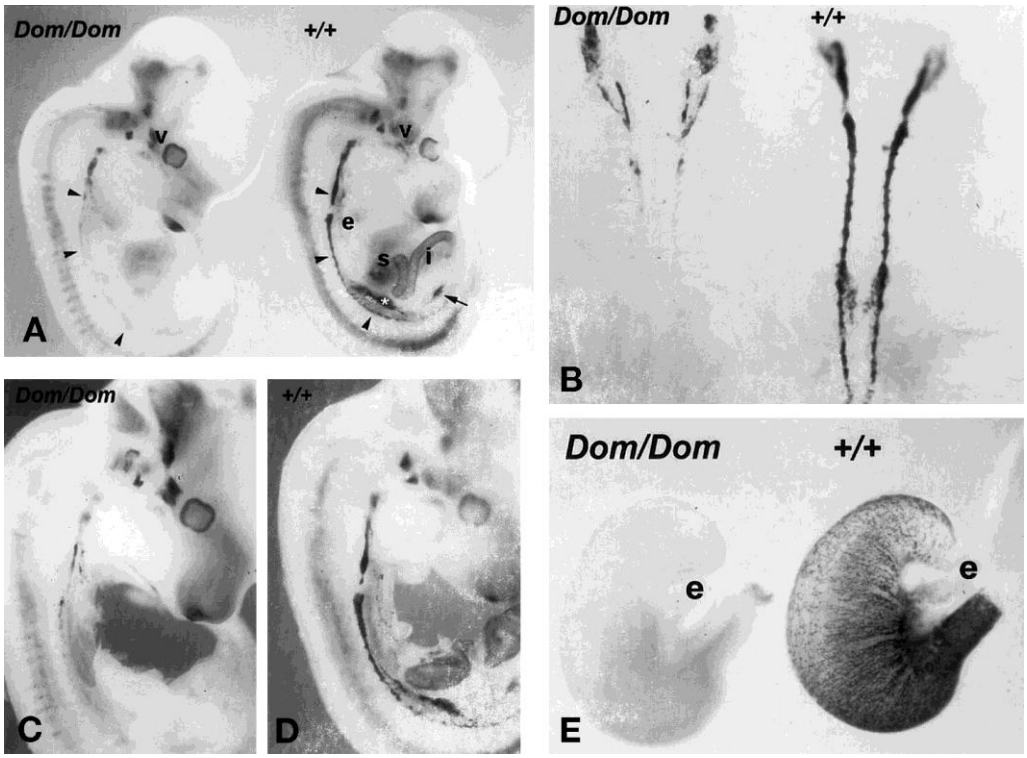

Figure 1.15 Characterisation of NCC defects in *Sox10Dom* mutant mice. In homozygous *Sox10Dom* mutant embryos, NCC are absent in the esophagus (e), stomach (s), and intestines (i). Innervation is also absent in the sympathetic ganglia (arrowheads), parasympathetic ganglia (arrow) and dorsomedial trigeminal ganglion (v). A: Intact embryos, B: Sympathetic ganglia and adjacent nodose ganglia, C and D: Embryos dissected to expose gut innervation. E: Stomach with esophagus. From Kapur et al. (1999).

Mutations in *SOX10* can cause neurocristopathies of varying severity. In Waardenburg Syndrome Type IV (WS-IV), patients have deficiencies in neural crest derived melanocytes, resulting in hypopigmentation, sensorineural hearing loss, and defects in enteric ganglia formation. Waardenburg syndrome type IV-C (OMIM ID 613266), also called Waardenburg-Shah syndrome, is caused by heterozygous *SOX10* mutation. WS-IV-A (OMIM 277580) and B (OMIM 613265) have similar features but are caused by *EDNRB* and *EDN-3* mutations respectively. Defects in glial cells causing hypomyelination, resulting in neuropathy, are sometimes later consequences of *SOX10* mutation and when accompanying the symptoms of WS-IV are part of PCWH (Peripheral demyelinating neuropathy, central dysmyelinating leukodystrophy, Waardenburg syndrome and Hirschsprung disease) (OMIM ID 609136) (Inoue et al., 2004). No respiratory symptoms have been described in WS-IV patients.

WS-IV-C is associated with haploinsufficient *SOX10* mutations, while PCWH is caused by dominant-negative *SOX10* mutations, indicating a difference in severity of mutation effect (Stolt and Wegner, 2010). The *Sox10Dom* mutation used as a mouse model for WS-IV (Hakami et al., 2006), (Hong and Saint-Jeannet, 2005) may be dominant-negative or haploinsufficient, as it has significant phenotypic effects when only one allele carries the mutation. Most truncated *Sox10* mutants show reduced transcriptional activity and a dominant-negative effect (Inoue et al., 2004).

1.7.4 Tbx1 and DiGeorge Syndrome

Tbx1 is a member of the T-box transcription factor family. It is necessary for the normal development of the NCC-derived pharyngeal arch structures and for the migration of cardiac NCCs within the arches (Lindsay et al., 2001). Tbx1 is necessary for the expression of the transcription factor Gbx2 which is necessary for the release of an unknown guidance factor from the pharyngeal arches that guides cardiac NCCs towards the heart (Calmont et al., 2009). Such non-cell-autonomous gene mutations can therefore disrupt NCC migration if they disrupt extrinsic factors or structures required for NCC migration. *Tbx1* is expressed in the pharyngeal arch mesenchyme and in the developing lung epithelium (Chapman et al., 1996).

DiGeorge syndrome, also called velocardiofacial syndrome, results from a heterozygous deletion in chromosome 22q11 (Epstein, 2001). The *TBX1* locus is within this region. Characteristics are highly variable and may include congenital heart defects, palate defects, craniofacial abnormalities and learning disabilities, most of which appear to stem from problems in pharyngeal arch development. Laryngotracheal abnormalities are observed in a proportion of patients, including tracheoesophageal fistulae, shortened trachea, missing or softened cartilage in the upper airways and tracheal bronchus, or blind-ending bronchus. These factors can cause restrictive lung disease, where the amount of air that can be inhaled is physically restricted (Huang and Shapiro, 2000). *Tbx1* heterozygous mutant mice show most aspects of the DiGeorge syndrome phenotype, most notably defects in cardiac outflow tract development (Jerome and Papaioannou, 2001; Lindsay et al., 2001). The role of Tbx1 in neural crest migration, particularly in cardiac neural crest migration, has been linked to DiGeorge syndrome (Kochilas et al., 2002).

Tbx1 mouse mutants display disruption of cranial nerve ganglia and migration (Vitelli et al., 2002) and homozygous *Tbx1* mutants have recently been shown to have decreased extrinsic vagal innervation of the stomach (Calmont et al., 2011). It has been hypothesised that NCCs migrate along the vagal nerve in order to populate the gut and lung, but in *Tbx1* mutants with hypoplasia of the vagal nerve intrinsic gut innervation appears to be normal. This indicates that NCCs in the gut do not require vagal nerve innervation within the gut to migrate and differentiate appropriately. The effect of homozygous *Tbx1* mutation on the development of the vagal nerve is interesting when considering the interaction between intrinsic NCC-derived lung neurons and extrinsic lung innervation from the vagal nerve. It is thus possible that Tbx1 may be involved in the guidance of NCCs or extrinsic innervation into the lung.

1.7.5 Other genes involved in NCC migration and development

NCCs migrate rostro-caudally along the length of the gut, guided by the chemoattractive ligand GDNF. Enteric NCC also undergo other modes of migration under the influence of different signalling cues in order to form a functional enteric nervous system. Deleted in Colorectal Cancer (DCC) is a receptor for netrin (Moore et al., 2007) and is expressed on enteric NCCs (Jiang et al., 2003), while netrin is expressed in the submucosal and pancreas (Jiang et al., 2003). *DCC* mutant mice have defects in NCC colonisation of the submucosa and pancreas, and cultured enteric NCCs migrate towards sources of netrin (Jiang et al., 2003). This indicates that a subset of NCCs in the gut mesenchyme migrate tangentially towards the gut lumen into the submucosa under the influence of the diffusible ligand netrin. Netrin attracts DCC-expressing enteric NCCs out of the gut and into the endoderm-derived pancreas (Jiang et al., 2003) in a tangential migration process analogous to the tangential migration of gut NCCs into the lung buds. The receptor neogenin is closely homologous to DCC but binds netrin more weakly. At E14.5 in the mouse neogenin is restricted to the mesenchyme of the developing lung (Fitzgerald et al., 2006), and has a role in lung mesenchyme development as a receptor for the growth-promoting netrin (Sun et al., 2011). The netrin/DCC/neogenin signalling pathway is thus a candidate for guiding NCCs into the lungs from the foregut, as the pathway guides NCCs into the pancreas from the foregut.

Other neural crest guidance molecules involved in NCC migration in the gut include Neuropilin1 (Nrp1), which is a co-receptor for several members of the semaphorin family of ligands that act as repulsive NCC guidance cues (Yazdani and Terman, 2006). Migrating NCCs express Nrp1 while the Nrp1 ligand Sema3A is expressed by the hindgut mesenchyme (Anderson et al., 2007). There is premature entry of sacral NCCs and extrinsic axons into the distal hindgut of fetal mice lacking Sema3A (Anderson et al., 2007), indicating that Sema3A expressed by the distal hindgut regulates the entry of sacral NCCs and extrinsic axons into the hindgut through its receptor Nrp1. It remains to be investigated whether Nrp1 regulates the migration of lung NCCs or extension of extrinsic innervation into the lung. Nrp1 is also important in the correct positioning of neural crest-derived sympathetic neurons in the sympathetic trunk, as Nrp1 transduces Sema3A signals that stop migrating NCC and cause them to aggregate in sympathetic chain ganglia. (Kawasaki et al., 2002).

Chd7 (chromatin helicase DNA binding domain 7) is a chromatin remodelling protein. By altering the chromatin packaging around genes it can alter patterns of gene expression. *Chd7* mutations are lethal early in development when homozygous and when heterozygous *CHD7* mutations are a cause of CHARGE syndrome (Coloboma of the eye, Heart defects, Atresia of the choanae, Retardation of growth and/or development, Genital and/or urinary abnormalities, and Ear abnormalities). Craniofacial abnormalities and PNS abnormalities have been reported in CHARGE syndrome patients. These features in particular have led to examination of the role of neural crest defects in the development of CHARGE syndrome, and the role of Chd7 in NCC development. Chd7 has been implicated in the activation of early neural crest transcriptional circuitry (Bajpai et al., 2010). *Tbx1* and the CHARGE-related gene *Chd7* are both necessary for blood vessel development, and mutations in the two genes have similar effects on artery development (Randall et al., 2009). DiGeorge syndrome and CHARGE syndrome appear to be developmentally related, often co-occurring (Huang and Shapiro, 2000). Chd7 has a part in the early neural crest cell development pathway. Investigation of this gene allows investigation of the effects of a non-signalling molecule, non-transcription factor gene in neural crest-derived intrinsic lung innervation.

1.8 Research Aims and Objectives

The development and role of the intrinsic lung innervation is an area that has received relatively little attention in the literature and there are many questions that are yet to be fully addressed. For example, although intrinsic lung neurons have been shown to be neural crest-derived in the chick embryo, and are likely to have the same origin in mammals, the spatiotemporal migration of NCC into the mammalian lung is incompletely described and the signalling mechanisms that guide NCC to final lung ganglion positions are not known. Intrinsic lung neurons are known to regulate or be involved in the regulation of important aspects of postnatal respiratory function such as bronchoconstriction, but their precise role in the regulation of targets of lung innervation such as ASM during embryonic development is unclear. In addition, the interactions between the development of intrinsic lung innervation and lung morphogenesis are incompletely described and could potentially be disrupted in congenital respiratory disorders in humans. NCC dysfunction is a well-established cause of many clinical syndromes, known as neurocristopathies, but the development of these cells has not been fully investigated in the context of congenital respiratory disorders. Thus a better understanding of the development of intrinsic lung innervation will not only help address some of these questions, but may also give insight to the mechanisms underlying congenital respiratory disorders in humans.

The overall aim of this PhD project was to investigate the mechanisms underlying the development of the neural crest-derived intrinsic innervation of the lung.

Objectives:

- Describe the spatiotemporal colonisation of the mammalian lung by NCC using *Wnt1Cre:Rosa26YFP* reporter mice.
- Determine whether NCC are prespecified to colonise the lung using chick intraspecies grafting to label and fate map NCC.
- Investigate signalling mechanisms involved in the guidance of NCC from the gut into the lung using organotypic lung culture and analysis of mutant mouse embryos.

2. Materials and Methods

2.1 Generation of mouse embryos

Wnt1Cre:Rosa26YFP mouse embryos were generated by crossing *Wnt1Cre* mice with homozygous floxed *Rosa26STOPYFP* mice on a C57B6 background as described (Danielian et al., 1998; Jiang et al., 2000; Srinivas et al., 2001). The day after mating, when the plug was confirmed, was taken as embryonic day (E) 0.5. Mice were killed by Schedule 1 methods in accordance with Home Office regulations.

Mutant mice were obtained from various sources. E14.5 *Sox10Dom* mutant embryos and littermates were obtained from Dr Wood Yee Chan at the Chinese University of Hong Kong; *Ret* mutant embryos and littermates were obtained from Dr Hideki Enomoto at the RIKEN Center for Developmental Biology, Japan; additional *Ret* and and *Gfra1* mutant mice were supplied by Dr Vassilis Pachnis at MRC National Institute for Medical Research, Mill Hill, UK; *Dcc* mutant embryos and littermates were obtained from Dr Elyanne Ratcliffe at McMaster University, Canada. Lungs from E14.5 *Tbx1* mutant mice and *Chd7* heterozygous mutants were obtained with littermate controls from Dr Peter Scambler at the UCL Institute of Child Health.

2.1.1 Preparation of mouse embryos

Pregnant mice were killed by Schedule 1 methods and dissected. The uterine tube was removed and immersed in ice cold phosphate-buffered saline (PBS) and the embryos were then dissected out of their membranes. Intact embryos, or dissected lungs (if embryos were older than E14.5), were then fixed in 4% paraformaldehyde (PFA) at 4°C for 1-3 hours depending on size. They were then washed for 15 minutes 3 times in 1xPBS. For cryopreservation, they were then stored in PBS/15% sucrose overnight before embedding in gelatine or OCT embedding medium and cryosectioning.

2.2 Transgenic mouse fate-mapping system

The *Wnt1Cre* and floxed *Rosa26STOPYFP* double transgenic system (Figure 2.1) allowed the permanent marking of NCC and all their descendants. The NCC marker gene *Wnt1* is transiently expressed in NCC and the dorsal neural tube early in NCC

development before their delamination (Echelard et al., 1994). The *Wnt1Cre* transgenic complex, in which the *Cre* gene is expressed under the control of the *Wnt1* promoter, causes the expression of the bacterial enzyme Cre recombinase in cells where *Wnt1* is expressed (Danielian et al., 1998). Cre recombinase excises the DNA between two lox sites. As the Cre-lox system is bacterial, Cre recombinase present in a normal mammalian cell will not cut DNA, because no lox sites should be present.

A second transgenic complex, *Rosa26STOPYFP*, is inactive unless Cre recombinase is present (Srinivas et al., 2001). It contains a universal Rosa26 promoter site and the gene for YFP (yellow fluorescent protein), separated by a floxed STOP sequence that prevents *YFP* transcription. If Cre recombinase is present, it excises the *Rosa26STOPYFP* transgene at the two lox sites either side of the STOP sequence, permanently removing it from the transgene. This allows *YFP* to be transcribed and expressed. Because the removal of the floxed STOP site is irreversible, the cell will continue to express *YFP* after *Wnt1* expression and Cre expression end. All the descendants of that cell will also carry the modified Rosa26YFP transgene and so will express *YFP* (Srinivas et al., 2001).

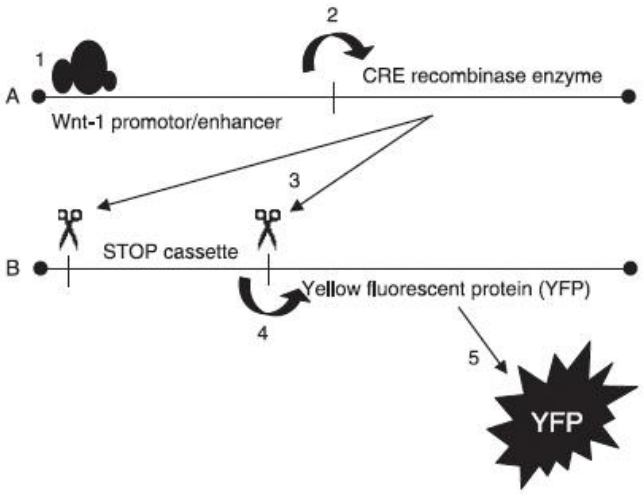

Figure 2.1 *Wnt1Cre:Rosa26YFP* double transgenic system for cell tracking. Lox sites are indicated by scissor icons. Transcription machinery binds at *Wnt1* promoter site (1) and transcribes *Cre* (2). Cre then excises the STOP sequence (3), allowing transcription of *YFP* (4). YFP is then expressed in the cell, even if Cre production stops (5).From Cassiman et al. (2006)

2.3 Genotyping *Wnt1Cre:Rosa26YFP* mice

Earclips were taken and frozen at -20°C until required. The earclips were immersed in 200µl tail lysis buffer (50mM Tris pH8, 5mM EDTA, 100 mM NaCl, 0.5% SDS,) with 10µl Proteinase K at 55°C overnight to break up the tissue. The next morning

the sample was centrifuged at 13K for 5 minutes to pellet the tissue. The DNA-containing supernatant was removed to a fresh tube and 90µl saturated NaCl solution added to each tube. The tube was vortexed to thoroughly mix the solutions, put on ice for 20 minutes, then centrifuged at 13K for 20 minutes. The supernatant was removed to a fresh tube containing 1ml 100% ethanol, and mixed by repeated inversion. At this point white feathery DNA became visible. The DNA was pelleted by centrifugation at 13K for 20 minutes, and the supernatant removed. The pellet was allowed to air dry before resuspending in 100µl TE buffer. PCR was run on the samples, using primers to amplify a region of the Cre locus. The PCR product was then put through gel electrophoresis in a 1.5% agarose gel. Presence of the Cre locus was confirmed by observation of a ~500MW DNA band in the gel.

Cre primer sequences: **Forward** accctgatcctggcaatttcgg
Reverse gatgcaacgagtgatgaggttc

2.4 Generation of chicken embryos

Fertilised chicken eggs were obtained from a commercial supplier and kept at 15□C until incubation. To commence development, eggs were placed in a forced air incubator, with constant humidity, at 37°C until harvesting. Fertilised eggs from a chicken strain that ubiquitously expresses green fluorescent protein (GFP) (McGrew et al., 2004; McGrew et al., 2008) were supplied by Prof. Helen Sang from the Roslin Institute and Royal Dick School of Veterinary Studies, University of Edinburgh, UK, and were incubated as above.

2.5 Source of human embryonic tissue

Human embryonic tissue was obtained from the Human Developmental Biology Resource (HDBR) at the UCL Institute of Child Health.

2.6 Neural tube grafting and back-grafting

GFP eggs from the Roslin Institute (described in section 2.5 above) and wild-type eggs were incubated until E1.5, then windowed to gain access to the embryo. Indian ink at 1:1 in PBS with 1:100 penicillin-streptomycin was injected beneath the surface of the yolk membrane using a mouth pipette, to allow better visualisation of the embryo. The vitelline membrane covering the embryo was then removed. In the wild type eggs, a microscalpel was used to ablate the vagal neural tube (NT) and

associated neural crest at the 10-12 somite stage (Figure 2.2, A). The NT was cut transversely at the levels of the 1st and 7th somite and then along its sides. Once detached from the embryo the NT was removed from the egg using a mouth pipette and discarded. To provide a stage-matched GFP NT for grafting, GFP embryos at the 10-12 somite stage were cut from the surrounding membrane *in ovo* with dissecting scissors. A dissecting spoon was used to move the GFP embryo from its egg into a dissecting dish of PBS containing 1% penicillin-streptomycin. The embryo was pinned out and dissecting scissors used to remove the NT between the 1st and 7th somites. The roughly dissected NT was put into 2% pancreatin-PBS solution for 15 minutes to break up the connective tissue, then separated from the somites/notochord using dissecting needles. The NT was then transferred to DMEM medium to prevent further pancreatin activity until transplantation. The GFP-positive NT was then transferred into a wild type host embryo that had undergone NT ablation (Figure 2.2, B) and the stage of the host and level of graft noted. Each graft was given an ID number. The host egg was then sealed with sellotape and put back in the 37°C incubator until harvesting.

For NCC back-grafting (Figure 2.2, C), the chimeric embryo that had received a NT from a GFP embryo was harvested at E5.5 and the gut and lungs dissected out. Under a fluorescent dissecting stereomicroscope, small pieces of gut and lung containing a high density of GFP-positive NCC were cut out and placed in DMEM medium. E1.5 wild-type host embryos were prepared for back-grafting by vagal neural tube ablation, described above. A piece of gut or lung from the chimeric donor was placed onto the ablated region of the neural tube. The egg was then sealed, returned to the incubator, and harvested at the desired embryonic stage. The gut and lungs were dissected out, pinned and fixed in 4% PFA for 1-2 hours, then further analysed.

2.7 GFP cell isolation for back-transplantation using FACS

As an alternative to transplanting segments of chimeric lung or gut into the neural tube region, GFP-positive cells from these tissues were isolated, cultured and transplanted. To do this, GFP cells were separated from the surrounding tissue using fluorescence-activated cell sorting (FACS). Lung lobes were minced in PBS 1% penicillin/streptomycin and transferred to a 50ml Falcon tube, then centrifuged at

1000rpm. The supernatant was removed and the lung tissue resuspended in 2ml Enzyme mix (Collagenase XI, Dispase II, 1% Penicillin/Streptomycin). The tissue was digested in enzyme mix for 20 minutes at 37°C to remove connective tissue. The action of the enzymes was aided by vigorous pipetting of the tissue suspension every 5 minutes. The enzyme mix was inactivated by the addition of culture medium (DMEM, N2, B27, Penicillin/Streptomycin) 1:1 with the existing suspension, and the mixture centrifuged for 5 minutes at 1000rpm. The supernatant was removed and the pellet of separated cells resuspended in 1ml culture medium, then passed through a 100μm cell strainer. The cells were then centrifuged again and the remaining pellet resuspended in 500μl medium. The suspension was transferred to FACS tubes and transferred on ice for sorting. Cell sorting was performed using a MoFlo XDP (Beckman Coulter) with Summit software. After FACS, the positive fraction was processed. The cells were pelleted by centrifuging for 5 minutes at 1000rpm and resuspended in medium at a high concentration. The suspension was then pipetted in 60μl drops upwards onto the underside of the lid of a Petri dish to form 'hanging drops'. Within these hanging drops of medium, cells collected together under the influence of gravity. The lid was placed on a Petri dish filled with 10ml DMEM 1% Pen/Strep to keep the air surrounding the droplets humid. The cells were then left overnight in a 37°C incubator. By the next morning the cells formed irregularly shaped aggregates 200-500μm across, which were then transplanted into the ablated neural tube region of E1.5 wild type host embryos. The host embryos were left to develop and processed as above.

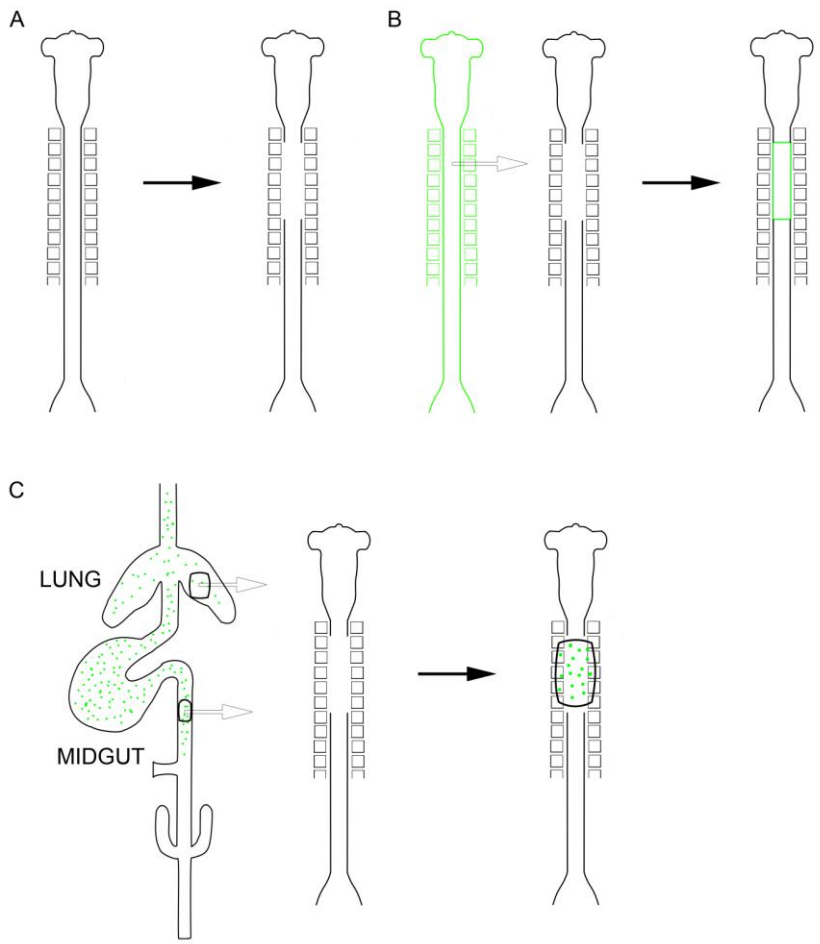

Figure 2.2 GFP neural tube grafting and backgrafting.
The vagal neural tube and associated neural crest of a wild-type chick was ablated at E1.5 (A) and the neural tube of an E1.5 GFP chick transplanted in its place (B). The chimeric embryo was allowed to develop to E5.5 and the lung and gut containing GFP NCC were harvested, cut into small segments, and then transplanted into the ablated vagal neural tube region of an E1.5 wild-type embryo (C). This is referred to as back-grafting, as the GFP NCC were grafted into a wild-type host twice.

2.8 Lung culture

Under a tissue culture hood, 1ml of culture medium (DMEM, 10% Fetal Bovine Serum, 1% Penicillin/Streptomycin) was put into one well of a 6 well culture plate. A membrane insert was then placed on top of the medium. Lungs from E12.5-E14.5 mouse embryos, F1 human embryos and E6.5 chick embryos were harvested and washed in sterile PBS. At E13.5 and beyond, the lung lobes were separated from each other and cultured separately due to their size. They were gently transferred onto the membrane inserts using spatulas. A maximum of 5 lobes were placed on one insert. They were then incubated at 37°C in a 5% CO2 atmosphere for up to 5 days.

2.9 Lung culture with chemoattractant-permeated beads

Agarose beads impregnated with candidate chemoattractants were prepared on the day of lung harvest. Agarose beads stored in sodium azide were washed in PBS 8

times for 15 minutes each time. For GDNF experiments, 2µl of GDNF in a 0.51µg/µl solution was added to 2µl of beads in PBS and left in the fridge for at least 2 hours before use.

For BDNF beads, 2µl of BDNF in a 0.1µg/µl solution was added to 2µl of beads in PBS and left in the fridge or at room temperature for 2 hours before use. The beads were placed on the lung lobes using a mouth pipette and a hand-drawn glass needle, with 1-2 beads per lung lobe. For human fetal lung tissue, a rubber bulb attached to a hand-drawn glass needle was used in place of a mouth pipette due to safety concerns.

2.10 Time-lapse microscopy of cultured lungs

Culture plates containing lungs were imaged using a Zeiss Axiovert microscope in a 37°C chamber. Images of each lung were taken daily using Velocity software under bright field and fluorescent microscopy at x10 and x20 magnification. Videos were filmed using the same software.

2.11 Whole mount immunohistochemistry

Intact mouse embryos or dissected mouse or chick embryonic lungs were fixed in 4% PFA for 1-3 hours and then rinsed 3 times in PBS before a 1 hour wash at room temperature. Antibody blocking solution (10% Sheep serum, 1% Triton X-100 in PBS) was applied for 1 hour at room temperature. Samples were incubated overnight at 4°C in primary antibody diluted in antibody block. Antibody dilutions used are shown in Table 2.1. The next day, samples were washed in PBS for 1 hour and then incubated in secondary antibody diluted in block at room temperature for 4 hours. Samples were washed for 1 hour at room temperature before observation under a Leica MZFLIII dissecting fluorescent stereomicroscope or mounting under a coverslip in Vectashield HardSet mounting medium with DAPI. Fluorescent microscopy was carried out on an Axioskop Zeiss fluorescent microscope.

Antibody (raised in)	Source	Dilution
Activated caspase 3 (rabbit)	New England Biolabs	1:250
ChAT (goat)	Santa Cruz	1:50
CGRP (rabbit)	Sigma	1:1000
Endomucin (rat)	Santa Cruz	1:100
GFP (chicken)	Abcam	1:300
GFP (mouse)	Invitrogen	1:100
GFP (rabbit)	Invitrogen	1:250
HNK1 (mouse)	culture supernatant	1:5
S100 (rabbit)	Dako	1:600
SMA (mouse)	Dako	1:200
SMA (rabbit)	AMS biotechnology	1:100
Sox10 (goat)	Santa Cruz	1:200
TUJ1 (mouse)	Covance	1:500
TUJ1 (rabbit)	Covance	1:1000
VIP (rabbit)	AbD Serotec	1:50

Table 2.1 Primary antibodies used in immunohistochemistry.

Antibody	Source	Dilution
Goat anti-rabbit Alexa-488 conjugated	Invitrogen	1:500
Goat anti-rabbit Alexa-568 conjugated	Invitrogen	1:500
Goat anti-mouse Alexa-488 conjugated	Invitrogen	1:500
Goat anti-mouse Alexa-568 conjugated	Invitrogen	1:500
Donkey anti-rat Alexa-568 conjugated	Invitrogen	1:500
Donkey anti-goat Alexa-568 conjugated	Invitrogen	1:500
Goat anti-chicken Alexa-488 conjugated	Invitrogen	1:300

Table 2.2 Secondary antibodies used in immunohistochemistry.

2.12 Whole mount immunohistochemistry for OPT (Optical Projection Tomography)

Mouse embryos or dissected lungs were fixed in 4% PFA for 0.5 to 1.5 hours depending on size. They were then washed in TBST (0.14M NaCl, 2.7mM KCl, 0.025M Tris HCl pH7.5, 1% Triton X-100). Samples were incubated in antibody block (TBST, 10% Sheep Serum) overnight at 4°C on a roller. After blocking, primary antibody (as shown in Table 2.1) was applied and samples were incubated overnight at 4°C on a roller. Following antibody incubation, samples were washed for 30 minutes at room temperature six times in TBST volumes greater than 5ml, and then overnight in TBST at 4°C. Alexa-568 conjugated secondary antibody was diluted in block and applied overnight at room temperature, before washing as

before in TBST. To mount the samples, 1% low melting point (LMP) agarose was prepared and filtered to remove impurities. The samples were embedded in LMP agarose and cooled to 4°C. A square block with the specimen at its centre was cut and attached to a magnetic chuck using superglue. The block was then shaped into a tapered octagonal cuboid using a microtome blade. The chuck and agarose were dehydrated in methanol for three days, with methanol changed once a day. After dehydration the samples were cleared in benzyl alcohol benzyl benzoate (BABB) for several days. The samples were then scanned under UV and visible light using a BiOPTonics OPT scanner 3001 (from BiOPTontics Microscopy, MRC technology). Computer-generated images were reconstructed using proprietary NRecon software.
After scanning, samples could be retrieved by washing the agarose mount in methanol for several days to remove BABB, then rehydrating the sample in an ethanol-PBS series. Agarose was cut from around the sample. The sample and remaining agarose were incubated in 57°C sucrose to melt and remove the agarose. The lungs were then cleaned using fine forceps and stored in PBS. Fluorescent immunostaining was still visible in whole lungs after this procedure.

2.13 Gelatine embedding and cryosectioning

Samples stored in PBS sucrose were incubated in liquid gelatine (PBS, gelatine 7.5%, sucrose 15%) at 37°C for 30 minutes. Samples were then placed in Petri dishes filled with liquid gelatine and placed on ice, causing the gelatine to set from the bottom up. Samples were oriented using forceps as the gelatine set. Once set, excess gelatine was removed to leave the sample in a cube of gelatine. The cube was attached to a cork disc using OCT cryoembedding medium. The samples were then flash-frozen in pentane, cooled to -65°C using liquid nitrogen and then stored at -80□C until cryosectioning. For cryosectioning, 10-12um sections were cut using a Leica CM1900UV cryostat at -22°C and placed on SuperFrost Plus slides. After air drying slides were stored at -20°C.

2.14 Immunohistochemistry on frozen sections

Gelatine was removed by immersing the slides in PBS for 30 minutes at 37°C. For OCT cryosections, OCT was removed by a 5 minute wash in PBS with 0.1% Triton X. The rest of the procedure is identical to that for gelatine. Antibody block (1xPBS,

0.1% Triton X, 1% Bovine Serum Albumen, 0.15% glycine) was applied and the slides incubated in a humid chamber at room temperature for 20 minutes. Primary antibody was then applied and the slides coverslipped and incubated overnight at 4°C. The slides were then washed 3 times for 5 minutes in PBS, and fluorescent Alexa-conjugated secondary antibody applied. The slides were coverslipped and incubated for 2 hours at room temperature in the dark before undergoing a further 3 PBS washes of 5 minutes each. Sections were finally mounted in Vectashield HardSet mounting medium with DAPI.

2.15 Immunohistochemistry on wax sections from the Great Ormond Street Hospital human tissue archive

Slides were dewaxed in a 60°C oven for 5 minutes, then immersed in xylene for 5 minutes to remove wax. They were then washed twice in 100% ethanol and water before being left in PBS/10% hydrogen peroxide for 20 minutes. For antigen retrieval, slides were placed in citrate buffer with EDTA and boiled for 40 minutes in a pressure cooker, then placed under running water to cool. Primary antibody was diluted in PBS, applied to the cooled slides and left to incubate at room temperature in a humidified chamber for 3 hours. Slides were then rinsed briefly in PBS followed by 5 minutes in PBS-4%Tween. Antibody visualisation was carried out using the REAL EnVision kit for peroxidase/DAB chromogenic immunohistochemistry. Slides were briefly counterstained with haemotoxylin before dehydrating with an alcohol/xylene series and mounting with DPX.

2.16 RNA probe production for *in situ* hybridisation

Plasmids containing sequences from Sox10 and c-Ret were the kind gift of Dr Amelie Calmont at the UCL Institute of Child Health. Plasmids containing sequences from ChAT, VaChAT, DBH and TH were the kind gift of Prof. Hermann Rohrer at the Max Planck Institute for Brain Research, Frankfurt. DH5-alpha E.Coli competent cells were transformed with plasmids using 45 seconds of 42°C heatshock and incubated in LB broth with 1:500 ampicillin before plating on LB agar/ampicillin plates and incubating overnight at 37°C. Colonies were then picked from the plates and grown in LB/ampicillin broth. For midiprep plasmid recovery, 50ml of bacterial culture was prepared. Plasmids were harvested using the Quiagen

midi-prep kit and protocol. The plasmids were linearized, and transcription carried out with DIG-labelled nucleotides to produce RNA sense and anti-sense probes. Sense probes were used as negative controls. RNA product was then cleaned using Clontech Chromaspin-1000 DEPC-H20 columns. The cleaned probe was mixed with 40µl formamide and 1µl RNAsin and stored at -20°C. Samples of DNA and RNA were taken throughout probe production for analysis via gel electrophoresis and spectrophotometry.

2.17 RNA *In situ* hybridisation on cryosections

Specimens were cryoembedded and sectioned as previously described (2.7), using DEPC-treated sucrose and gelatine. Gelatine was removed by placing slides in 37°C DEPC-treated PBS for 30 minutes. Probe was diluted to 1µg/300µl in 65°C hybridisation buffer (50% formamide, 10% dextran sulphate, 5mM EDTA, 20mM Tris pH8, 10mM Dithiothreitol, 1x Denhardts solution, 0.05% yeast tRNA, 300mM NaCl). 300µl of probe-containing buffer was applied to each slide. Slides were covered with baked coverslips and incubated overnight at 65-70°C in a chamber humidified with 65°C wash buffer (50% formamide, 50% SSC). The next day, slides were washed in MABT (Maleic acid buffer pH7.5 with 1% Tween) twice for 5 minutes, then 65°C wash buffer twice for 30 minutes, then MABT twice for 5 minutes. Slides were then placed in a humid chamber and 500µl blocking solution applied to each (2% Roche blocking reagent, 10% heat-inactivated sheep serum in MABT) for 1 hour at room temperature. Anti-DIG AP-conjugated antibody from Roche was diluted 1/1500 in blocking solution and applied to slides, which were then coverslipped and incubated overnight at 4°C. The next day, slides were washed for 10 minutes in MABT 3 times, 2 minutes in pre-developing buffer (100mM Tris pH9.5, 100mM NaCl, 50mM $MgCl_2$) and then incubated at room temperature in the dark with developing buffer (5% PVA, 100mM Tris pH9.5, 100mM NaCl, 50mM $MgCl_2$) with NBT (4.5µl/ml) and BCIP (3.5µl/ml). After 1-8 hours, purple coloration developed in the labelled regions. Staining was stopped by washing the slides in running water. The slides were then air-dried, mounted with Vectamount and photographed.

3. Chapter 3: Development of the intrinsic innervation of the mouse lung

In order to examine the role of the neural crest in the formation of mammalian intrinsic lung innervation, a transgenic mouse system was used to fate-map neural crest cells (NCCs) in the developing foregut, trachea and lungs through several stages of development.

We used *Wnt1Cre:Rosa26YFP* (Wnt1Cre:YFP) mice to trace NCCs and map the fate of NCCs during embryonic development. These double transgenic mice express yellow fluorescent protein (YFP) in all NCCs and their progeny from E9.5, when *Wnt1* expression in NCCs begins. A detailed description of the transgenic constructs and their function in these mice can be found in the materials and methods chapter (section 2.1). *Wnt1Cre:Rosa26YFP* embryos develop normally and so can be used to track the pattern of NCC migration via the presence of the marker protein YFP. As neural crest-derived cells continue to express YFP after differentiation, the fate of NCCs in the lung can be traced by co-staining for YFP and markers of cell differentiation.

3.1 The spatiotemporal pattern of neural crest cell migration into the lung

During early lung bud growth, which occurs at E10.5-E11 in mouse, the lung buds form as outgrowths of the foregut. At E10.5, YFP-positive NCCs begin to migrate tangentially from the foregut mesenchyme, where they are present in large numbers, into the lung buds (Figure 3.1, A, B). NCCs are seen close to the trachea and bronchi, the earliest respiratory epithelial tubules at E10.5 (Figure 3.1, A, B) and E11.5 (Figure 3.1, C, D). As the proximal airways, the bronchi and bronchioles, develop within the lung buds they become colonised by NCCs (Figure 3.1, A-D). Over the next 3 days from E11.5 (Figure 3.1, C, D) to E13.5 (Figure 3.1, H-J), NCCs move into the distal lung and are seen adjacent to epithelial tubules (Figure 3.1, D, G, J) as the lobes of the lung (Figure 3.1, F, I) are formed and the future airways extend. NCCs are seen bilaterally next to epithelial tubules by E13.5 (Figure 3.1, H-J), when the lungs have substantially increased in size and lobe separation is more pronounced.

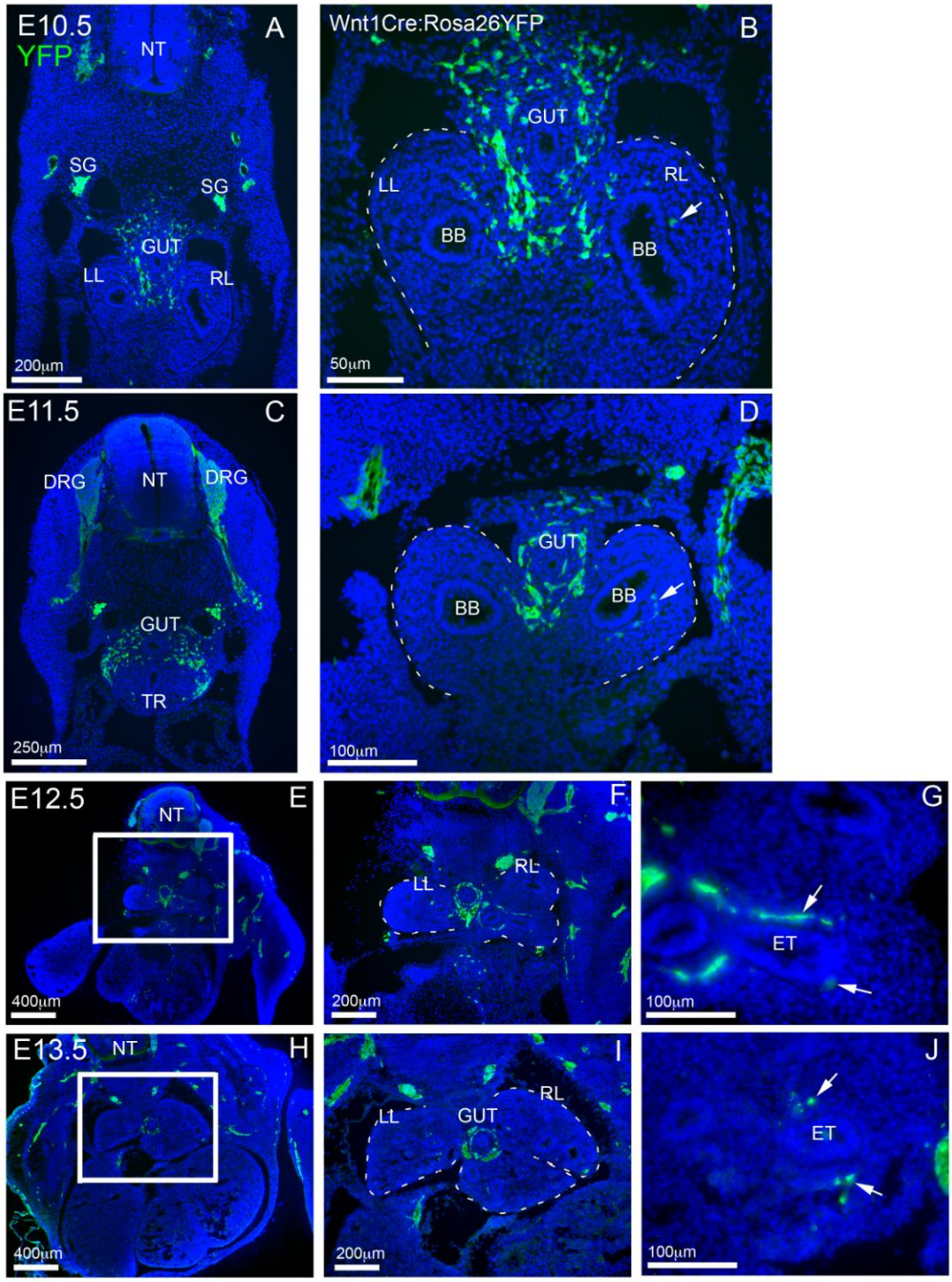

Figure 3.1 Series of *Wnt1Cre:Rosa26YFP* embryo cryosections from E10.5 to E13.5, immunostained for YFP (green). NCCs (arrows) migrate from the neural tube to the foregut and then into the lung. YFP-positive NCC migrate from the dorsal neural tube to the area around the foregut and from there tangentially into the lung buds, moving along airways to colonise the distal lung. F and I are the boxed areas in E and H, respectively. Dashed lines indicate lung boundary. BB: bronchus, DRG: dorsal root ganglia, ET: epithelial tubule, GUT: foregut, LL: left lung, NT: neural tube, SG: sympathetic ganglia, RL: right lung, TR: trachea.

At E12.5 (Figure 3.2i and ii) NCC density is greater in rostral lung tissue, near the trachea and bronchi (Figure 3.2i and ii, A-H) than in more caudal lung tissue, in the early lungs (Figure 3.2ii I-L). In the trachea (Figure 3.2i, B), bronchi (Figure 3.2i, D) and rostral lung tissue (Figure 3.2i and ii F, H), numerous NCCs surround the epithelial tubules while in caudal lung tissue (Figure 3.2ii, J, L) fewer NCCs can be seen in the lung. This difference in NCC distribution in regions of the early lung, before the mesenchyme expands, appears to be due to incomplete NCC migration into the lungs at this stage of development. This suggests that tangential migration of NCCs into the lung buds moves in a rostral-caudal wave, with colonisation of the trachea and bronchi occurring first, and then colonisation of the rostral lung bud occurring before colonisation of the caudal lung bud (Figure 3.2ii, J, L). As the lungs mature and the mesenchyme and airways grow, the boundary of the lung grows away from the bronchi, necessitating ongoing NCC migration in order to colonise more peripheral lung tissue. This qualitative observation was made in four E12.5 embryos and was not quantified due to the difficulties in standardising the level of section and precise embryonic age for analysis.

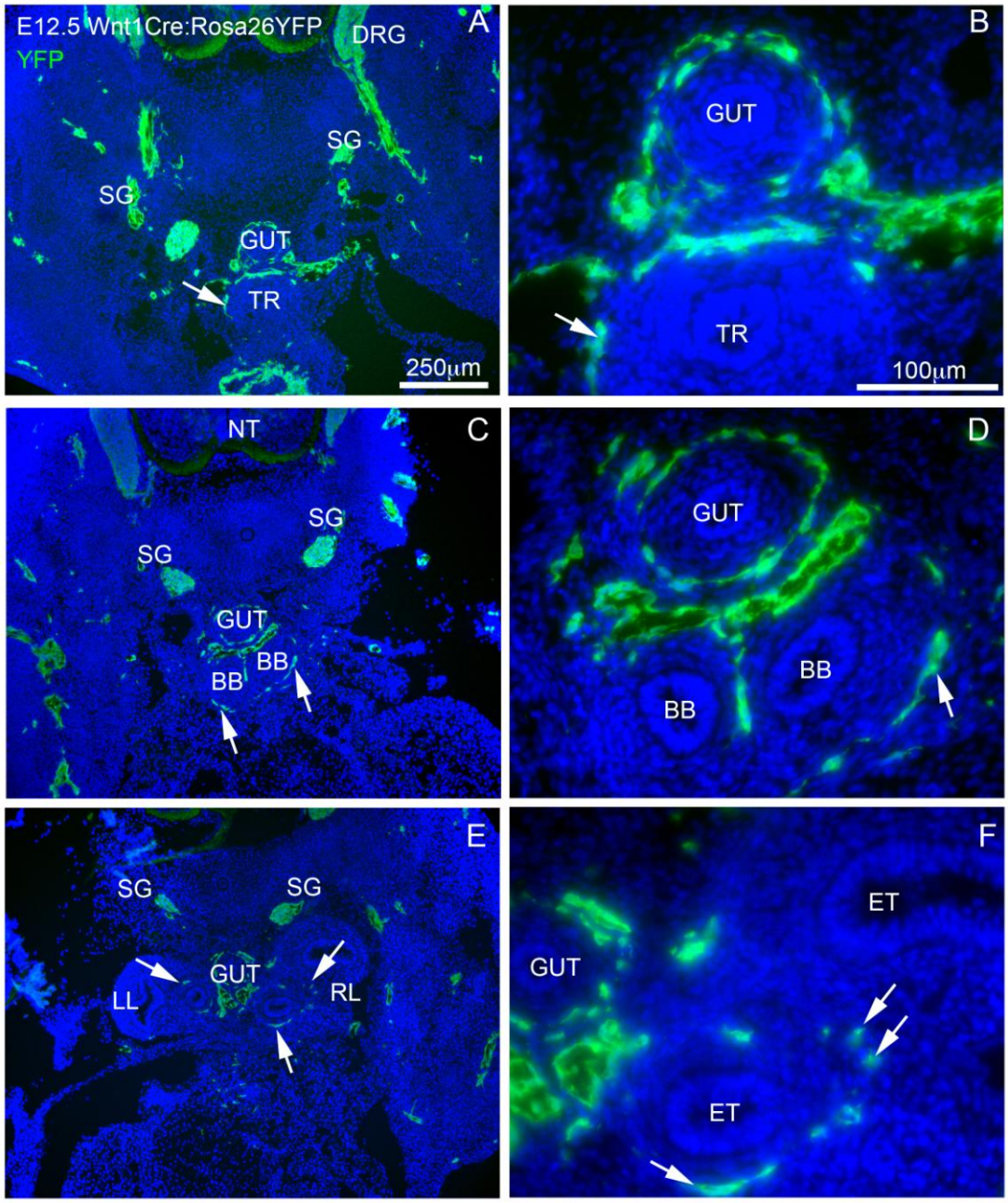

Figure 3.2i NCC denser in rostral than caudal sections through E12.5 *Wnt1Cre:Rosa26YFP* mouse embryo (rostral region). There are more NCCs present in rostral than in caudal lung tissue. Arrows indicate NCCs. BB: bronchus, DRG: dorsal root ganglia, ET: epithelial tubule, GUT: foregut, LL: left lung, NT: neural tube, SG: sympathetic ganglia, RL: right lung, TR: trachea.

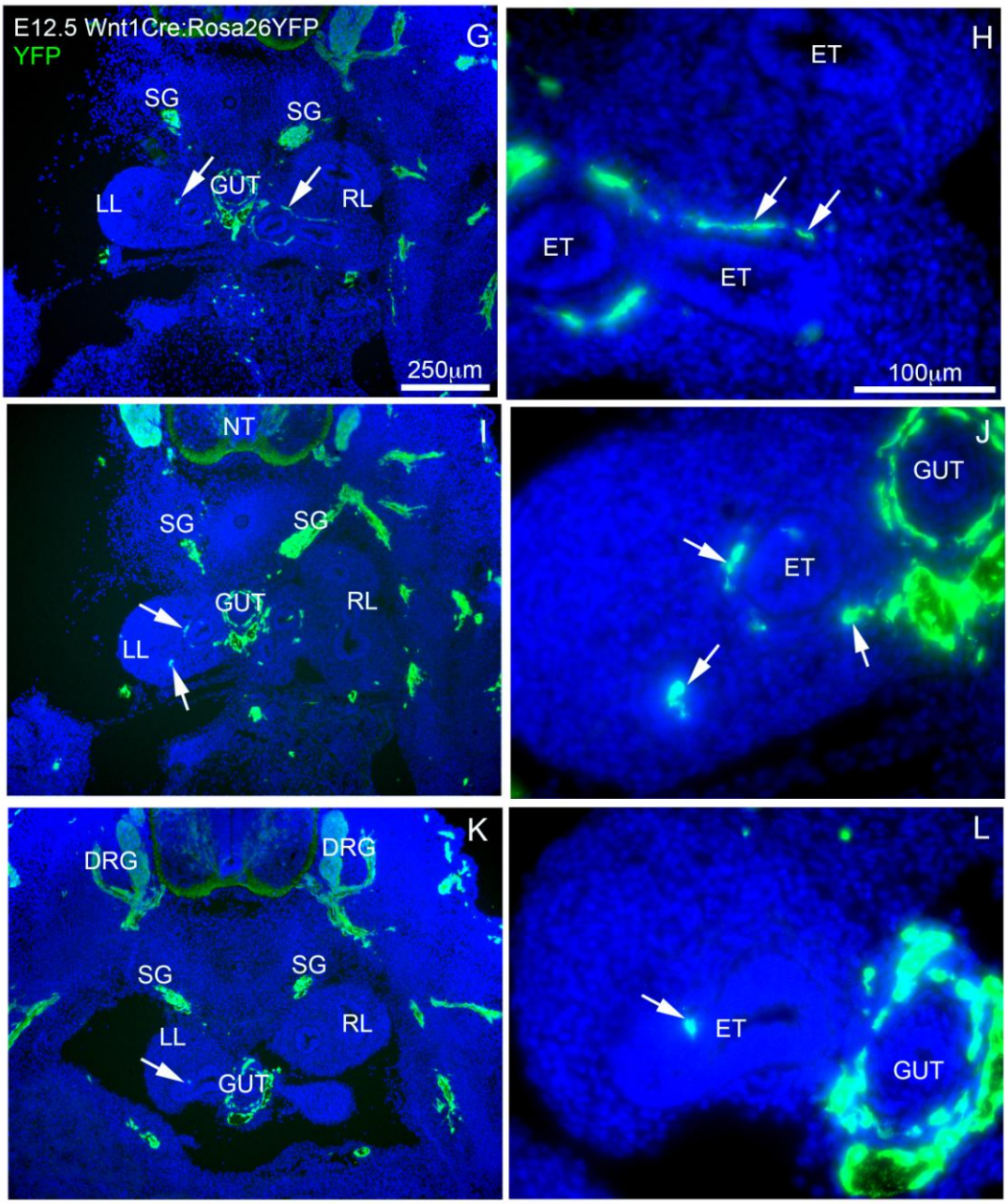

Figure 3.2ii NCC denser in rostral than caudal sections in E12.5 *Wnt1Cre:Rosa26YFP* mouse embryo (caudal region). A lower density of NCCs is seen in the more posterior lung. Arrows indicate NCCs. BB: bronchus, DRG: dorsal root ganglia, ET: epithelial tubule, GUT: foregut, LL: left lung, NT: neural tube, SG: sympathetic ganglia, RL: right lung, TR: trachea.

As the lungs grow, the branching of the respiratory tree produces an increasing number of epithelial tubules of decreasing size. The large upper airways, the bronchi and bronchioles, are still developing at E12.5 but are well established by E14.5 (Figure 3.3) and have given rise to several airway generations. At E14.5 the lobes of the lung have separated, each containing its own branch of the respiratory tree (Figure 3.3, A, B, C). NCCs are still denser around the bronchi (Figure 3.3, A) and in more central lung tissue (Figure 3.3, B) than in the peripheral lung (Figure 3.3, C), probably due to the outward growth of the lung mesenchyme. NCCs and neuronal projections migrate and extend into the growing lung in close proximity to the airways. At E14.5 (Figure 3.3) NCC migration along the future airways is more advanced. NCCs migrate next to the epithelial tubules (Figure 3.3, I, J, K, L) and begin to group together to form intrinsic lung ganglia (Figure 3.3, I). Neuronal processes extend around the airways (Figure 3.3, L). At E14.5 NCCs migrate along the epithelial tubules, shown in an epithelial tubule cross-section (Figure 3.3, K).

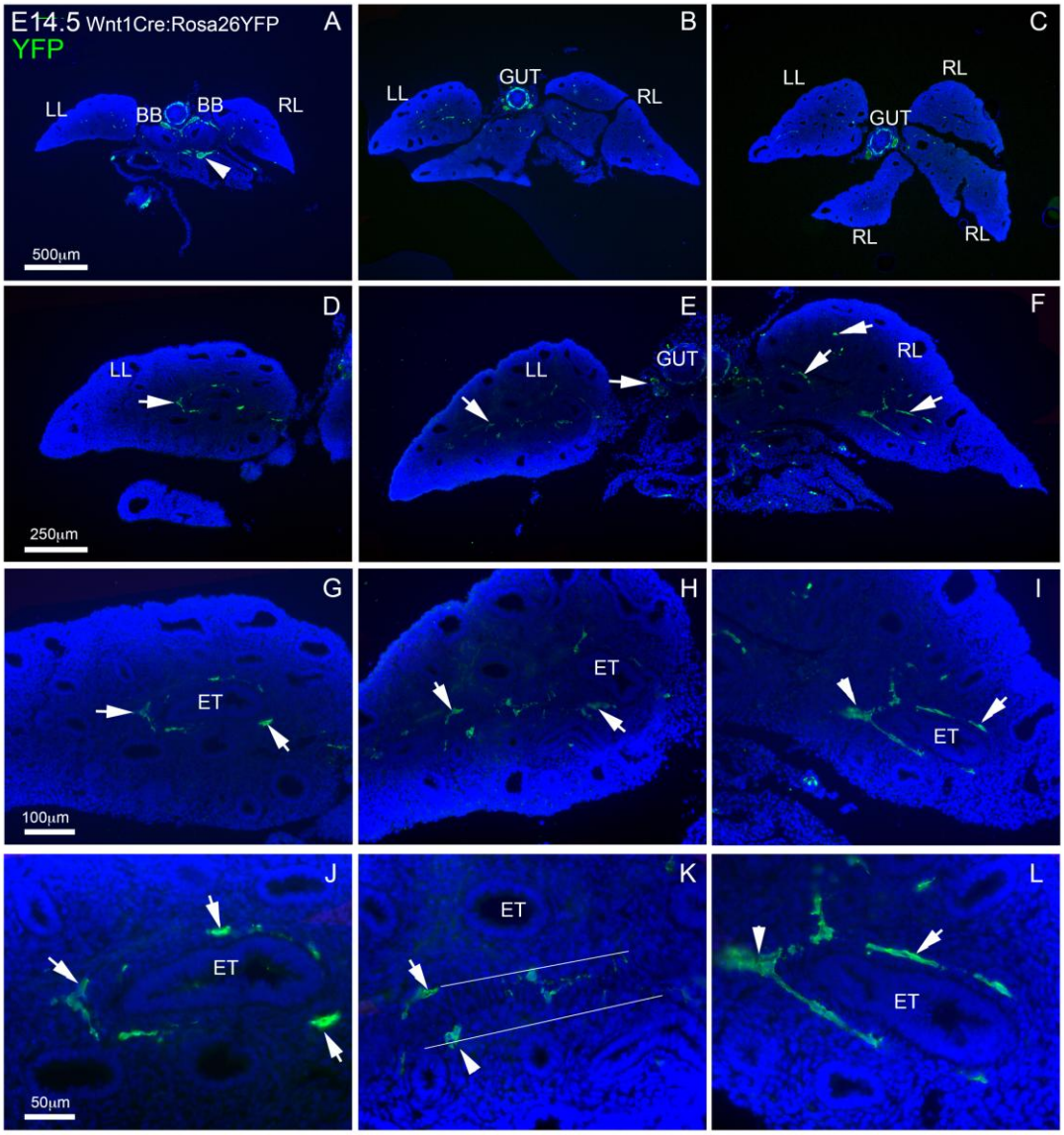

Figure 3.3 E14.5 *Wnt1Cre:Rosa26YFP* mouse lungs stained for YFP expression. Arrows indicate neural crest-derived tissue, arrowheads indicate ganglia composed of several cell bodies. The lines in K indicate the boundaries of an obliquely sectioned epithelial tubule. A-C are low power sections of the lung, rostral to caudal levels. D-L come from varying levels.
BB: bronchus, ET: epithelial tubule, GUT: foregut, LL: left lung lobe, RL: right lung lobe.

From E16.5 to birth at P0 the airspaces in the lung mesenchyme become established and enlarge (Figure 3.4, A, E, I). By E18.5 (Figure 3.4, E, F, G, H) lung alveolarisation begins to change the structure of the lung mesenchyme, producing the large surface area necessary for respiration. In the lungs from E16.5 onwards, neural crest-derived tissue is present only around the larger, more proximal airways (Figure 3.4, B, F, J). These neural crest-derived cells have a neuronal phenotype, extending long processes that surround the airways (Figure 3.4, C, D, G, H). Neural crest-derived cells group together to form ganglia (Figure 3.4, K, L). Airway ganglia made up of multiple neural crest-derived neurons can be seen next to the larger proximal airways, especially the bronchi (Figure 3.4, A, I, K, L). Neural crest-derived tissue is most dense around the primary bronchi and the upper and earlier-formed respiratory tubules.

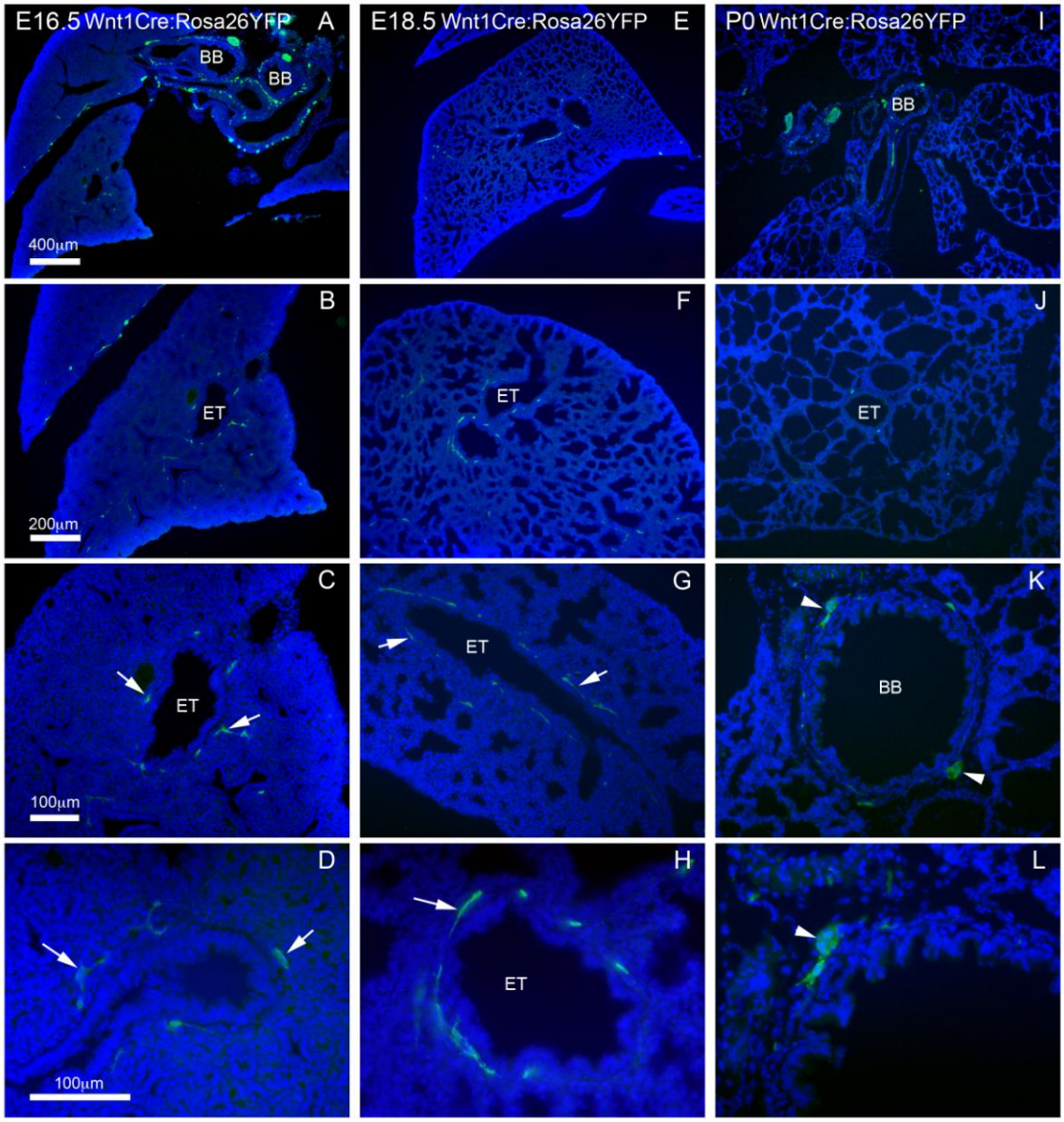

Figure 3.4 E16.5, E18.5 and postnatal day 0 *Wnt1Cre:Rosa26YFP* mouse lungs, stained for YFP expression. Arrows indicate neuronal tissue, arrowheads indicate neuronal ganglia composed of several cell bodies. Airway shown in oblique section in G. BB: bronchus, ET: epithelial tubule.

3.2 Developmental fate of neural crest cells in *Wnt1Cre:Rosa26YFP* mouse lungs

In order to confirm that the NCCs that migrate into the lung differentiate into neurons, the *Wnt1Cre:Rosa26YFP* mouse strain was used to track neural crest-derived cells after differentiation. Sections of E14.5 *Wnt1Cre:Rosa26YFP* mouse lungs were co-stained for the neural crest marker YFP and the neuronal marker Tuj1 (neuronal beta-III tubulin) (Lee et al., 1990) (Figure 3.5). Ganglia in *Wnt1Cre:Rosa26YFP* mouse lungs coexpress YFP and the neuronal marker Tuj1 (Figure 3.5, A-F). The overlap of YFP and Tuj1 expression in cell bodies in the lung indicates that all the neuronal cell bodies in the lungs are neural crest-derived at this stage.

We also examined *Wnt1Cre:Rosa26YFP* lungs to determine whether YFP-positive neural crest cells in the lung differentiated into glia (Figure 3.6), using antibodies against the calcium binding protein S100, which marks glial cells (Stefansson et al., 1982). Within the neural crest-derived neuronal ganglia described above, some cells co-express YFP and the glial marker S100 (Figure 3.6, A-F), indicating that NCCs give rise to glia in intrinsic lung ganglia as well as neurons.

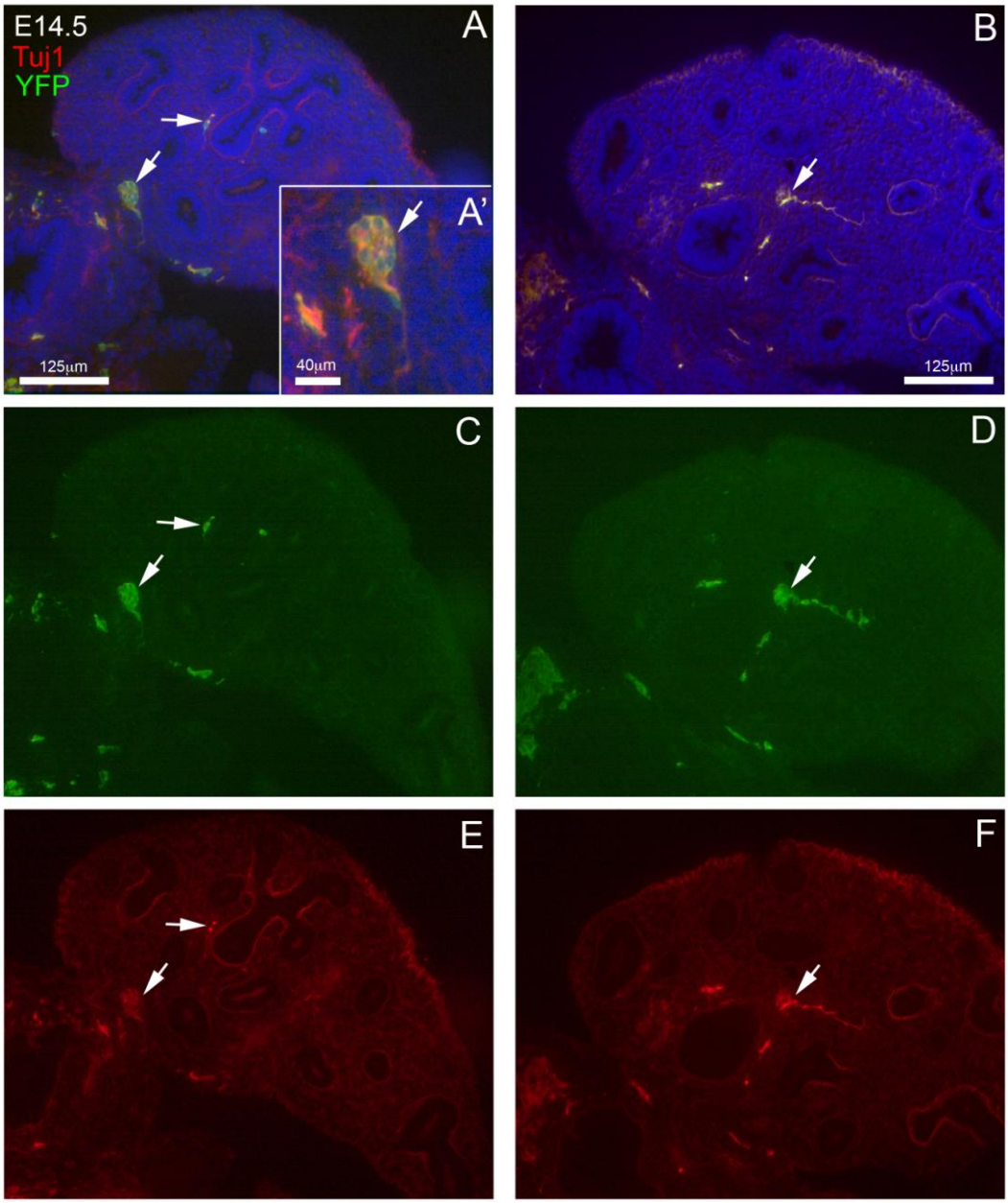

Figure 3.5 E14.5 *Wnt1Cre:Rosa26YFP* mouse embryonic lungs co-stained for YFP and the neuronal marker Tuj1. Tuj1 expression (red) is seen in YFP-expressing neural crest-derived (green) cells. Arrows indicate cell bodies expressing both YFP and Tuj1.

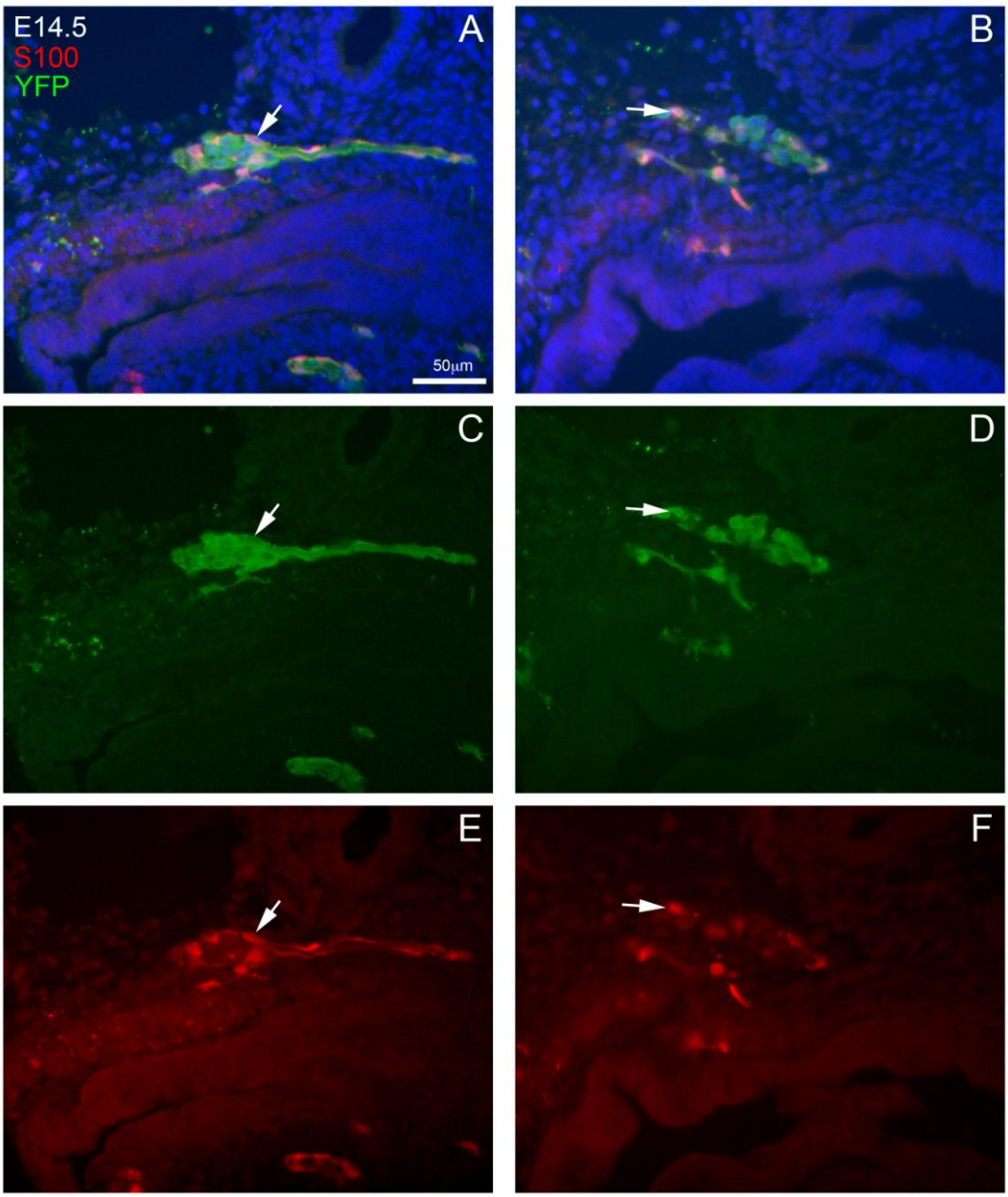

Figure 3.6 E14.5 *Wnt1Cre:Rosa26YFP* mouse embryonic lungs stained for YFP and the glial marker S100. S100 expression (red) is seen in some YFP-expressing neural crest-derived (green) cells in lung ganglia. Arrows indicate cell bodies expressing both YFP and S100.

3.3 Airway smooth muscle development and neural crest cell migration

In the section above, we demonstrated that NCCs migrate into the developing lungs and differentiate into neurons and glia, forming intrinsic ganglia. These intrinsic lung ganglia, also called airway parasympathetic ganglia (APGs), have various functions in the adult lung, including involvement in the the regulation of airway smooth muscle (ASM) contraction.

The development of ASM, the major target of intrinsic ganglion innervation, was characterised in the mouse lung along with NCC migration and differentiation. The timing of ASM formation and the relative timing of NCC colonisation of the lung was investigated using immunohistochemistry for an early ASM differentiation marker, smooth muscle actin (SMA) (Wallace and Burns, 2005) and the neuronal marker Tuj1, which marks the lung neurons that were shown to be derived from the neural crest (section 3.2). ASM develops in situ around the airways as the airways grow and branch, as discussed in the introduction (section 1.5.1). In the developing mouse lung SMA is expressed in the airway wall in advance of neuronal colonisation of the airway at E13.5 (Figure 3.7, C, E, F). ASM is present around the airways in the distal lung in the absence of intrinsic neurons. ASM and NCCs are present in proximal lung tissue (Figure 3.7, D, E) but NCCs have not yet migrated into distal lung tissue (Figure 3.7, F). In sections through mouse embryos, the concentric bands of smooth muscle in the gut (Figure 3.7, D, E) act as internal control tissue, indicating that the SMA staining has worked in the lungs. In E14.5 lungs (Figure 3.8) the distribution of ASM and neurons is similar to that at E13.5 but ASM has developed and is thicker and more extensive than at E13.5. ASM is seen around the bronchi (Figure 3.8, A) and larger airways, while NCCs are present in the lung mesenchyme adjacent to the ASM (Figure 3.8, D, E, F). The smaller airways from later generations of the respiratory tree are not surrounded by ASM (Figure 3.8, B, D, F). At E16.5 and 18.5 (Figure 3.9) ASM is still present around the larger airways (Figure 3.9, B, D, F), but not around the alveolar spaces that now make up the majority of the lung (Figure 3.9, A, C, E).

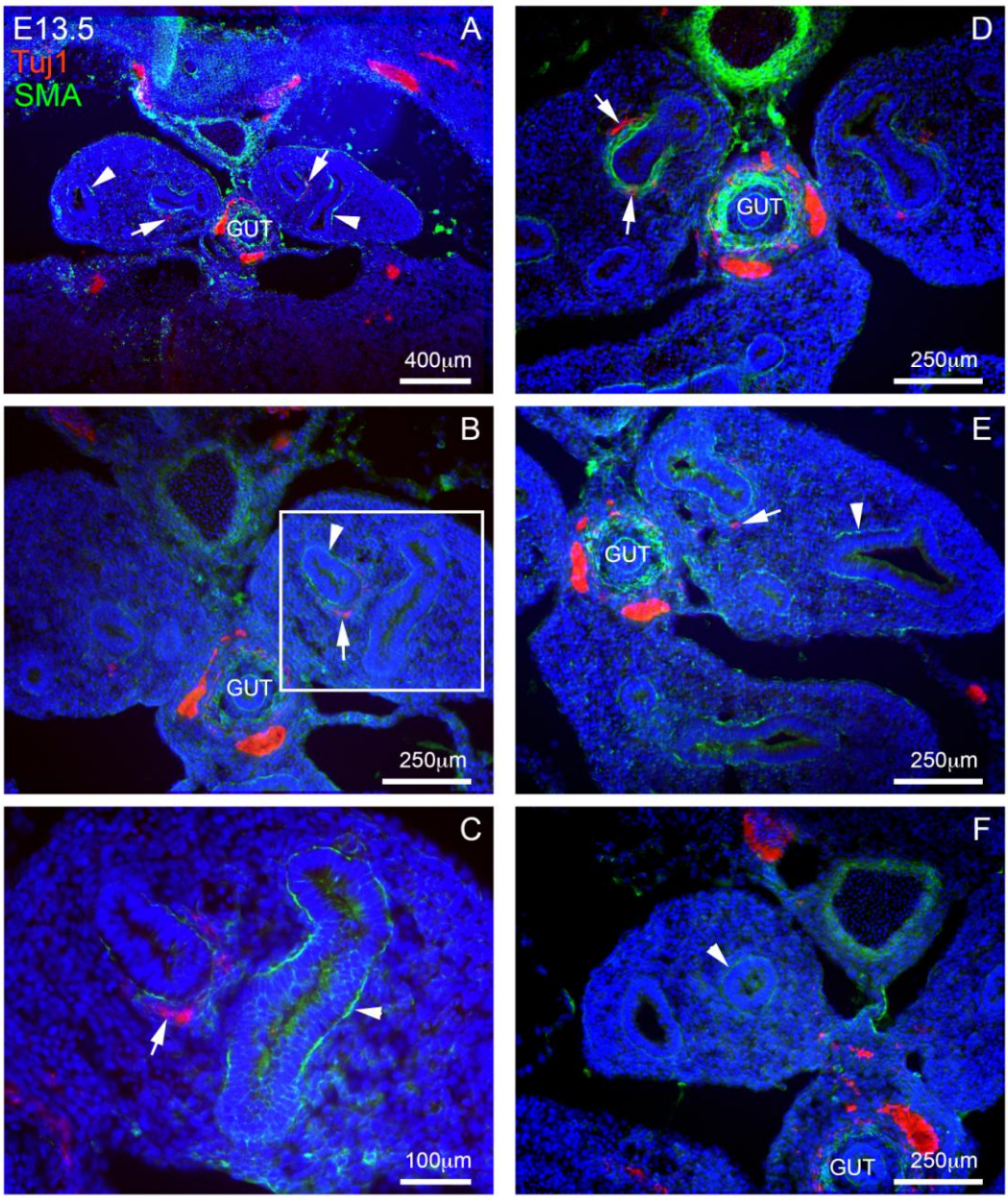

Figure 3.7 ASM and neurons in E13.5 mouse lungs. E13.5 mouse lungs costained for the neuronal marker Tuj1 (red) and the smooth muscle marker SMA (green). Neurons are indicated by arrows and ASM by arrowheads. A-C are increasing magnifications of the same section, C being the boxed area in B. D-F are three different sections at the same magnification. ASM is seen in distal tissue in the absence of neurons (E).

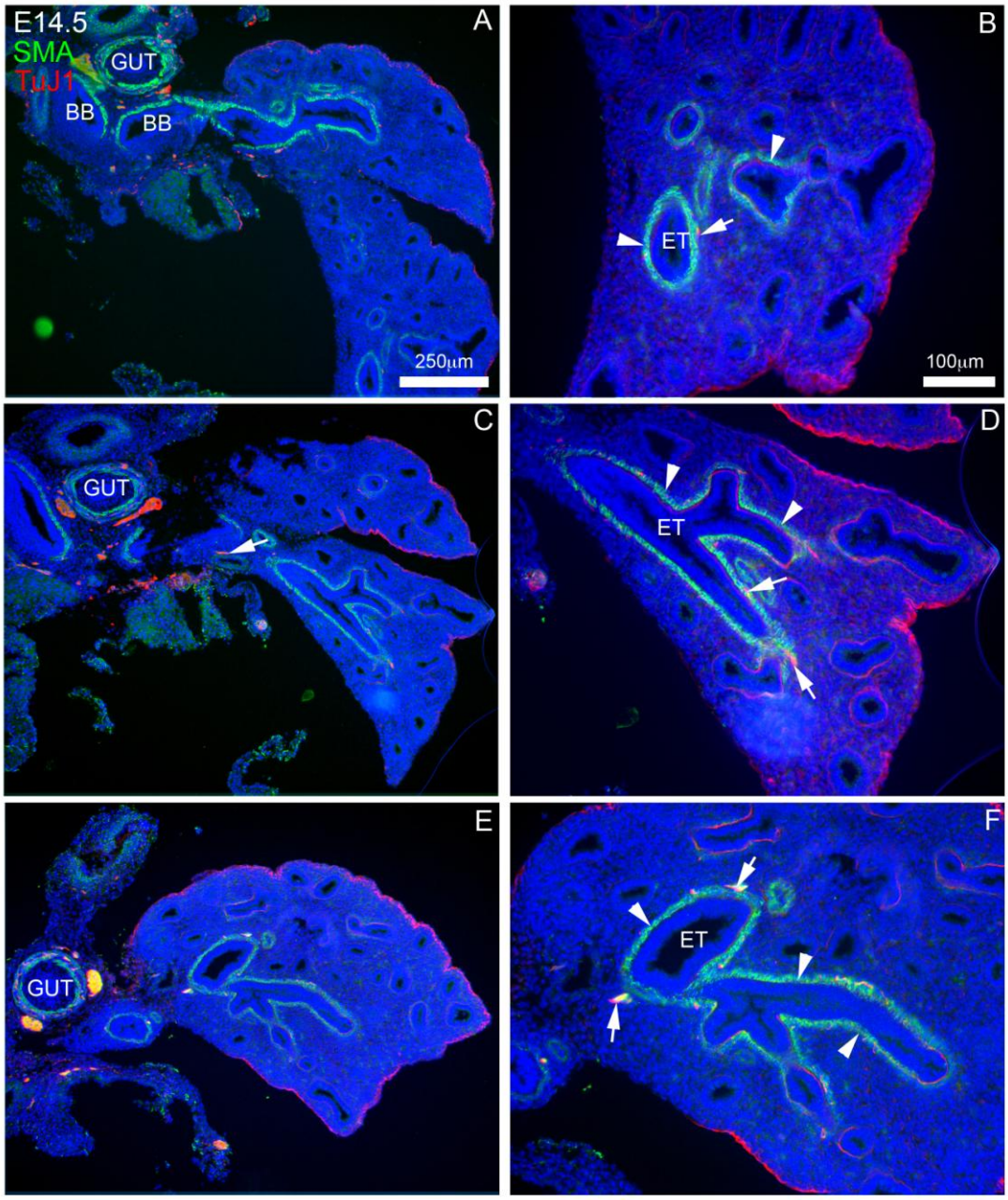

Figure 3.8 ASM and neurons in E14.5 mouse lungs. Sections of E14.5 mouse lung, costained for the neuronal marker TuJ1(red) and smooth muscle marker SMA (green). Some red staining is seen at the lung edges due to background staining of the anti-mouse secondary antibody on mouse tissue. Neuronal tissue is indicated by arrows and ASM by arrowheads. Neurons are located adjacent to the airways, in close association with the airway smooth muscle. BB: bronchi. ET: epithelial tubule.

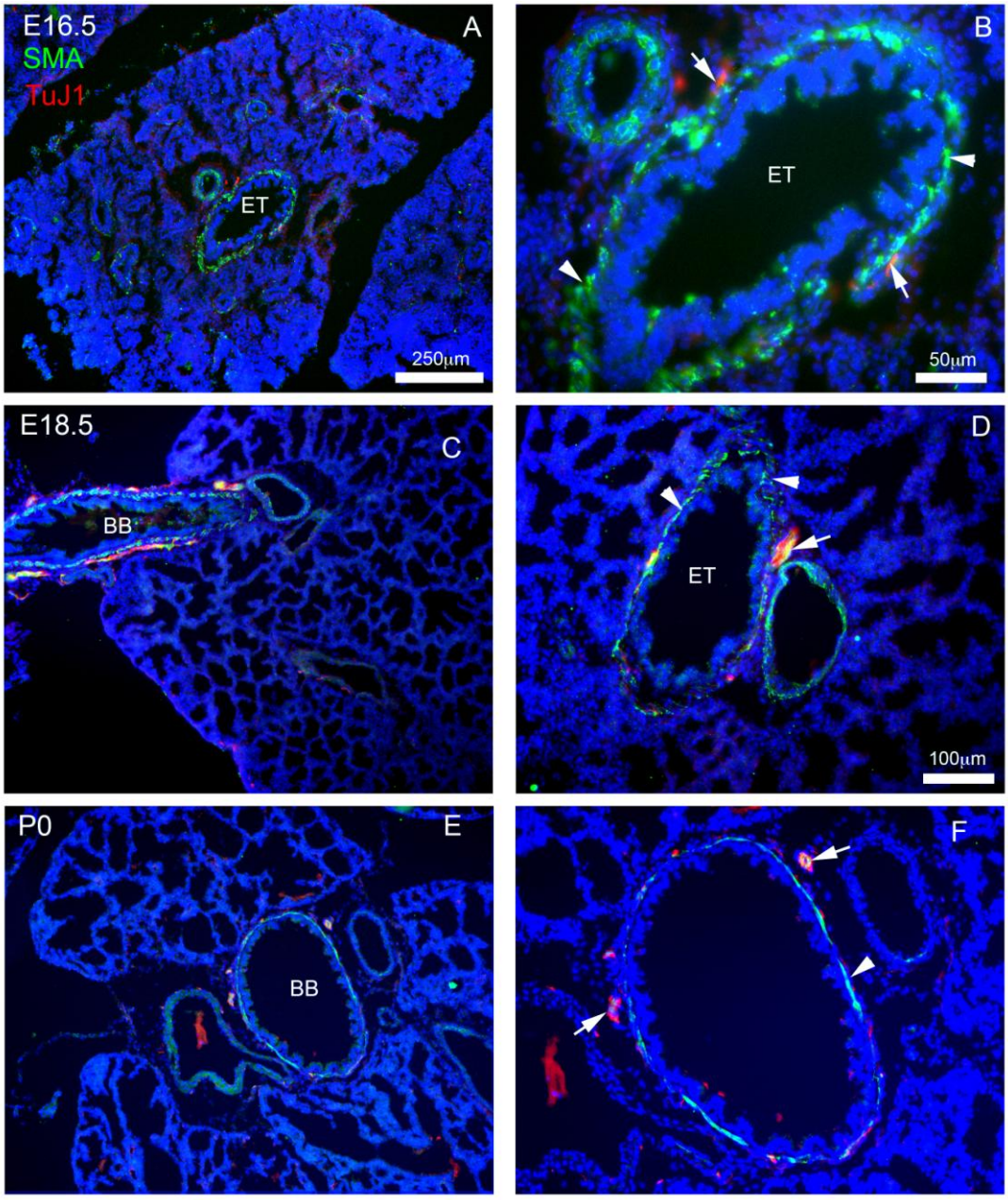

Figure 3.9 ASM and neurons in E16.5 and E18.5 mouse lung. Sections of E16.5 and E18.5 mouse lung costained for SMA (green) and Tuj1 (red). Neuronal tissue indicated by arrows and ASM by arrowheads. Smooth muscle continues to surround the major airways but is absent around alveolar spaces. BB: bronchus, ET: epithelial tubules.

3.4 Distribution of NCCs in the lung as shown by optical projection tomography (OPT)

The distribution of neural crest-derived tissue in the lung was characterised in frozen sections, as shown in section 3.1 above. However, because neural tissue is relatively sparse in the lungs it is difficult to fully describe the distribution of neurons and their three-dimensional structure in the embryonic lung using only 2-dimensional sections. In order to better describe the architecture of neural crest-derived lung innervation, using the *Wnt1Cre:Rosa26YFP* mouse strain, whole mount immunostaining for the NCC marker YFP was carried out in E14.5 lungs, followed by OPT scanning (Sharpe et al., 2002) to obtain three-dimensional images of the complex organisation of intrinsic pulmonary innervation (Figure 3.11 and 3.12). This novel technique permitted the imaging of NCC or neuronal marker staining in whole lung tissue at a resolution sufficient to see the distribution of ganglia and projections within the lung.

In fluorescent OPT, samples are first immunostained with a fluorescent marker and then cleared. Light of the excitatory wavelength for the fluorescent marker then illuminates the sample and a camera-imaging chip captures the pattern of emitted fluorescent light (Figure 3.10). The sample rotates so that images are taken from all angles. Each image records the total amount of light emitted along a straight line through the specimen. Where the staining is stronger the light emitted is greater. Proprietary software then uses this intensity data to construct a three-dimensional model of the pattern of staining (Sharpe et al., 2002). This model can then be rotated or virtually sectioned through several axes, and videos produced of the resulting series of views to show multiple aspects of the sample.

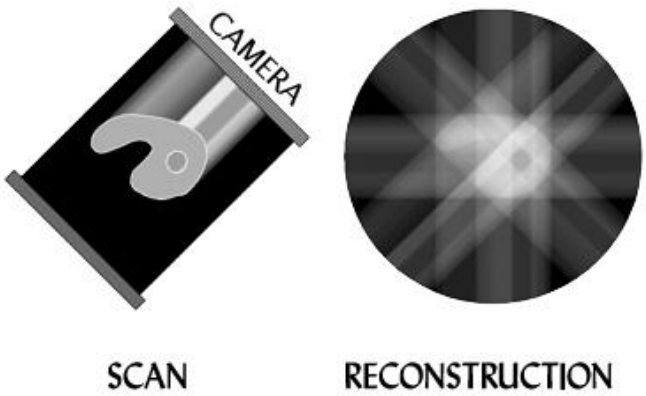

Figure 3.10 OPT reconstruction. By combining intensity data from several angles, the internal structure of the sample can be reconstructed. Adapted from J. Sharpe, Edinburgh MRC website.

In OPT scans of E14.5 *Wnt1Cre:Rosa26YFP* lungs stained for the NCC marker YFP (Figure 3.11 and 3.12) the branching structure outlined by YFP-positive tissue corresponds to the shape of the branching airways in all lungs scanned (n=3). YFP-positive projections, presumably axons (Figure 3.11, A-E) are seen as thin lines of YFP staining with occasional cell bodies or varicosities visible along them. Larger groups of NCCs form neuronal ganglia (Figure 3.11, C). Virtual sections through OPT reconstructions (Figure 3.12, Ai-Avi) show similar patterns of innervation to those seen in cryosections, as described above. The similarity between the staining seen in virtual and actual sections therefore validates the OPT scans obtained. NCCs and neural crest-derived projections (Figure 3.11, B-F) are found in close association with the airways and occur at high density around the trachea (Figure 3.11, A-C).

At E14.5, NCCs and neural crest-derived innervation are denser in the trachea than in the lung lobes (Figure 3.11 and 3.12). NCC are seen along the major airways into the lobes of the lung, most clearly seen in the upper left lobe (Figure 3.13, A, E, I) and uppermost right lobe. Larger groups of NCCs near the upper airways are visible (Figure 3.13, A, D-F, I). The three-dimensional scan shows the extension of YFP-expressing NCCs and neural crest-derived tissue away from the trachea into ventral and rostral lung tissue (Figure 3.13, C, G). The vagal nerve is distinct from the intrinsic tracheal innervation (Figure 3.12, D, H). A video of a rotating three-dimensional reconstruction of E14.5 *Wnt1Cre:Rosa26YFP* lungs, stained for YFP, can be seen in the supplementary information for the publication by Freem et al (Freem et al., 2010).

These scans provide a useful overview of the distribution of neural crest-derived tissue in the lung. They confirm that NCC migration takes place along the airways in close association with neuronal projections, which extend and branch along the airways. Large neural crest-derived ganglia are present next to the primary bronchi.

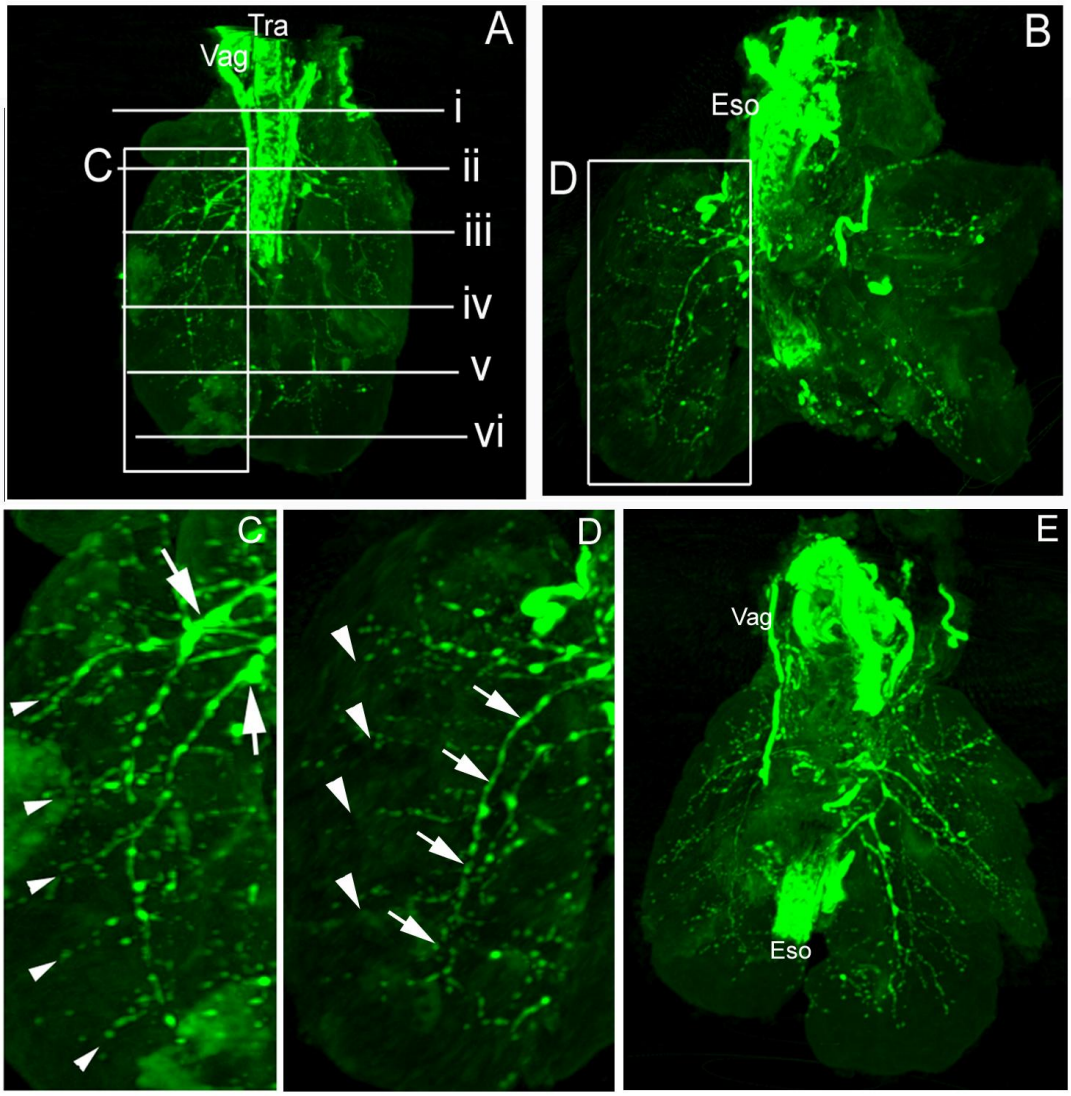

Figure 3.11 OPT scans of 3 different E14.5 *Wnt1Cre:Rosa26YFP* mouse embryonic lungs immunostained for the NCC marker YFP. A, B, E: Whole E14.5 lungs. C: Zoom of left lobe of the lungs in A. Arrows indicate ganglia, arrowheads indicate projections along airways. D: Zoom of left lobe in B. YFP-positive NCCs can be seen in ganglia along the main descending airway (arrows) and thinner projections along ancillary branches (arrowheads). Eso: esophagus, LL: left lobe, RL: right lobe, Tra: trachea, Vag: vagus.

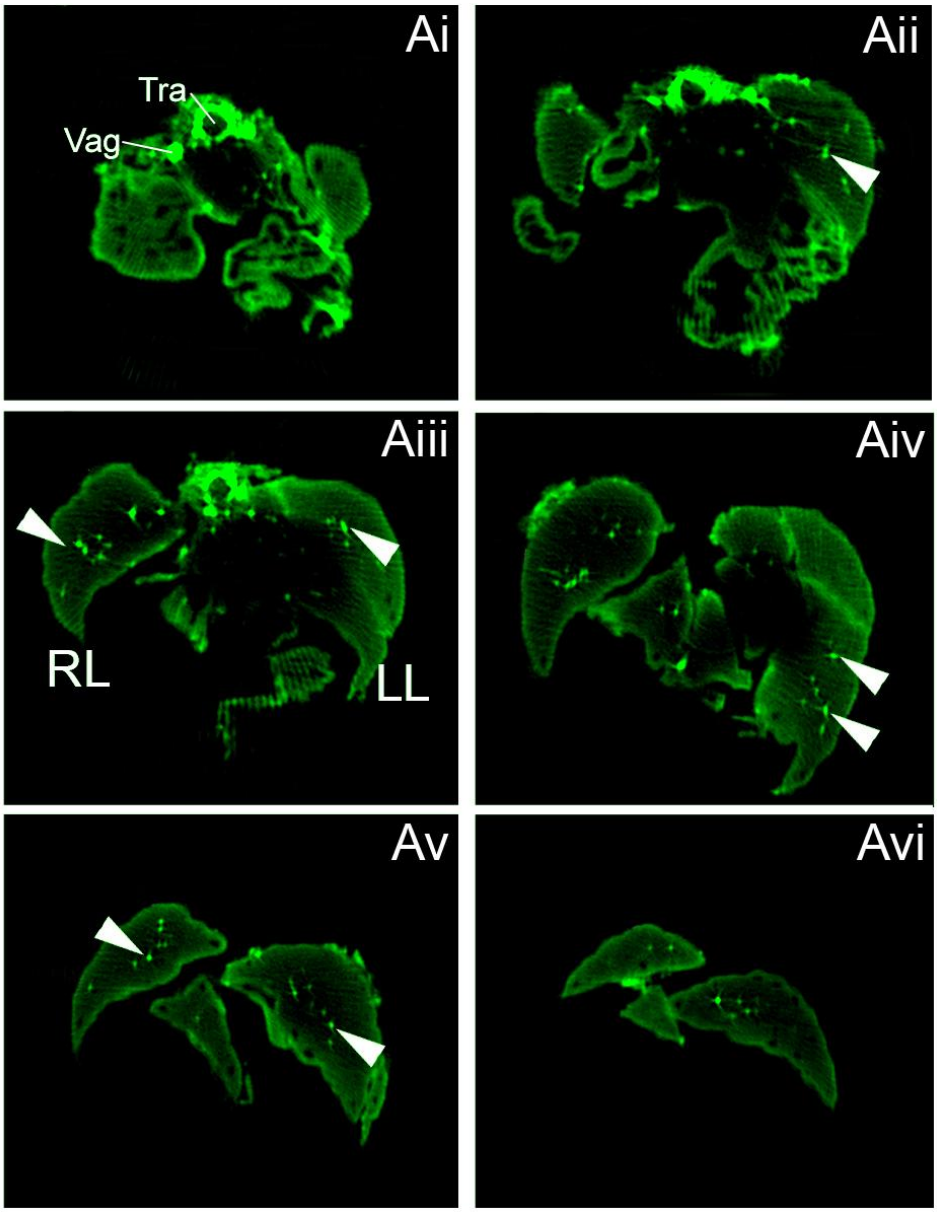

Figure 3.12 Virtual transverse sections through OPT scan of E14.5 *Wnt1Cre:Rosa26YFP* mouse embryonic lung stained for YFP (Figure 3.11, A). Sections shown in Ai-Avi correspond to the levels labelled i-iv in Figure 3.11, A. YFP-positive neural crest derived tissue (arrowheads) is seen next to airways and surrounding the trachea. LL:

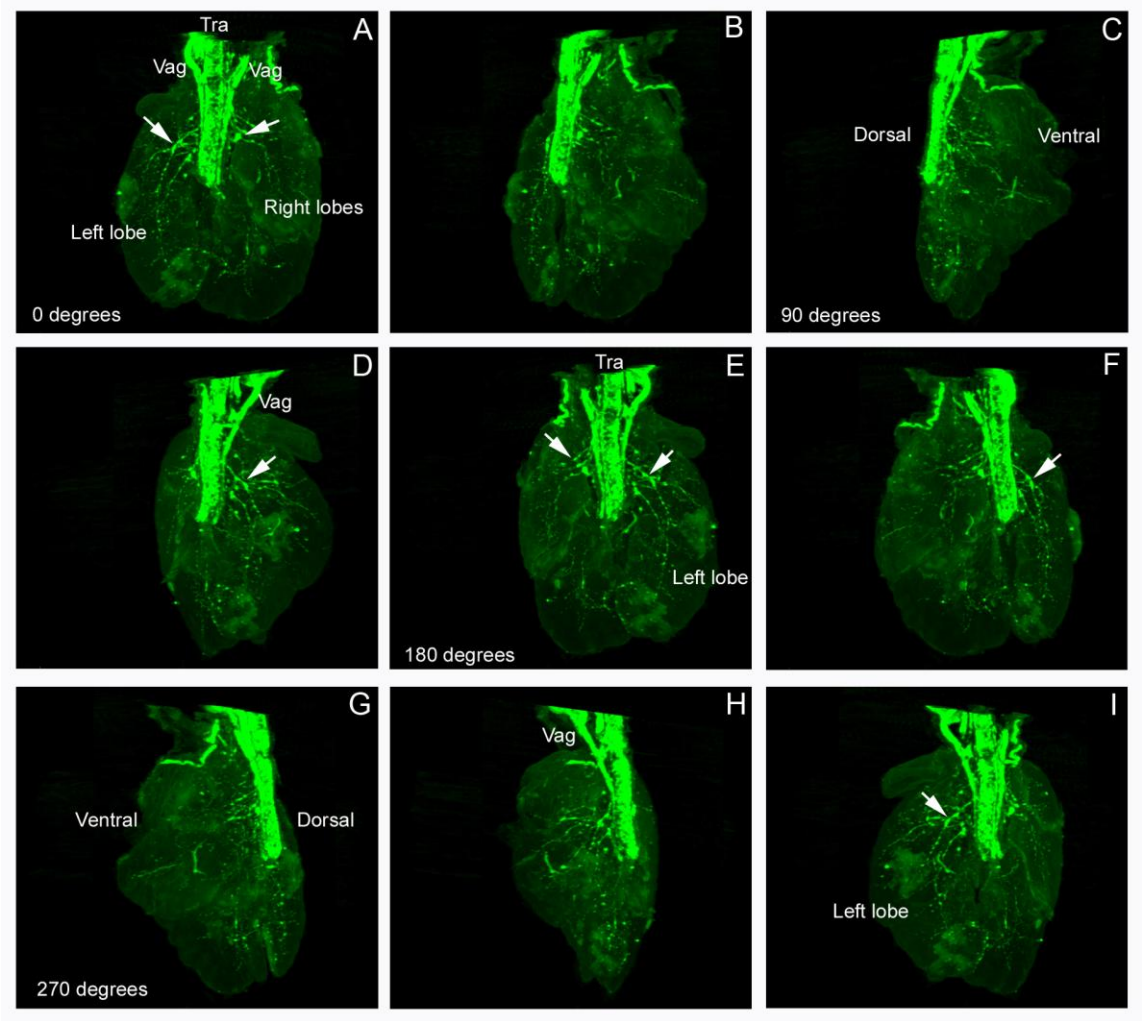

Figure 3.13 Stills from 360-degree rotation of three-dimensional reconstruction of OPT scan of E14.5 *Wnt1Cre:Rosa26YFP* mouse lungs immunostained for YFP. The rotation of the lung allows better visualisation of the three-dimensional architecture of pulmonary innervation. Arrows indicate groups of NCCs. Tra: trachea, Vag: vagus.

3.5 Discussion

The R26R-YFP reporter line was first described by Srinivas et al (Srinivas et al., 2001) and this transgenic line was combined with the Wnt1-Cre transgenic mouse described by (Danielian et al., 1998) to develop the *Wnt1Cre:Rosa26YFP* double transgenic mouse strain used here. A similar double transgenic strain, using LacZ rather than YFP to mark NCCs, has been used to track NCC migration to the heart (Jiang et al., 2000). The *Wnt1Cre:Rosa26YFP* double transgenic mouse is a powerful experimental model for the analysis of NCC migration and differentiation in mammals. *Wnt1* is expressed in the neural crest region and roof plate before NCC delamination, thus marking NCC progenitors and the future dorsal neural tube (Echelard et al., 1994). YFP is expressed in all NCCs and their descendants, as well as the dorsal neural tube, once *YFP* expression is activated by the expression of Cre recombinase under the control of the *Wnt1* promoter during early embryonic development. This allows the fate of NCCs to be traced after they have stopped expressing *Wnt1* and have begun migration. Native markers in mice do not allow this definitive and comprehensive tracing of NCCs and their offspring over a long time period. Neural crest migration and differentiation takes place over several days. During this time, NCCs may express several different marker proteins, and marker expression can change as cells differentiate (Young et al., 2003) or become progressively limited to increasingly differentiated subsets of NCC (Britsch et al., 2001). Early NCC markers, including Sox10 (Kelsh, 2006) do not persist in all NCCs after NCC differentiation.

There are numerous advantages to using a transgenic fluorescent cell lineage marker system for NCC fate mapping, as compared to using native markers. In the case of neural crest-derived neurons, YFP marks neuronal projections as well as cell bodies, allowing neural crest-derived neuronal networks and targets of neural crest-derived innervation to be traced. This approach has an advantage over quail-chick interspecies grafting techniques which have been extensively used to trace the NCC lineage in the chick (Burns and Delalande, 2005), where only cell nuclei are marked by the quail cell-specific antibody QPCN. In this (Freem et al., 2010) and other studies (Barraud et al., 2010; Cassiman et al., 2006) the expression of the fluorescent YFP marker allowed NCCs and neural crest-derived cells to be traced throughout the embryo from the onset of Wnt1 expression at E9.5 onwards. Other Wnt1Cre

double transgenic studies have used a LacZ-expressing construct to mark NCCs and their progeny (Langsdorf et al., 2011; Nassenstein et al., 2010). Unlike YFP, which can be visualised in live tissue, this construct only allows marked cells to be traced after fixation and staining, which limits its use. As discussed later in chapter 5, the migration of YFP-expressing NCCs can be tracked in live cultured tissue over several days, using fluorescent time-lapse microscopy. Although organotypic lung culture has been used to examine the migratory behaviour of NCCs and subsequent differentiation of neurons, without a fluorescent marker live imaging cannot be used to examine NCCs within the cultured lung and analysis must be carried out after tissue fixation (Tollet et al., 2002).

Vagal NCCs migrating tangentially from the foregut have been previously demonstrated to be a source of intrinsic lung innervation in the chick (Burns and Delalande, 2005). Therefore, the migration of NCCs in mice was studied, in order to investigate how NCC in mammals colonised the lung and gave rise to intrinsic lung neurons. The investigation also provided a baseline for further studies of lung innervation in mutant mice.

The first appearance of NCCs in the *Wnt1Cre:Rosa26YFP* mouse embryonic lung occurred at E10.5, during early lung bud formation. A subset of NCCs migrated tangentially from the area surrounding the foregut towards the trachea and bronchi. NCCs were thus seen to enter the lung buds laterally from the foregut. This was the most prevalent form of NCCs migration in the lung up to E13.5. In the later stages of embryonic lung development, NCCs migration from proximal to distal lung tissue took place along the airways. These findings are consistent with previous observations of pulmonary neural development in confocal images of whole mouse lungs up to E14, using immunostaining for p75 to mark NCCs (Tollet et al., 2001; Tollet et al., 2002). Rostro-caudal differences in the timing of NCC colonisation of the lungs were seen in E12.5 lungs, where the rostral lung was colonised in advance of the caudal lung. Rostro-caudal migration of NCCs has been described in the gut (Burns and Thapar, 2006), and so the migration of NCCs from the gut into the rostral lung bud before the caudal lung bud could be similar to the pattern of NCC migration in the gut. NCC delamination also occurs in a rostro-caudal wave, along the antero-posterior body axis (Bronner-Fraser, 1993).

As NCCs in the lung differentiated to form neurons, neuronal projections from both intrinsic lung neurons and extrinsic neurons extended along the airways to form a neuronal plexus. The formation of this neuronal plexus around the airways, closely associated with airway smooth muscle, has been previously described in whole lungs (Sparrow et al., 1995), but not in sections. As the major source of extrinsic lung innervation, the vagal nerve, is marked by YFP expression in the *Wnt1Cre:Rosa26YFP* mouse, it was not possible to distinguish whether neuronal projections came from intrinsic neurons or extrinsic nerve fibres using this transgenic mouse line. The vagal nerve may be marked by YFP expression for several reasons. Firstly, the vagus contains projections from the neural crest-derived jugular ganglia. Secondly, migrating NCCs and neural crest-derived Schwann cells can be present on the surface of the vagal nerve. Nassenstein et al have shown that extrinsic innervation can be separated into neural crest-derived and placode-derived fibres in the mouse (Nassenstein et al., 2010), but they did not examine intrinsic neurons in the lung. The sequence of NCC migration and development into and within the mouse lung and the relationship between ASM and neuronal development that we describe here have been shown to be similar in the embryonic and fetal human lung (Burns et al., 2008; Sparrow et al., 1999).

After E14.5 NCCs, neural crest-derived neurons and neuronal projections within the lobes of the lung were always seen in close association with the future airways. As the lung mesenchyme expanded from E14.5 to P0 and underwent alveolarisation, neural tissue in the lung became increasingly sparse, possibly because lung innervation does not grow over time to the same extent as the lung mesenchyme. The majority of intrinsic lung innervation was found in the early-formed, upper, conducting airways. At P0 (Figure 3.4), lung innervation resembled that previously described in earlier anatomical papers on the adult lung (Dey and Hung, 1997; Larsell, 1922), with large ganglia present near the upper bronchi and projections and dispersed, small ganglia present in the peripheral lung, with neural tissue not extending as far as the lower respiratory tree or alveoli. Though mouse lungs undergo some postnatal development (see table 1.1, section 1.3), this is mainly related to lung mesenchyme growth and alveolarisation. Therefore, the innervation of the lung appears to develop in the prenatal period (Dey and Hung, 1997).

The lateral migration of vagal NCCs into the mouse lung from the gut was not described previous to this work, though the neural crest origin of intrinsic lung innervation was suggested (Dey and Hung, 1997). The development of neural crest-derived neurons in mouse embryonic lungs older than E14.5 has recently been investigated in wholemount lungs (Langsdorf et al., 2011) using a *Wnt1Cre:Rosa26LacZ* double transgenic mouse line as well as the *Wnt1Cre:Rosa26YFP* line also used in this project. Langsdorf et al also characterised early NCC colonisation of the lung using a RET-EGFP transgenic mouse strain, which allowed *Ret*-expressing NCC to be traced. They described tangential NCC migration from the gut into the mouse lung and subsequent NCC differentiation to form intrinsic lung neurons, and demonstrated that all intrinsic lung ganglia are neural crest-derived using the *Wnt1Cre:Rosa26LacZ* mouse line, in agreement with the results reported in this thesis.

Neural crest-derived intrinsic pulmonary neurons and a smaller number of associated neural crest-derived glia were seen in large ganglia near the bronchi and smaller ganglia next to the airways, corresponding in position to the cholinergic and NANC airway parasympathetic ganglia (APGs) described in the introduction in section 1.4.3. These intrinsic lung neurons must begin to express neurotransmitters during development in order to become functional. The development of a number of neurotransmitter markers in chicken lung innervation has been described (Burns and Delalande, 2005; Vaccaro et al., 2006). Parasympathetic ganglia formation and function in ASM signalling in the cultured fetal pig lung has also been studied using synaptic and neuronal markers, confocal microscopy and electrophysiology (Weichselbaum et al., 1996; Weichselbaum and Sparrow, 1999). Glia have not been described in APGs during development in any detail.

ASM arises early in lung development from the lung mesenchyme and surrounds the growing airways as they develop as described earlier (introduction, section 1.5.1) and as reviewed in Sparrow and Lamb (2003). ASM forms as rings of circular muscle around the airways. A neuronal plexus is present around the fetal airways in association with ASM in embryonic lungs and has been investigated in human (Burns et al., 2008; Sparrow et al., 1999), pig (Sparrow and Weichselbaum, 1997;

Weichselbaum et al., 1996; Weichselbaum and Sparrow, 1999), mouse (Tollet et al., 2001) and avian (Burns and Delalande, 2005) embryonic and fetal lung development. The smooth muscle marker smooth muscle actin marks early smooth muscle in the lung (Leslie et al., 1990). The function of the pulmonary neuronal plexus in stimulating smooth muscle contractions in developing fetal pig lung has been described (Sparrow and Weichselbaum, 1997). ASM is present in the distal lung in advance of NCC colonisation (Figure 3.7) as previously described (Tollet et al., 2001). Although intrinsic lung innervation is closely associated with ASM and airways, ASM is not necessarily associated with neural tissue in the developing lung. Although initially present in thick, diffusely-edged bands around the airways (Figure 3.7), ASM develops to become a thinner, more condensed band around the major conducting airways in the perinatal lung (Figure 3.9).

ASM is the major target of innervation from intrinsic lung neurons. The temporal link between the formation and maintenance of ASM and the development of neural crest-derived intrinsic neurons in the lung was therefore examined. As expected from previous work (Sparrow et al., 1999; Tollet et al., 2001; Tollet et al., 2002) the intrinsic innervation of the lung appears in more distal lung epithelial tubules after ASM has formed. ASM is laid down in the wake of the tip of the growing epithelial tubule early in airway formation (Cardoso and Lu, 2006) and is present at E11 in mouse (Mitzner, 2004). It was therefore expected that the innervation of the lung appeared after the formation of the smooth muscle layer around the airways, as was demonstrated in these experiments.

The relatively sparse nature of lung innervation meant that limited information on the three-dimensional geometry of the pattern of lung innervation was obtained from tissue sections. In order to obtain more detailed three-dimensional information, we took advantage of Optical Projection Tomography (OPT) imaging technology. In fluorescent OPT, samples are immunostained with a fluorescent marker and then cleared and scanned to produce a three-dimensional computer model. This model can then be rotated or virtually sectioned through several axes, and videos produced of the resulting series of views. OPT can be used to look at general tissue morphology, using tissue autofluorescence (Ijpenberg et al., 2007; Kirkby et al., 2011), in situ hybridisation staining patterns (Fisher et al., 2011; Sato et al., 2008),

or immunostaining as in this (Freem et al., 2010) and other studies (Walls et al., 2008). The three-dimensional images produced by OPT scanning can be further analysed to give quantitative information, for example using branch mapping to produce a numerical description of branching morphology in the kidney (Short et al., 2010). Such computational mapping techniques could be transferred to branching morphogenesis in the lung.

OPT scans of E14.5 lungs produced more complete and useful data on the anatomy and localisation of neuronal projections and neurons in intact lungs than that obtained from sections. The combination of OPT with the use of the *Wnt1Cre:Rosa26YFP* transgenic mouse line is unique and provides a novel method of NCC lineage tracing. Three-dimensional reconstructions of OPT scanned lungs can be digitally sectioned in multiple planes and the scanned lungs can also be processed after OPT for conventional microscopy, allowing detailed analysis of lung morphology by multiple methods. OPT scanning allows the assessment of general lung morphology as well as revealing the localisation of staining for specific markers. OPT is also a useful technique for assessing the phenotype of transgenic or mutant model animal embryos and organs. Three-dimensional reconstructions allow multiple aspects of internal and external morphology to be analysed. We also used OPT to examine lung innervation in mutant mouse embryonic lungs (chapters 5 and 6), allowing better comparison of the architecture of lung innervation than could be accomplished using analysis of lung innervation in frozen sections alone. Some previous studies have looked at innervation and NCCs in the wholemount mouse lung using confocal microscopy (Langsdorf et al., 2011; Sparrow and Lamb, 2003; Tollet et al., 2001). However, examining lung innervation by this method requires flattening of the lung tissue during mounting, which can deform the tissue and obscure regions of staining. The anatomy and architecture of lung innervation can therefore be distorted. OPT has the advantage of allowing the preservation of three-dimensional lung morphology and thus greater imaging fidelity.

At E14.5, when several generations of airway branching had occurred, NCCs and neural crest-derived cells could be seen in OPT scans in close proximity to the airways and were more dense in proximal than distal lung tissue. Neural crest-derived nerve fibres appeared to extend into the lung along the airways, possibly

from an intrinsic source. The branching pattern of neuronal processes seen in OPT images of E14.5 lungs corresponds to the branching pattern of the early airways. In sections of embryonic lungs of the same stage neurons were always seen next to airways. The virtual transverse sections through digital three-dimensional reconstructions of OPT-scanned lungs showed the same distribution of YFP-positive tissue as physical transverse sections, allowing us to validate the information from these scans. Virtual sections in the sagittal and coronal planes (not shown) could also be produced from the same scanned lung, although owing to the sparse nature of lung innervation the three-dimensional reconstructions were more informative than these additional sections.

In summary, we have shown that NCCs colonise the mouse lung using a novel combination of a transgenic mouse reporter strain and a three-dimensional imaging technique (OPT). We have also demonstrated that NCCs in the lung give rise to neurons and glia that form ganglia next to the airways in close association with ASM.

4. Chapter 4: Neural crest cell prespecification in the chick gut and lung

Having characterised the anatomy of NCC migration in the mouse lung, the next step was to investigate the mechanisms underlying NCC migration into the lung. NCCs are guided away from the neural tube and to their respective target organs by a combination of contact inhibition, permissive pathways, repulsive signals and attractive cues, as reviewed in Kulesa and Gammill (2010) and discussed in the introduction in section 1.6. NCCs migrate along permissive pathways and migratory scaffolds in cohesive streams, confined by repulsive surrounding signals and drawn to chemoattractive signalling sources. Different groups of NCCs with different spatial or temporal origins may have diverse responses to these guidance molecules and mechanisms due to NCC subgroup prespecification to follow particular migration pathways, as reviewed in Ruhrberg and Schwarz (2010).

Lung NCCs and gut NCCs have a common vagal neural crest developmental origin and early migratory pathway, so it is reasonable to hypothesise that these NCCs may respond to common signalling pathways. In order to determine whether lung NCCs are likely to be guided into the lung by cues that also guide gut NCC, a series of neural crest grafting experiments were carried out in the chick to test lung and gut NCC prespecification (Figure 4.4, below). These studies investigated whether lung and gut NCCs are prespecified to migrate into their respective target organs and allowed us to ascertain whether their common origin means that lung and gut NCCs respond to common signalling cues.

4.1 Intraspecies grafting to investigate NCC colonisation of the lung

The degree of prespecification of lung NCCs was investigated using intraspecies NCC grafting with GFP transgenic and wild-type chick embryos. GFP transgenic chickens have been engineered to express GFP ubiquitously (McGrew et al., 2004; McGrew et al., 2008). Previous to the generation of the GFP chicken strain, quail-chick neural tube grafting has been used extensively to trace quail NCC migration in chick embryos (Kalcheim and Le Douarin, 1999), including tracing quail vagal NCC migration into the chick lung (Burns and Delalande, 2005). Here a protocol similar

to that used for quail-chick grafting was employed to transplant GFP vagal neural tube and associated neural crest from GFP chicken embryos into wild-type recipients. Chick embryo microsurgery *in ovo* for intraspecies grafting and back-grafting was carried out by Dr Alan Burns.

At E1.5, the vagal neural tube and associated neural crest from GFP chicken embryos was grafted into wild-type chicken embryos at the same stage of development (n=20). GFP chick intraspecies grafting allows GFP-positive NCCs to be effectively and reproducibly traced in host embryos (Figure 4.1). The grafted GFP-positive neural tube integrates with host tissue (Figure 4.1, A, B) and GFP-positive NCCs migrate into host tissue and colonise the early gut, trachea and lung bud mesenchyme (Figure 4.1, D-F). GFP-positive NCCs from stage-matched GFP vagal neural tube grafts were found to migrate into both the gut and lungs of graft recipient embryos and form neurons in ganglia in the gut and lungs (Figure 4.2i and 4.2ii), similar to those seen in previous work (Burns and Delalande, 2005). GFP-positive ganglia and projections can be seen in the intact chick lung (Figure 4.2i and 4.2ii, C, G, K, N). In lung sections at E5.5 and E6.5 (Figure 4.2i, D, H) it is evident that more grafted GFP-positive NCCs migrate into the lung as development progresses. Tangential migration of NCCs from the gut into the lung is evident (Figure 4.2i, D, H). GFP-positive projections (Figure 4.2i and 4.2ii, G, K, N) are present in the lungs along with NCC cell bodies. Some of these projections may be extrinsic lung innervation from the vagal nerve and some may come from GFP NCCs in the lung that have differentiated to give rise to neurons. The vagal nerve is also labelled by vagal GFP neural tube grafting (Figure 4.2ii, I, L).

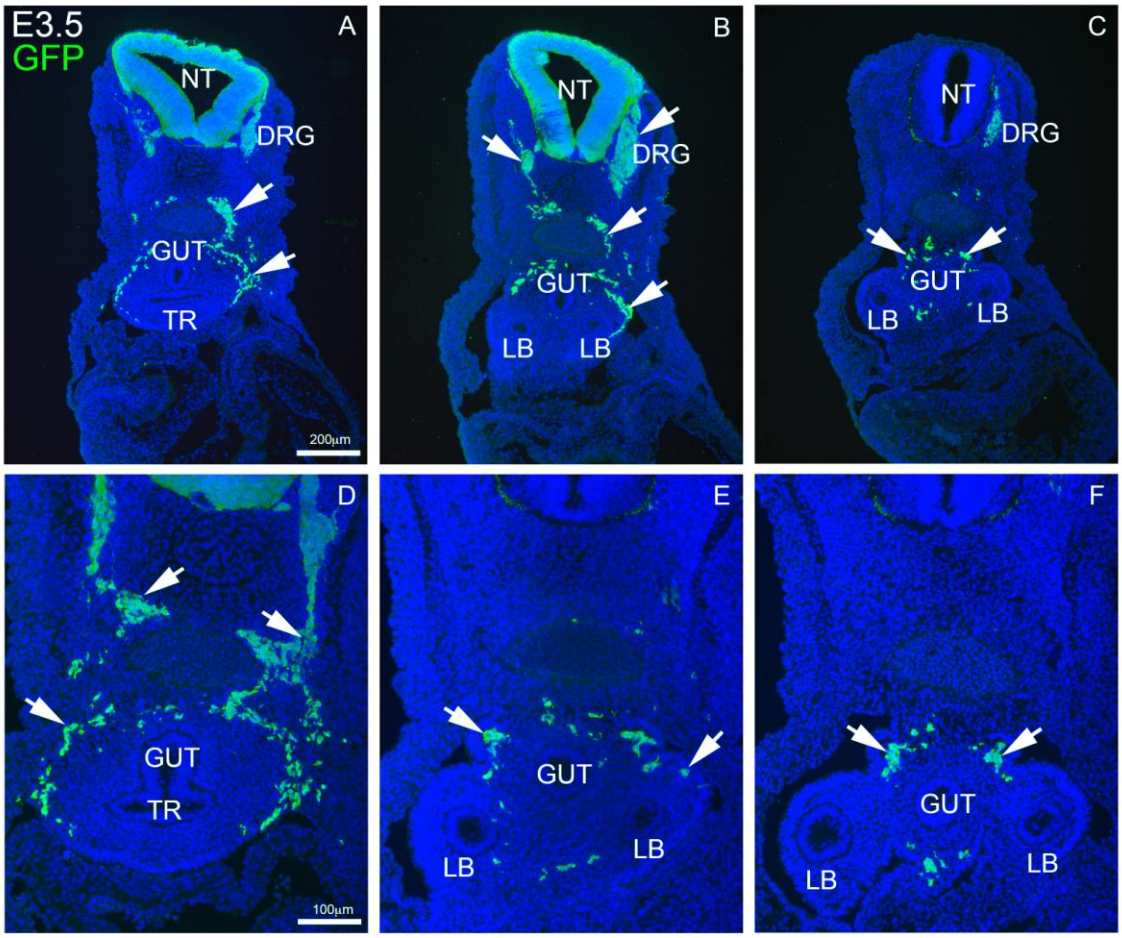

Figure 4.1 GFP chick intraspecies vagal neural tube grafting recipients at E3.5. GFP-positive vagal NCC (arrows) migrate into the host lung buds and gut. DRG: dorsal root ganglia, GUT: gut, LB: lung bud, NT: neural tube.

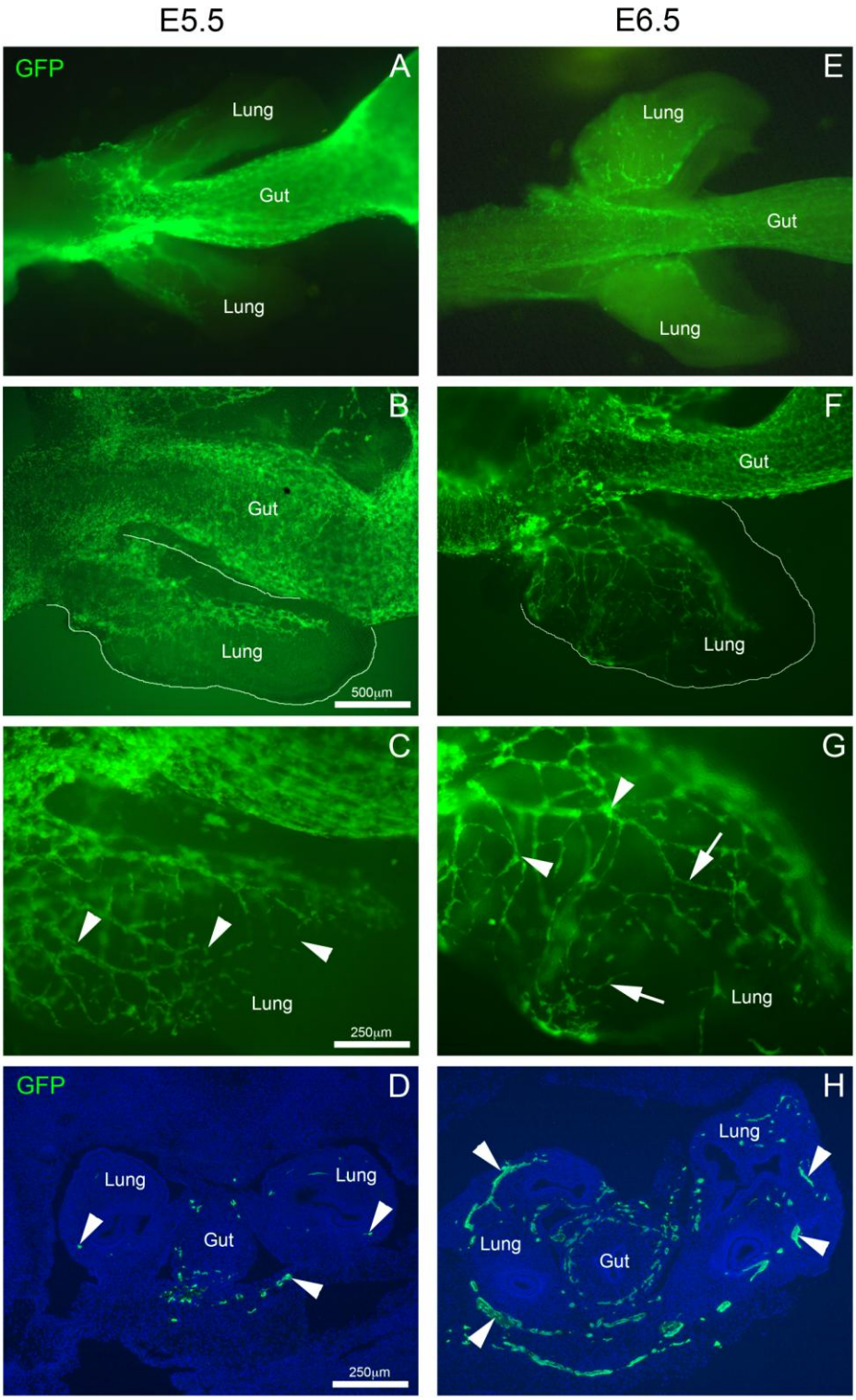

Figure 4.2i GFP vagal neural tube graft recipient lungs at E5.5 and E6.5. GFP cells are visible in lung tissue both in whole lungs (A-C, E-G, I-N) and sections (D,H) without immunohistochemical staining. A, E are unmounted and B, C, F, G are whole-mounted under coverslips. Arrows indicate projections, arrowheads indicate cell bodies and ganglia. Lungs and gut are oriented so that left = rostral, right = caudal.

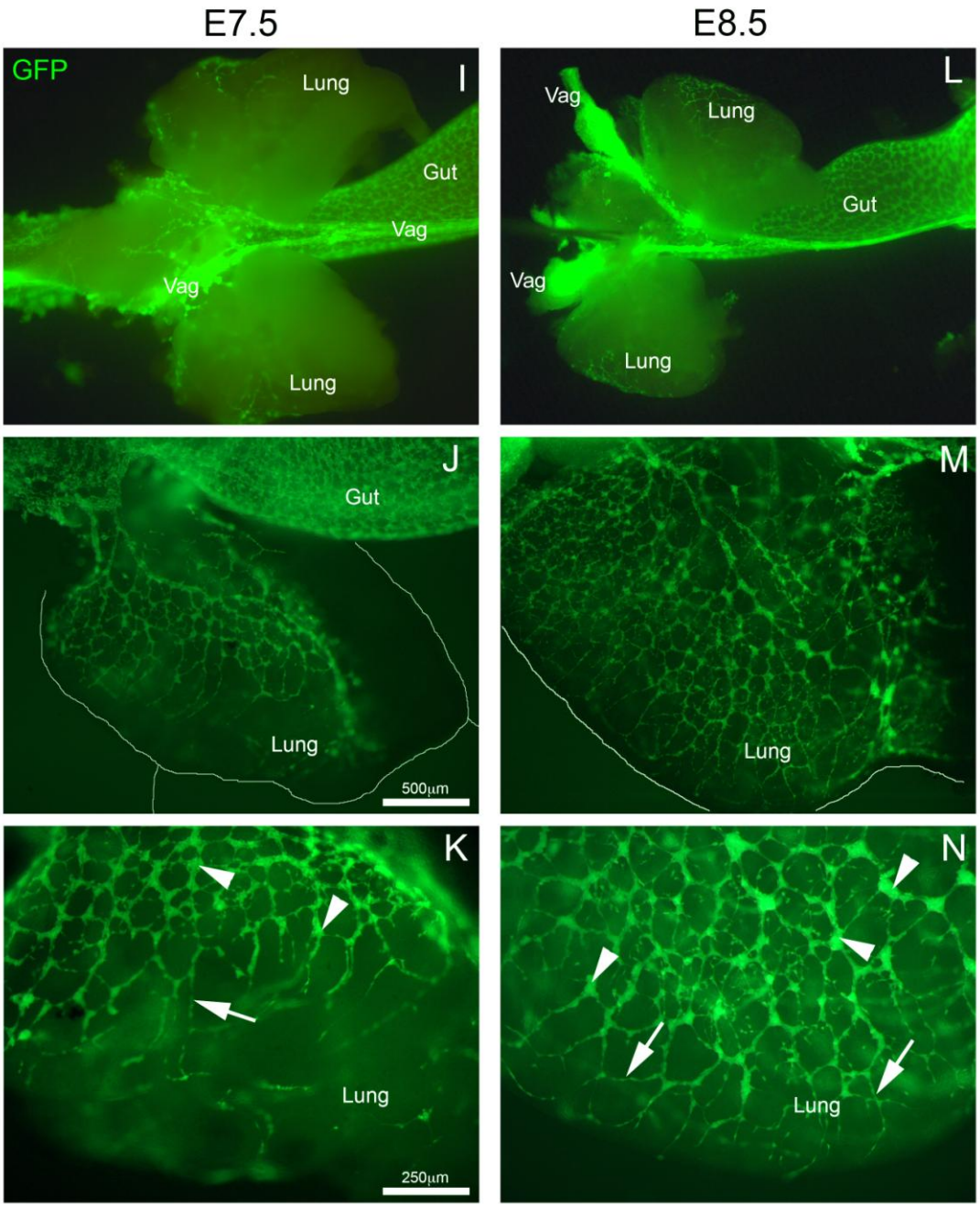

Figure 4.2ii GFP vagal neural tube graft recipient lungs at E7.5 and E8.5. GFP cells are visible in lung tissue in wholemount lungs without immunohistochemical staining. By E8.5 a neuronal network has formed in the lung. I, L are unmounted and J, K, M, N are whole-mounted under coverslips. Arrows indicate projections, arrowheads indicate cell bodies and ganglia. Vag: vagal nerve.

4.2 Intraspecies back-grafting to investigate NCC prespecification

Having characterised the migration of grafted GFP NCCs into the chick lung and gut, these chimeric chick embryos were used to further investigate the developmental potential of lung and gut NCCs. Transplanting the vagal neural tube (NT) of a GFP chick embryo into a wild-type embryo produces a chimeric embryo carrying a vagal NCC population marked by GFP expression, including NCCs in the gut and lungs. In order to investigate NCC prespecification, the lungs or gut from this chimeric embryo were dissected out and the GFP-positive NCCs in a segment of chimeric lung or gut tissue were back-transplanted into the early NCC migration pathway in the vagal neural tube region of a wild-type host (Figure 4.3). The migration of GFP-positive NCC within the recipient embryo was then traced. Testing whether NCCs in the gut are committed to colonise the same region on remigration may provide clues as to whether younger NCCs, before migration, are likely to be prespecified to enter the gut.

There are several possible outcomes of back-grafting gut and lung NCCs (Figure 4.4). If lung NCCs are committed to only enter the lung, back-transplanted GFP-positive lung NCC should migrate only into the lungs of the wild-type host embryo and not along the gut caudal to the lungs (Figure 4.4, A), whereas if lung NCCs are not committed to enter the lung, then when back-grafted they would enter both the lung and gut (Figure 4.4, C). Conversely, if gut NCCs are committed to colonise only the gut and not the lungs, then back-transplanted GFP-positive gut NCCs would migrate into and along the gut and not migrate into the lungs (Figure 4.4, B) as they would if they are not committed to the lung or gut as a target organ (Figure 4.4, C).

It is possible that gut or lung NCCs acquire specification for their target organs after entering them, and thus that experimental outcomes indicating prespecification (Figure 4.4, A) could be due to NCC differentiation with age, but by back-grafting NCCs as young as possible the potential for this effect was minimized.

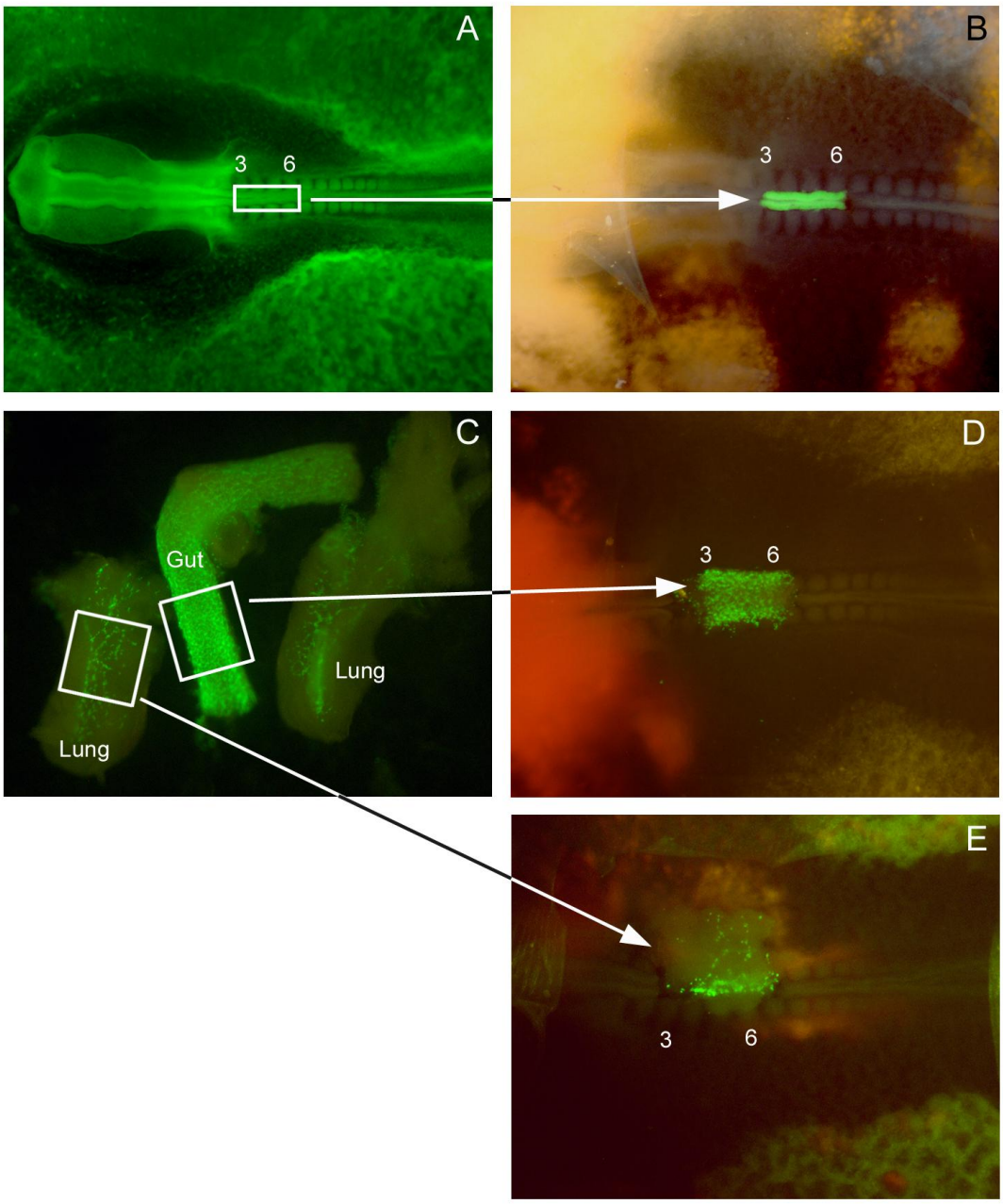

Figure 4.3 Intraspecies grafting and back-grafting of GFP-labelled NCC. GFP-positive vagal neural tube and associated neural crest from somites 3-6 is grafted into the corresponding region of a wild-type host (A, B) and the embryo allowed to develop. At E5.5 the lung and gut containing GFP NCC are harvested (C) and segments of these tissues back-grafted into wild-type hosts (D, E).

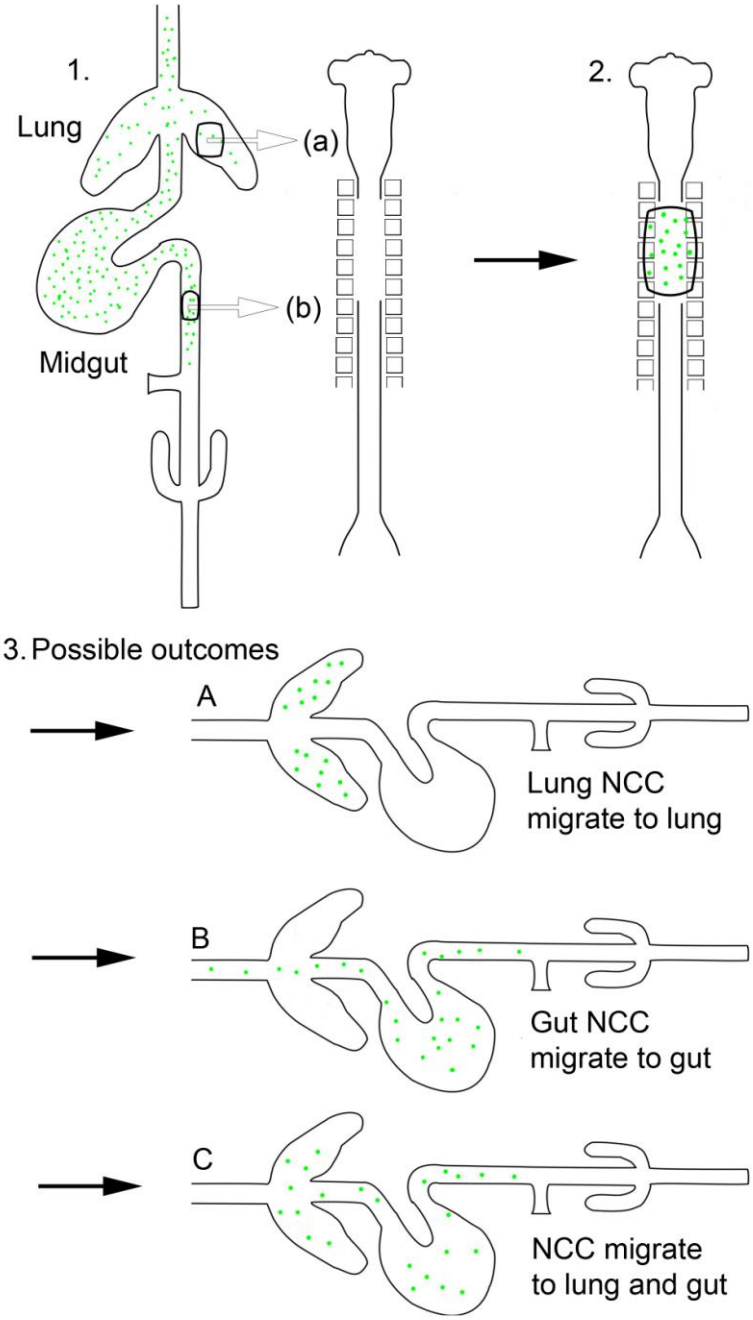

Figure 4.4 Diagram of GFP NCC back-grafting experiments and possible outcomes. 1. Segments of lung (a) or gut (b) from chimeric embryos, containing GFP-positive NCC (green) are removed from E5.5 chicks and transplanted into the ablated NT region of an E1.5 wild-type chick. 2. The back-graft recipient chick embryo is allowed to develop for a further 4 days. 3. The possible outcomes of lung and gut back-grafting are shown. Lung and gut NCC may migrate only to their original sites (A, B) indicating that they are prespecified for these targets, or they may migrate into both lung and gut regardless of their organ of origin (C).

In the next set of experiments, segments of E5.5 chimeric gut containing GFP-positive NCCs were back-grafted into the early migration pathway of E1.5 embryos (n=12). The migration pattern of back-grafted GFP-positive gut NCCs was compared to that of GFP-positive vagal NCCs from a vagal neural tube graft (n=20), to see whether back-grafted gut NCCs appear to be prespecified to enter the gut in comparison to a mixed population of vagal NCCs.

GFP-positive NCCs from back-grafted E5.5 gut tissue migrate into and colonise the gut and lung in a similar distribution to GFP-positive NCCs from an E1.5 vagal neural tube graft (Figure 4.5). The gut and lungs in dissected E5.5 chick embryos that received gut NCC back-grafts at E1.5 have a normal morphology (Figure 4.5, B), similar to that seen in vagal neural tube graft recipients (Figure 4.5, A). GFP-positive NCCs can be seen in the gut and lungs of both graft recipients at initial dissection under a fluorescent dissecting microscope (Figure 4.5, C, D) and appear to be present at similar densities in the lungs and esophagus. Back-grafted GFP-positive gut NCCs are present in recipient lungs at E7.5 (Figure 4.5, H) and these back-grafted gut NCCs are present in a similar distribution, density and morphology to vagal NCCs in the lungs of vagal neural tube graft recipients (Figure 4.5, G). However, when NCCs at the NCC migration wavefront in the gut are compared, back-grafted NCCs are less numerous at this site than NCCs from a vagal graft and have a different morphology, appearing longer and thinner (Figure 4.5, E, F). This spindle-shaped morphology appears to be restricted to back-grafted NCCs at the migration front in the gut (Figure 4.5, E, F) and is not seen in back-grafted NCCs in the rostral gut or lungs (Figure 4.5, C, D). This effect on NCC morphology may be due to the smaller number of GFP-positive NCCs transferred in gut back-grafts compared to neural tube grafts.

These findings show that NCCs back-grafted into the early neural crest migration pathway enter both the lung and gut, indicating that gut NCCs are not prespecified to enter only the gut.

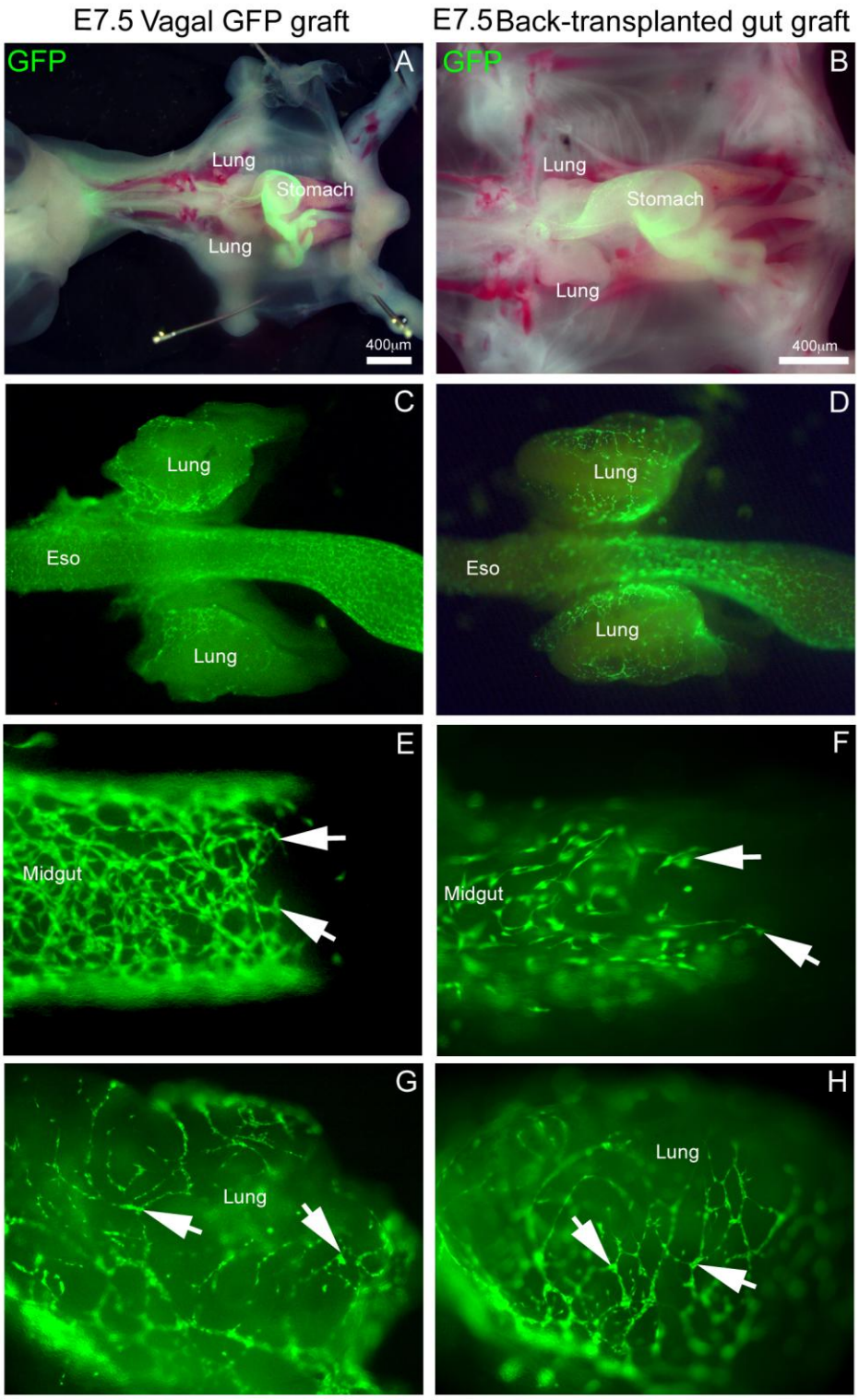

Figure 4.5 Comparison of neural tube graft and gut back-graft recipients at E7.5. GFP NCC from both vagal neural tube graft and gut back-graft colonise the gut (E, F) and lung (G, H). Arrows indicate GFP-positive NCC. Eso: esophagus.

GFP-positive NCCs from back-grafted gut tissue colonise the lung and form ganglia-like structures (Figure 4.6, B, D, F, H), as do GFP NCCs from a GFP neural tube graft (Figure 4.6, A, C, E, G). Back-grafted GFP-positive NCCs from the gut contribute extensively to the lung ganglia and extend projections (Figure 4.6, H). GFP-positive NCCs are sparser in the lung in back-grafted embryos (n=3) (Figure 4.6, C, E) than in neural tube grafted embryos (Figure 4.6, D, F). As previously discussed, this may be due to the lower number of GFP-positive NCCs present in the back-grafted gut tissue compared to the number of GFP-positive NCCs in grafted GFP neural tube, or to experimental variation in the effectiveness of the grafting process.

Fewer GFP-positive neuronal projections are visible within lungs from a gut back-grafted embryo (Figure 4.6, F, H) than in lungs from a neural tube-grafted embryo (Figure 4.6, E, G). Back-grafted gut NCCs from E5.5 donors are thus highly migratory in host E1.5 embryos despite stage differences between the graft and host, as back-grafted gut GFP-positive NCCs are present in the distal lung in similar positions to GFP-positive NCCs from a stage-matched neural tube graft (Figure 4.6, B, A).

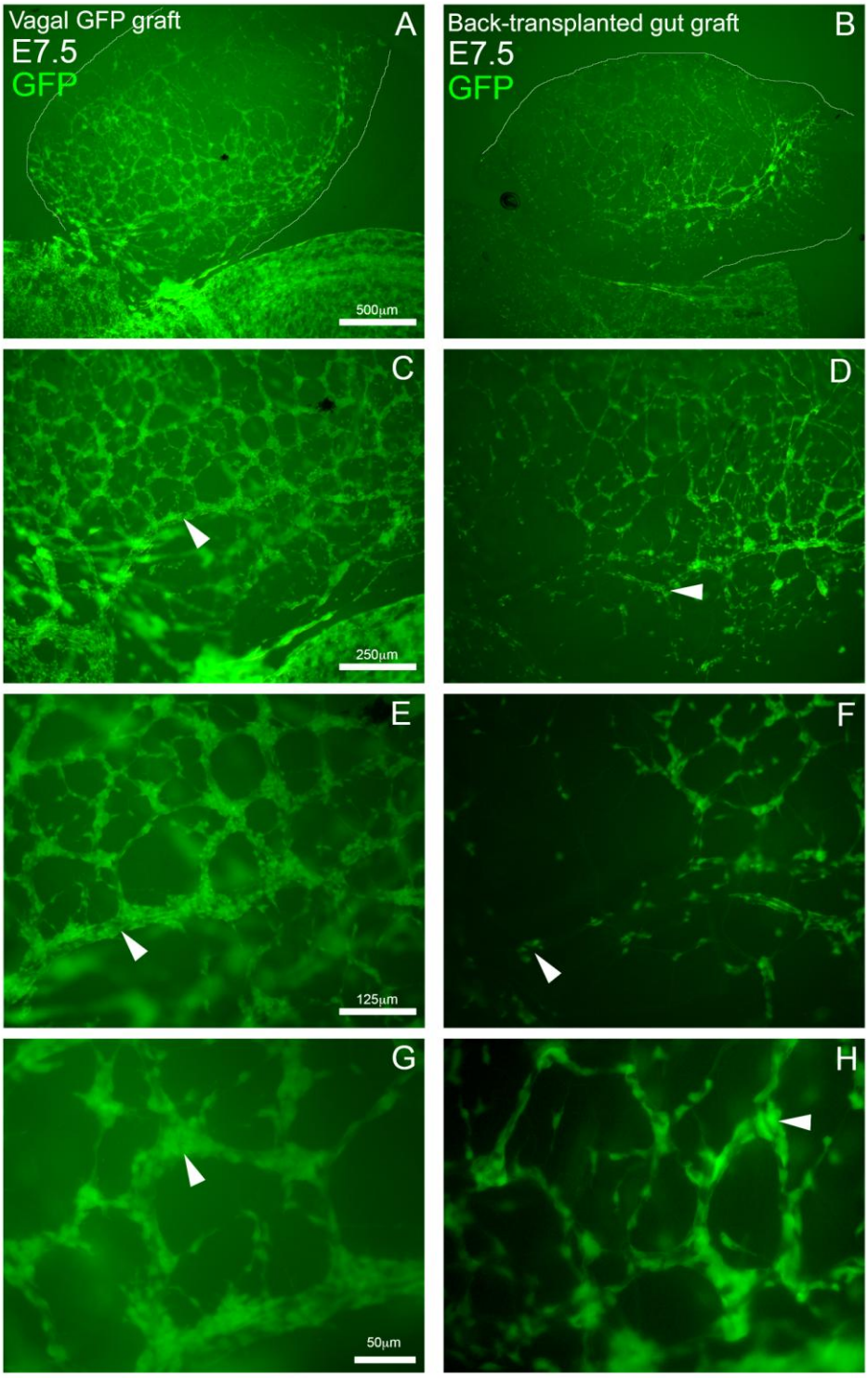

Figure 4.6 E7.5 chick lung after GFP neural tube grafting (left panel) compared to E7.5 chick lung after GFP gut NCC back-grafting (right panel). GFP NCC (green) can be seen in neural networks in lungs from both grafts. GFP cells have grouped together and extended neuronal projections, forming ganglia (arrows).

Lungs from gut back-graft recipient embryos contain GFP-positive neural crest-derived cells, GFP-negative host neural crest–derived cells and GFP-negative extrinsic innervation (Figure 4.7). Back-grafted gut NCCs contribute extensively to the lung ganglia (Figure 4.7, E-H), send out GFP-positive projections (Figure 4.7, F, G) and express the neuronal marker Tuj1 (Figure 4.7, G, H), showing that GFP NCCs from the gut can give rise to neurons in the lung.

In some cases, back-transplanted NCCs appear sparser in the lung at E8.5 than at E7.5 (Figure 4.7, A-D). However, this is likely to be due to variation in the effectiveness of the graft between different embryos, differences in the integration of the graft, or slight differences in the tissue grafted, any of which can affect the number of cells delivered to the host by different grafting experiments. Another possibility is that the expansion of the lung tissue between E7.5 and E8.5, without matching expansion of the lung NCC population and lung innervation, leads to sparser lung innervation at E8.5.

It also appears that gut GFP NCCs from back-grafted gut tissue do not contribute to the vagal nerve, as the major vagal extrinsic projections into the lung are unmarked by GFP (Figure 4.7, C, E). This is in contrast to GFP neural tube grafts, which give rise to GFP-positive cells or fibres within the vagal nerve (see Figure 4.2ii, I, L). This difference may contribute to the smaller number of GFP-positive neuronal projections seen in lungs from back-grafted embryos.

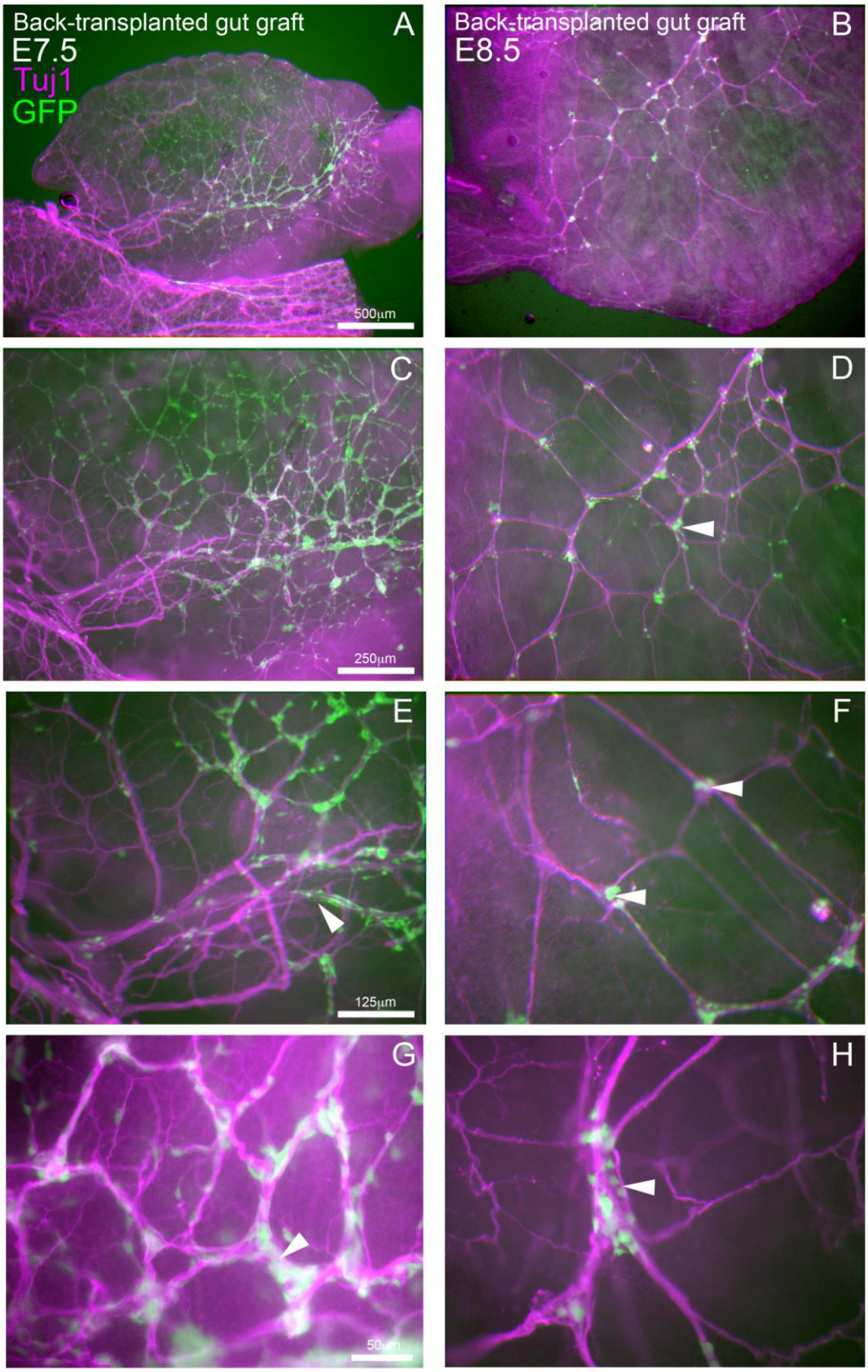

Figure 4.7 E7.5 and E8.5 chick lungs from gut back-graft recipient chick embryos. Chimeric donor tissue containing gut GFP NCC was grafted at E1.5. Tissue stained for the neuronal marker Tuj1 (magenta). GFP NCC (green) co-localise with neural tissue in both lungs. Arrowheads indicate GFP cells in ganglia.

In a second set of back-grafting experiments, back-grafts were carried out with segments of lung tissue containing GFP-positive NCCs. In all lung back-grafts that were carried out (n=18) no GFP NCCs were seen in the lung or gut in any of these embryos at E5.5 to E8.5 (not shown). In order to transplant developmentally younger, potentially more migratory lung NCCs, E5.5 lung tissue was transplanted, but GFP-positive NCC were sparse in the grafted lung tissue at this early stage. Lung tissue was also transplanted at E6.5, when GFP NCCs were present in greater numbers and at a higher density, but with similar results. In order to determine why back-grafted lung NCCs did not colonise the host embryo, unlike back-grafted gut NCCs, the graft sites in recipient chick embryos were examined (Figure 4.8). Sections through the graft sites revealed that there are fewer NCCs in the lung back-graft (Figure 4.8, C) than in the gut back-graft (Figure 4.8, B) and only very limited migration of NCCs out of the grafted tissue. In contrast, NCCs from back-grafted gut had migrated in large numbers from the grafted tissue into surrounding host tissue (Figure 4.8, B). The higher density and numbers of NCCs in the gut (Figure 4.8, E) compared to the lung (Figure 4.8, F) may be a factor that enables NCC migration from grafted gut tissue but not grafted lung tissue. Additionally, the presence of what appear to be neuronal projections from NCCs in the grafted lung (Figure 4.8, F) where gut NCCs still appear undifferentiated (Figure 4.8, E) suggests that the lack of lung NCC migration away from the graft site may be due to differentiation of the lung NCCs into neurons that are no longer migratory.

In an effort to increase the numbers of lung and gut NCCs back-transplanted into the early embryo, lung and gut NCCs were isolated from chimeric chick tissues by Fluorescent Activated Cell Sorting (FACS) and cultured before transplantation. FACS-sorted GFP-positive NCCs were cultured overnight in a ‘hanging drop’ culture system, which caused the cells to aggregate. The NCC aggregates were then transplanted into wild-type host embryos. The GFP-positive lung NCC aggregate back-grafts (n=5) did not result in GFP NCC colonisation of the lung or gut (not shown) and back-grafting of gut NCC aggregates (n=8) had a similar result, suggesting that cell aggregate transplantation is not a viable method of NCC back-grafting. No GFP cells were seen in the neural tube of grafted embryos, suggesting that cells within the aggregates did not survive or were displaced from the neural

tube. The number of cells that could be transplanted in these NCC aggregate grafts, even when multiple aggregates were transferred, was small.

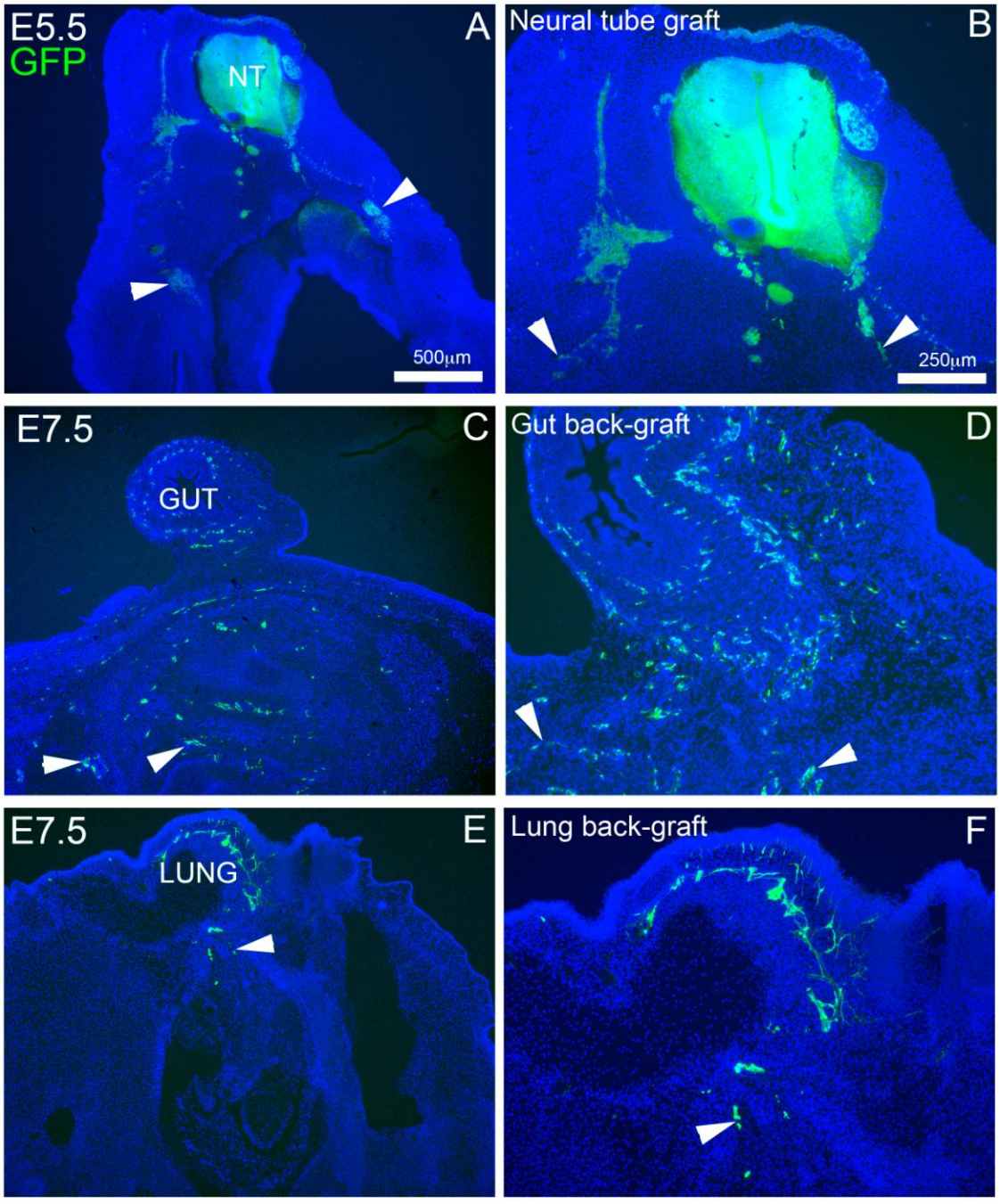

Figure 4.8 Sections through graft sites in the chick vagal neural tube for a GFP neural tube graft (A, D), chimeric gut back-graft (B, E) and chimeric lung back-graft (C, F). GFP NCCs are present in the grafted lung and gut tissue at the level of the ablated neural tube. Arrowheads indicate grafted GFP NCCs that have migrated out of the graft into host tissue. Only a few GFP-positive cells appear to have migrated a small distance from the grafted lung tissue (F).

4.3 Discussion

Vagal NCC migration into the chick lung has previously been investigated using interspecies quail-chick grafting (Burns and Delalande, 2005). In order to further examine NCC migration into the chick lung, a novel intraspecies grafting protocol was employed. The use of donor embryos from a transgenic chicken strain that expresses GFP ubiquitously (McGrew et al., 2004) allowed grafted cells and all their derivatives to be fate-mapped. In the case of intraspecies NCC grafting, the expression of GFP in grafted NCCs allowed these cells to be tracked throughout the developing embryo including the lung and gut, using either intrinsic GFP fluorescence or anti-GFP immunohistochemistry. Intraspecies GFP chick tissue grafting has recently been used to trace NCC fate in olfactory glia formation (Barraud et al., 2010). In this study, the vagal neural tube and associated neural crest of GFP chick embryos was grafted into stage-matched wild-type hosts. The migration of GFP-positive NCCs into the lungs and gut, and the formation of GFP-positive ganglia in the lung, were characterised in host embryos over several days of development. GFP-positive NCCs migrated from the grafted vagal neural tube to colonise the lung and gut. Within the lung, GFP-positive NCCs aggregated into ganglia-like structures and extended neuronal projections. The vagal nerve was also marked by GFP expression in chimeric GFP-positive neural tube-grafted embryos. This could be due to GFP-positive NCC migration along the vagal nerve in these embryos, as described in mouse development (Tollet et al., 2001). Alternatively, it is remotely possible that the grafting procedure may have transferred some cranial NCCs from above the vagal neural tube region, resulting in GFP-positive NCC contribution to the jugular ganglia and hence the vagal nerve as sensory neuron progenitors (Nassenstein et al., 2010; Thompson et al., 2010). Another alternative though unlikely source of GFP-positive vagal nerve fibres could be the nodose ganglion, which contains neural crest-derived glial cells (Ayer-Le Lievre and Le Douarin, 1982; Baker and Bronner-Fraser, 2001) that can give rise to neurons if placodal nodose ganglion neurons are ablated (Harrison et al., 1995). Nodose ganglion neurons are placode-derived. GFP-positive NCCs within the host lung expressed the neuronal marker Tuj1 and therefore differentiated to form neurons as demonstrated previously using quail-chick grafting (Burns and Delalande, 2005) and contributed to intrinsic lung ganglia. More GFP-positive cells and more organised

neuronal architecture were seen in the host chick lung as it developed and grew from E5.5 to E8.5.

Previous to the generation of the GFP chicken strain, the technique of interspecies grafting of quail tissue into chick embryos has been used for cell fate tracing (Le Douarin and Kalcheim, 1999; Le Lievre and Le Douarin, 1975). Quail embryo tissue grafted into a chick embryo host survives and integrates with the host tissue without rejection. Quail tissue can be distinguished from chick tissue using immunostaining against the quail cell nuclear marker protein QCPN, allowing the fate of grafted quail tissue and its derivatives to be traced. Quail and chick embryos have very similar embryology, which contributes to the integration of grafted quail tissue in chick recipients, although chick embryo growth is greater in the later stages of development. Quail-chick neural tube grafting has been used to trace quail NCC migration in the chick embryonic gut (Burns et al., 2002; Le Douarin, 1993; Le Douarin and Teillet, 1973) and was used in the characterisation of vagal NCC migration into the chick lung from the foregut (Burns and Delalande, 2005). It has also been used to investigate NCC specification and potential in back-grafting experiments (Rothman et al., 1990; Rothman et al., 1993). Although more difficult to accomplish and sustain than in chick, back-grafting has been used in mouse embryos, for example to investigate the cell-autonomous and non-autonomous effects of *Ret* deletion on NCC behaviour (Bogni et al., 2008). Mammalian tissue has also been transplanted into chick hosts to trace cell developmental potential (Fontaine-Perus et al., 1997; White and Anderson, 1999) and to study mammalian cell behaviour in the accessible *in vivo* environment provided by the chick embryo, as reviewed in Goldstein (2010). Other methods, including electroporation with fluorescent markers (Itasaki et al., 1999) and cell injection with vital dyes (Serbedzija et al., 1991), have also been used to track cell migration in the chick embryo, as reviewed in de Bellard and Bronner-Fraser (2005); Kulesa et al. (2009). However, these methods are less useful as they may mark unwanted cell populations and the vital dye or electroporated construct can dilute over cell divisions. For a proliferating cell population such as NCCs, the latter may mean that the signal will be lost in the descendants of marked cells.

The GFP chick intraspecies grafting protocol has several advantages over quail-chick grafting. GFP-positive cells can be seen in the live chimeric graft recipient without staining, allowing the success of the graft to be checked *in ovo*, whereas the quail-chick graft requires the embryo to be killed, fixed and stained before the success of the graft can be assessed. GFP chick grafting makes back-grafting of NCCs easier, as GFP-positive NCCs in live graft tissue can be examined and their density checked before grafting the tissue into a host embryo. Also, GFP expression in this transgenic chick line is cytoplasmic and so marks the entire cell, allowing projections to be seen in GFP-positive graft-derived neurons. This allows us to see neuronal networks that are not visible when using quail-chick grafting, as the quail cell marker used to visualise quail cells marks only the cell nucleus. Additionally, intraspecies grafting eliminates any species differences that could be present between grafted quail tissue and chick recipient embryos.

NCCs can be prespecified to follow certain migration pathways by the expression of receptors that respond to certain signalling cues, and can have restricted differentiation potential within subgroups (Mosher et al., 2007; Ruhrberg and Schwarz, 2010). One example is the expression of the signalling receptor Neuropilin1 in intermediate-migrating but not early-migrating trunk NCC subgroups as they migrate away from the dorsal neural tube, so that they are prespecified to respond differently to semaphorin signalling and follow different migration pathways (Schwarz et al., 2009b). Another example occurs in enteric NCCs where the netrin receptor DCC is thought to be expressed in a subpopulation of NCCs and guides them into the submucosa and pancreas (Jiang et al., 2003; Young et al., 2004). Earlier in migration, a subset of NCC undergoes contralateral migration and is prespecified to form nociceptors in the dorsal root ganglia (George et al., 2007). NCC prespecification, as opposed to environmental determination of fate, is an ongoing field of study, as reviewed in Lefcort and George (2007); Ruhrberg and Schwarz (2010). If NCCs that colonise the lung are prespecified to enter the lung by the expression of different receptors than those on gut NCC, then back-transplanted gut NCCs should not enter the lung, as they would be unable to respond to the hypothetical lung-specific signalling cue.

The results of the gut and lung neural crest back-grafting experiments that we carried out in the chick embryo showed that back-transplanted GFP-positive gut NCCs migrated indiscriminately into both lung and gut tissue, and thus that gut NCCs are not prespecified to enter only the gut. Since the lung can be colonised by back-grafted gut NCCs it is unlikely that NCCs that have migrated into the lung were prespecified to enter the lung, although this was not proven. It is possible that NCCs that migrate into the lung transiently express a particular receptor during migration into the lung in response to local environmental cues, and so that back-transplanted gut NCC can be induced by migration conditions to express this receptor.

The results shown here indicate that vagal NCCs in the gut are likely to migrate into the lung under the influence of a signalling cue or cues that also guides NCCs in the gut and suggests that because of their shared developmental origin and lack of prespecification, lung and gut NCCs are able to respond to the same set of signalling cues. It is also possible that NCCs migrating along the foregut do not initially migrate into the lungs through a response to a chemoattractive signalling molecule, but are diverted into the tissue surrounding the trachea or bronchi by stochastic migration. In contact inhibition between NCCs in the early migration pathway, NCCs are induced to migrate away from areas of high NCC density, near the neural tube (Carmona-Fontaine et al., 2008). Contact inhibition could theoretically drive lateral migration into the lung through the mesenchyme early in development, when the lung buds have not separated from the gut. This hypothesis will be discussed further in the conclusion (chapter 7).

It has been demonstrated here that back-grafted gut tissue integrated with the host neural tube region and GFP-positive NCCs migrated out of the graft and into the surrounding tissue. Gut NCCs back-grafted into the trunk rather than the vagal neural tube region have previously been shown to re-enter the migration stream and migrate to distant sites, but not back into the gut, in younger host embryos in quail-chick chimera back-grafting experiments (Rothman et al., 1990; Rothman et al., 1993). These results were thought to be likely due to the axial position of the back-grafts rather than loss of NCC potential to enter the gut (Rothman et al., 1990), which is supported the results shown here from back-grafting into the vagal region.

The use of GFP chick tissue for grafting and back-grafting made the analysis of graft success and the placing of grafted tissue easier in this project than in previously published studies, as GFP-positive NCCs are visible in live grafted chimeric chick tissue using a fluorescent dissecting microscope. In addition to colonising the gut and lung, GFP-positive NCCs from the back-grafted gut contribute to intrinsic lung ganglia and differentiate to form neurons, as shown by their expression of the neuronal marker Tuj1.

There appeared to be a reduced number of GFP-positive cells in gut back-transplant graft hosts compared to neural tube graft hosts, in addition to some variation between individual grafts. This was probably due to the reduced number of GFP-positive NCCs in the grafted tissue, as more NCCs were transplanted with the grafted vagal neural tube than were transplanted in a similarly sized piece of chimeric gut. The reduced number of grafted NCCs did not appear to impair NCC colonisation of the lung, as GFP-positive NCCs were seen throughout the lung and in a similar distribution to NCCs from a vagal neural tube graft. The gut back-grafted GFP-positive NCCs were also developmentally older than the vagal NCCs attached to the grafted vagal neural tube, as the former were grafted at E5.5 and the latter at E1.5, but this appeared to have no effect on their motility or their ability to colonise the lung.

Back-grafted gut NCCs had a different appearance at the gut migration front to NCCs from a vagal neural tube graft (Figure 4.5). This differing morphology may stem from the smaller number of NCCs transferred in gut back-grafting than in neural tube grafting, as similar spindle-shaped NCC morphology was observed at the migration wavefront in the gut when vagal NCCs were experimentally reduced (Barlow et al., 2008). In that study, NCCs at E4 in the gut had a thinner, less networked appearance after vagal NCC ablation. Interestingly, the decreased density of NCCs at the enteric NCC migration front in the midgut does not seem to have affected NCC colonisation of the lung, suggesting that NCC colonisation of the lung depends on NCC density on the foregut rather than the total number of NCCs that pass through the gut.

Although gut NCCs successfully migrated in the host embryo when back-transplanted, lung NCC from back-grafted lung tissue failed to migrate into the host embryo. Further examination of the graft site revealed that although the lung graft had integrated with the host tissue, GFP-positive cells had not migrated away from the graft site as they did in gut back-grafts. GFP-positive NCCs in the grafted lung tissue appeared to have a more differentiated phenotype than NCCs from grafted gut tissue. Neural crest-derived cells in the lung had projections and appeared to have aggregated into ganglia-like structures in contrast to NCCs in the grafted gut tissue, which were not aggregated and had no long neuronal projections. Interestingly, this indicates that NCCs in the lung may differentiate sooner than NCCs in the gut, losing their migratory capability and thus their ability to re-enter the migratory pathway when back-grafted. This potential difference in the timing of NCC differentiation could be further investigated by examining the timing of acquisition of neuronal markers such as HuC/D or NeuN in lung and gut neural crest-derived tissue. Cranial NCCs in different subpopulations have been shown by back-grafting to have differences in the timing of differentiation, as late-migrating cranial NCCs in the branchial arches lose migratory ability earlier than early-migrating cranial NCCs that contribute to the trigeminal ganglia (McKeown et al., 2003). Different NCC subpopulations may have differences in their timing of differentiation due to the differing environmental cues they encounter during migration, as reviewed in Ruhrberg and Schwarz (2010). Due to the relatively long distances that they travel in order to fully colonise the gut, NCCs that remain in the gut could be expected to retain their migratory ability longer than NCCs that migrate from the gut into the lung, which travel a comparatively short distance. This hypothesis could also be tested by backgrafting gut NCCs from older embryos, when the gut NCCs have differentiated to form neurons and glia, and comparing their behaviour to that of backgrafted lung NCCs. It is also possible that the lower numbers of NCCs in grafted lung tissue compared to grafted gut tissue meant that there were too few GFP-positive NCCs transferred in lung back-grafting to colonise the host embryo in significant numbers. Another possibility is that with fewer NCC present in the grafted lung tissue, population pressure on NCC sto migrate out into the host embryo was lower and so NCC migration out of the graft was less prevalent. This hypothesis could be assessed by successfully FACS-sorting GFP-positive vagal or gut NCCs and embedding them in a migration-permissive matrix at various densities,

then grafting pieces of this matrix into the vagal neural tube region and observing differences in migratory behaviour of NCCs grafted at different densities.

Lung and gut NCCs have a shared developmental origin and follow similar early migration pathways. If lung and gut NCCs are not prespecified to enter their target organs, as is indicated by these experiments, they are likely to respond to a common set of signalling cues. The signalling cues and transcription factors that are involved in gut NCC migration have been extensively investigated, providing a list of candidate molecules including RET, GDNF, DCC and Sox10 that could be assayed to see whether they play a role in NCC colonisation of the lung (Table 1.2, section 1.7.4).

5. Chapter 5: The RET signalling pathway in neural crest cell development in the lung

Having characterised NCC migration into the lung (chapter 3), and shown that gut NCCs do not appear to be prespecified to enter their target organs (chapter 4), the shared developmental origin of lung and gut NCCs was considered in order to compose a list of potential signalling cues that could be involved in NCC migration into the lung. If lung and gut NCCs are not prespecified they are likely to respond to a common set of signalling cues, indicating that similar pathways could be involved in lung and gut NCC migration. The next step was to investigate whether any of several signalling molecules already known to be involved in gut NCC guidance (Table 1.2, section 1.7.4) also play a role in guiding NCCs to migrate into the lungs.

The GDNF receptor RET and its co-receptor GFRa1 were selected as candidate molecules for neural crest guidance into the lung for the following reasons: (i) previous reports using organotypic mouse lung culture with GDNF beads show lung NCC are attracted to GDNF, indicating GDNF involvement in the formation of lung innervation (Tollet et al., 2002). (ii) RET and GFRa1 have previously been shown to be expressed in enteric and lung NCCs in the chicken embryo (Burns and Delalande, 2005). (iii) The RET-GDNF pathway is important for the migration of NCCs along the gut to form the intrinsic ganglia of the enteric nervous system as shown in *Ret* mutant mouse analysis (Schuchardt et al., 1994) and as reviewed in Burns and Thapar (2006), as well as in parasympathetic PNS and kidney development as reviewed in Airaksinen and Saarma (2002). In *Ret* (Schuchardt et al., 1994) and *Gfra1* -/- (Enomoto et al., 1998) mice the majority of the gut caudal to the stomach is not colonised by NCCs. (iv) In addition to gut aganglionosis, *Ret* mutant mice have a depressed ventilatory response to inhaled CO_2 (Burton et al., 1997), suggesting that development of chemosensitive lung neurons might be deficient in *Ret* mutants. (v) Finally, after the experiments in this thesis were carried out and published, a deficiency in intrinsic ganglia in the lung and trachea was described in *Ret* homozygous mutant mice (Langsdorf et al., 2011), suggesting that the RET signalling pathway is necessary for the development of intrinsic lung innervation.

In order to test the involvement of the RET signalling pathway in guiding NCC migration into the lung an organotypic culture system was utilised to test whether GDNF is sufficient to attract NCCs within the lung (section 5.2), and to test the putative guidance molecule BDNF (section 5.4). In complementary experiments it was tested whether the RET receptor and GFRa1 co-receptor are necessary for NCC lung colonisation by analysing the lungs of *Ret* -/- and *Gfra1* -/- mutant mouse embryos (section 5.2). Lung innervation in a number of other candidate gene mutant mouse strains was also analysed, but no lung innervation defects were observed in *Dcc* and *Nrp1* mutant mouse analysis (section 5.4).

In addition to investigating signalling molecules that could guide NCCs into the lung, the interaction of NCCs with blood vessels in the lung was examined to investigate potential guidance mechanisms other than diffusible signalling molecules for NCCs in the lung, such as migration along a substrate (section 5.3).

Although RET has been shown by *in situ* hybridization to be expressed in NCCs in the developing chicken lung (Burns and Delalande, 2005), this finding had not been demonstrated in mouse. Therefore it was first confirmed that RET is expressed in enteric and lung NCCs in the mouse at E12.5 using *in situ* hybridisation (Figure 5.1). This stage was chosen for examination because it is the stage at which NCCs begin migrating into the mouse lung, and so a receptor necessary for the migration of NCCs into the lung is likely to be expressed at this stage. The results showed that RET was clearly expressed in tissues used as internal positive controls, including the sympathetic ganglia (Figure 5.1, A). RET expression was confirmed in NCCs around the gut (Figure 5.1, C) and in individual NCCs in the lung buds (Figure 5.1, C, D). The extent of RET staining was consistent with the numbers of NCCs usually seen in the mouse lung at E12.5, as shown in previous chapters (chapter 3, Figures 3.1 and 3.2). RET could therefore plausibly be involved in guiding NCCs to their targets in the lung given its spatiotemporal pattern of expression.

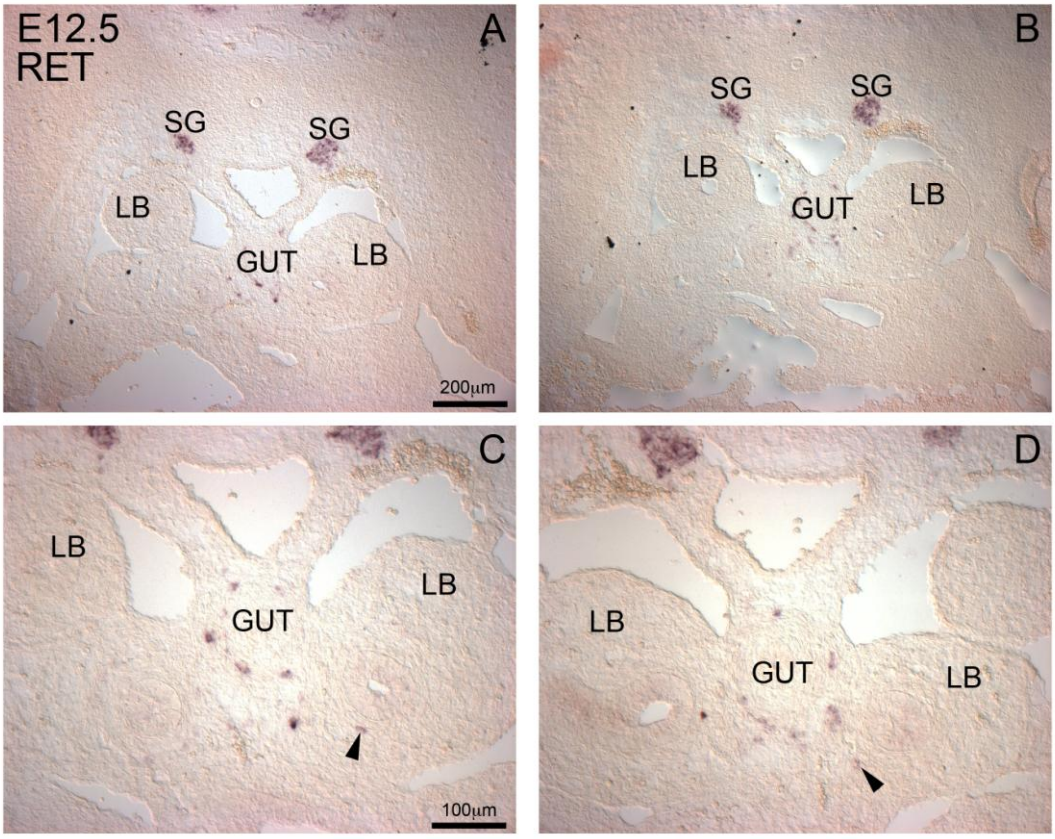

Figure 5.1 E12.5 mouse transverse sections after *in situ* hybridisation against RET transcripts. RET is expressed in NCCs surrounding the gut and in NCCs that are migrating tangentially from the gut into the lung buds (arrowheads). GUT: Gut, LB: Lung bud, SG: Sympathetic ganglia.

5.1 Migration of neural crest cells in organotypic lung culture

An organotypic lung culture system based on the protocol used by Tollet et al (Tollet et al., 2002) was established and optimised in order to examine the migration of NCC within the lungs and to investigate their migratory responses to the diffusible chemoattractive RET ligand GDNF. Lungs from chick, mouse and human embryos were initially cultured at several stages: mouse lungs and lung segments from stages E11.5 to E15.5, chick lungs at E6.5 and E7.5, and human lung segments at 10 and 11 weeks of development.

Mouse lungs were used for the majority of organotypic culture experiments for three reasons. 1) They survived best in culture, for periods of up to 6 days while chick and human lung cultures only survived 4 days. Airway peristalsis was observed in mouse lungs until day 5, a sign that the airway smooth muscle tissue was functional over an extended period of time. 2) Using *Wnt1Cre:Rosa26YFP* mouse lungs, YFP-

expressing NCC could be easily tracked over several days using live imaging fluorescence microscopy. 3) Mouse lungs were also much more consistently available at a range of suitable stages than human fetal lungs, although the latter were used in some experiments when available. Mouse E12.5-E13.5 lungs were used for analysis, as at this stage the lungs had a visible population of YFP cells and they survived well in culture due to their young age and small size. Older stages were more prone to necrosis, probably because the larger sized lungs were unable to receive sufficient nutrients in culture to sustain the tissue. In younger E11.5 lungs very few YFP cells were visible, as insufficient NCC migration into the lung had occurred before the lung was dissected and cultured.

Following culturing of E12.5 to E13.5 *Wnt1Cre:Rosa26YFP* mouse lungs, lung tissue was collected and immunostained for the marker smooth muscle actin (SMA) in order to examine airway smooth muscle (ASM) preservation. Tissue was also immunostained for the NCC marker YFP, in order to look at NCCs and neural crest-derived tissue, or the neuronal marker Tuj1 in order to see neuronal tissue. In E13.5 cultured lungs, lung structure continues to develop as evidenced by the branching of airways (Figures 5.2 and 5.3, A, B, C, D), although the lung undergoes flattening, as seen in the cross sections in the centre panel. NCCs, ganglia and neuronal projections are present around the airways (Aii, Bii, Cii, Dii, Figure 5.2 and Figure 5.3). YFP-positive neural crest-derived cells (Figure 5.2, Aii, Bii, Cii, Dii) and Tuj1-positive neuronal tissue (Figure 5.3, Aii, Bii, Cii, Dii) are present adjacent to the SMA-positive ASM layer surrounding epithelial tubules over the first four days of culture, as previously described in freshly dissected embryonic mouse lungs (chapter 3, section 3.3). ASM and NCC distribution in cultured lungs is similar to that in embryonic mouse lungs (Figures 3.7 and 3.8), validating the organotypic lung culture system.

Organotypic culture was also carried out using E6.5 chick lungs (Figure 5.4) and E7.5 chick lungs. Chick lungs survived less well in culture than mouse lungs, but airway peristalsis was observed in culture until day 3. By day 4 (Figure 5.4, D, H) the lungs had decreased in size and large areas of black necrotic tissue could be seen. The structure of the airways was not maintained in culture, as the airways and air sacs in the lung grew but did not appear to undergo branching. Chick lungs are

larger than mouse lungs at comparable embryonic stages, contributing to the difficulty of culturing them. In addition, chick lung NCCs could not be visualised in culture as was possible with YFP-expressing NCCs in *Wnt1Cre:Rosa26YFP* mouse lungs.

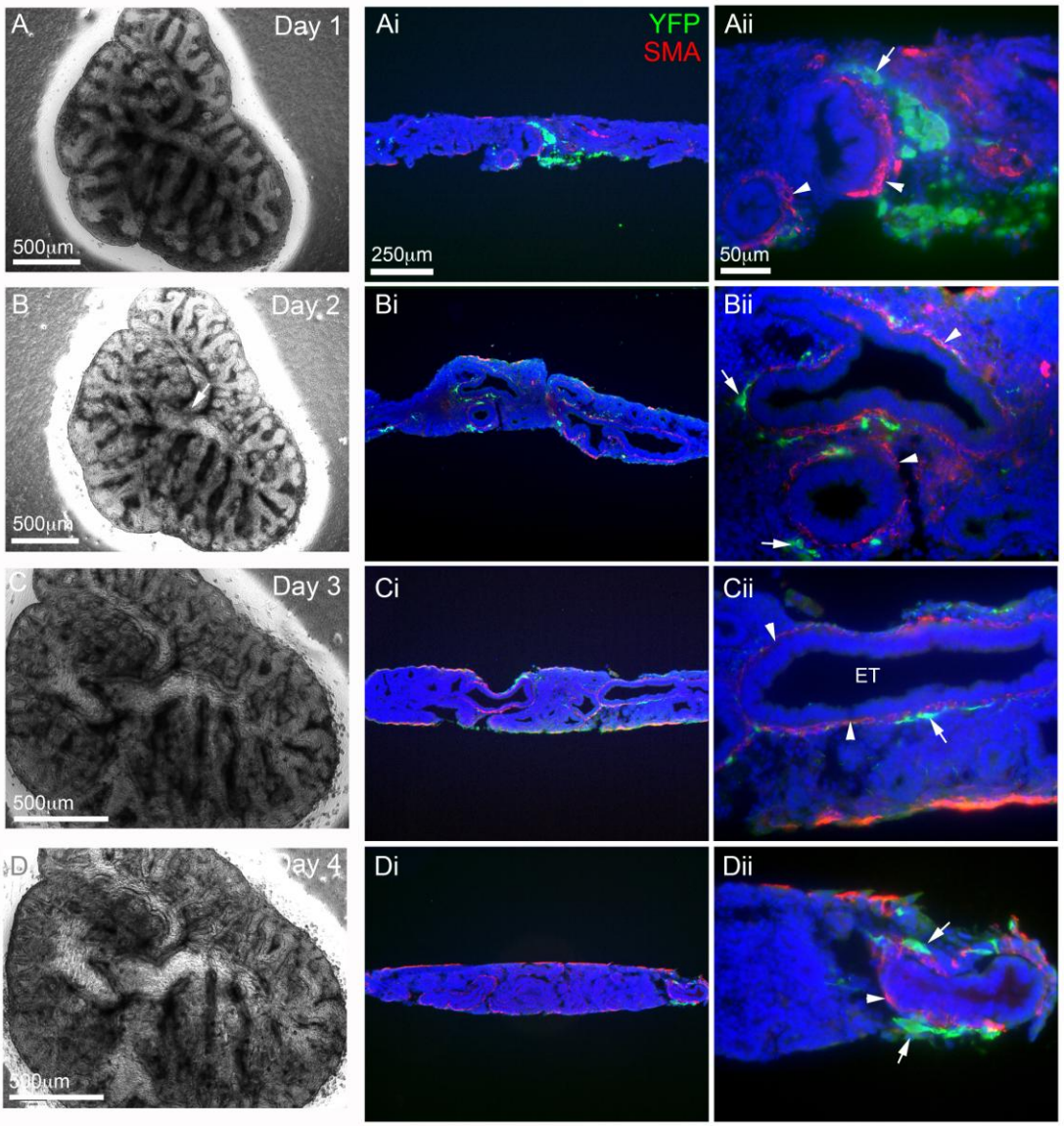

Figure 5.2 E13.5 *Wnt1Cre:Rosa26YFP* lungs and lung NCCs survive and develop in culture for 4 days. Cryosections from lungs cultured for 1 to 4 days (middle and right panels) were stained for YFP (green) and SMA (red). Neural crest-derived tissue (arrows) and ASM (arrowheads) continue to develop in culture (Aii-Dii). Light micrographs of cultured E13.5 lungs (A-D) show an increasingly intricate branching structure of airways over four days. The lungs maintain internal epithelial tubule structure, but undergo some flattening in culture (Ai-Di).

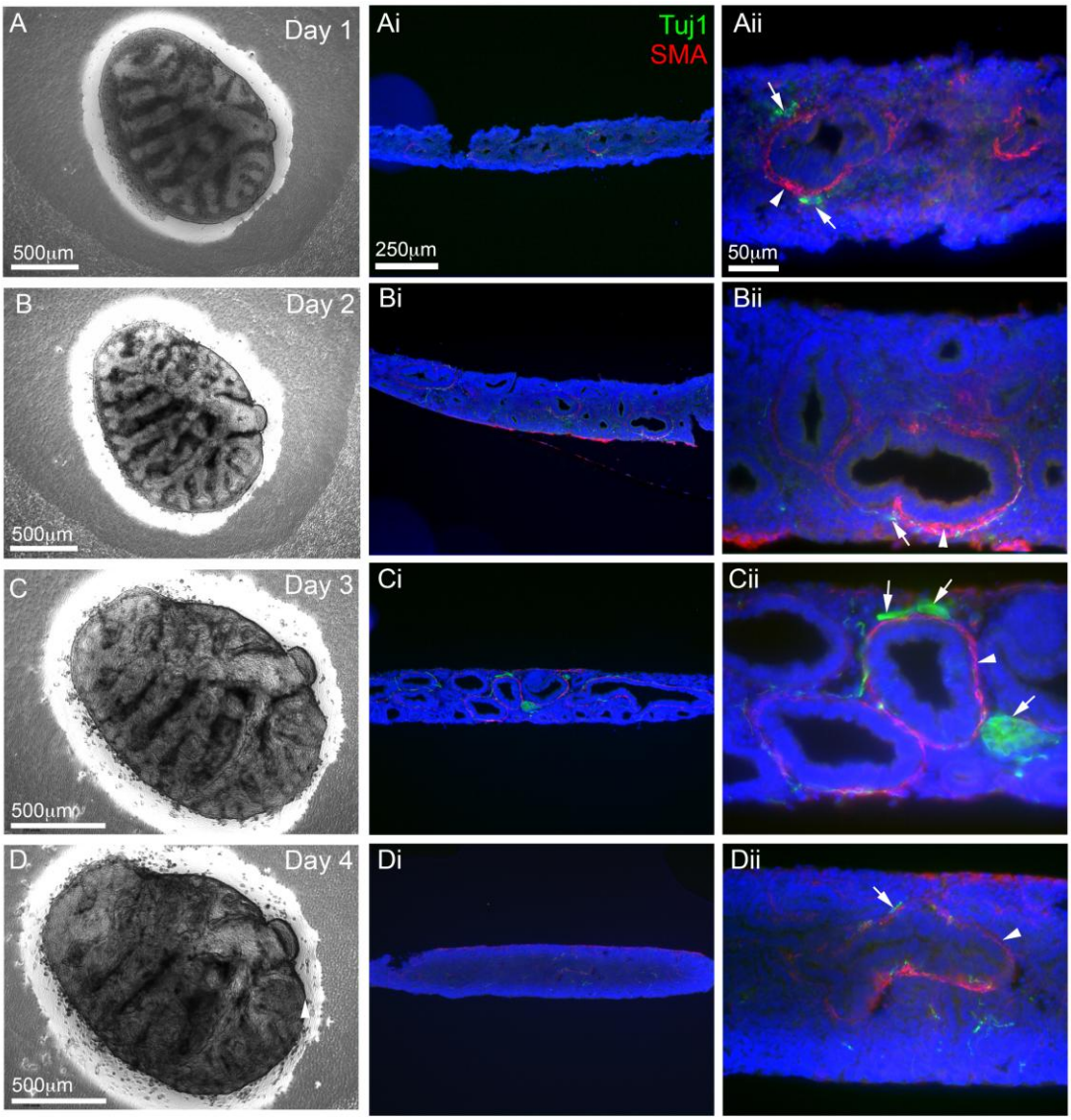

Figure 5.3 Intrinsic neurons and neuronal tissue survive in cultured lungs for 4 days. Light micrographs of E13.5 wild-type lungs in culture (A-D) show airway branching. Cryosections through cultured E13.5 lungs from 1 to 4 days in culture were stained for the neuronal marker Tuj1 (green) and SMA (red) (Ai-Di, Aii-Dii). Neurons (arrows) and ASM (arrowheads) continue to develop around the airways in culture as shown in vivo (chapter 3). Tuj1 staining is seen in similar positions and cells as YFP staining (Figure 5.2).

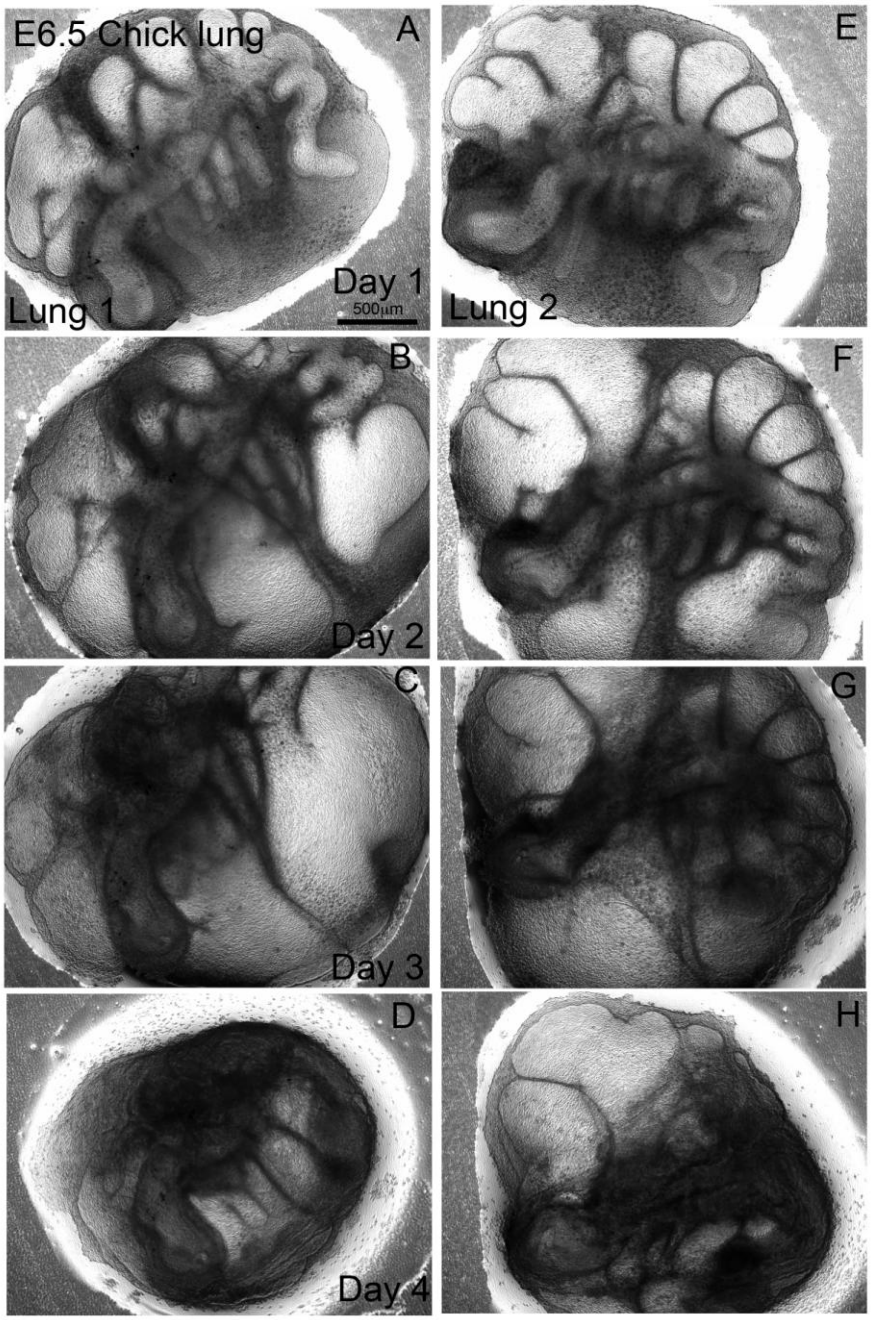

Figure 5.4 E6.5 chick lung culture. The chick lung survives in culture for 3 days, but is not as robust as the mouse lung. The development of the airways and air sacs continues, but by day 3 (C, G) dark necrotic tissue is visible around the central airway. By day 4 (D, H), the lungs had visibly decreased in size and large areas of necrotic tissue (black) could be seen. The structure of the airways is not well preserved, as the air spaces in the lung grow but do not subdivide.

Having optimised a protocol for E12.5-E13.5 mouse lung organotypic culture, the next step was to test the effect of diffusible GDNF on lung NCC migration by placing GDNF-soaked beads onto E12.5 *Wnt1Cre:Rosa26YFP* cultured lungs (n=15) (Figure 5.5i and ii). Figure 5.5ii shows the green channel data from Figure 5.5i in isolation. Control beads soaked in PBS did not attract NCCs (Figure 5.13, below). Up to 3 beads were placed on each lung in various positions and accumulation of YFP-positive cells observed in culture. Neurite extensions, previously described around GDNF beads in cultured lungs (Tollet et al., 2002) were not observed due to the low resolution available in live imaging of the cultured lungs.

Neural crest cells were seen to migrate towards beads containing GDNF at a concentration of 250 ng/μl (indicated by arrows) in whole organ lung cultures over several days. Beads placed near existing NCCs at the trachea (Figure 5.5i, B, E, H, K, N) attracted NCCs more quickly and at greater qualitative density than beads placed near the periphery of the lung (Figure 5.5i, C, F, I, L, O), probably due to the closer proximity of NCCs. While proximal beads were surrounded by NCCs on day 2 of culture, it took until day 3 for a number of NCCs to reach more peripherally located GDNF beads. However, even GDNF beads on the lung periphery attracted NCCs, indicating that GDNF is an effective lung NCC chemoattractant even at long distances. Alternatively, GDNF may promote undirected NCC movement causing NCC to aggregate around GDNF beads over time, but this interpretation was not further investigated.

These results suggest that the RET signalling pathway, acting through GDNF, may be involved in NCC guidance into the lung, confirming the earlier results of Tollet et al (Tollet et al., 2002) using a similar culture system.

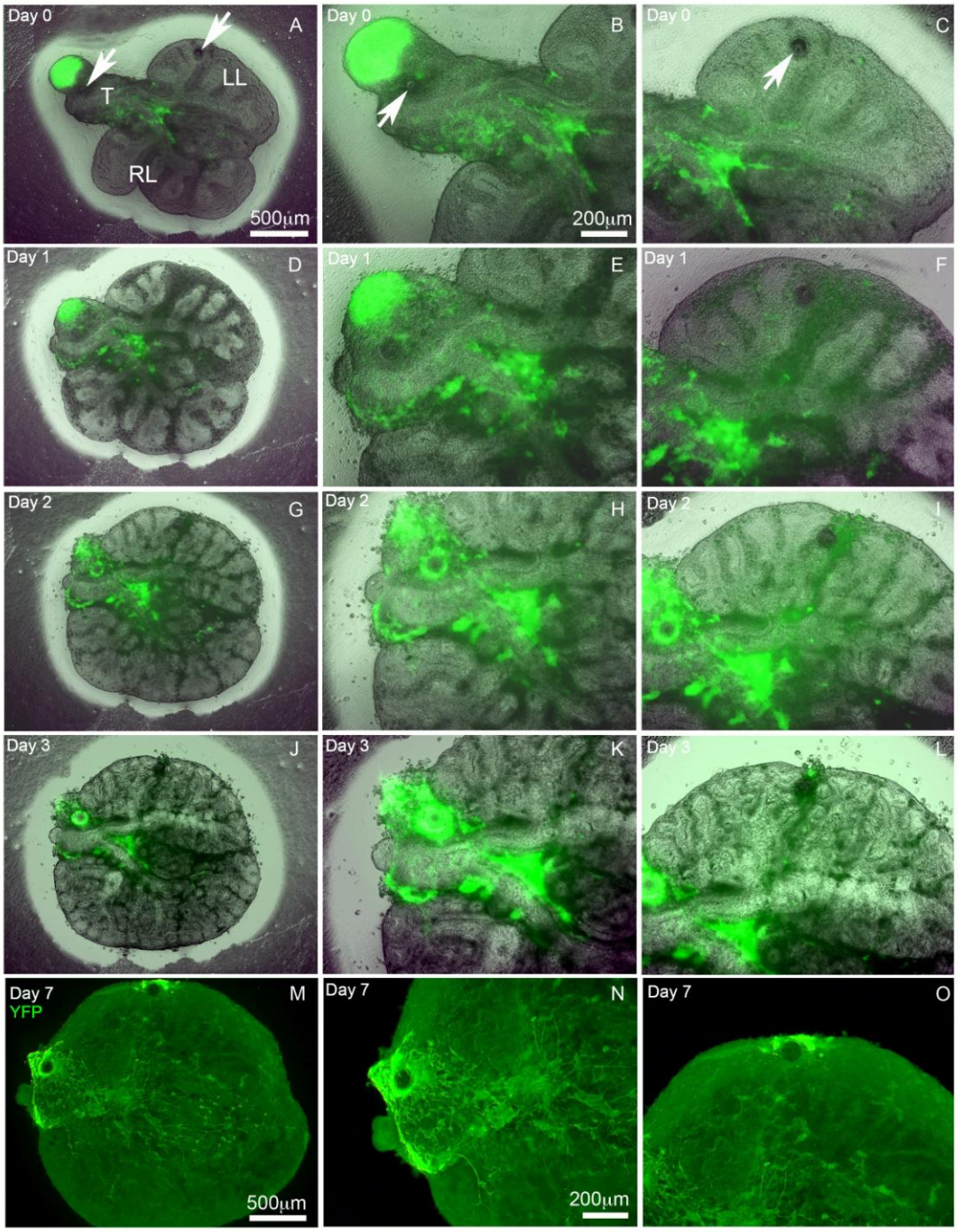

Figure 5.5i GDNF beads attract NCC in cultured E12.5 *Wnt1Cre:Rosa26YFP* lungs. Day 0 to 3 (A-I) show light micrographs superimposed with fluorescent micrographs of YFP fluorescence. Day 7 pictures (M-O) show whole-mount immunohistochemistry against YFP in the cultured lung after fixation. NCCs (green) accumulate around GDNF beads (arrows).

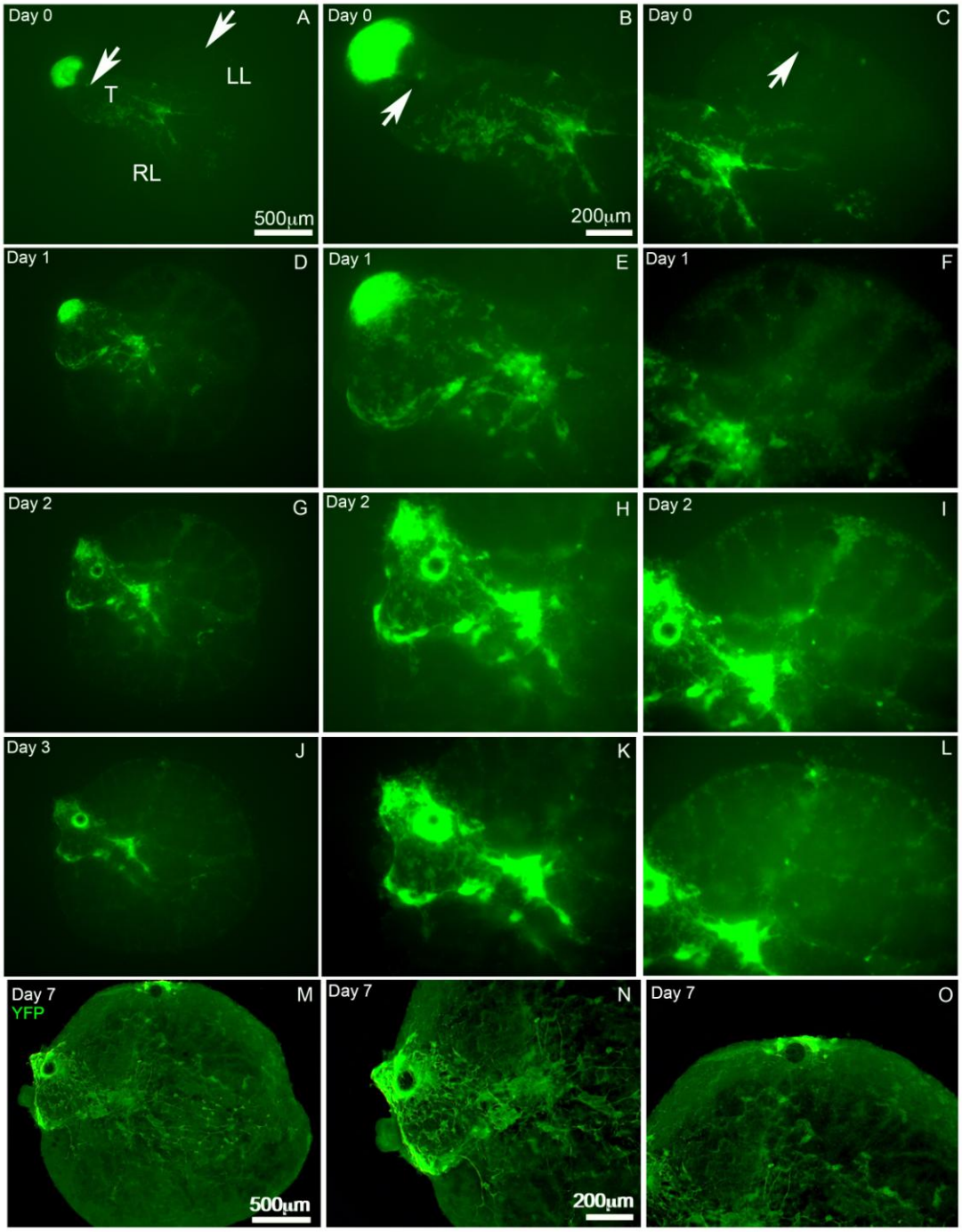

Figure 5.5ii. Green channel from Figure 5.5i, showing that GDNF beads attract NCC in cultured E12.5 *Wnt1Cre:Rosa26YFP* lungs. Day 0 to 3 (A-I) show fluorescent micrographs of YFP fluorescence. Day 7 pictures (M-O) show whole-mount immunohistochemistry against YFP in the cultured lung after fixation. NCCs (green) accumulate around GDNF beads (arrows).

Organotypic lung culture using pieces of F1 (10 week old) human fetal lungs was also carried out in the presence of GDNF beads (Figure 5.6). In 10-week-old human fetal lungs airway structure and branching were maintained in culture for 4 days, though large areas of necrotic tissue could be seen by day 4 (Figure 5.6, C, D). 10-week-old human fetal lungs could be used in isolated GDNF bead experiments for up to 6 days (not shown) but older human lung tissue did not survive as long in culture.

Beads containing GDNF at a concentration of 250ng/ul were placed on several pieces of human lung tissue on the first day of culture and lungs harvested and stained at two-day intervals to observe any effect of GDNF on neural crest-derived tissue within the lung. No aggregations of neural crest-derived neurons were seen around GDNF beads, possibly due to the age and level of neuronal differentiation of neural crest-derived cells in the human fetal lung samples used, as NCCs may have ceased migration at this late stage of lung development. Neurite extension towards GDNF beads was not measured, as neurites were easily disrupted during staining and mounting and so could not reliably be seen.

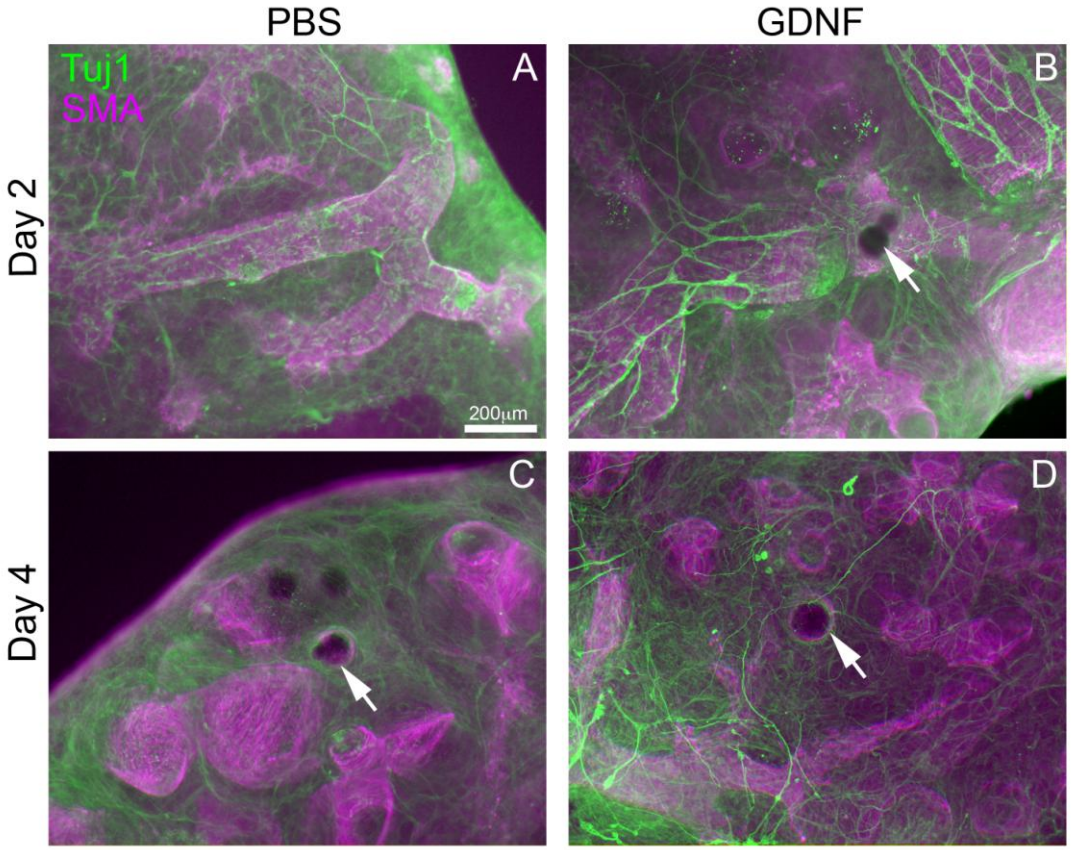

Figure 5.6 Tuj1 and SMA staining of pieces of cultured human fetal lung at F1 with PBS and GDNF beads (arrows). Neurons did not aggregate around GDNF beads in lung culture, possibly due to the advanced age of the tissue compared to the mouse lungs used in culture experiments.

5.2 Analysis of NCC migration into the lung in RET pathway mutant mice

In order to assess whether RET pathway receptors are necessary for normal NCC migration into and within the lung, NCC colonisation of the lung in *Ret* and *Gfra1* mutant mice was examined.

Neural crest-derived innervation of the lung in mutant mouse embryos was examined at E14.5 as lung innervation is well established at this stage. Embryos were serially cryosectioned and sections immunostained for the neuronal marker Tuj1, which, as shown in chapter 1, is expressed in neural crest-derived neuronal tissue within the mouse lung at E14.5. In order to analyse NCC colonisation of the lung in the absence of the RET and GFRa1 receptors, the innervation in homozygous mutant mouse lungs was compared with that in wild-type littermate lungs. The results show that lung colonisation by NCCs in *Ret* -/- mouse embryos and in *Gfra1* -/- mouse embryos is indistinguishable from that in littermate controls. Neuronal cell bodies and neural tissue are present in similar densities and distributions in mutant and control lungs. In *Ret* -/- lungs (n=3) (Figure 5.7) neuronal projections and neuronal cell bodies can be seen around the epithelial tubules in a similar distribution to that in wild-type littermates (n=3). As an internal positive control, neuronal tissue can be seen around the foregut in both wild-type embryos (Figure 5.7, A) and mutant embryos (Figure 5.7, D). Neuronal cell bodies and ganglia, indicated by arrows, can be seen in similar positions next to the larger epithelial tubules in both wild-type (Figure 5.7, B, C) and mutant (Figure 5.7, E, F) littermate lungs.

Gfra1 -/- lungs (n=3) (Figure 5.8) also have a similar distribution of neuronal tissue to that in the lungs of wild-type littermates (n=2). Neurons and neuronal projections can be seen around the future bronchi in the wild-type (Figure 5.8, B) and mutant (Figure 5.8, D) lungs.

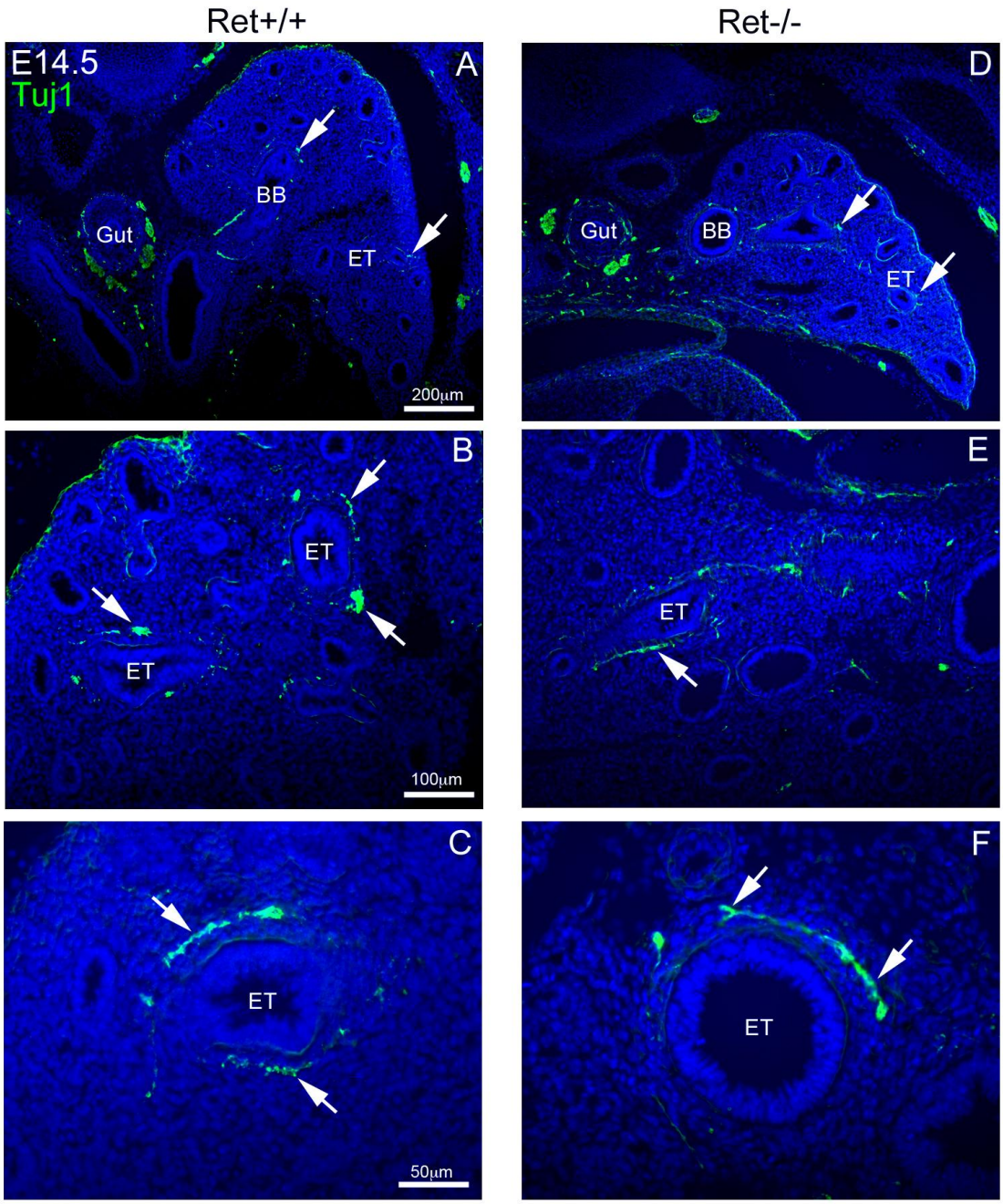

Figure 5.7 E14.5 *Ret* +/+ and -/- littermates show similar distribution of neurons, immunostained for Tuj1 (green). The distribution of neuronal cell bodies and projections (arrows) is indistinguishable between wild-type and mutant littermates. BB: bronchus, ET: epithelial tubules.

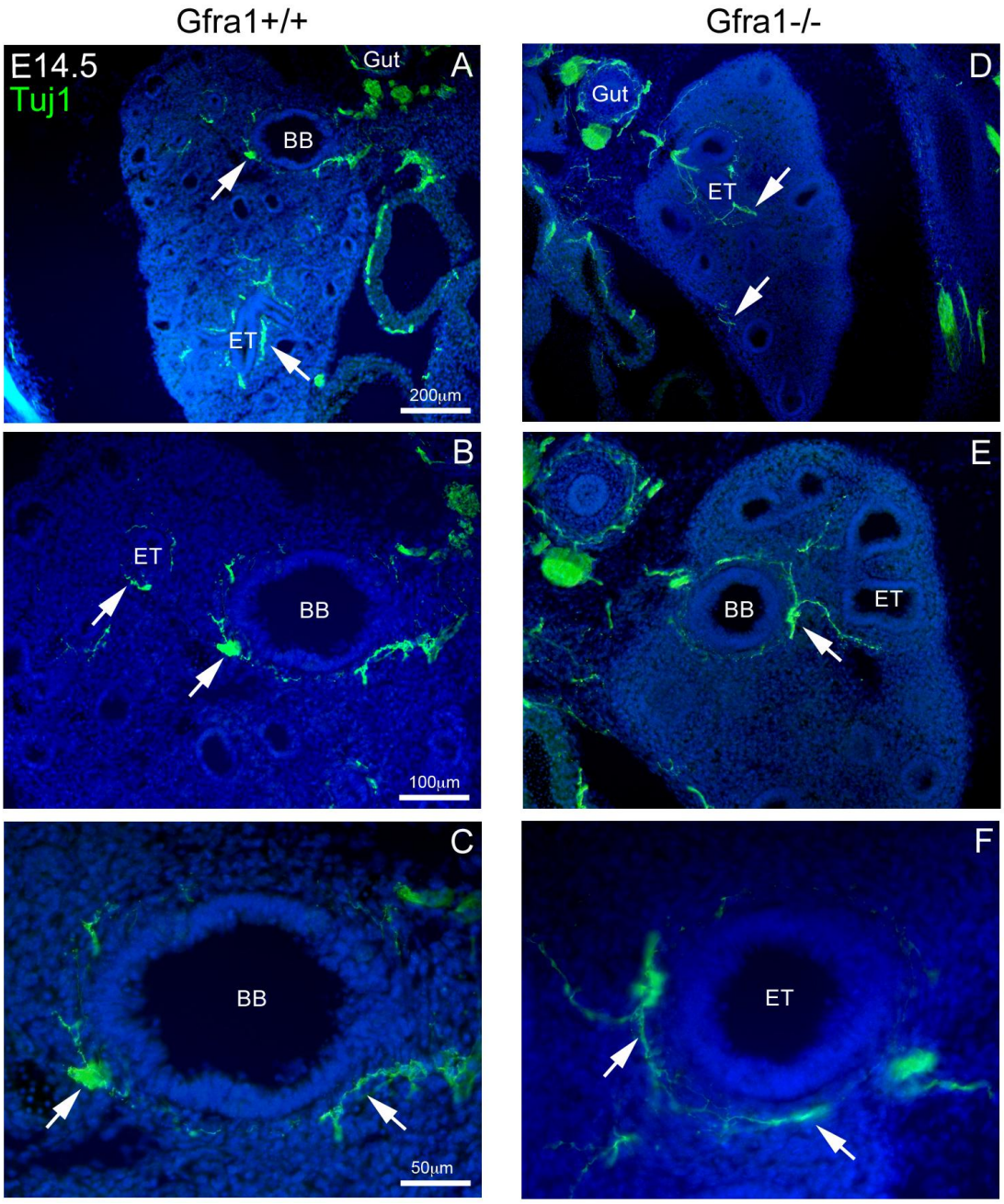

Figure 5.8 E14.5 *Gfra1* +/+ and -/- littermates show similar distribution of neurons, immunostained for Tuj1 (green) . The distribution of intrinsic neuronal cell bodies and projections (arrows) is indistinguishable between wild-type and mutant littermates. BB: bronchus, ET: epithelial tubules.

A technique was previously utilised for assaying the extent and pattern of lung innervation in whole lungs using optical projection tomography (OPT) (chapter 3, section 3.3). This technique was also applied to whole *Ret* mutant, heterozygote and wild type littermate E14.5 lungs immunostained for the neuronal marker Tuj1. When the extent and distribution of neuronal tissue in the lungs was compared between genotypes, no obvious differences in the density or patterning of lung innervation were apparent (Figure 5.9). In all genotypes the organisation of neuronal tissue and the neuronal projections in the lungs follow a similar pattern. The left lung has a consistent pattern of innervation (Figure 5.9, B', D' and F'), with a central line of neuronal tissue along the main bronchus punctuated by periodic offshoots that follow the ancillary airways in a stereotyped pattern. The anti-Tuj1 staining used on these lungs did not distinguish between extrinsic neuronal projections and neuronal cell bodies, so I could not compare the size of the intrinsic lung ganglia using OPT scans of anti-Tuj1 staining. OPT scans were used to produce video reconstructions of the lungs that are available online as supplementary figures for the publication by Freem et al (Freem et al., 2010).

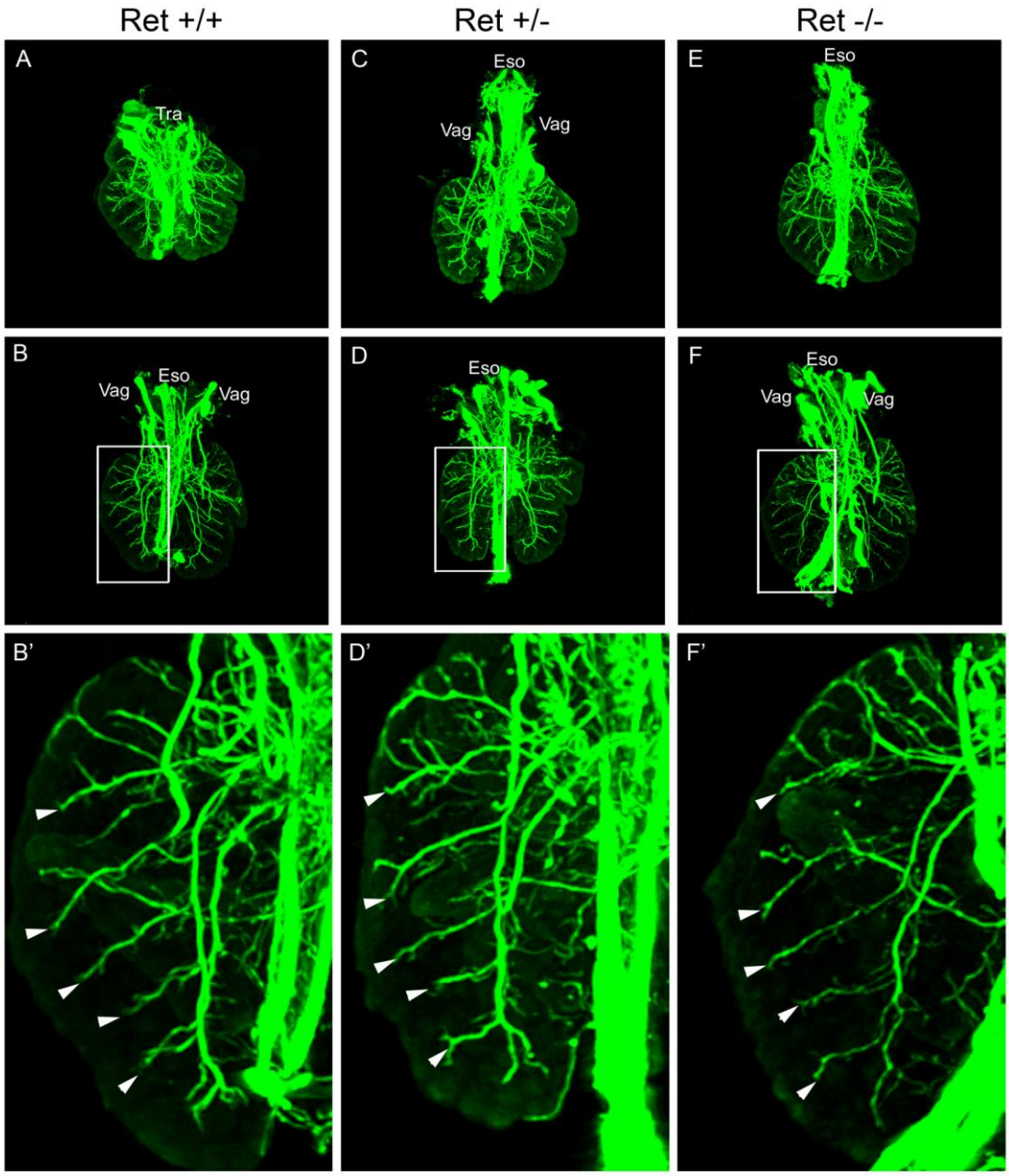

Figure 5.9 OPT scans of *Ret* mutant lungs and controls. E14.5 *Ret* wild type (A, B, B') heterozygote (C, D, D') and mutant lungs (E, F, F') from littermate embryos. The branching pattern of neuronal projections (arrowheads) and density of neuronal tissue is similar in all three phenotypes. The left lung has been magnified to compare patterns of innervation (B', D', F'). Eso: Esophagus, Tra: Trachea, Vag: Vagal nerve.

In order to confirm that the numbers of neurons in intrinsic lung ganglia were similar in littermate *Ret* +/+, +/- and -/- embryonic lungs, these lung ganglia were examined in greater detail (Figure 5.10). After OPT scanning, the scanned lungs were rehydrated and retrieved from the agarose in which they were embedded for OPT scanning. Fluorescent anti-Tuj1 staining was still visible in the lungs after scanning and rehydration. The lobes of the lungs were separated from the bronchi and mounted separately under glass coverslips. Using high-power fluorescence microscopy, individual Tuj1-stained neuronal cell bodies could be seen within lung ganglia (Figure 5.10, C', C", D', D"). Quantification of Tuj1-stained neuronal cell bodies within all the ganglia in these lungs was then carried out by examining ganglia at multiple focal lengths and counting neurons seen. The ganglia within the lung at E14.5 were present in anatomically stereotyped positions (Figure 5.10, arrows and arrowheads in C, D), aiding comparative quantification – rather than counting all neurons in the lung at once, neurons within each ganglion were counted and added together during analysis. Similar numbers of neurons were counted in corresponding ganglia in *Ret* +/+, +/- and -/- lungs. The mean total number of neurons also showed little difference between genotypes (Table 5.1). Further statistical tests were inappropriate due to small sample sizes (n=2 for each group).

	Mean	SD
Neurons in Ret+/+ lung	292	41.7
Neurons in Ret +/-lung	253	35.4
Neurons in Ret -/- lung	244	5.7

Table 5.1 Neurons counted in lung ganglia from different *Ret* genotypes. The number of neurons in homozygous mutant lungs is similar to that in wild-type lungs at E14.5.

The total number of intrinsic parasympathetic neurons in the postnatal mouse lung has been estimated to be about 200 (Undem and Larry, 2009). Comparing this number to the numbers of neurons counted in wholemount wild-type and *Ret* mutant lungs (Table 5.1), it appeared that NCC colonisation of the lung is nearly complete at E14.5. This means that analysis of mutants at E14.5 was near optimal, as at this stage the lungs are small enough to scan in full but have a substantial complement of intrinsic neurons.

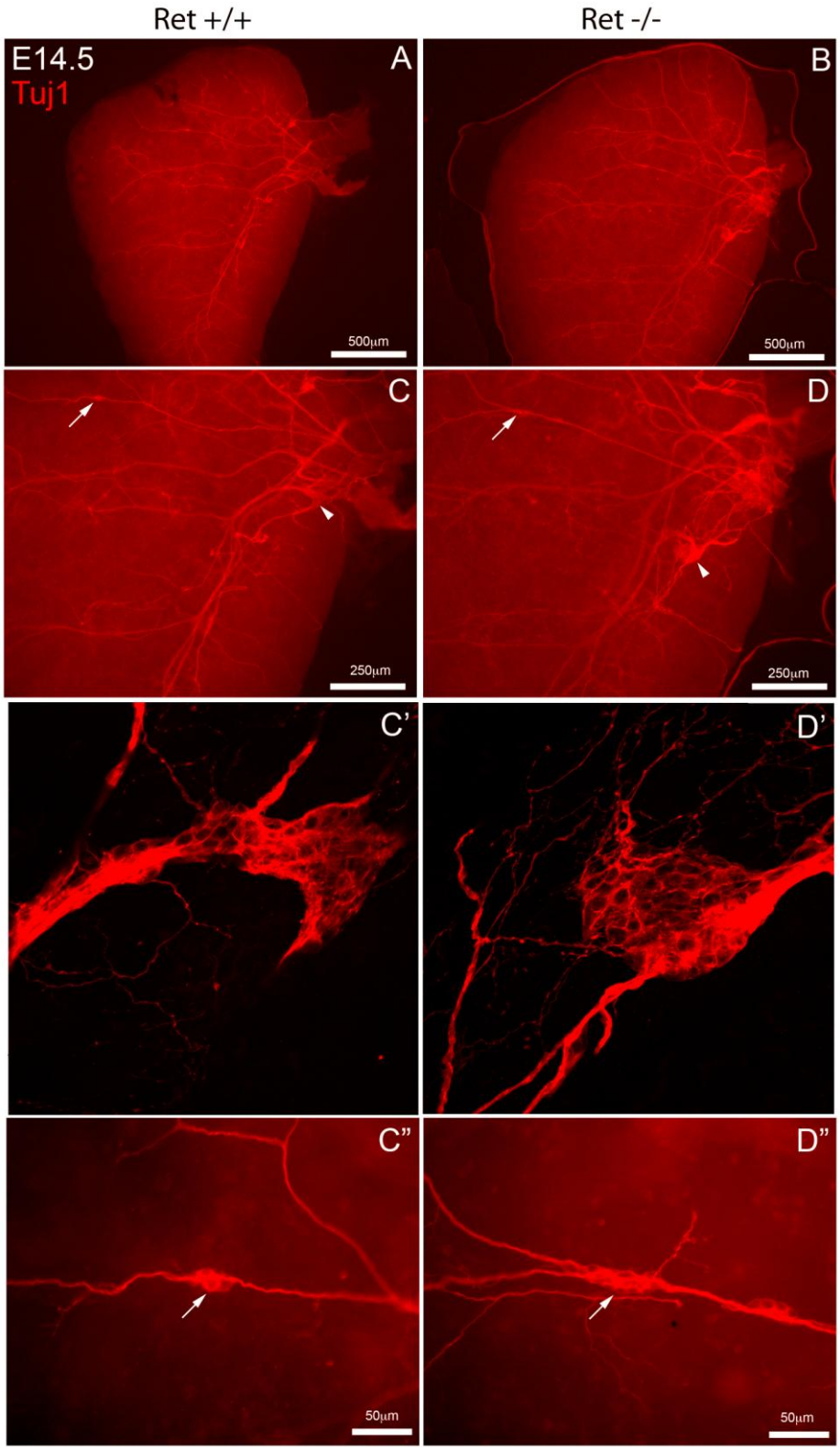

Figure 5.10 E14.5 *Ret* +/+ and -/- whole lungs stained for Tuj1 (red) show similar distribution of neurons. Lung lobes were separated from each other and mounted under coverslips. Ganglia were present in stereotyped locations (C, D). Neurons within ganglia were counted under a fluorescent microscope. Arrowheads in C and D indicate ganglia shown in C' and D', arrows indicate ganglia shown in C" and D".

5.3 NCC migration and the vascular system

As well as investigating signalling molecules that could guide NCCs into the lung, other guidance mechanisms that could potentially be involved in directing NCCs into the lung, such as migration along a substrate, were examined. Enteric NCCs have been shown in endothelial cell and NCC co-culture experiments to use the extracellular matrix of endothelial cells on the outer surface of blood vessels as a substrate for migration within the gut, and NCC migration is deficient in avascular gut (Nagy et al., 2009). NCC migration and angiogenesis also use the same semaphorin signalling cues to guide the segmented development of ganglia and blood vessels, as shown in neuropilin mutant mouse analysis (Fantin et al., 2009). In order to investigate whether migration along blood vessels was a plausible method of guidance for NCCs entering and migrating within the lung the juxtaposition of NCCs and blood vessels within the lung was looked at in several stages in *Wnt1Cre:Rosa26YFP* mouse embryos. The diffusely distributed vascular plexus and the larger pulmonary blood vessels in the lung were both examined, as both were marked by antibodies against the vascular epithelium marker protein endomucin (Liu et al., 2001). Blood vessels in the lung were easily distinguished from airways by gross anatomy as well as by endomucin staining, as the endomucin-stained blood vessels lack the epithelial layer seen around the airways.

At E12.5 (Figure 5.11, A-D) there are few NCCs within the lung. Endomucin staining is markedly absent in the epithelial layer around the future airways (Figure 5.11, C, D). NCCs are not seen in proximity to blood vessels (Figure 5.11, A-D, arrows) and appear to remain around the future airways where the blood vessel marker endomucin is not expressed. Airways and blood vessels are therefore distinguishable by endomucin staining as well as morphology. At E14.5 (Figure 5.11, E-H) although major airways surrounded by NCC-derived neural tissue are adjacent to blood vessels (Figure 5.11, H), NCCs are not seen in close association with blood vessels. Later in development at E16.5 and E18.5 (Figure 5.12), the vascularisation associated with increasing alveolarisation means that endomucin is present in a large proportion of the lung mesenchyme (Figure 5.12, I-N) as well as larger blood vessels (Figure 5.12, P). However, the epithelial tubules that will become the airways are not marked by endomucin (Figure 5.12, K-P). Together, these results showed that YFP-positive NCCs are not seen in close association with blood vessels

in the developing lung. This suggests that blood vessels do not serve as a scaffold for NCC migration in the developing lung.

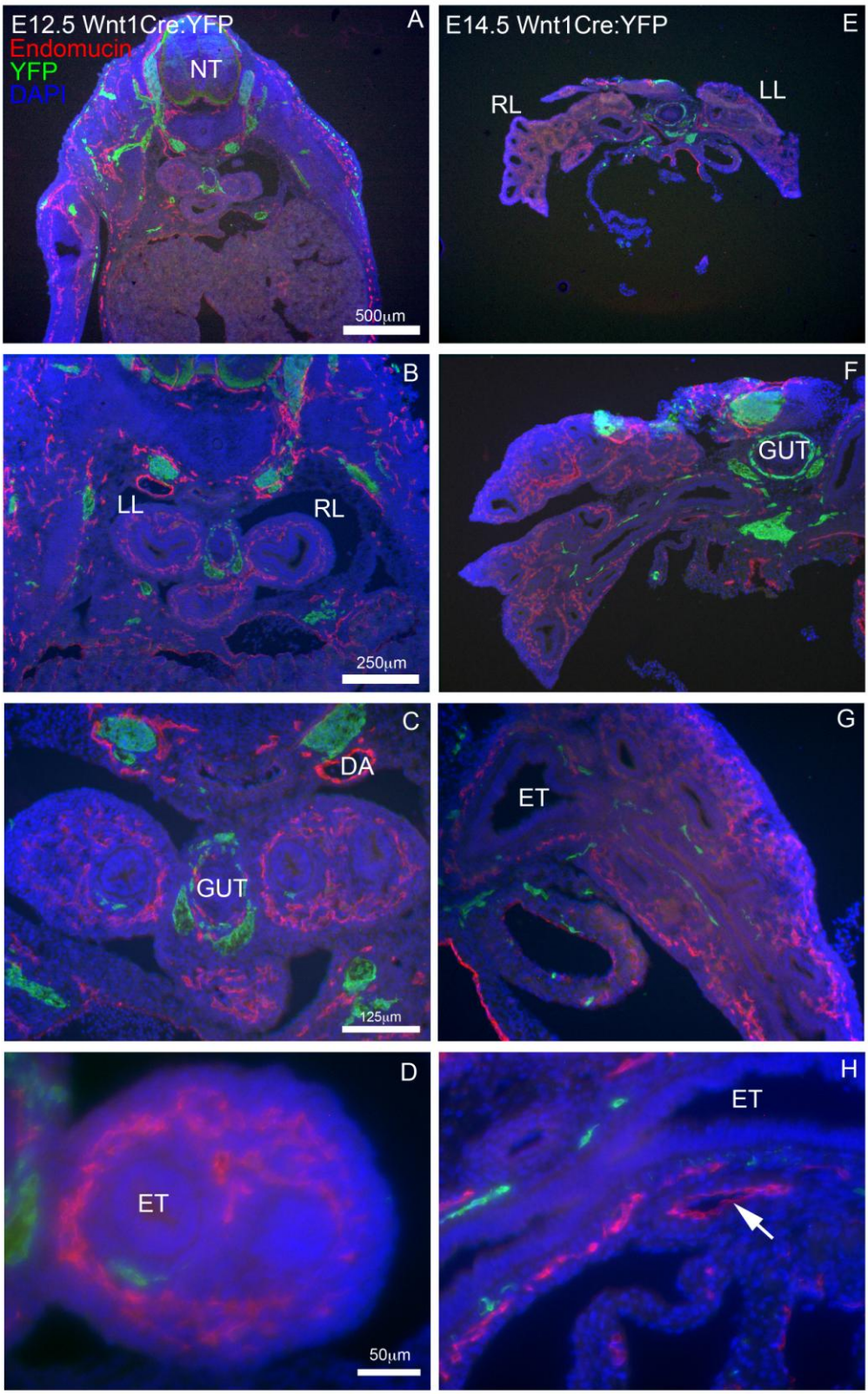

Figure 5.11 Blood vessels in E12.5 (A-D) and E14.5 (E-H) *Wnt1Cre:Rosa26YFP* mouse lungs. Sections stained for endomucin (red) and YFP (green). Arrow indicates blood vessel. DA: dorsal aorta, ET: epithelial tubule, LL: left lung, NT: neural tube, RL: right lung.

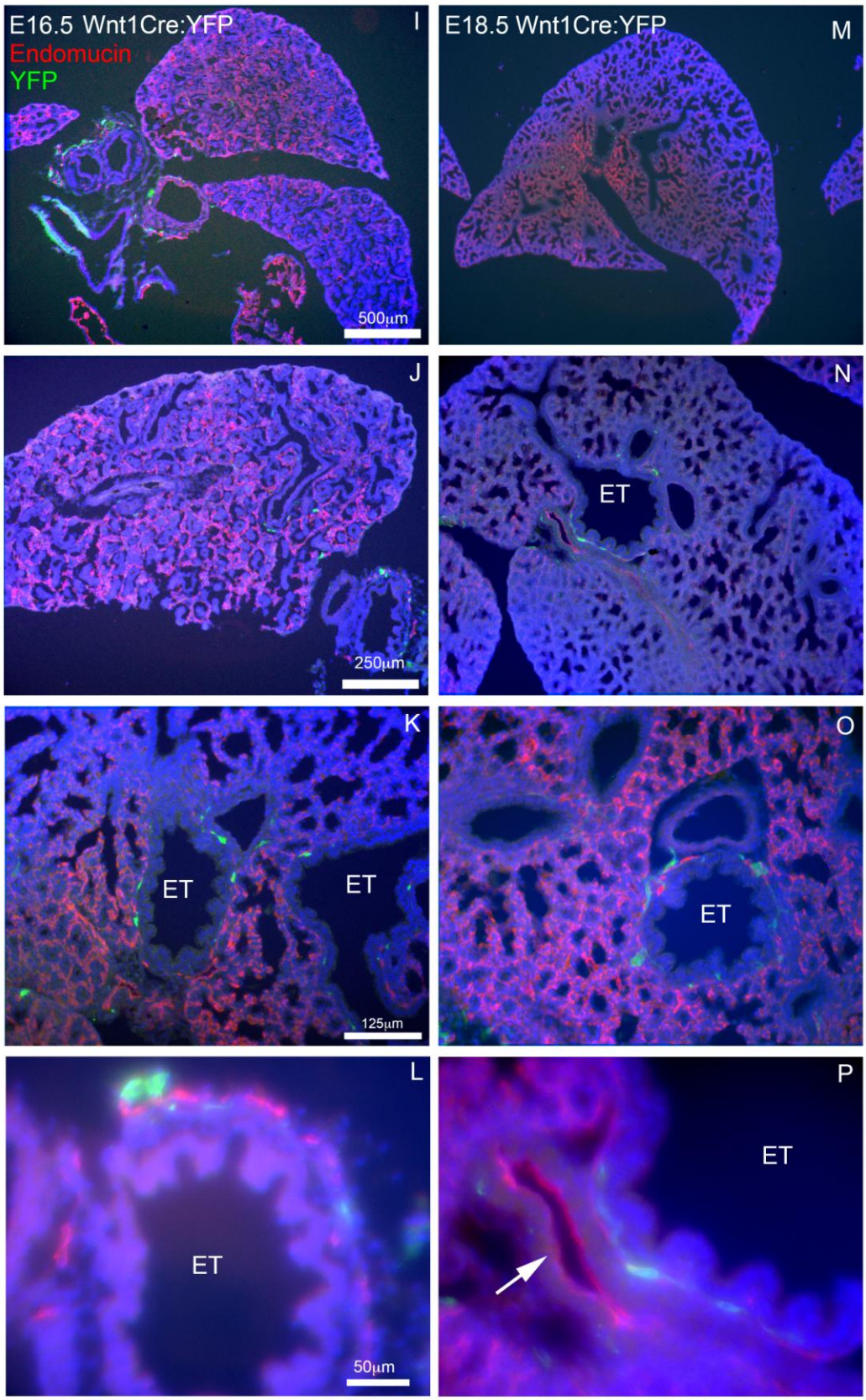

Figure 5.12 Blood vessels in E16.5 (I-L) and E18.5 (M-P) *Wnt1Cre:Rosa26YFP* mouse lungs. Sections stained for YFP (green) and endomucin (red). Arrows indicate blood vessels. ET: epithelial tubule.

5.4 Other signalling pathways in NCC migration into the lung

Having characterised NCC migration into the lung, and investigated the role of the RET signalling pathway in lung NCC migration, further signalling pathways were examined to investigate signalling molecules that potentially play a role in guiding NCC to migrate into the lungs. The signalling molecules analysed below did not appear to be involved in NCC migration into the lung.

It was tested whether candidate ligands were sufficient to attract NCC within the lung using an organotypic culture system. Results using this system to investigate the RET signalling pathway are presented in section 5.1 and 5.2 above. In addition to these experiments, similar experiments were carried out using the potential chemoattractant BDNF (Brain-Derived Neurotrophic Factor), presented below. Once the lung culture test system had been established as described in section 5.1, the effect of potential NCC chemoattractants on NCC migration was tested by placing chemoattractant-soaked beads onto E12.5 *Wnt1Cre:Rosa26YFP* cultured lungs. Having validated this culture system using a known NCC chemoattractant, GDNF (Figure 5.5), it was then used to test the novel candidate molecule BDNF. BDNF was considered to be a candidate because it is the ligand for the receptor TrkB, and TrkB mutant mice have been reported as having no intrinsic ganglia or other lung innervation (Garcia-Suarez et al., 2009). BDNF is also thought to be required as a survival factor for the development of vagal sensory nerves in the lung and breathing difficulties have been reported in BDNF mutant mice (Erickson et al., 1996).

In experiments with the putative chemoattractant BDNF, GDNF was used as a positive control. Beads were impregnated with GDNF at a concentration of 250 ng/μl. Mouse lungs were photographed at day 0 of culture before bead placement (Figure 5.13, A, B, C) and daily thereafter. On day 6 the lungs were fixed and immunostained for the transgenic NCC marker YFP. While cells accumulated around GDNF beads as expected (Figure 5.13, F, I, L O), only a few NCCs were seen in proximity to BDNF beads (Figure 5.13 E, H, K, N). The NCC response to BDNF beads was similar to the response to negative control PBS bead (Figure 5.13, A, D G, J M). These findings suggest that BDNF does not act as a chemoattractant for NCC within the embryonic lung.

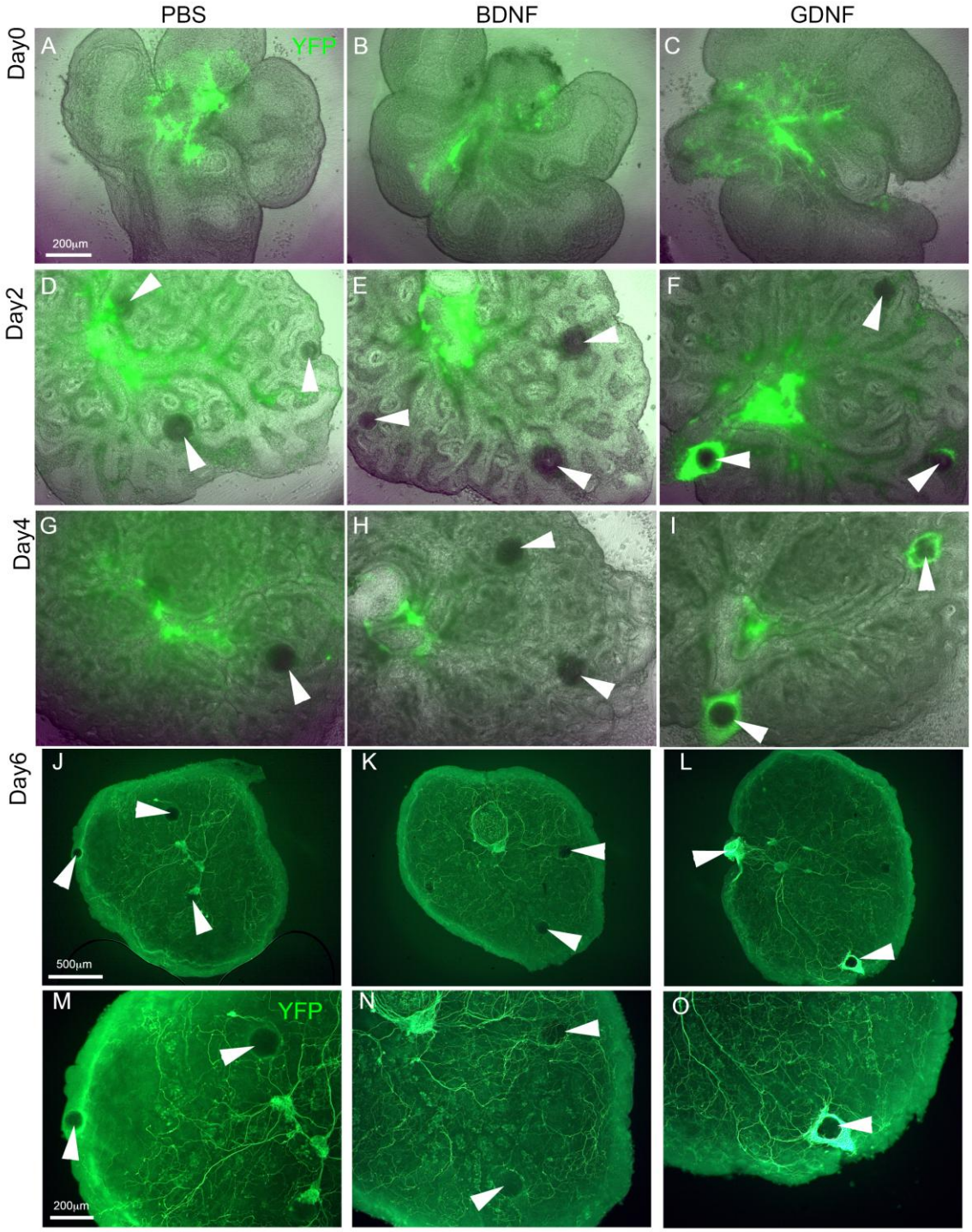

Figure 5.13i BDNF beads do not attract NCC. Culture of E12.5 Wnt1Cre:Rosa26YFP lungs in the presence of BDNF, GDNF/positive control and PBS/negative control beads (arrowheads). Timelapse images with green channel overlay (A-I) and immunohistochemtry against YFP in wholemount lungs after culture (J-O). The YFP-expressing NCC do not migrate towards BDNF (A, D, G, J, M) or PBS (B, E, H, K, N) beads, while they do migrate to and aggregate around GDNF beads (C, F, I, L, O).

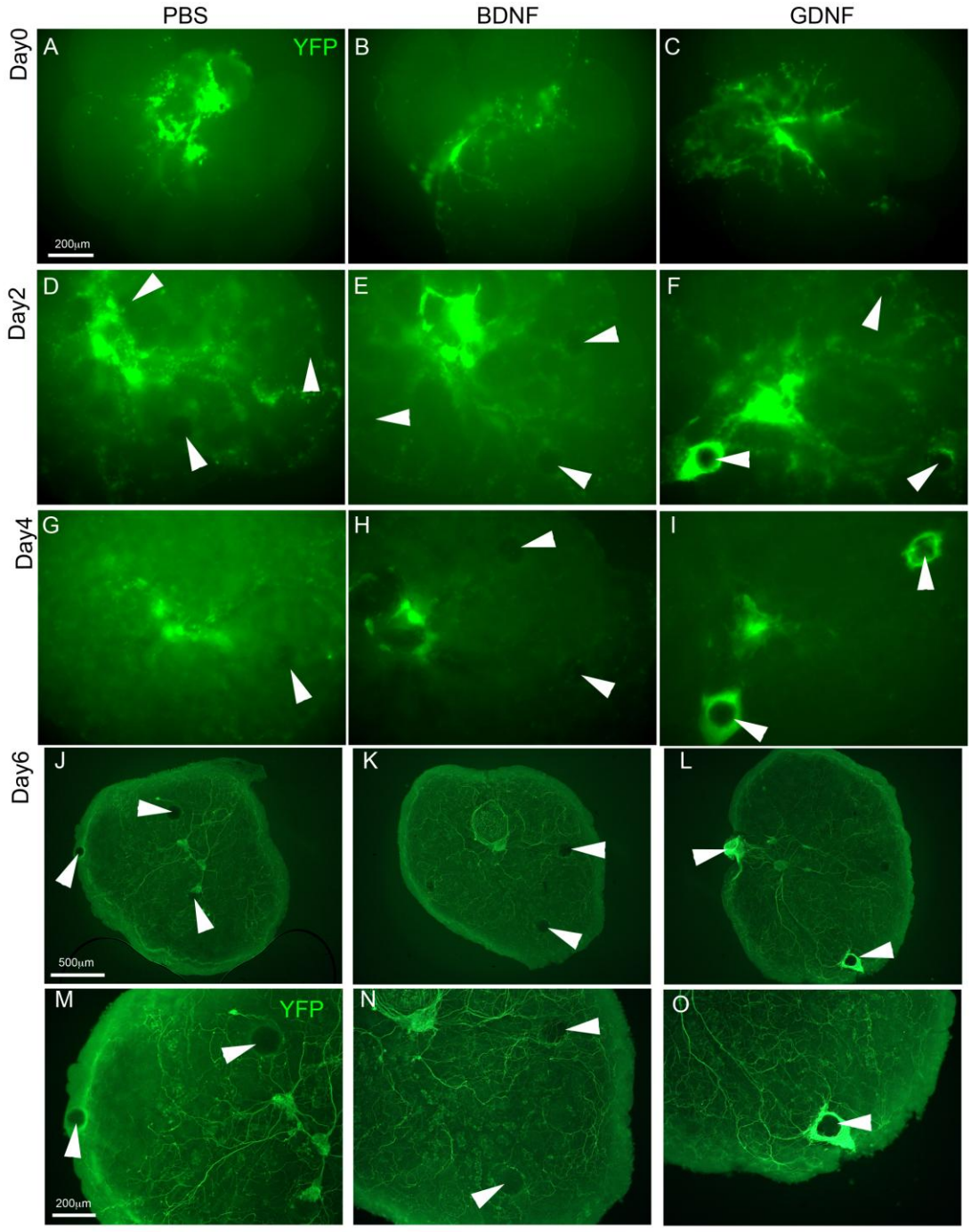

Figure 5.13ii BDNF beads do not attract NCC. Green channel only of Figure 5.13ii: Culture of E12.5 Wnt1Cre:Rosa26YFP lungs in the presence of BDNF, GDNF/positive control and PBS/negative control beads (arrowheads). The YFP-expressing NCC do not migrate towards BDNF (A, D, G, J, M) or PBS (B, E, H, K, N) beads, while they do migrate to and aggregate around GDNF beads (C, F, I, L, O).

In other experiments, it was examined whether candidate molecules were necessary for NCC colonisation of the lung by analysing the lungs of mutant mouse embryos. In *Dcc* mutant mice tangential migration of NCCs from the foregut into the pancreas is impaired (Jiang et al., 2003). E14.5 *Dcc* mutant embryos and littermate controls were obtained from Dr Elyanne Ratcliffe at McMaster University, Canada and analysed lung innervation in these embryos to see whether tangential NCC migration from the gut into the lung is also impaired (Figure 5.14). Tuj1 staining showed that the distribution of neural tissue lungs in *Dcc* mutant embryos is similar to that in controls and so that DCC does not appear to mediate tangential NCC migration from the gut into the lungs.

However, examination of *Dcc* mutant lung morphology in sections revealed a previously undescribed lung mesenchymal phenotype, in which fissures (Figure 5.14, E, red arrows) are present in homozygous *Dcc* mutant E14.5 lungs but not in wild type littermate lungs. These fissures may be due to the role of netrin in lung epithelial tubule morphogenesis (Liu et al., 2004). Netrin and DCC have been hypothesised to be involved in lung development due to their expression patterns in the lung (Dalvin et al., 2003), but the lung mesenchyme particular phenotype does not appear to have been previously described. Further investigation of this phenotype was outside the scope of this project.

Lungs from E13.5 Neuropilin1 (Nrp1) conditional mutant mice were obtained from the group of Dr Christiana Ruhrberg at UCL. These mice appear to have subtle defects in ENS formation (Dr Christiana Ruhrberg, unpublished communication). In these mice, *Nrp1* expression is only knocked down in Wnt1-expressing cells (Gu et al., 2003), allowing the cell-autonomous role of Nrp1 in NCC migration to be examined. Conditional-null floxed mutants for *Nrp1 (Nrp1$^{fl/fl}$)* (Gu et al., 2003) were mated to mice expressing Cre recombinase under the control of the Wnt1 promoter. Mice with conditional knockout of *Nrp1* in their NCC have been labeled *Nrp1* -/- (Figure 5.15). Lung innervation is present in E13.5 *Nrp1* -/- mouse lungs in a similar distribution to that in wild-type littermates.

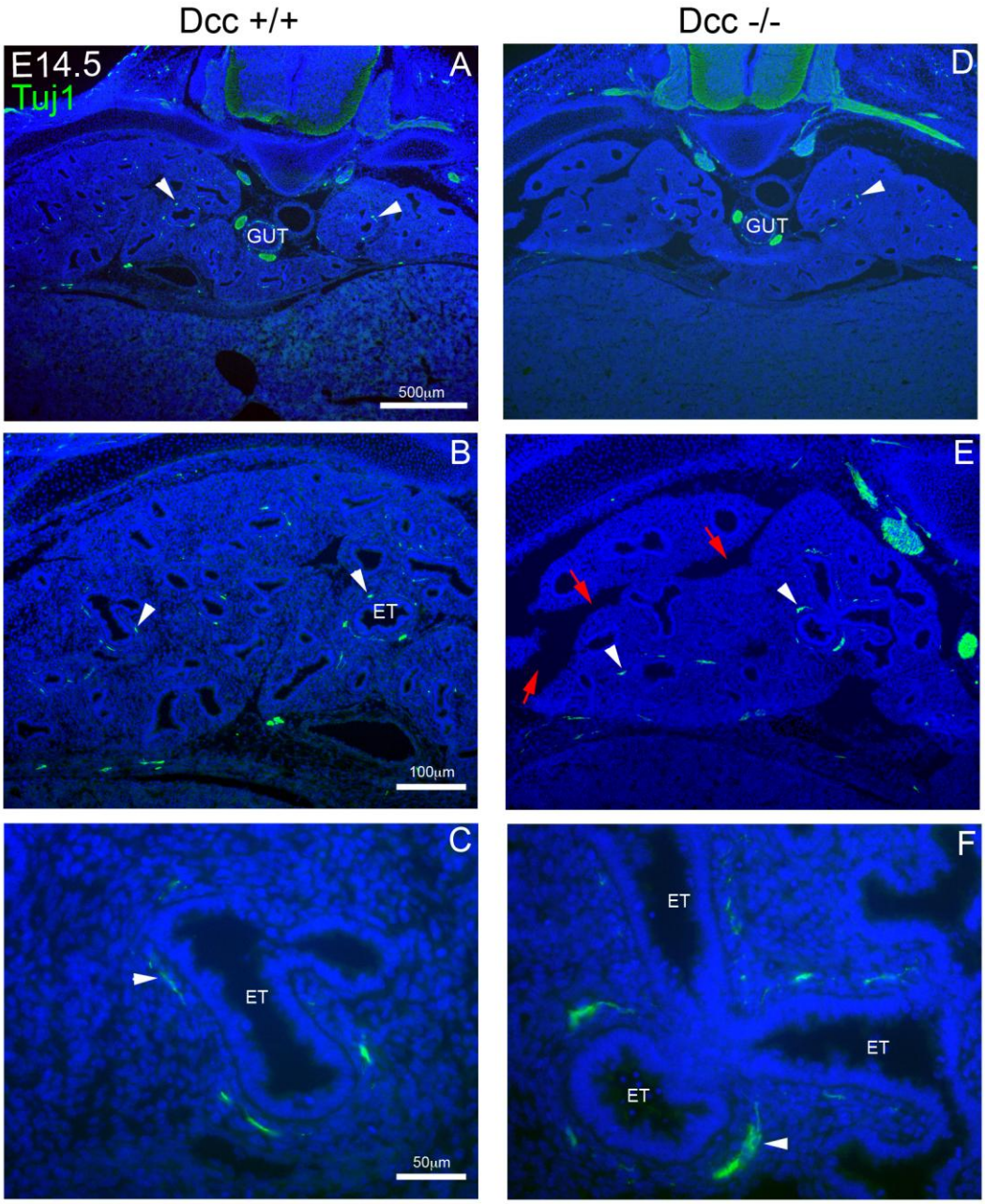

Figure 5.14 E14.5 *Dcc* -/- and +/+ littermates show similar distribution of neurons, immunostained for Tuj1 (green). The distribution of neural tissue (arrowheads) is indistinguishable between mutants and wild type littermates. Note malformation of the lungs, with fissures (red arrows) present in the mesenchyme in E but not B.

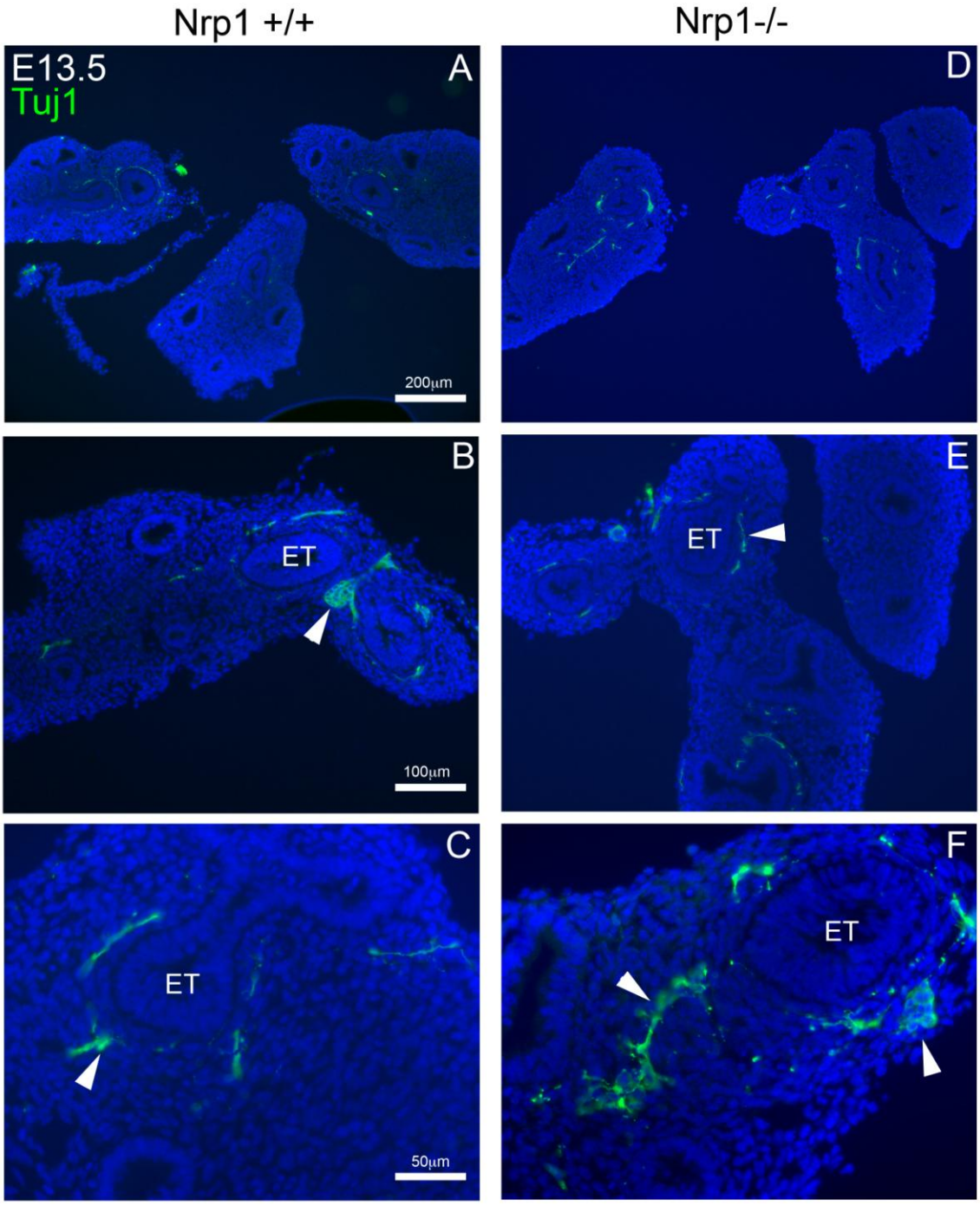

Figure 5.15 Lungs from E13.5 Neuropilin1 Wnt1Cre conditional mutant -/- and +/+ littermates show similar distribution of neurons, immunostained for Tuj1. Neuronal cell bodies (arrowheads) are visible in both wild type and homozygous *Nrp1* mutant

5.5 Discussion

Previous studies have shown that neural crest-derived enteric innervation is deficient in *Ret* and *Gfra1* mutant mice (Enomoto et al., 1998; Schuchardt et al., 1994). GDNF, the ligand for RET and its co-receptor GFRa1, has been shown to attract NCCs in both gut (Young et al., 2001) and lung (Tollet et al., 2002) in organotypic tissue culture systems, and this has been confirmed in this study using lung culture experiments. *RET* mutations have been linked to respiratory dysfunction in Haddad syndrome (Amiel et al., 1998) as well as being a common cause of enteric aganglionosis in Hirschsprung's disease (Parisi and Kapur, 2000). *Ret* mutant mice display respiratory dysfunction resulting from decreased carbon dioxide chemosensitivity (Burton et al., 1997) indicating that this respiratory dysfunction has a neuronal basis. *Ret* mutations have been suggested to decrease the number of neural crest-derived intrinsic ganglia in the lung (Langsdorf et al., 2011) and so the RET pathway could be involved in NCC colonisation of the lung. However, these results showed that, perhaps unexpectedly, lung innervation appears normal in *Ret* and *Gfra1* mutant mice at E14.5. This indicates that *Ret* and the RET signalling pathway are not necessary for neural crest colonisation of the lung.

To help determine the mechanisms underlying the migration of NCCs into the lungs, an organotypic culture system was established for testing potential chemoattractant molecules that could guide NCCs into the lungs. Lung survival and the preservation of lung morphology were assessed by examining airway branching and peristalsis in culture and the expression of neuronal, neural crest and smooth muscle markers in cultured lungs. The distribution of these cell types over time was comparable to that seen in freshly dissected mouse lungs at similar stages (chapter 3), with a band of smooth muscle seen around the epithelial tubules and neurons or NCCs seen in apposition to that smooth muscle layer. The organotypic mouse lung culture system coupled with the use of *Wnt1Cre:Rosa26YFP* transgenic mouse lungs allowed NCC migration and chemotaxis to be tracked over several days in culture. The culture system was based on a similar approach developed by Tollet et al (Tollet et al., 2002). However, in this system the use of lungs from the *Wnt1Cre:Rosa26YFP* mouse allowed NCC migration to be tracked over several days in culture using fluorescent time-lapse microscopy, an improvement on previous lung culture

systems. This tracking of NCC migration within the cultured lung has proven to be useful in tracking NCC migration towards chemoattractant beads. In contrast, other studies on potential NCC chemoattractants in cultured tissue such as GDNF (Tollet et al., 2002; Young et al., 2001) and netrin (Jiang et al., 2003), required the lungs to be fixed and stained before NCC location could be analysed.

The protocol described in this thesis was used to confirm and extend previous results (Tollet et al., 2002) that indicated that GDNF is a chemoattractant for lung NCCs in culture. GDNF is also a chemoattractant for gut NCCs in culture (Young et al., 2001). It was found that over several days, YFP-expressing NCCs migrated to and surrounded the GDNF beads, indicating that GDNF is a chemoattractant for NCC. In addition these methods allowed observation of the continuation of airway branching in cultured lungs and recording of the progress of YFP-expressing NCC migration within cultured lungs over several days. This protocol was also used to test the novel potential chemoattractant BDNF (see section 5.4), which did not attract lung NCCs in the organotypic lung culture system.

The organotypic culture system was also applied to segments of fresh human fetal lungs obtained from the Human Developmental Biology Resource (HDBR) managed by UCL Institute of Child Health. This resource allowed the testing of chemoattractants on human lung NCC, to add to the results on GDNF signalling obtained from mouse lung tissue. Human fetal lungs at approximately 10 weeks gestation (Fetal Stage 1) have been shown to contain a network of neurons around the layer of ASM that surrounds the future airways (Burns et al., 2008; Sparrow et al., 1999). These neurons and ASM were maintained in the lung in the organotypic culture system, allowing similarities between mouse and human lung to be assessed. The human lungs used were at Fetal Stage 1, and therefore at a comparatively older stage than the mouse lung used in tissue culture. By week 10 in the human lung (Burns et al., 2008) many cells of NCC origin displayed projections and markers of neuronal differentiation. Differentiated neurons do not migrate as readily as NCCs, so this may be why neural crest-derived neurons were not seen aggregated around GDNF beads in F1 human lung. Neuronal tissue in organised networks was established around the airways and NCCs did not appear to be present, explaining why NCC aggregation around GDNF beads could not be seen in cultured human

lungs. Human lungs at a less advanced developmental stage were not available for culture.

Organotypic culture experiments suggested that the RET-GDNF signalling pathway is sufficient to guide NCCs within the embryonic lung. If GDNF signalling through the RET receptor is necessary for NCC migration into the lung, *Ret* mutant mice would be expected to have a deficiency in intrinsic neural crest-derived lung neurons. However, lung sections from E14.5 *Ret* and *Gfra1* homozygous mutant embryos did not show decreased numbers of intrinsic pulmonary neurons compared to littermate controls, indicating that RET is not necessary for neural crest cell colonisation of the lung.

Although E14.5 *Ret* -/- lungs appear to have normal neural crest-derived innervation, examination of older lungs may shed light on a role for RET in NCC maintenance in the lung. Recent work, published after the findings of this thesis, suggested that there are decreased numbers of intrinsic pulmonary neurons in the *Ret* mutant trachea and lungs (Langsdorf et al., 2011) at E18.5, four days later than in the E14.5 lungs examined in this thesis. It is possible that RET signalling has a role in NCC maintenance in the lung, and therefore that the previously reported reduction in intrinsic neuronal numbers in the *Ret* mutant lung is due to problems with neural crest-derived neuron differentiation or survival rather than NCC migration. RET has been suggested to be necessary for maintenance of neural crest-derived sympathetic neuroblasts (Durbec et al., 1996) and GDNF for controlling ENS precursor proliferation (Gianino et al., 2003) and neuronal survival (Schafer and Mestres, 1999). This hypothesis could be further tested by quantifying the levels of neuronal cell death in *Ret* mutant and control lungs over several embryonic stages, and determining whether there is a difference in the level of neuronal cell death that could account for the decreased neuronal numbers observed in *Ret* mutant lungs at E18.5 by Langsdorf et al.

It is possible that the reported association of *Ret* mutations with respiratory dysfunction in some Haddad Syndrome cases (Amiel et al., 1998) is due to the role of RET in the formation or maintenance of neural crest-derived tracheal innervation, as a significant reduction in intrinsic neurons in the trachea has been reported in the

Ret mutant (Langsdorf et al., 2011). RET pathway involvement in the development of central respiratory carbon dioxide sensitivity, as previously hypothesised (Burton et al., 1997) could also lead to respiratory defects in *Ret* mutant mice without significant defects in lung intrinsic neuron formation.

In addition to NCC cell autonomous effects of the *Ret* mutation, it is possible that non-cell autonomous effects of the *Ret* mutation may also affect NCC colonization of the lung. The migration of wild-type NCC, transplanted into the *Ret* mutant mouse gut, is deficient compared to that of wild-type NCC in a wild-type gut (Bogni et al., 2008).

Optical Projection Tomography (OPT) scanning of Tuj1-stained E14.5 *Ret* -/-, -/+ and +/+ littermate mouse lungs was used to generate three-dimensional reconstructions of neuronal tissue in the lung for further phenotypic analysis. This approach allowed the pattern and density of neuronal projections to be compared throughout the whole lung, rather than between sections. It also allowed the approximate size and general morphology of the lungs to be assessed and compared. OPT has previously been used to assess the general morphology of mutant mouse phenotypes (Ijpenberg et al., 2007) and to characterise immunostaining patterns in normal embryos (Walls et al., 2008).

Analysis of OPT scans showed that neuronal projections were present in the same pattern and had similar diameters in *Ret* mutant and wild-type lungs. Ganglia were also present in the same positions in mutant and wild-type lungs. In sections from *Ret* and *Gfra1* E14.5 mutant embryos there was no visible difference in the distribution and density of neuronal projections and cell bodies between mutant and wild type littermate control lungs. The innervation in *Ret* mutant lungs was also investigated in greater depth using OPT and neuronal quantification. The use of OPT to compare lung innervation phenotypes in mutant mouse models is a novel technique which allowed us to look in greater detail at the architecture of lung innervation. Combined with neuronal quantification using microscopy, these techniques allowed a global assessment of lung innervation. No apparent difference could be seen between *Ret*-/-, +/- and +/+ mouse lungs at E14.5.

These results suggest that the GDNF receptors RET and GFRa1 may not be involved in lung colonisation. However, the results of GDNF bead organotypic culture experiments appear to contradict the results of *Ret* and *Gfra1* mutant mouse analysis. *Ret* and *Gfra1* mutants show no defects in lung innervation, yet in organotypic lung culture lung NCCs migrate towards GDNF beads. There are several possible explanations for this. The most likely is that lung NCCs express RET and GFRa1 receptors due to their origin as foregut NCCs and so are capable of responding to GDNF when exposed to it in culture even though GDNF is not a guidance cue for NCCs in the lung *in vivo*. In previous studies, although RET and GFRa1 receptors were found to be expressed on NCCs within the lung, GDNF expression was not detected in the lung (Burns and Delalande, 2005).

An alternative hypothesis to explain these results is that the two GDNF receptors have redundant roles in guiding lung NCCs towards GDNF during normal development, as GFRa1 is reported to be capable of transducing GDNF signals in the absence of RET (Airaksinen et al., 1999). In order to test this latter hypothesis a double knockdown of *Ret* and *Gfra1* expression could be carried out and the effect on NCC migration into the lung observed.

It is also possible that other RET co-receptors, GFRa2, 3 or 4, are present on lung NCCs and are involved in mediating normal NCC migration into the lung in response to alternative RET ligands such as neurturin, artemin and persephin (Manie et al., 2001). Due to cross-selectivity within the GFRa family, these receptors also weakly bind GDNF (Airaksinen et al., 1999) and could therefore mediate NCC migration towards an artificial source of GDNF in the lung organotypic culture system. Similarly, soluble GFRa1, shown to be present in the human lung (Burns et al., 2008), could act as a guidance cue for lung NCC. However, the normal lung colonization seen in the *Ret* mutant lung makes this unlikely as signalling through these pathways would require a functioning RET receptor.

While diffusible guidance cues are important in NCC migration in the gut, NCC migration can also be constrained by migration along a spatially restricted permissive substrate or scaffold. Endothelial cells on the outer surface of blood vessels have been shown to be a substrate for migration of NCCs within the gut

(Nagy et al., 2009), constraining NCCs to migrate in particular regions. NCC migration and blood vessel development have also been linked at an earlier stage of NCC migration, where NCCs and growing blood vessels both use semaphorin signalling through the receptor neuropilin to guide their growth from the neural tube region into the gaps between future vertebrae in the developing spinal cord (Fantin et al., 2009). Blood vessels and nerves use similar signalling pathways to pattern their growth, and NCCs and neuronal projections can use growing blood vessels as guides (Carmeliet, 2003). In order to investigate whether migration along blood vessels was a plausible method of guidance for NCCs entering and migrating within the lung, the positioning of NCCs and blood vessels within the lung was examined in several stages in *Wnt1Cre:Rosa26YFP* mouse embryos. The vascular plexus was not condensed into blood vessels at E12.5, when NCCs first entered the lung, and NCCs were not seen in endomucin-expressing lung tissue, instead remaining near the future airway epithelial tubules. NCCs were not present in association with larger blood vessels seen in older lungs, indicating that NCCs do not migrate along these vessels within the lung.

BDNF beads do not attract lung NCCs in culture, indication that BDNF does not act as a chemoattractant for lung NCCs, despite reported lung innvervation defects in *Bdnf* mutant mice (Garcia-Suarez et al., 2009). Alternatively, signalling through BDNF may be necessary for successful pulmonary intrinsic neuron projection growth or differentiation, as previously suggested (Garcia-Suarez et al., 2009). Other results from this thesis (see chapter 6) indicate that vagal nerve fibres are required for correct positioning of neural crest-derived intrinsic ganglia. Given that deficiencies in the vagal nerve have been reported in *Bdnf* mutant mice, and the suggested role for vagus innervation as a scaffold for NCC migration identified in *Tbx1* mutant mice (chapter 6), it seems likely that the lung innervation defects reported in *Bdnf* mutant mice result from defects in vagal nerve formation.

6. Chapter 6: Role of transcription factors in NCC colonisation of the lung

Having characterised NCC migration into the lungs (chapter 3) and investigated signalling pathways involved in NCC migration (chapters 4 and 5), the next step was to examine the role of transcription factors in NCC colonisation of the lungs. Transcription factors potentially involved in NCC migration into the lungs were investigated by examining lung innervation in mice with mutations in transcription factor genes, which had deficiencies in gut innervation and a reported deficiency in NCC colonisation of the gut or other organs. The transcription factor genes selected for investigation are known to cause neural crest defects when mutated in transgenic mouse strains and are mutated in human congenital diseases (see introduction, section 1.7). Investigating the effects of transcription factor gene mutations on neural crest-derived innervation in the lung allowed examination of the pathways upstream of chemotactic signalling in NCC colonisation of the lung.

6.1 Sox10 in NCC migration and development

Sox10, discussed in the introduction (section 1.7.2), is a transcription factor important in several stages of NCC development as a survival, proliferation and differentiation factor. In order to investigate its potential role in lung NCC function, it was first examined whether Sox10 is expressed in the NCCs that migrate into the lung. Using *in situ* hybridisation, it was found that *Sox10* is expressed in NCCs in the mouse lung and gut at E12.5, when NCCs begin to migrate into the lung (Figure 6.1). Dorsal root ganglia, which have been shown to express *Sox10* (Britsch et al., 2001), were used as internal controls to show that the *in situ* hybridisation staining pattern for *Sox10* expression was as expected (Figure 6.1, A, B). *Sox10*-positive NCCs surrounded the foregut (Figure 6.1, C-F) and were present around the bronchi (Figure 6.1, C) and in the lung buds near the epithelial tubules (Figure 6.1, E-H). These results confirmed that *Sox10* is expressed in NCCs that colonise the lung.

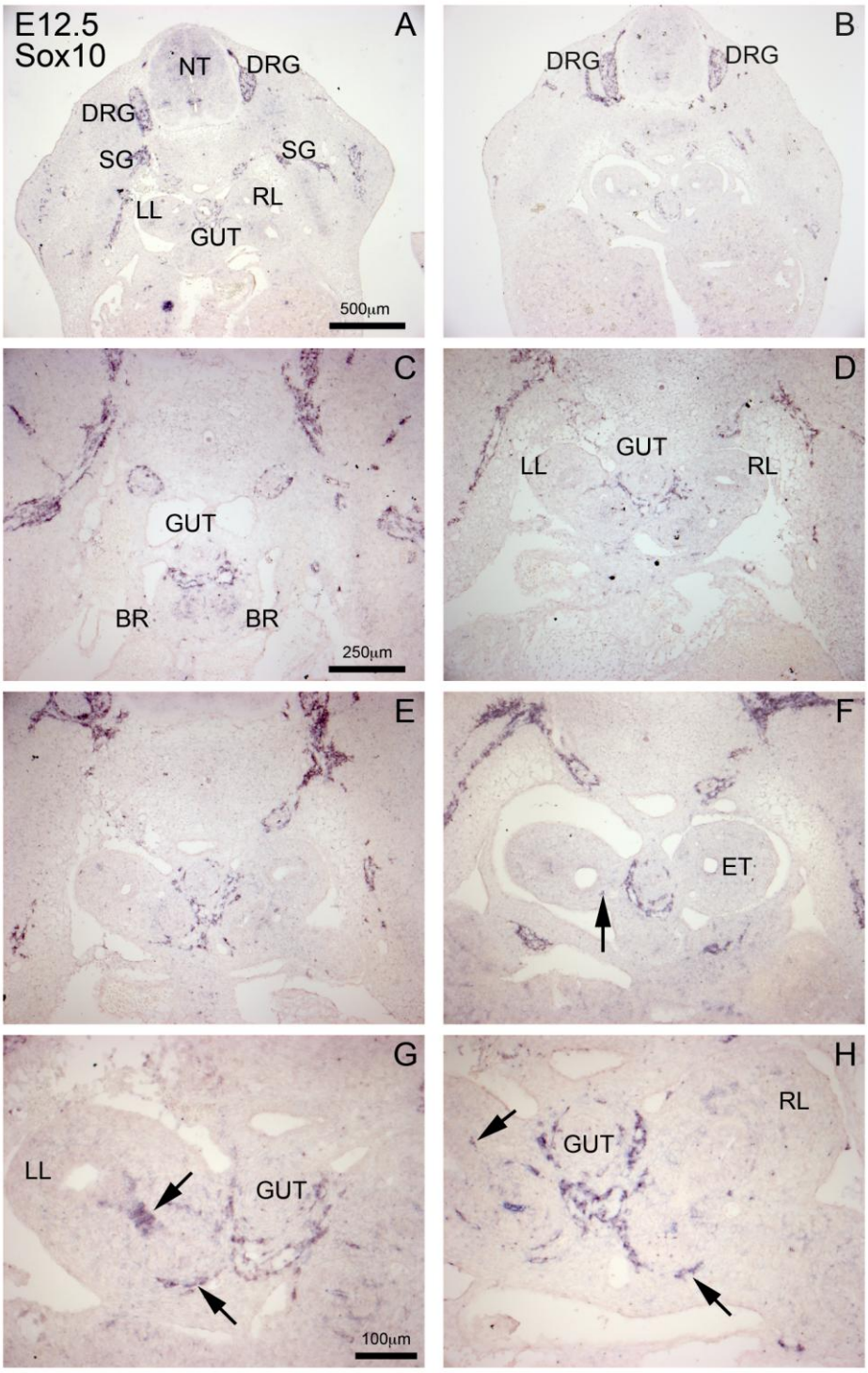

Figure 6.1 *Sox10* expression in sections of E12.5 wild-type mouse embryo. *Sox10*-expressing NCCs are seen around the developing gut and in the developing lung buds (arrows). BR: bronchus, DRG: dorsal root ganglia, ET: epithelial tubule, GUT: gut, LL: left lung, NT: neural tube, RL: right lung, SG: sympathetic ganglia.

6.1.1 Analysis of *Sox10Dom* mutant mouse lungs

Having confirmed that *Sox10* is expressed in NCCs that colonise the lung, the next step was to investigate whether Sox10 is necessary for normal NCCs colonisation of the lung, by examining lung innervation in a *Sox10* loss-of-function mouse mutant. There are a number of *Sox10* mutant mice including a *Sox10* open reading frame deletion mutant (Britsch et al., 2001) and less severe hypomorphic codon substitution and single base deletion mutants (Schreiner et al., 2007). Embryonic lungs from a mouse strain carrying the *Sox10Dom* (Dominant Megacolon) mutation (Herbarth et al., 1998) were examined. The *Sox10Dom* heterozygote mutant has a well-documented variable-length intestinal aganglionosis similar to human Hirschprung's disease (Southard-Smith et al., 1998). This aganglionosis results from severely reduced NCC migration into and along the gut due to NCC death early in the NCC migration pathway (Kapur, 1999). The homozygous *Sox10Dom* mutant has total intestinal aganglionosis, though extrinsic gut innervation from the vagal nerve is still present in the upper gut. Homozygous *Sox10Dom* mutants die *in utero* by E15 (Kapur, 1999).

Lung innervation was first examined in cryosections of E14.5 *Sox10Dom* (*Dom*) wild-type and homozygous mutant littermate embryos stained for the neuronal marker Tuj1 (Figure 6.2). Neural crest-derived intrinsic lung neurons (Figure 6.2, A-C) were identified by their position and by their expression of Tuj1. In *Dom* homozygous mutant mouse lungs, intrinsic neurons are absent within the lung in contrast to intrinsic neurons in wild-type littermate controls. At similar lung levels, shown by the pattern of epithelial tubules (Figure 6.2, B, E), neuronal cell bodies can be seen in wild-type littermates whereas only thin neuronal projections are present in mutants. Neuronal projections (Figure 6.2, C, F) are present in both wild-type and homozygous mutant lungs. Lung morphology, including lobe separation and airway size, appears similar in mutant and wild-type lungs (Figure 6.2, A, D).

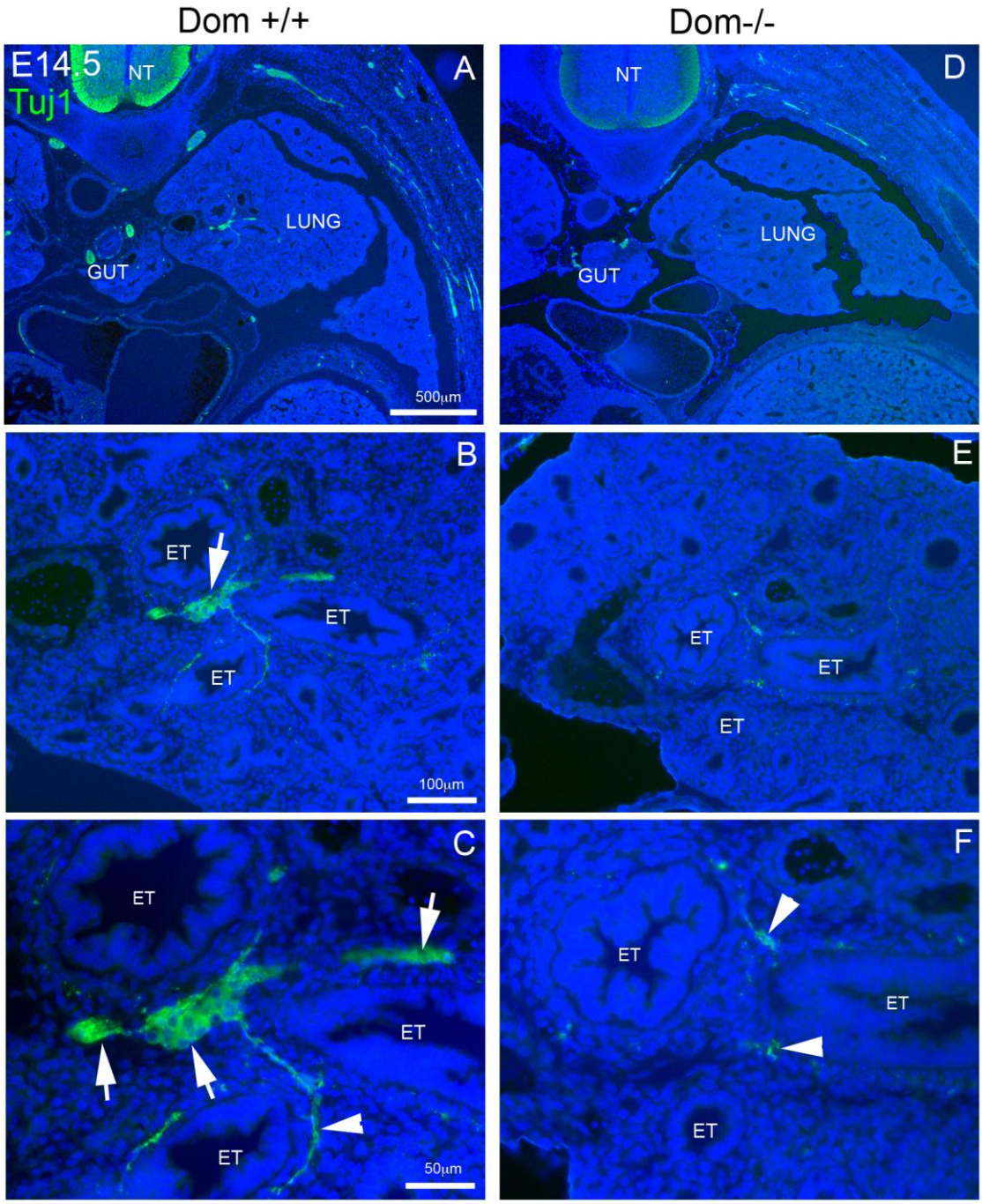

Figure 6.2 E14.5 *Dom* +/+ and -/- littermate embryos show absence of neurons in mutant, immunostained for Tuj1. Neuronal cell bodies and ganglia are present in the wild-type lung (white arrows) but absent in the *Dom* mutant lung in sections taken from similar levels in the lung (C, F). Nerve fibres (arrowheads) are present in both genotypes. ET: epithelial tubule.

In order to look at innervation throughout the lung and to gain information on the three-dimensional distribution of neuronal tissue within the lung, E14.5 littermate lungs from wild-type (n=3), *Dom* heterozygote (n=3) and *Dom* homozygote (n=3) embryos were scanned using optical projection tomography (OPT) (Figure 6.3) according to the technique described in chapters 3 and 5. OPT scanning allowed analysis of lung morphology and neuronal marker distribution throughout the whole lung in three dimensions.

Neurons and ganglia are absent in *Dom* homozygous mutant lungs (Figure 6.3, F') but ganglia are present in similar positions and at approximately similar sizes in *Dom* heterozygous mutant lungs and stage-matched wild-type lungs. Neuronal projections (arrowheads) are present in stereotyped positions along the branching airways (Figure 6.3, D'-E'). A few thin extrinsic neuronal projections are seen in approximately normal positions in *Dom* homozygous mutant lungs (Figure 6.3, F'). Lungs of the same genotypes (Figure 6.3, A and D, B and E, C and F) had similar staining patterns, indicating that the lack of intrinsic neurons seen in the *Dom* mutant lung is a consistent feature.

Some lungs were prepared for scanning by removing the gut and vagal nerves (Figure 6.3, D-F) while the gut and vagal nerves were left attached to others (Figure 6.3, A-C). In the *Dom* homozygous mutant specimen (Figure 6.3, C) intrinsic gut innervation appears absent, while the vagal nerve projecting along the gut appears normal. This confirms the gut phenotype previously reported (Kapur, 1999).

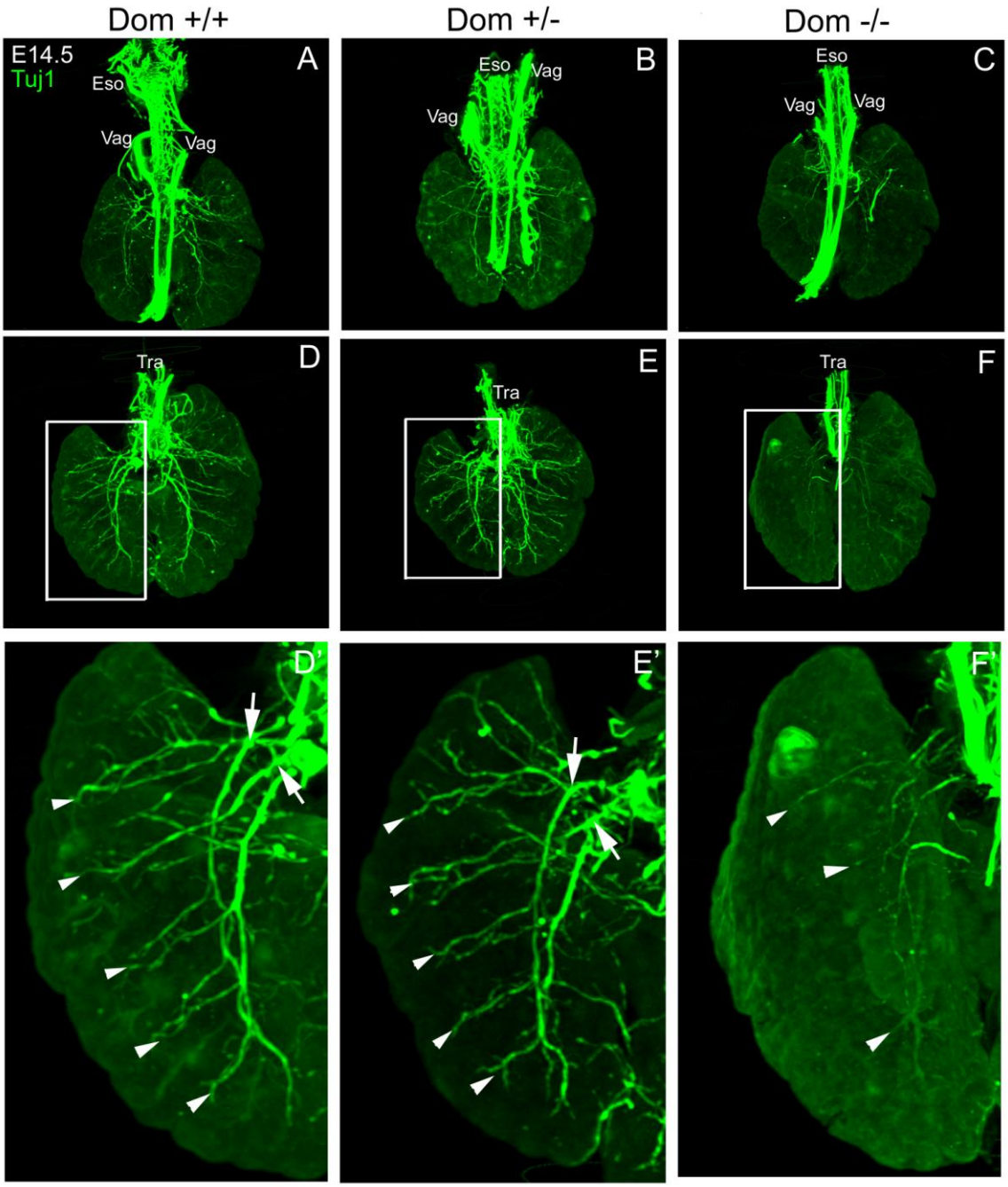

Figure 6.3 Three-dimensional reconstructions of OPT scans of neuronal tissue in E14.5 *Dom* +/+, +/- and -/- lungs. Tissue stained for Tuj1 (green). A-C have gut and vagal nerve attached, D-F are different specimens with trachea only. Ganglia (arrows) are seen in *Dom* +/+ and *Dom* +/- lungs but not homozygotes. Fine projections (arrowheads) occur in all lungs but are sparser in *Dom* -/- lungs. Eso: Esophagus, Tra: Trachea, Vag: Vagal nerve.

After OPT scanning, the *Dom* lungs were retrieved and mounted intact for closer examination of individual ganglia (Figure 6.4). Intrinsic lung ganglia are present in wild-type and heterozygous mutant lungs but absent in *Dom* homozygous mutants (Figure 6.4, B, D, F). *Dom* homozygous mutant mice have normal patterns of extrinsic lung innervation but reduced thickness of neuronal fibres (Figure 6.4, E, F). The nerve fibres that project into the *Dom* -/- lung maintain their positioning and branching but are thinner than those seen in the wild-type lungs. This may be because in *Dom* -/- lungs projections from intrinsic neurons, which would usually contribute to these nerve bundles, are missing. Vagal nerve pathfinding in the *Dom* -/- lung thus appears to follow branching airways in a normal pattern, if not at normal density, in the absence of intrinsic lung neurons.

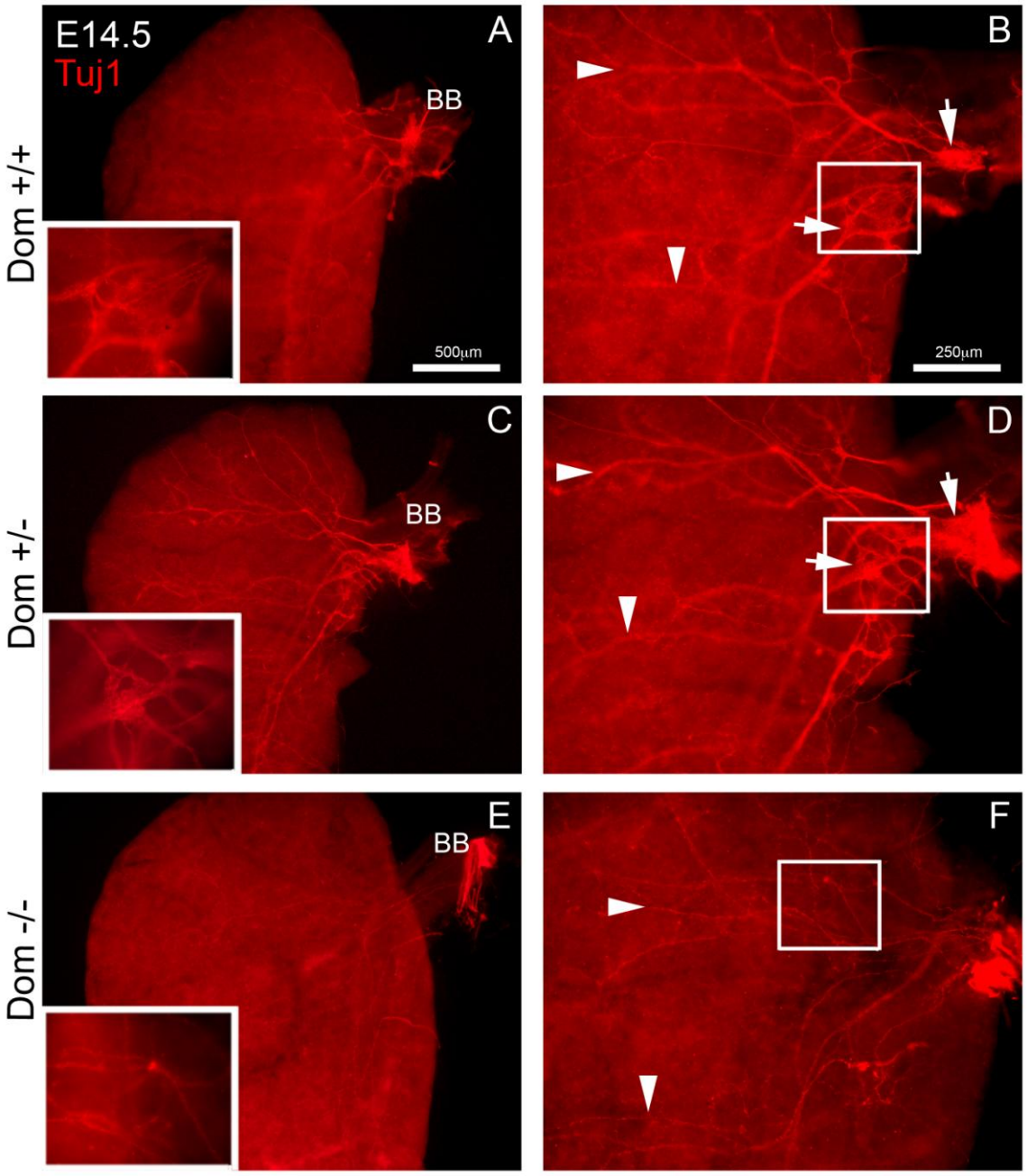

Figure 6.4 E14.5 wholemount *Dom* +/+, +/- and -/- lungs Tuj1-stained to show ganglia. Arrowheads indicate nerve fibres, arrows indicate major ganglia near the primary bronchus. Ganglia and neuronal cell bodies are absent in *Dom* homozygous mutants, and nerve fibre thickness is severely reduced. Boxes in A, C and E are magnified areas in B, D and F. BB: bronchus.

The size and distribution of lung ganglia were then examined more closely (Figure 6.5). In *Dom* wild-type and heterozygote left lungs, large (Figure 6.5, A, B), middle-sized (Figure 6.5, D, E) and small (Figure 6.5, G, H) ganglia can be seen in stereotypical positions, but in *Dom* homozygous mutant lungs nerve fibres are present without accompanying ganglia (Figure 6.5,C, F, I).

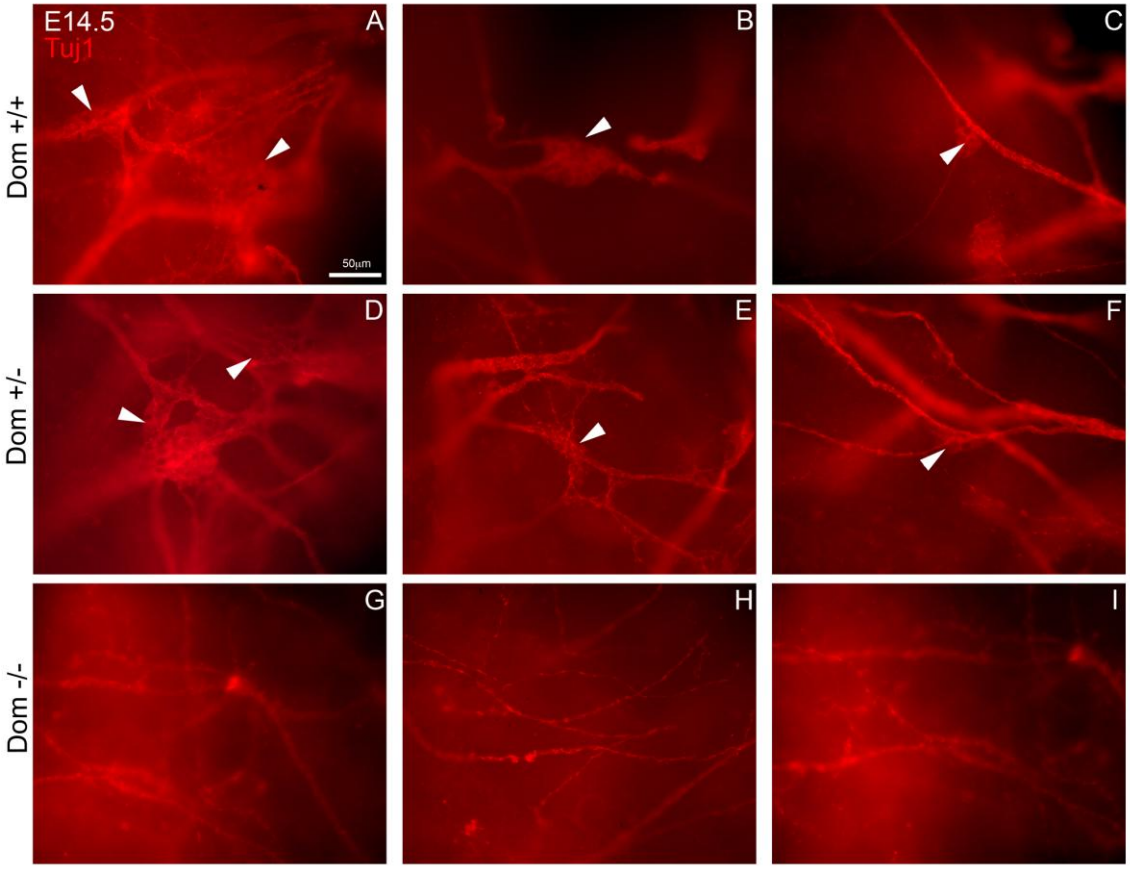

Figure 6.5 Ganglia positions in wholemount *Dom* and control lungs. Ganglia (arrowheads) are present near the bronchus (A-C), near the upper bronchiole (D-F) and peripheral lung (G-I). In *Dom* +/+ and +/- large, mid-sized and small ganglia can be seen in stereotypical positions, but in *Dom* -/- lungs projections are present without accompanying ganglia (C, F, I).

Tuj1 staining was sufficiently strong and specific to allow neurons to be counted within the lung. Results showed that there was a significant difference in numbers of neuronal cell bodies in the lung between homozygous mutants and stage-matched heterozygotes and wild-type embryos (Graph 6.1). There was also more variation in the number of lung neurons in heterozygotes compared to the wild-type group. This fits with previous descriptions of variable penetrance of the *Dom* allele in heterozygotes, where genetic background has been reported to affect the extent of NCC deficit (Walters et al., 2010).

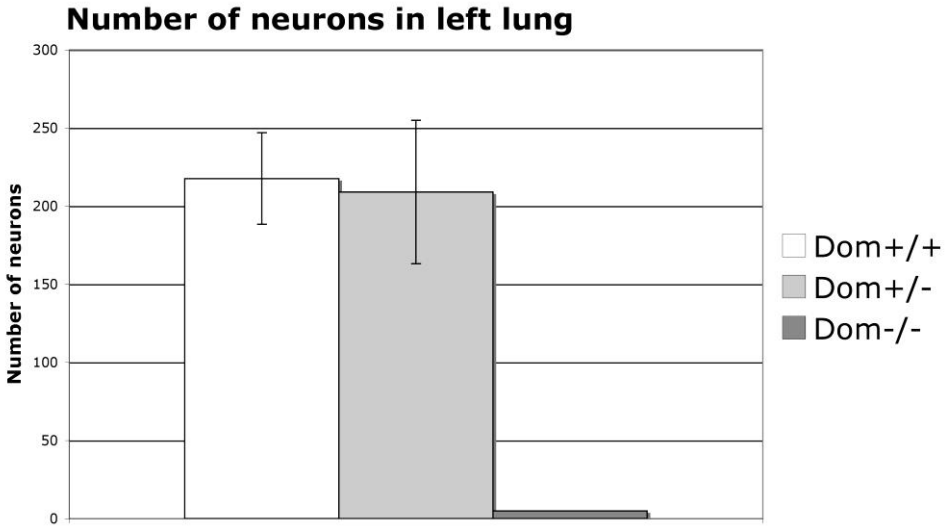

	MEAN	SD	SEM
Dom +/+	217.6	50.7	29.3
Dom +/-	209.0	65.0	46.0
Dom -/-	0	0	0

Graph 6.1 *Dom* -/- (n=3) lungs have significantly fewer neurons (P=0.003, One Way ANOVA) than *Dom* +/+ (n=3) and *Dom* +/- (n=2) lungs. There is no significant difference between wild-type and heterozygote lungs (p=0.835). Error bars show SEM.

Observation of the *Dom* wholemount lungs indicated an unexpected potential difference in lung size between different *Dom* genotypes. *Dom* homozygous mutant lungs appeared larger than those of stage-matched embryos. Given the deleterious effects of Sox10 mutation on general development, it seems unlikely that these embryos are generally developmentally advanced. This aspect of the *Dom* phenotype was investigated and quantified (Graph 6.2). Further investigation of this phenotype would be necessary to conclusively reject or confirm the statistical significance of the findings, as the experiment was statistically underpowered.

The pattern of lung branching is similar in mutant and wild-type lungs judging by branching patterns observed in wholemount (Figure 6.4) and by airway distribution and morphology in cross-sections (Figure 6.2). This indicates that increased airway branching does not seem to have occurred.

	MEAN	SD	SEM
Dom +/+	2.16	0.07	0.04
Dom +/-	1.98	0.21	0.12
Dom -/-	2.5	0.4	0.23

Graph 6.2 There is no significant difference in left lung size between *Sox10Dom* genotypes (p=0.128 one way anova). However, the test has insufficient power at n=3 per group to conclusively reject a difference in lung size between genotypes. Error bars show SEM.

Earlier work (Kapur, 1999; Southard-Smith et al., 1998) has shown that NCCs in *Dom* mutants and heterozygotes are more susceptible to cell death early in their migratory pathway, near the dorsal neural tube at E9 and E10, and has suggested that the decreased numbers of NCCs underlie the subsequent deficiencies in enteric nervous system formation seen in these mice. Later degeneration of neurons due to lack of glial differentiation caused by the absence of Sox10 has also been reported to cause neuronal death (Paratore et al., 2002), and *Dom* heterozygous mutants were observed to have increased apoptosis in vagal NCCs outside the gut (Stanchina et al., 2006). It was decided to see whether apoptosis in neural crest-derived cells was a factor in reducing intrinsic neuronal numbers in the *Dom* homozygous mutant lung at E14.5 using activated caspase-3 staining (Figure 6.6) which detects cell death (Kumar, 2007). Tuj1 is not expressed in apoptotic cells, so caspase-positive cells near neuronal tissue or ganglion sites were examined.

Results showed that caspase-3 positive cells are present in lung ganglion positions, in close proximity to neuronal projections (Figure 6.6, A-F). Caspase staining is seen in both wild-type (Figure 6.6, A, C, E) and mutant lungs (Figure 6.6, B, D, F). There appeared to be a slight increase in caspase-positive cells in mutants (Figure 6.6, B), but there is no clear difference. These results suggest that the substantial NCC death reported to occur earlier in the NCC migration pathway is likely to account for the reduction in NCCs in the lungs at this point in development. NCC death in lungs does not appear to contribute to the absence of NCCs in *Dom* homozygous mutant lungs.

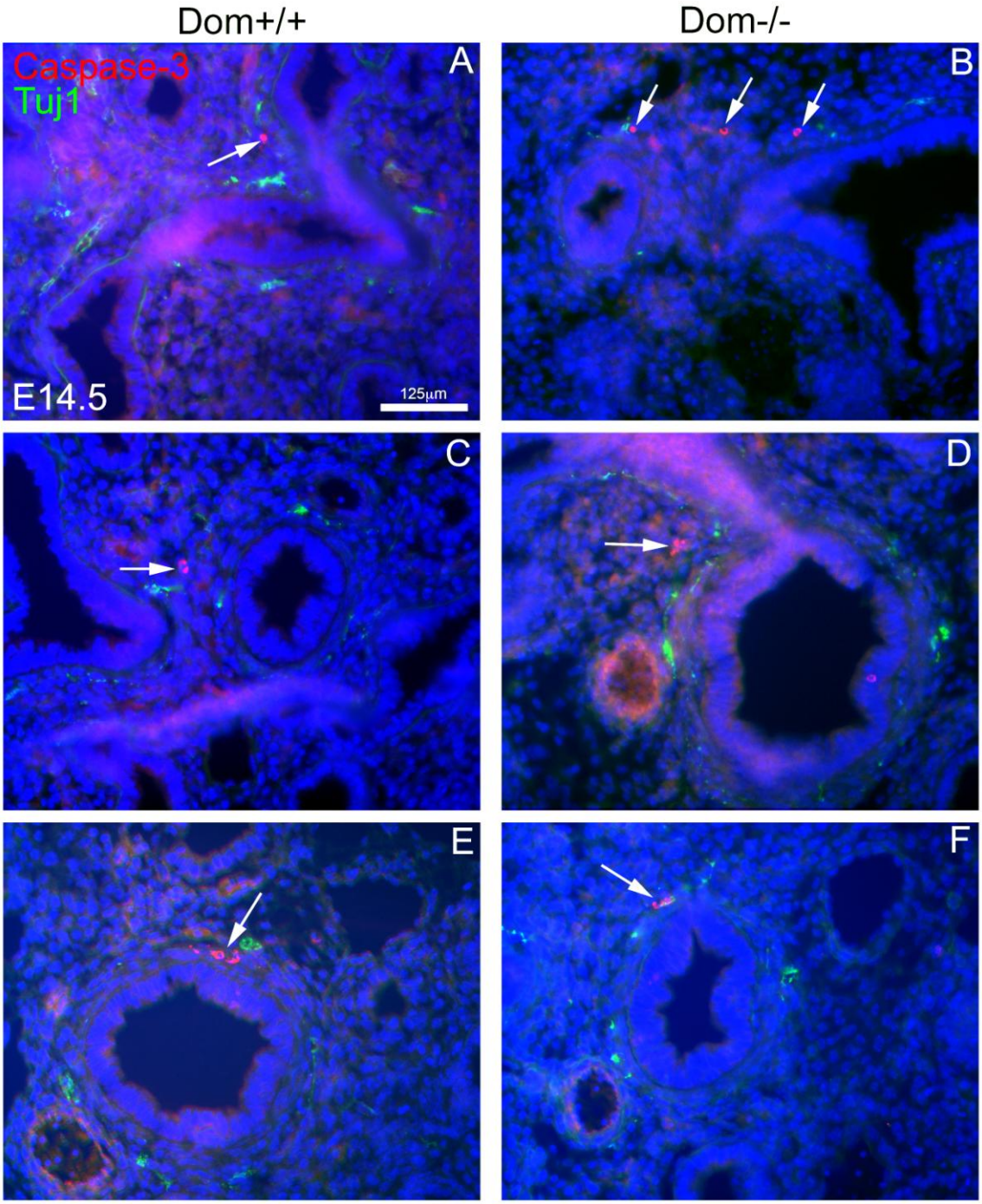

Figure 6.6 Caspase-3 staining in *Dom* +/+ and *Dom* -/- lungs indicates similar levels of cell death. E14.5 *Dom* wild-type and homozygous mutant lungs, stained for activated caspase-3, a marker of apoptosis. Cells positive for activated caspase-3 indicated by arrows.

6.2 Analysis of *Tbx1* mutant mouse lungs

The transcription factor Tbx1 is expressed in multiple regions including the pharyngeal arches, where it is involved the development of the branchial arches and is necessary for the expression of the transcription factor Gbx2, which is necessary for normal NCC guidance along the branchial arches (Calmont et al., 2009; Vitelli et al., 2002) and in the developing lung epithelium (Chapman et al., 1996). Although Tbx1 is not expressed in NCCs, *Tbx1* mutations can cause non-cell autonomous defects in the formation of some neural crest-derived structures, including the cardiac outflow tract (Vitelli et al., 2002). NCCs migrate within the branchial arches, which are disrupted in *Tbx1* mouse mutants. Extrinsic vagal nerve innervation is reduced in the *Tbx1* homozygous mutant mouse foregut (Calmont et al., 2011) and these mutants also have defects in neural crest-derived heart tissue (Lindsay et al., 2001). Further details of Tbx1 function are discussed in the introduction (section 1.7.3).

Lungs from E14.5 *Tbx1* mutant mice, described in (van Bueren et al., 2010) were obtained with littermate controls. Lung innervation was examined in sections of wild-type lungs and *Tbx1* homozygous mutant littermate lungs (Figure 6.7). Lung innervation appeared normal in the upper lung (Figure 6.7, A-D) in *Tbx1* -/- mice, with innervation present around the major airways. The size and distribution of the airways in mutant lungs also appeared normal. Intrinsic neurons and neuronal projections were present in both wild-type and mutant lungs, with ganglia seen near the bronchus in *Tbx1* -/- lungs (Figure 6.7, B, D). However, neuronal tissue distribution appeared to be significantly altered in *Tbx1* -/- lungs, with less neuronal tissue present in the caudal lung (Figure 6.7, E-H).

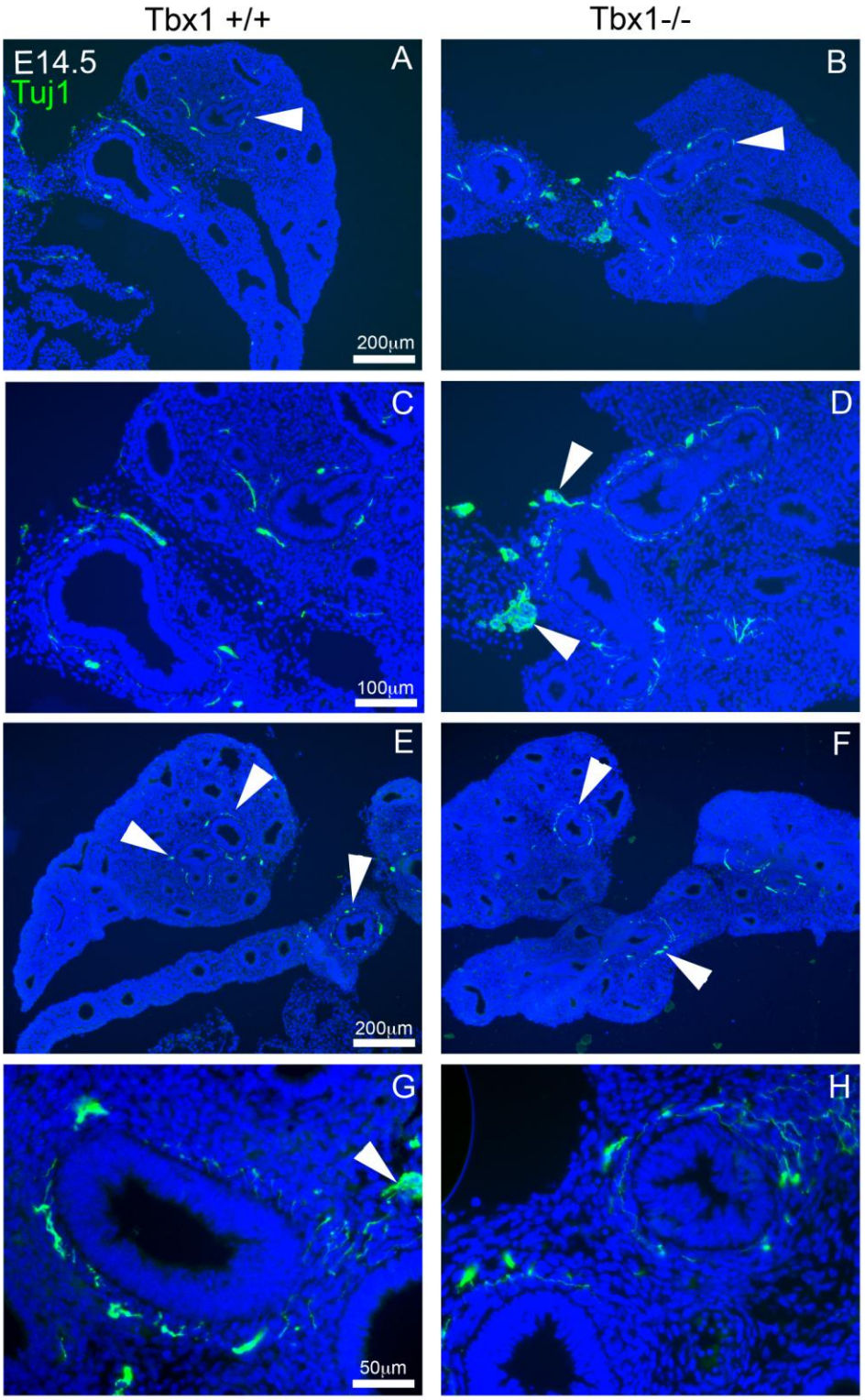

Figure 6.7 Lungs from E14.5 *Tbx1* +/+ and -/- littermates stained for Tuj1 show presence of neurons in both. Neuronal tissue (arrowheads), some in ganglia (D) is visible in both wild type and homozygous mutant lungs. However, neurons and neuronal tissue are sparser in caudal lung tissue (E-H) in mutant lungs (F, H) than in wild-type lungs (E, G).

In order to analyse the distribution of innervation throughout the whole lung, the phenotype was further investigated using wholemount immunohistochemistry. Whole *Tbx1* mutant and littermate lungs were stained for Tuj1 and the left lung was examined to determine the distribution of ganglia and projections (Figures 6.8, 6.9 and 6.10). In the wild-type lung the pattern and distribution of intrinsic ganglia and extrinsic projections appeared normal, following the stereotypical pattern of airway branching (Figure 6.8, A). However in *Tbx1* homozygous mutant lungs (Figure 6.8, E), there were no ganglia around the distal bronchioles. Instead, a large number of neurons were clumped together near the bronchus (Figure 6.8, F), suggesting that their migration into the lung has halted at this point. In addition, neuronal projections in the distal lung, either from intrinsic or extrinsic neurons, terminated at around 500 micrometres into the lung and, although associated with the airways up to that point, did not progress further along the airways into the lung.

Looking more closely at the bronchus and proximal lung (Figure 6.9) there were multiple ganglia in various positions in wild-type and heterozygote lungs (Figure 6.9, A, C) while in mutant lungs there was a single large aggregation of neurons at the bronchus and no ganglia in the more distal lung (Figure 6.9, E). At a position in the distal lung where small ganglia are normally observed in wild-type lungs (Figure 6.9, B) there is an absence of neuronal projections in homozygous mutant lungs (F).

Next, neurons were quantified within the *Tbx1* mutant and control lungs (Graph 6.4, below) by counting the Tuj1-positive cell bodies in ganglia in wholemount lungs under high magnification. Their distribution was also more closely examined (Figure 6.10). While in wild-type and heterozygote lungs there were numerous ganglia in a range of sizes at stereotyped positions (Figure 6.10, A-F), in the *Tbx1* mutant lung a single large group of neurons larger than any single normal intrinsic lung ganglion was present near the bronchus (Figure 6.10, G) and, even where projections are present, there were no neurons in association with those projections (Figure 6.10, H, I).

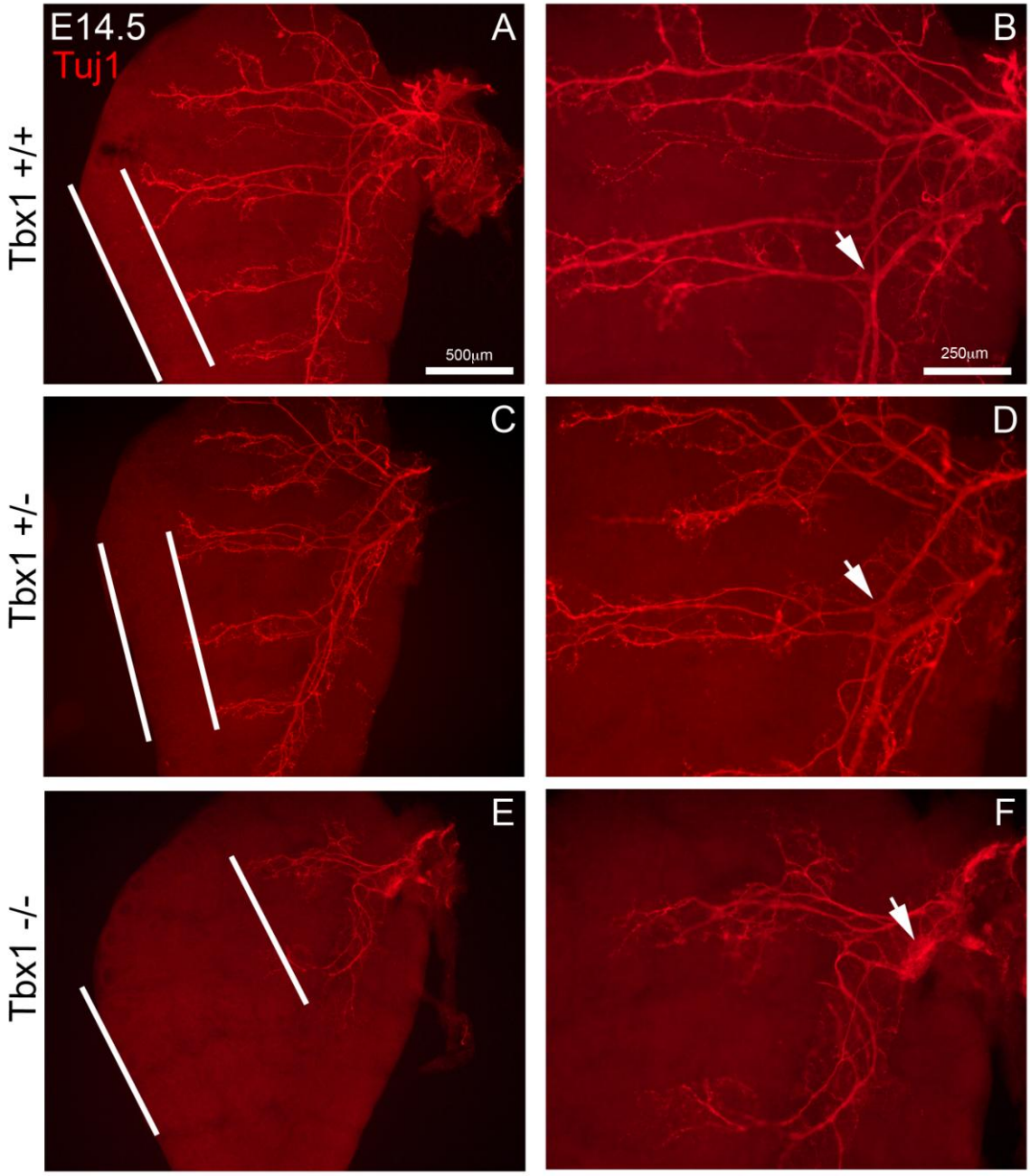

Figure 6.8 Neuronal projections extend less far into the distal lung in *Tbx1*-/- lungs. E14.5 wholemount *Tbx1* +/+, +/- and -/- lungs stained for Tuj1. Arrows indicate ganglia. White lines indicate end of projections and periphery of lung tissue, used to measure the distance between projections and lung boundary for analysis in Graph 6.3.

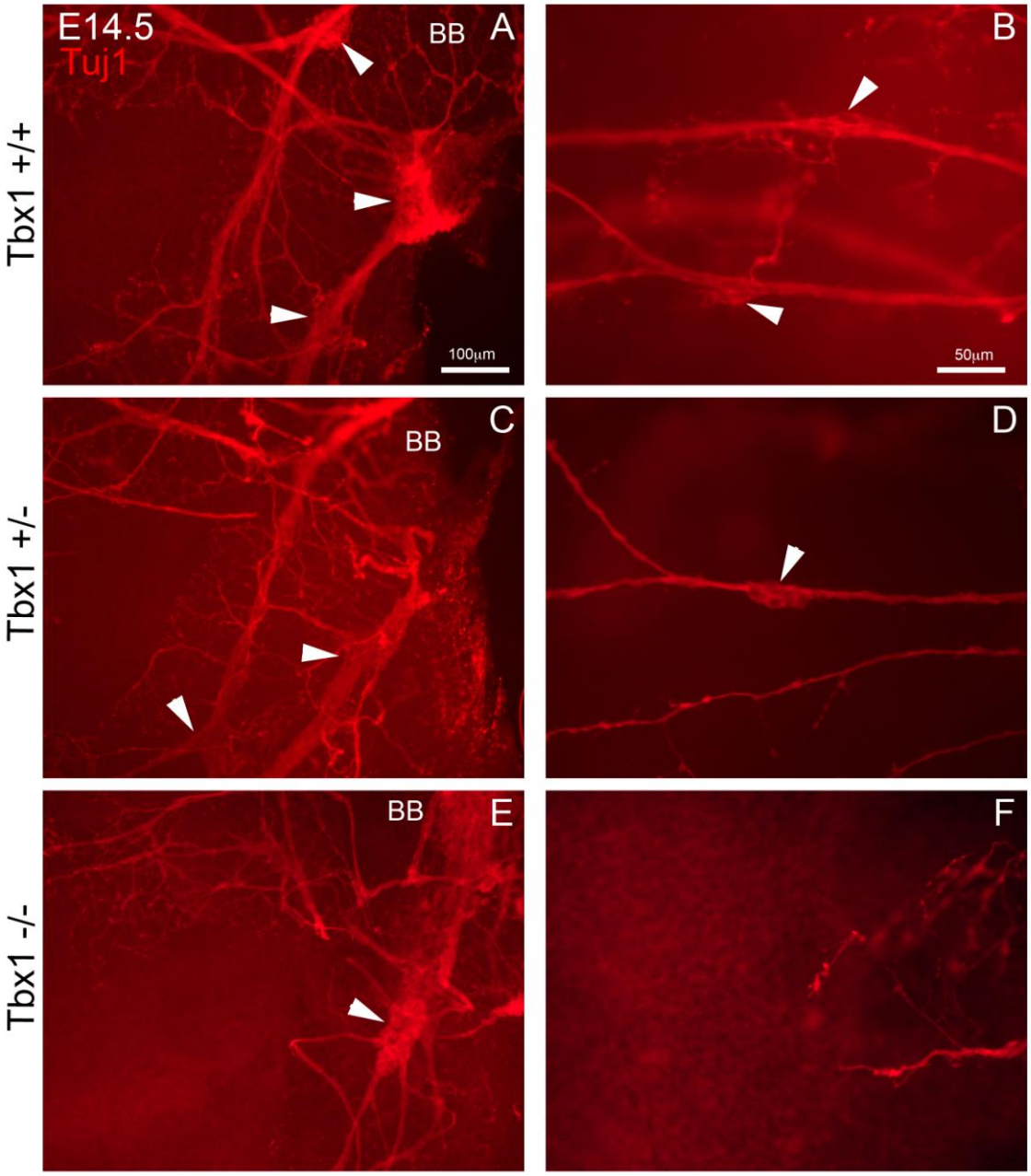

Figure 6.9 Neurons and nerve fibres in E14.5 *Tbx1* +/+, +/- and -/- lungs. Ganglia (arrowheads) are present in *Tbx1* +/+ and +/- lungs near the bronchus (A, C) and in the peripheral lung (B, D). In *Tbx1* -/- lungs, there are many neurons near the bronchus (E) but not in more distal tissue (F). BB; bronchus.

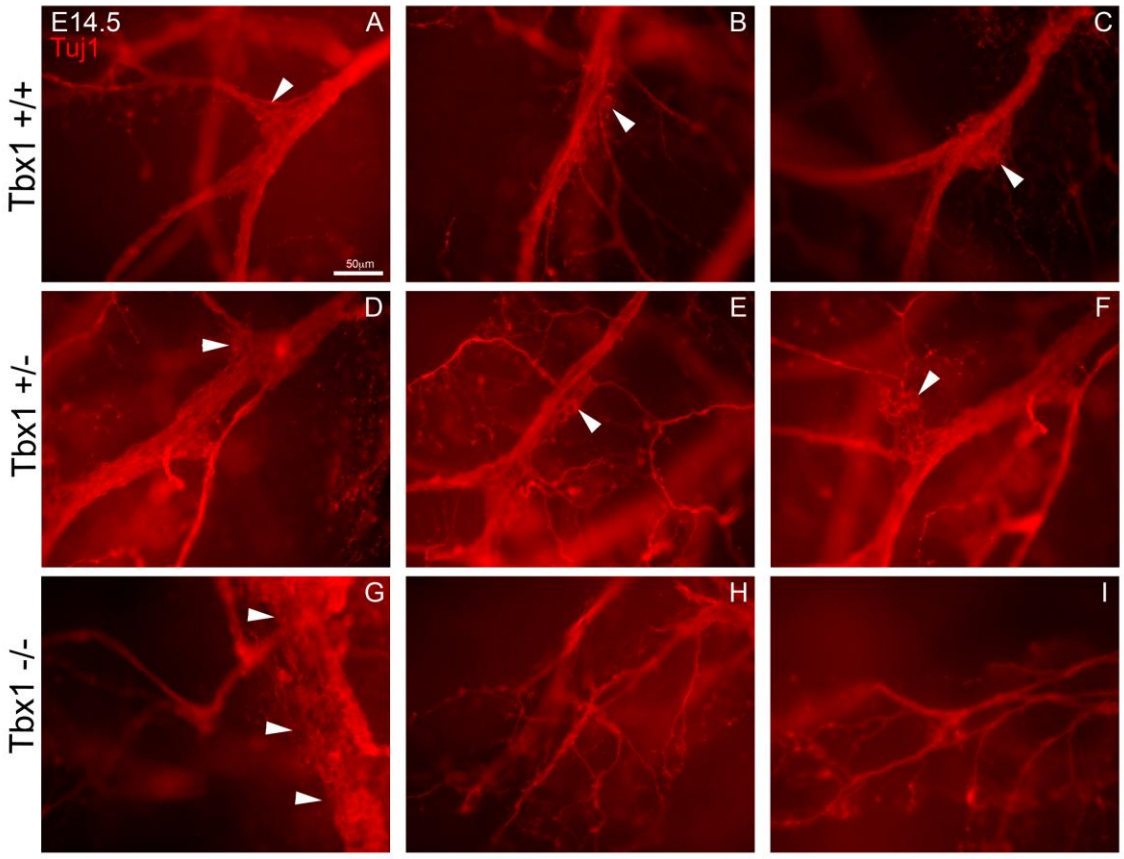

Figure 6.10 Ganglia in *Tbx1* +/+, +/- and -/- lungs. Ganglia (arrowheads) of various sizes are present in *Tbx1*+/+ and *Tbx1*+/- lungs (A-F), but in *Tbx1*-/- lungs most neurons are found in a single large aggregate that is located near the bronchus (G).

Next, the extent of lung innervation in *Tbx1* -/- and control lungs was quantified (Graph 6.3) by measuring the distance between the most distal lung innervation and the outer edge of the left lung, as shown in Figure 6.8. The larger the distance measured, the less extensive the lung innervation. There was a significant reduction in the extent of lung innervation in *Tbx1* -/- lungs. Projections in *Tbx1* +/+ and +/- lungs extended approximately four times further into the lung than projections in *Tbx1* -/- lungs.

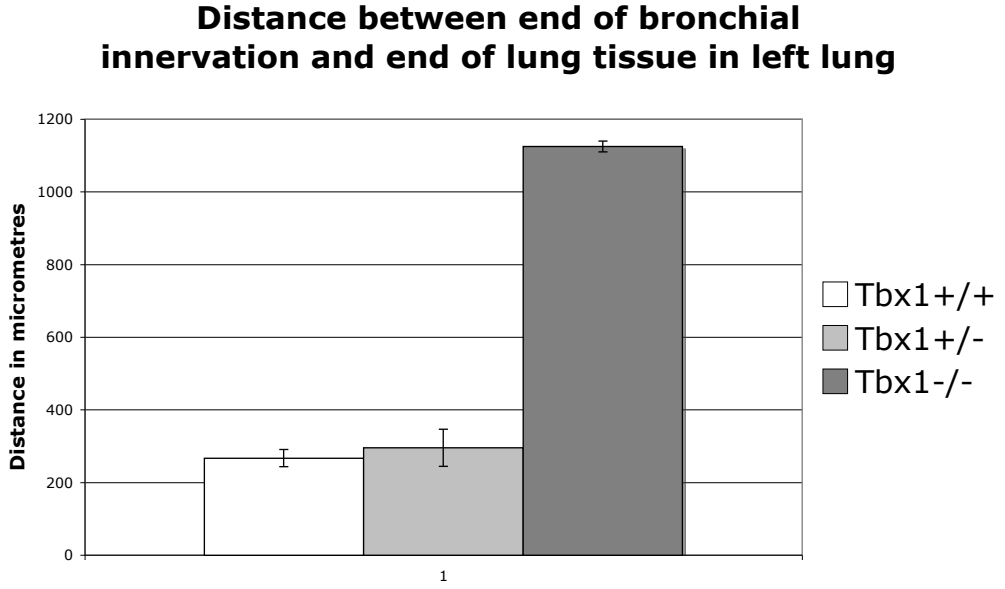

	MEAN	SD	SEM
Tbx1 +/+	267	42	24
Tbx1 +/-	295	88	51
Tbx1 -/-	1125	21	15

Graph 6.3 There is a significant difference in the extent of lung innervation ($p<0.001$, One Way Anova) between *Tbx*1 -/- (n=2) and both *Tbx*1 +/+ (n=3) and *Tbx1* -/+ (n=3). No significant difference was found between *Tbx1* +/+ and *Tbx1* -/+. Error bars show SEM.

To determine whether the presence of intrinsic neurons in one large ganglion in *Tbx1* -/- lungs was due to a lack of intrinsic neurons in the lung, the number of neurons within *Tbx1* mutant and littermate lungs was quantified. The mean number of neurons in *Tbx1* +/+ lungs was 120, and the mean in *Tbx1* -/- lungs was 156. There was no significant difference in the number of neurons in the lungs between the genotypes ($p=0.324$, One Way ANOVA on Ranks, n=3,2). The results show that NCC migration into the proximal lung appears to be unimpaired in *Tbx1* -/- lungs.

Therefore, the difference in ganglion positioning between *Tbx1* -/- lungs and *Tbx1* +/- or +/+ lungs is probably not due to a deficiency in the numbers of neurons that enter the *Tbx1* -/- lungs and is likely to be due to other factors.

6.3 Airway smooth muscle development in *Sox10Dom* and *Tbx1* mutant mice

NCCs migrate into the developing lungs and form intrinsic lung ganglia that are involved in the regulation of airway smooth muscle (ASM) contraction. It has been shown in fetal lung culture that stimulation of cholinergic intrinsic ganglia in the fetal lung causes ASM contraction (Sparrow et al., 1995), indicating that lung innervation could have a role in fetal ASM activity. This ASM activity has been proposed by Jesudason et al. to be important in shaping lung development by influencing intraluminal pressure and hence lung growth (Jesudason, 2009).

The role of neural crest-derived intrinsic ganglia in lung development and potentially in congenital lung disease was investigated by examining the lung structure and ASM in mouse mutants with altered lung innervation. ASM develops around the airways before those airways are colonised by NCCs. Having demonstrated a defect in intrinsic lung innervation in *Sox10Dom* (*Dom*) homozygote mutant mouse embryos (section 6.1), the expression of the ASM marker SMA in *Dom* homozygote mutant lungs was examined to test whether the absence of intrinsic lung innervation in these mutant lungs affected ASM development. The density and distribution of smooth muscle in *Dom* mutant lungs at E14.5 is very similar to that seen in wild-type littermate lungs (Figure 6.11). Smooth muscle surrounds the major airways in a dense band (Figure 6.11, C, D) and is present as a sparser band around smaller airways (Figure 6.11, E, F). The extent and density of ASM is thus similar in mutant and wild-type lungs, suggesting that intrinsic lung neurons are not necessary for normal ASM formation.

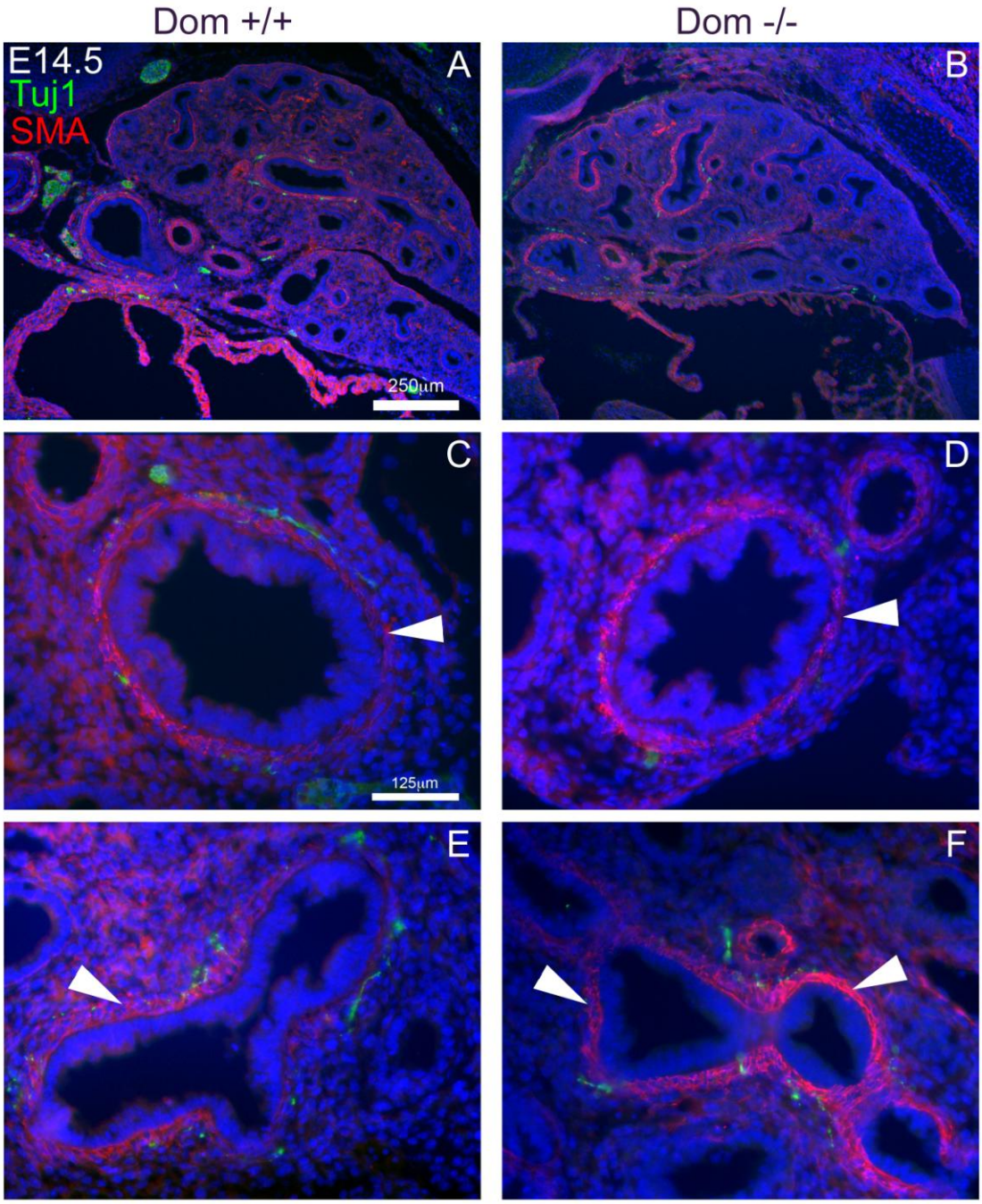

Figure 6.11 ASM appears unaffected in *Dom* mutant lungs. E14.5 *Dom* mutant and wild-type littermate lungs stained for SMA (red) and Tuj1 (green). A layer of smooth muscle is present around the airways and has similar thickness and density in *Dom* +/+ and *Dom* -/- lungs. Arrowheads indicate ASM.

In order to investigate whether the extrinsic and intrinsic lung innervation defects described in *Tbx1* -/- mutant lungs (section 6.2) affect ASM development, ASM distribution in *Tbx1* -/- mutant lungs was examined (Figure 6.12). At similar levels in the lung, wild-type and mutant lungs show similar airway morphology and ASM distribution (Figure 6.12, A, B). As described previously (chapter 3), ASM is present in distal lung tissue in the absence of innervation in normal development, and the same staining pattern is seen in *Tbx1* -/- lungs (Figure 6.12, D, F). The thickness and distribution of ASM around the airways is similar in *Tbx1* mutant and wild-type E14.5 lung (Figure 6.12, C-F). This suggests that the deficiency in extrinsic innervation and ganglion positioning in Tbx1 -/- lungs does not affect ASM formation.

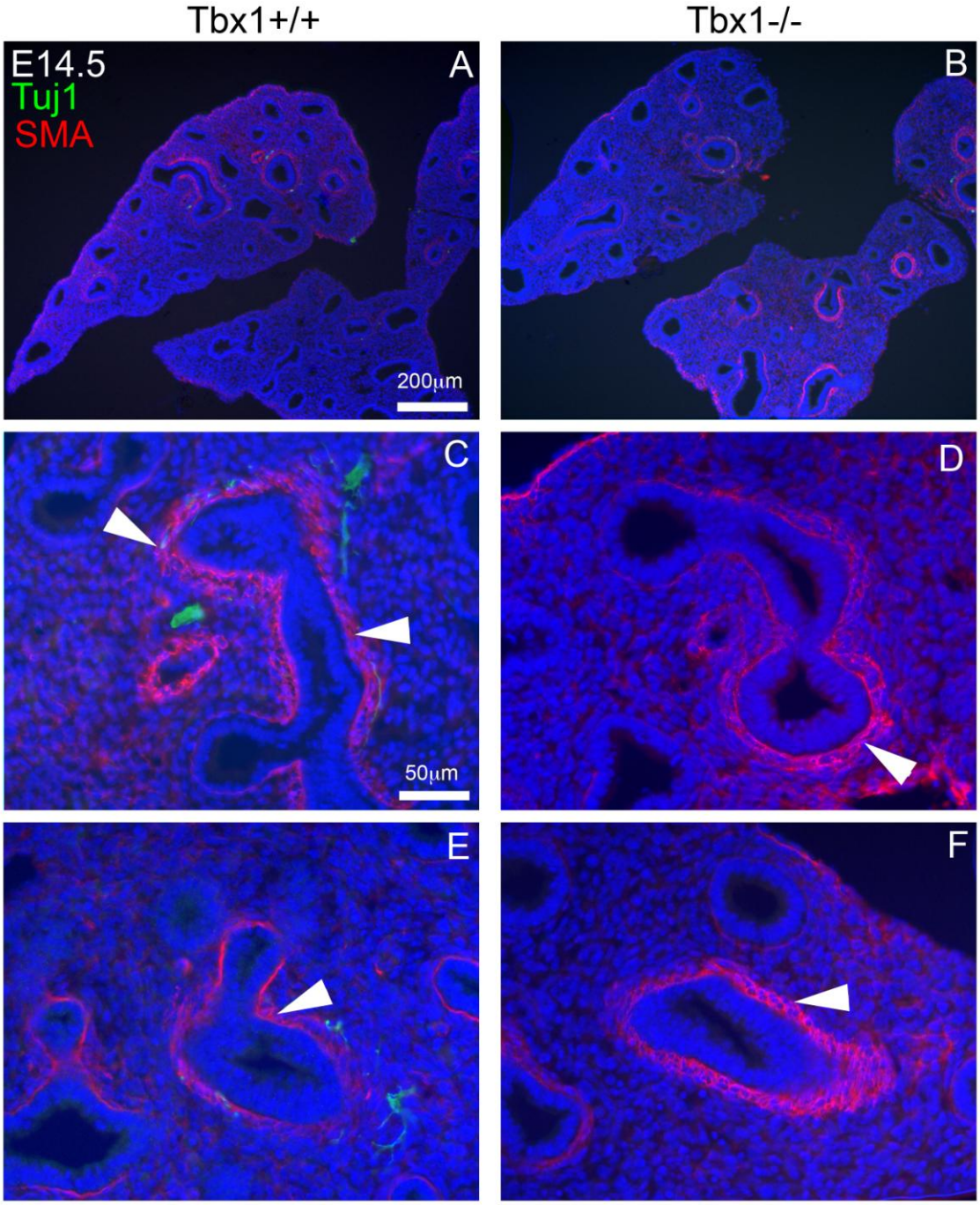

Figure 6.12 ASM appears similar in *Tbx1* +/+ and -/- lungs. *Tbx1* homozygous mutant and wild-type littermate lungs stained for SMA (red) and Tuj1 (green). A layer of smooth muscle is present around the airways and has similar thickness and density in *Tbx1* +/+ and -/- lungs. Arrowheads indicate ASM.

6.4 Discussion

The *Sox10Dom* (*Dom*) heterozygous mutant mouse has a number of NCC defects including failure of NCCs to colonise the caudal gut, causing variable length intestinal aganglionosis. The *Dom* heterozygous mouse is a model for Waardenburg Syndrome type IV (Southard-Smith et al., 1999; Southard-Smith et al., 1998), while the *Dom* homozygous mutant mouse has total enteric aganglionosis and does not survive past E15 (Kapur, 1999; Southard-Smith et al., 1998).

The previously described gut NCC defects in the *Dom* mutant guided the choice to analyse neural crest-derived innervation in the lungs in this mouse line, as gut and lung NCCs share a common developmental origin (Burns and Delalande, 2005). E14.5 *Dom* homozygous and wild-type littermate embryos were analysed using frozen sections. In mutants homozygous for the *Dom* mutation, neuronal cell bodies were absent within the lung. No airway ganglia were seen in mutant lungs, although thinner neuronal fibres not associated with cell nuclei, a characteristic of extrinsic neuronal projections, were present in *Dom* mutant lungs in a similar pattern to the thicker fibres seen in wild-type lungs. Nerve bundles in the *Dom* homozygous mutant lung had the same anatomical layout but were markedly thinner than nerve bundles in heterozygotes. The reduced thickness of projections in the *Dom* -/- lung may be due to the loss of projections from intrinsic neurons that would normally add to and thicken these branching nerve trunks. In *Dom* mutants, the pattern of extrinsic lung innervation was similar to that seen in the wild-type.

OPT scanning of *Dom* +/+, +/- and -/- stage-matched E14.5 lungs was used to compare the extent of intrinsic neurons and projections within these lungs and also allowed comparison of the density of gut innervation and vagal nerve innervation between genotypes. Using OPT scanning to analyse neuronal marker staining in the lungs allowed the initial observation of potential size differences between stage-matched lungs of different genotypes, which was followed up with statistical investigation. OPT scans thus enabled the comparison of multiple aspects of lung morphology, and gave a detailed, three-dimensional picture of lung innervation for phenotypic analysis, as previously used to analyse *Ret* mutant lung innervation (chapter 5).

In addition to the absence of intrinsic lung neurons, there was also a possible reduction in extrinsic vagal nerve innervation in *Dom* -/- lungs that could contribute to the decreased diameter of nerve fibres and sparser neuronal projections observed in OPT scans of *Dom* -/- lungs. However, the vagal nerve appeared normal in OPT scans of *Dom* -/- lungs so this does not seem likely. Despite this, it is possible that the neural crest-derived extrinsic vagal nerve fibres are affected by the *Dom* Sox10 mutation while extrinsic vagal nerve placode-derived fibres, dorsal motor nucleus and nucleus ambiguus fibres are not. Both neural crest- and placode-derived sources contribute to extrinsic sensory innervation of the lung via the pulmonary branch of the vagal nerve (Nassenstein et al., 2010).

The *Tbx1* heterozygous mouse has non-cell autonomous NCC migration defects in the pharyngeal arches (Calmont et al., 2009), while the *Tbx1* homozygous mutant mouse has deficiencies in vagal nerve formation resulting in vagal nerve hypoplasia (Calmont et al., 2011). However, NCC colonisation of the gut appears normal in these mutants. Lung innervation in E14.5 *Tbx1* +/+ and -/- mice was examined in sections, which showed that intrinsic neurons were present in *Tbx1* -/- lungs. More information was obtained from the analysis of lung innervation in *Tbx1* +/-, +/- and -/- whole lungs, which allowed us to better examine the pattern of neuronal distribution in these lungs.

In contrast to the lack of intrinsic innervation and reduced but apparently normally patterned extrinsic innervation in *Sox10Dom* mutant lungs, in *Tbx1* homozygous mutants extrinsic vagal lung innervation was severely disrupted while intrinsic neuronal cell bodies were present within the lungs. Intrinsic neurons were present in normal numbers in the proximal lung but they did not appear to migrate into the lung beyond the bronchi. Neurons appeared in large clumps, 'backed up' around the bronchus and did not move further into the lung lobes. As deficiencies in vagal nerve development leading to vagal nerve hypoplasia have been observed in *Tbx1* homozygous mutants (Calmont et al., 2011), it seems likely that the deficiency in nerve projections within the *Tbx1* -/- lung are due to the absence of vagal nerve innervation. Surprisingly, this deficiency in vagal nerve innervation appears to have affected the migration of NCCs into the lung and the positioning of neural crest-derived intrinsic ganglia.

The results indicate that NCCs may normally migrate into sub-bronchial airways along extrinsic nerve fibres, the projections providing a substrate for migration. The position of intrinsic neurons suggests that they use vagal nerve fibres to guide them into their correct locations in the peripheral lung after they have migrated from the gut into the lungs. Since Tbx1 is needed for normal vagus formation, and in its absence the vagus is disrupted, I hypothesise that in *Tbx1* -/- mice lung NCCs cannot use vagal nerve projections to guide them into the lung and so their migration is halted at the point where the vagus innervation stops. It has previously been suggested, owing to their close association during development, that migrating NCCs use the vagal nerve as a conduit for migration in the lung and NCCs have been shown to be present along the vagal nerve (Tollet et al., 2001), supporting these results. Similarly, cranial nerves have been suggested to be a scaffold for NCC migration to form facial parasympathetic ganglia and for motor neuron migration in the hindbrain (Coppola et al., 2010). In contrast, in the gut NCCs do not appear to use the vagal nerve as a guide (Calmont et al., 2011; Powley and Phillips, 2002) and intrinsic gut neural crest-derived neurons are needed for the development of some sensory vagus gut innervation (Ratcliffe et al., 2011). The neuronal projections that persisted in the upper airways of the *Tbx1* -/- lung may be the remnants of vagal nerve projections or they may be projections from intrinsic lung neurons, which would normally thicken the vagal nerve bundles that extend throughout the E14.5 lung. A possible experiment to determine whether the projections seen in *Tbx1* -/- lungs are from intrinsic neurons could be to use DiI tracing to determine the extent of the intrinsic neuronal projections and extrinsic vagal nerve innervation, by staining vagal nerve projections and intrinsic neuronal projections using DiI labelling in separate lungs or by using double labelling for intrinsic neurons and the vagus with DiI and DiO, which are differently coloured, in the same lung.

The vagal nerve hypoplasia seen in the *Tbx1* -/- mutant mouse may have an effect on lung development through disrupting lung innervation from the vagal nerve. However, since the homozygous mutants in which vagal nerve hypoplasia is seen do not survive past E15, the effect of *Tbx1* -/- vagal nerve hypoplasia on lung development and function cannot be analysed at later stages. The vagal nerve hypoplasia seen in *Tbx1* homozygous mutants resembles a congenital disorder in which lung innervation and development are affected. In congenital diaphragmatic

hernia (CDH) a section of bowel protrudes into the thoracic cavity through a defective, incomplete diaphragm during fetal development (Paterson, 1888). This protrusion reduces space in the thoracic cavity and impedes lung growth, resulting in lung hypoplasia (Campanale and Rowland, 1955). Pulmonary defects are the primary cause of death in CDH (Kitagawa et al., 1971). Although CDH is not considered to be a classical neurocristopathy, neural crest-derived structures are affected in a rat model of CDH produced by prenatal nitrofen exposure (Yu et al., 2001)., with effects including reduction in the number of intrinsic enteric neurons (Martinez et al., 2009), a reduction in tracheal innervation (Pederiva et al., 2008) and malformation or narrowing of the heart outflow tract (Yu et al., 2001). This indicates that a neural crest defect may underlie or contribute to the CDH phenotype. Thus, neural crest disorders may be a cause of CDH (Tovar, 2007; Yu et al., 2001). The intrusion of the bowel into the thoracic space is accompanied by lung hypoplasia. There is some evidence from physiological examination of the fetal lung that ASM dysfunction precedes hernia formation (Featherstone et al., 2006) and thus that lung hypoplasia in CDH may be a primary defect rather than a response to bowel intrusion into the thoracic space. The vagus and laryngeal nerves which provide extrinsic innervation to the trachea and esophagus are absent or hypoplastic in the nitrofen model of CDH (Martínez et al., 2004). More distal lung innervation in this model has not been examined to date. Alternatively, the lung hypoplasia in seen CDH may be secondary to bowel hernia or an effect of the nitrofen treatment on signalling molecules important in lung growth. Lung epithelial tubule development is delayed in nitrofen-treated mouse embryos (Coleman et al., 1998). Shh expression in the mouse lung has been described as altered by nitrofen treatment (Sato et al., 2009), as has Wnt expression (Doi and Puri, 2009) and FGF10 expression (Teramoto et al., 2003), and these signalling molecules are important in lung epithelial tubule development and lung growth (Affolter et al., 2009). However, the role of lung innervation in lung growth may be a factor worth investigating when looking at the role of intrinsic lung innervation in general lung development. One possible investigation could be to block neuronal signalling in a wild-type mouse embryonic lung during organotypic lung culture by using a neurotoxin, and the effect on lung developmental processes such as airway branching or airway peristalsis could then be observed and compared to that in control lungs.

Investigation of the role of intrinsic ganglia in lung development and function in this project has been hampered by the lack of access to an intrinsic innervation-deficient model. Mice with reported NCC defects were analysed as part of an investigation to find a model aganglionic lung to test the role of intrinsic lung neurons during development. The discovery of lung innervation defects in *Tbx1* and *Dom* mutant mice has opened avenues for the further investigation of lung and ASM development in the absence or disruption of intrinsic ganglia. In the *Dom* homozygous mutant mouse, this investigation has identified a model that can be used to examine the effects of the absence of intrinsic lung neurons on early lung development, in particular on airway smooth muscle development and prenatal activity. Although *Dom* -/- mutant mice had a severe deficiency in intrinsic lung neurons, homozygous mutants do not survive past E15 due to the effect on development of the *Dom* mutation and so their postnatal lung function could not be investigated.

There was an unexpected potential difference in lung size between different *Dom* genotypes although the experiment was statistically underpowered. The potentially increased size of *Dom* homozygous mutant lungs may be related to the absence of intrinsic innervation. The function of intrinsic lung neurons in development has not previously been addressed. Culturing embryonic lungs from *Dom* homozygous mutants could allow the examination of airway peristalsis in these lungs compared to that in wild-type lungs, and thus the analysis of the effect of intrinsic neurons on airway peristalsis. It is possible that the potential larger *Dom* -/- lung size is related to the role of intrinsic neurons in lung development. If lungs are larger in the absence of intrinsic innervation, this suggests intrinsic neurons may have a role in regulating airway peristalsis, which then may become over-active without them and thus causes lung overexpansion or hyperplasia. More *Dom* -/- mutant lungs, with wild-type littermates, are needed to confirm whether the alteration in lung size is a real or statistically significant effect. A further experiment, if the difference in lung size is confirmed, could be to culture *Dom* -/- lungs or other aganglionic embryonic lungs and comparing their airway peristaltic activity to that in control cultured lungs, to see whether the absence of intrinsic neurons increases the pace of airway peristaltic contractions.

Intrinsic neurons innervate smooth muscle, which generates peristaltic contractions during lung development (Schittny et al., 2000). These contractions increase intraluminal pressure, driving epithelial branching as shown *in vitro* (Unbekandt et al., 2008). Airway peristalsis is hypothesised to contribute to lung growth *in utero*, driving tissue expansion (Jesudason, 2009). There are a number of studies on the intrinsic contractility of ASM through the generation of calcium currents (Featherstone et al., 2005; Jesudason et al., 2006; Sparrow et al., 1994), but the effect of intrinsic lung innervation on these peristaltic contractions is unknown. Cholinergic innervation can stimulate contraction of ASM in the fetal lung *in vitro* (Sparrow and Weichselbaum, 1997). The role of neural crest-derived intrinsic lung innervation in smooth muscle activity and maintenance in the embryonic lung has not been fully investigated to date. In *Dom* and *Tbx1* homozygous mutant mouse embryos, two mouse models have been identified with which to examine the effects of neural crest-derived intrinsic lung neuron deficiency and disorganisation on the development of ASM, a target of intrinsic lung innervation. Investigation of the development of ASM in these mutant lungs has found that ASM distribution and density appeared normal in the absence of intrinsic neurons in the *Dom* -/- mouse (Figure 6.11). It has also been demonstrated that ASM appears normal in the caudal *Tbx1* -/- mouse lung in the absence of neural tissue (Figure 6.12). This suggests that normal lung innervation is not necessary for the development of ASM. However, the impact of the lack of lung innervation on ASM function remains to be investigated. ASM undergoes peristaltic contractions prenatally and in cultured embryonic and fetal lungs. ASM activity before birth has been investigated in the fetal pig lung (Sparrow et al., 1995; Sparrow et al., 1994). The pig fetal lung has been used as a model for human lung development owing to its similar size. As lung peristalsis may contribute to lung growth (Jesudason, 2009), intrinsic neuron function in development could be important if it affects ASM contraction in the embryonic lung as it does in the adult. Intrinsic pulmonary neurons could potentially act to control the rhythm of peristaltic contractions in embryonic ASM, slowing them and thus counteracting the generation of intraluminal pressure that drives lung expansion. This hypothesis could be further examined by culturing the Tbx1 and Dom mutant lungs and observing or physiologically measuring airway peristalsis in culture.

Chapter 7. Preliminary investigation into the potential involvement of intrinsic lung innervation in Sudden Infant Death Syndrome

SIDS (Sudden Infant Death Syndrome) is the term applied to the sudden, unexpected death of infants from unknown causes, usually during sleep. There is no clear aetiology, but congenital defects are suspected to be a predisposing factor due to the age of mortality. Cases are currently described as Sudden Unexpected Death in Infancy (SUDI) and if no cause is found after post-mortem are attributed to SIDS. Risk factors include prone sleeping position and parental smoking perinatally (Vennemann et al., 2007). Defects in respiratory control are strongly suspected to be responsible for at least some SIDS cases, as such defects could cause sudden death with little observable morphological abnormality. The difference in risk between prone and supine sleep positions also seems to implicate respiratory control and function. The presence of intrinsic lung neurons is not routinely screened for in pathological analysis of SIDS cases, although an increase in the number of NEBs has been described in SIDS cases (Cutz et al., 2007a; Gillan et al., 1989). Delayed maturation of the vagus nerve, a source of extrinsic lung innervation, has also been reported in SIDS (Becker et al., 1993). The morphology, distribution and extent of intrinsic ganglia in the lungs in SUDI/SIDS cases, which may have congenital respiratory function defects, have not previously been analysed.

Wax-embedded lung tissue from a number of SUDI cases is preserved in a post mortem tissue archive in the Histopathology Department of Great Ormond Street Hospital. This archive, made available to us by Professor Neil Sebire, is a unique resource for the investigation of the involvement of intrinsic neurons in SIDS. The archive is sizable as over 1500 cases are represented in the archived lung tissue. Of these cases, all were initially classified as SUDI. Following post-mortem investigation, some were assigned a known cause of death while for others the cause of death remained unknown. These latter cases were classified as SIDS and are likely to have heterogeneous causes. The 'known' (known cause of death) SUDI samples in which respiratory dysfunction is not implicated are from cases of a

similar range of ages to the 'unknown' (unknown cause of death) SUDI/SIDS samples. The 'known' SUDI samples can thus be used as internal controls when examining SUDI lung tissue samples for intrinsic pulmonary neuron abnormalities. We carried out a proof of principle investigation to determine whether the tissue available in this archive can be processed, immunohistochemically stained and analysed.

7.1 Lung innervation in human SUDI lung samples

We investigated lung innervation in wax sections of SUDI lung samples obtained from GOSH Histopathology archives. These cases were all postnatal deaths in early childhood from unknown causes, classified as SUDI. Sections from four different SUDI cases were immunostained for TuJ1, counterstained with the nuclear stain haematoxylin and analysed (Figures A1.1 and A1.2). Although airway ganglia and neuronal projections were observed in close proximity to the larger airway in most samples, preliminary analysis suggests that some lungs may have unusual patterns of innervation. In the slide from case 08p225 (Figure A1.2, M-P), a ganglion is present in the mesenchyme distant from any airway (Figure A1.2, P). There are also airway ganglia with unusual, irregular morphology (Figure A1.2, M, N), which do not resemble the pattern of innervation seen in any other sample.

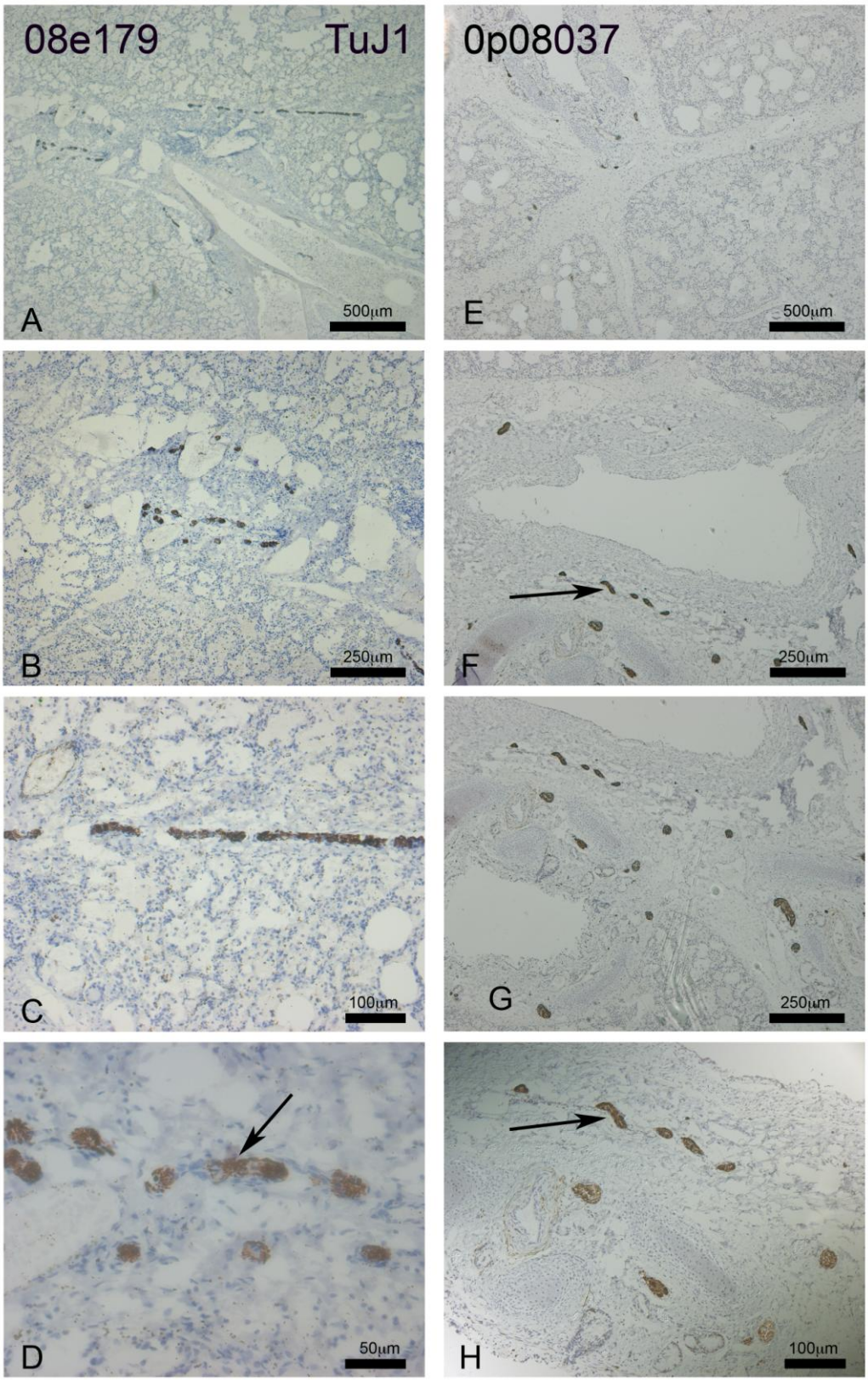

Figure 7.1 Lung innervation in SUDI lungs. Sections from wax-embedded SUDI postnatal human lungs after immunohistochemical staining for the neuronal marker TuJ1 (brown) and haemotoxylin counterstaining (blue). Arrows indicate neuronal tissue usually seen surrounding larger, conducting airways.

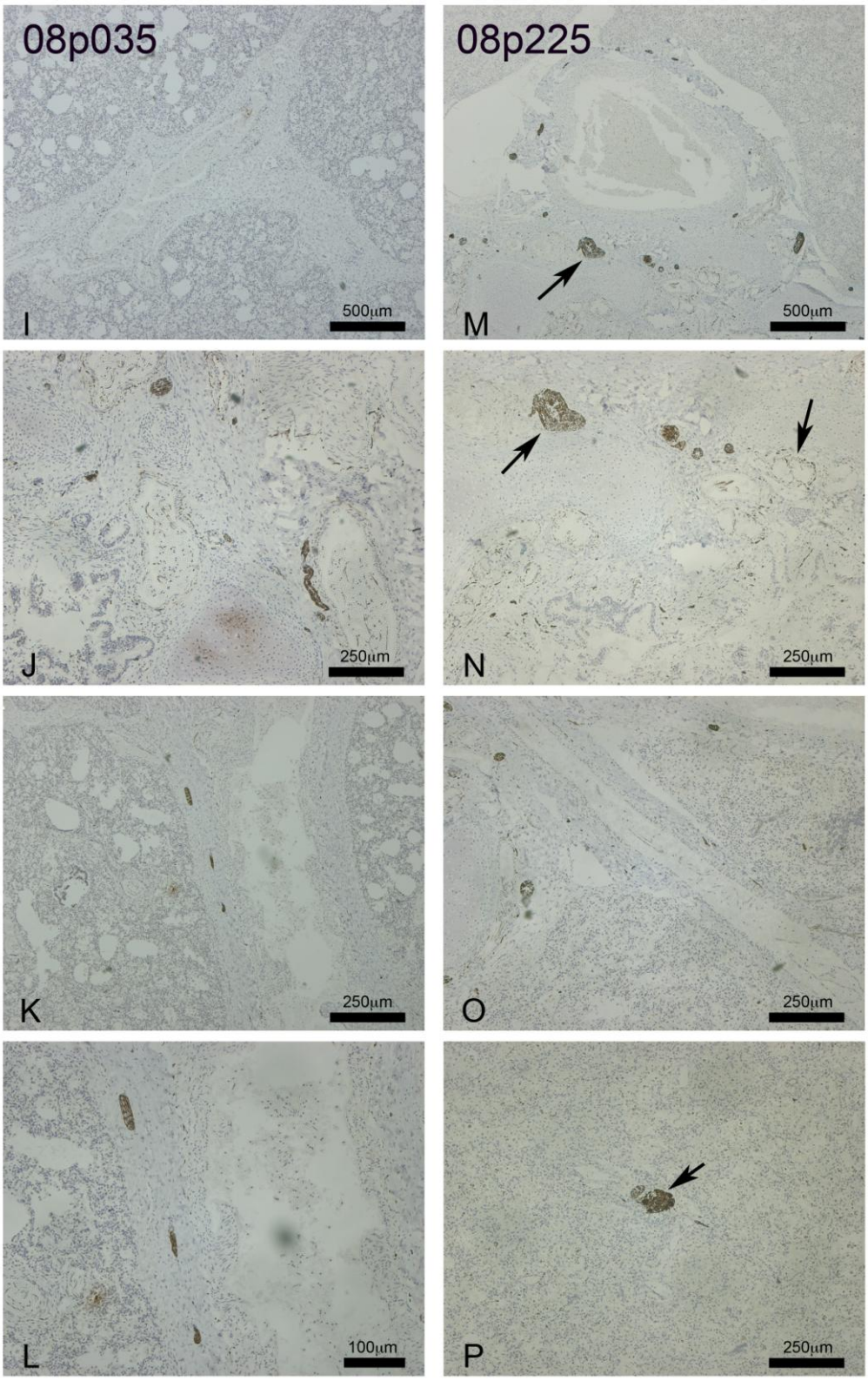

Figure 7.2 Lung innervation in SUDI lungs. Sections from wax-embedded SUDI postnatal human lungs after immunohistochemical staining for the neuronal marker TuJ1 (brown) and haemotoxylin counterstaining (blue). Arrows indicate neuronal tissue usually seen surrounding larger, conducting airways.

Following immunohistochemical analysis on wax sections, a procedure to analyse lung innervation was developed, taking precautions to ensure that the samples analysed were comparable to each other. Given the heterogeneity of the origin of sections, airway diameter was used as a proxy for airway generation and hence the level of the lung from which the tissue was taken. In order to standardise the branching level of the lung examined to more feasibly compare numbers of neuronal ganglia between samples, ganglia were only counted within 0.5mm of airways that were at least 0.5mm in diameter. The number of airways in each slide that met the size criteria for counting varied from 2 to 7. There was variation in the numbers of ganglia seen around similarly sized airways (Graph 7.1). As more specimens become available through the GOSH tissue archives, statisical analysis of intrinsic neuron number or ganglion size will become necessary to better characterise lung innervation in a range of samples. The current protocol that we have established can be refined and used in future studies.

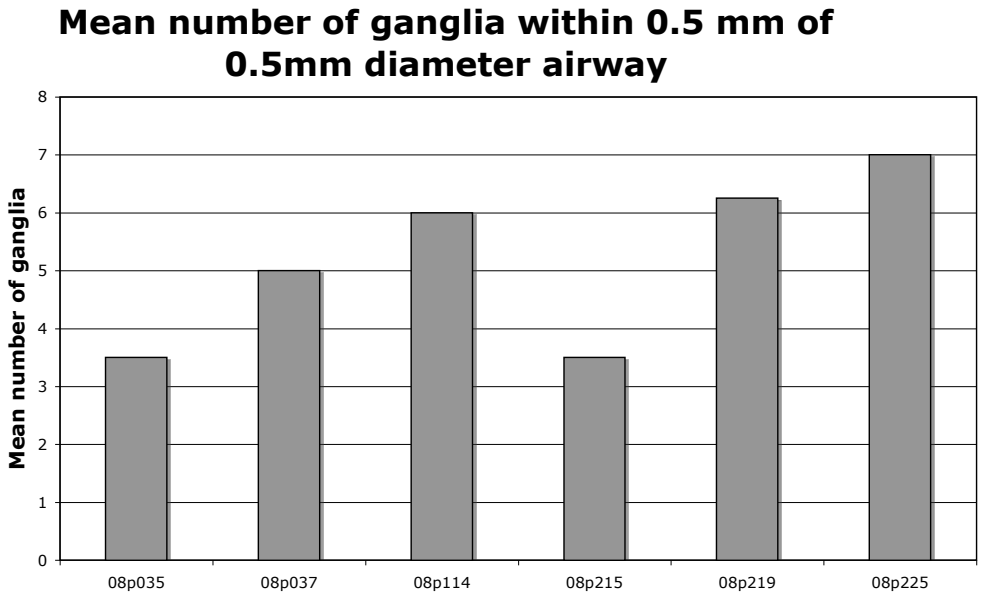

Graph 7.1 Mean numbers of ganglia counted in SUDI lungs. 2 – 7 airways were of sufficient diameter to be counted in each slide. There is variation in the number of ganglia seen around similarly sized airways.

Previous studies suggest that changes in the distribution of neuroepithelial bodies (NEBs) may be involved in SIDS as they have been shown to be present in increased numbers in lungs from SIDS cases (Cutz et al., 2007b). NEBs are found in

close proximity to NCC-derived intrinsic ganglia, (Brouns et al., 2009) and PNECs within NEBs could be affected by acetylcholine release from neural crest-derived intrinsic lung neurons (Freitag et al., 1996; Schuller et al., 2003). Innervation in lung tissues from human SUDI cases was therefore analysed to determine whether intrinsic neurons had abnormalities in numbers, distribution or morphology in some of those cases.

7.2 Discussion

A protocol for immunohistochemical staining of the archived tissue for the neuronal marker Tuj1 was been developed, and the tissue has been shown to be amenable to immunohistochemical evaluation and so can be used to analyse innervation in the human postnatal lung in SUDI. To date, sections from 8 cases have been immunostained and preliminary analysis conducted but no control tissue has so far become available. Of the SUDI cases from which lungs were collected, none have a known cause of death. One case appears to have unusual lung innervation, where airway ganglia were present in the mesenchyme, away from any airways.

A method for quantitative analysis of neuronal density and location was developed, taking into account that the specimens received come from varying areas of the lung. Airways greater than 0.5mm in diameter were selected for analysis, as the size of the airways should relate to their generation in the respiratory tree. Ganglia within 0.5mm of the airway were analysed. There were some issues, due to the nature of the samples available, which needed to be taken into account when analysing this tissue. Airway diameter is a useful proxy for level in the respiratory tree, but variation in airway diameter can also be affected by disease, environmental factors or variation in the age of the children from whom the samples were taken. There are also other factors affecting ganglion number and positioning apart from the position in the respiratory tree. For example, ganglia are more numerous around airway branching points, but as only single slides were available for each sample and each sample itself came from varying areas of the lung, proximity to airway branching points could not be analysed.

Nevertheless, this preliminary study indicated that archived lung samples can be retrieved, stained and analysed, and thus could be more extensively analysed in future studies.

8. Concluding remarks

The intrinsic innervation of the lung is derived from the neural crest, as shown in both avian (Burns and Delalande, 2005) and mammalian (Freem et al., 2010; Langsdorf et al., 2011) model organisms. Intrinsic neurons are closely associated with extrinsic vagal lung innervation (Tollet et al., 2001). Intrinsic neurons migrate into the lung to positions at airway branch points, where they form airway parasympathetic ganglia. In this project, the migration of NCCs into the lung in mouse and chick embryos was characterised using innovative fate-mapping techniques to follow NCCs as they migrate and differentiate. Differing defects in neural crest-derived intrinsic lung ganglia development have been described in two mouse mutant strains. Through analysis of these mutants, some of the mechanisms by which NCCs migrate to their final positions in the developing mouse lung have been elucidated.

8.1 NCC colonisation of the lung

NCC migration into and within the developing mouse lung was investigated using the *Wnt1Cre:Rosa26YFP* mouse. Results indicated that early NCC migration into the lung from the gut, before E12.5, consisted of single cells migrating to non-stereotyped positions in the lung buds. NCC migration within the lung, in contrast, occurred only along the airways and neural crest-derived intrinsic ganglia had consistent, stereotyped positions. Stereotypy in lung airway and blood vessel development has been previously described (Lazarus et al., 2011; Metzger et al., 2008) and so the stereotypy seen in the development of lung innervation is consistent with other aspects of lung development.

Close observation of NCC migration into the early lung in the *Wnt1Cre:Rosa26YFP* mouse and chimeric chick embryos showed that early NCC migration into the lung buds appeared haphazard in comparison to later NCC migration within the lung. The combination of these results allowed the proposal of a novel hypothesis: that NCCs migrating along the foregut may be diverted into the mesenchyme of the trachea or bronchi by stochastic migration rather than migrating into the lungs through a response to a chemoattractive signalling molecule. In contact inhibition between NCCs in the early migration pathway, NCCs are induced to migrate away from areas

of high NCC density, near the neural tube (Carmona-Fontaine et al., 2008). NCCs are much more numerous in the gut than in the lung, and so a subset of NCCs could migrate into the lung buds through population pressure early in development when the lung buds have not separated from the gut. This could apply only to the early diversion of NCCs from the foregut into the lung buds, and not to migration of NCCs within the growing lung to stereotypical ganglion positions, as in the latter the pattern and targets of migration are much more stereotyped and the density of NCCs much lower. Supporting this idea, NCC migration into the lung appears normal where there are normal numbers of NCCs in the foregut. NCCs colonise the foregut and lungs in *Ret* and *Gfra1* mouse mutants despite their defects in colonisation of the intestines (chapter 5). Also, back-grafted chick embryos, which receive fewer grafted GFP-positive NCCs than vagal GFP grafted embryos, show a similar density of GFP-positive NCCs in the lungs (chapter 4). However when NCCs are not present in the foregut, NCCs do not migrate into the lungs, as was described in the *Dom* mutant mouse (chapter 6). This hypothesis could be further investigated in future studies by using observation of lung and gut NCC behaviour in the early gut and lung buds in culture, either using chimeric GFP chick tissue or *Wnt1Cre:Rosa26YFP* mouse tissue so that fluorescently marked NCC migration could be observed over time. To differentiate stochastic NCC migration from a diffusible signalling cue response, one possible approach could be to use ROCK inhibitors on cultured tissue to block the RhoA pathway that enables cell protrusion collapse in contact inhibition (Carmona-Fontaine et al., 2008), to test whether NCCs migrate into the lungs in the absence of contact inhibition, although this could also disrupt the NCC migratory response to chemoattractants or other aspects of NCC behaviour (Stewart et al., 2007). Another possibility could be to experimentally reduce the number of NCCs in the gut as has been done previously, when a critical number of NCCs was shown to be necessary for normal gut colonisation (Barlow et al., 2008) and then examine NCCs in the lung and foregut to see whether reduced population pressure in the foregut results in an absence of NCCs in the lungs, although again this approach has flaws. Reduced NCC numbers in the gut could result in reduced NCCs in the lungs in either case.

8.2 Signalling pathways and mutant analysis

Intraspecies grafting using the GFP transgenic chick was used to trace NCC migration in the chick lung and gut and to carry out NCC backgrafting to test the developmental potential of lung and gut NCC. Gut NCCs were shown to enter the lung after backgrafting, indicating that lung and gut NCCs are not prespecified to enter their target organs. This result suggested that NCCs migrate into the lung in response to a cue that gut NCCs can also respond to and thus that the cue that directs NCCs into the lung is likely to be one that also directs gut NCCs.

In an effort to discover the mechanisms underlying NCC migration into the lungs, the lung innervation phenotypes of mutant mice were analysed. The candidate mutant strains chosen for analysis were deficient in genes already known to be involved in NCC migration. Intrinsic neuronal density and distribution in the lungs of *Ret*, *Gfra1* (chapter 5), *Tbx1* and *Sox10Dom* (chapter 6) mutant mouse embryos were examined. I also examined innervation in *Dcc* mutant and *Nrp1* conditional knockout embryonic lungs, which had no observable defects in lung innervation (chapter 5). These mouse mutant strains were analysed either because they had defects in intrinsic enteric innervation (*Ret, Gfra1*, *Sox10Dom*), or defects in NCC migration in other organs (*Dcc*, *Nrp1*, *Tbx1*). Some of the results obtained were unexpected. For example, the RET-GDNF signalling pathway was suggested by some studies to be necessary for NCC colonisation of the lung (Langsdorf et al., 2011; Tollet et al., 2002), a hypothesis contradicted by analysis of lung innervation in E14.5 *Ret* and *Gfra1* mutant mouse lungs. RET and GFRa1 receptors, although present on lung NCC (Burns and Delalande, 2005) and capable of mediating lung NCC migration towards artificial GDNF sources in culture (Tollet et al., 2002), are not necessary for NCC colonisation of the mouse lung or for normal intrinsic ganglion positioning. Further studies could indicate whether the innervation defects reported in older *Ret* mutant mouse lungs (Langsdorf et al., 2011) stem from a NCC survival defect. Langsdorf et al addressed tracheal and bronchial innervation in greater detail than intrinsic lung innervation, although the innervation of these three regions appears to be fairly continuous and have a common source.

Analysis of signalling molecule involvement in lung NCC colonisation through mutant mouse analysis revealed that the primary candidate guidance system, the RET pathway, was not necessary for NCC migration into the lung, and neither were the other signalling systems tested.

8.3 Developmental interaction between extrinsic and intrinsic lung innervation

Because the *Wnt1Cre:Rosa26YFP* double transgenic mouse construct marks a portion of vagal nerve lung innervation (Nassenstein et al., 2010), extrinsic vagal nerve and intrinsic lung innervation could not be fully discriminated in these mice. Evidence from *Tbx1* mutant mice, where the vagal nerve is severely hypoplastic but neuronal projections are seen in the upper lung, suggests that intrinsic neurons are the source of many of the nerve fibres in the pulmonary plexus. This is corroborated by evidence from the *Dom* mutant mouse, where persistent extrinsic projections are much thinner in the absence of intrinsic lung neurons, suggesting that projections from these neurons may normally contribute to nerve trunks in the lung. A possible future experiment to determine whether the projections seen in *Tbx1*-/- lungs arise from intrinsic neurons could utilise DiI tracing to show the extent of projections from lung intrinsic neurons. In reciprocal experiments using whole lungs with the gut and vagal nerves attached, DiI crystal could be placed on the cut vagal nerve to show, anterogradely, the extent of extrinsic vagal nerve projections in wild-type lungs, as has been done in the gut (Murphy and Fox, 2007). The apparently truncated neuronal projections that persist in *Tbx1* -/- lungs could extend from the hypoplastic vagal nerve or, more likely given their normal diameter, from the intrinsic neurons. DiI tracing could be used on control lungs to determine the relative contribution of vagal nerve and intrinsic neurons to the nerve bundles in the lung, and in *Tbx1* mutants to find the source of the shortened but still thick projections within the lung.

Mice with mutations in the BDNF receptor TrkB have been shown to have lung innervation defects (Garcia-Suarez et al., 2009) and breathing difficulties (Erickson et al., 1996), and BDNF appears to guide vagal nerve projections in the stomach (Murphy and Fox, 2010). However, BDNF does not appear to attract lung NCC (chapter 5, section 5.4). Examination of *TrkB* mutant mice during embryonic development could allow investigation into the source of their lung innervation

defect, especially in comparison to the defects seen in *Tbx1* -/- embryos, and could be useful in examining the interrelationship of extrinsic lung innervation from the pulmonary branch of the vagal nerve and intrinsic lung innervation in development.

8.4 NCC guidance into the lung

As NCCs are closely associated with the branching respiratory tree, it is possible that NCC use the lung epithelial tubules as a guiding scaffold for migration, but given the reported close association between NCCs and the vagal nerve in the lung (Tollet et al., 2001) and the results of *Tbx1* mutant mouse analysis, the vagal nerve is more likely to play a guiding role for lung NCC. A next step could be to examine what guides vagal nerve projections within the lung. The parallel projections along the main airway are positioned in a stereotypical manner on either side of the epithelial tubule suggesting that the outgrowth of vagal nerve fibres is precisely guided and positioned. NCCs and neuronal projections have been shown to use endothelial tubules as migratory scaffolds in the gut (Nagy et al., 2009) and in early NCC migration (Fantin et al., 2009), where the endothelial tubules are blood vessels rather than future airways. In this study NCCs did not appear to use blood vessels as a scaffold for migration (chapter 5) and there was no neuronal tissue associated with blood vessels. It is also clear from earlier results (chapter 3) that NCCs and lung innervation are usually seen in close association with the respiratory tree, which, like the blood vessels in the lung, is composed of epithelial tubules during embryonic development. It is possible, given the close association between lung innervation and the lung airways, that the respiratory tree is a scaffold for extrinsic vagal projection extension into the lung. This could be investigated by testing the ability of vagus projections to grow along lung epithelial explants in culture, or by examining the cell surface and ECM markers expressed on the outer surface of the future airway epithelium to see whether any known vagus guidance molecules such as laminin or netrin (Ratcliffe, 2011) are present. Cell adhesion between NCCs has been shown to be needed for normal NCC migration in the gut (Anderson et al., 2006b).

In the proposed model for the formation of lung innervation, NCCs migrate along the vagal nerve. However, there is no evidence as yet for how NCCs migrating along the vagus in the lung could cease their migration and aggregate in appropriate

positions to form intrinsic ganglia. This question could be investigated through the analysis of neuronal differentiation in the lung. By determining the timing of lung NCC differentiation and investigating whether the cues triggering the end of NCC migration and initiation of differentiation in the lung are environmental or cell-autonomous using lung NCC culture, a better attempt at finding the signalling cues that halt NCC migration could be made. For example, lung NCC could be cultured with lung epithelial tubule tissue from near an intrinsic ganglion site, and compared to NCC cultured with epithelial tubule tissue from a site where intrinsic ganglia do not form, to see whether a local property of the epithelial tubule can induce lung NCC differentiation. This approach would also be useful in following up results on lung NCC differentiation from experiments on NCC prespecification in the chick. In these experiments, lung NCCs appeared to lose migratory potential when back-grafted, while gut NCCs did not, suggesting that NCCs in the lung differentiate into neurons at an earlier stage than NCCs in the gut. This could be further investigated by comparing the timing of expression of neuronal differentiation markers such as NeuN in lung and gut neural crest-derived neurons.

8.5 Model for neural crest-derived intrinsic ganglia formation

Taking into account the results from NCC tracing in the *Wnt1Cre:Rosa26YFP* mouse (chapter 3), NCC fate mapping using intraspecies chick grafting (chapter 4) and *Sox10Dom* and *Tbx1* -/- mouse embryo analysis (chapter 6), I propose a model for intrinsic lung innervation development as follows. In early lung development, NCCs migrate into the lung buds in the absence of extrinsic vagal innervation, possibly through stochastic migration under the influence of contact inhibition from the greater density of NCCs in the early gut than the early lung. However, the lung tissue expands greatly from E12.5, when individual NCCs could be seen in sections, to E14.5, when extrinsic lung innervation is extensive. NCCs migrate tangentially from the gut into the early lung stochastically, supported by the apparent lack of prespecification of lung and gut NCC shown using chick NCC back-grafting. Once within the lung, NCCs use extrinsic vagal nerve fibres as a permissive substrate or scaffold for further migration, enabling colonisation of the expanding distal lung tissue. In support of this idea, NCCs were seen in the absence of neuronal projections in the early lungs, before the lung buds have separated from the gut endoderm. However, later in development at E14.5, no lung NCCs or neurons were

seen that were not in contact with neuronal projections. Once neural crest-derived neurons are established they are always present in association with neuronal projections that appear to be from the vagal nerve, in agreement with previous reports (Tollet et al., 2001).

8.6 Neurotransmitters in intrinsic lung innervation

Analysis of neurotransmitter expression in neural crest-derived neurons in the lung was attempted using both *in situ* hybridisation and immunohistochemistry to detect markers for the neurotransmitters acetylcholine (ACh), vasoactive intestinal peptide (VIP), nitric oxide (NO), dopamine and serotonin (Table 7.1). Some of the neurotransmitters listed have been found to be expressed in lung intrinsic neurons or extrinsic lung innervation in postnatal lungs, including ACh (Gabella, 1987; Tallini et al., 2006) VIP (Dey et al., 1981), NO (Guembe and Villaro, 1999) and serotonin (Vaccaro et al., 2006). Substance P, tachykinins and other transmitters have also been described in the lungs (Myers, 2001; Wine, 2007). Acetylcholine is expressed in some non-neuronal lung tissue (Wessler et al., 1999), so the vesicular marker VAchT was used to confine acetylcholine marker detection to neurons (Wessler and Kirkpatrick, 2001). However the analysis of neuronal subtypes during embryonic development has been unsuccessful in this project to date. Finding a way to detect neurotransmitter expression in intrinsic lung neurons would allow characterisation the timing of neurotransmitter onset. Such studies could be useful in determining the point at which these neurons become functional in regulating ASM contraction. In the gut, different neurotransmitters begin to be expressed at different stages (Branchek and Gershon, 1989) and it is possible that there is also variation in the onset of neurotransmitter expression in lung intrinsic neurons.

Neurotransmitter	Marker (function)
acetylcholine	ChAT (synthetic enzyme) VAchT (vesicular transporter)
nitric oxide	NOS (synthetic enzyme)
vasoactive intestinal peptide (VIP)	VIP (neurotransmitter)
dopamine/serotonin	DBH and TH (synthetic enzymes) serotonin (neurotransmitter)

Table 8.1 Neurotransmitters suggested to be present in lung innervation and the markers used to attempt neurotransmitter expression analysis.

The characterisation of neurotransmitters in neural crest-derived intrinsic ganglia would also allow further investigation of the developmental distinctions between NANC intrinsic neurons and cholinergic intrinsic neurons in the lung, for example by confirming that both sets of intrinsic ganglia are neural crest-derived and further investigating how the fate choice for these neurons is made. NANC intrinsic lung neurons are not present in some mammalian species, notably some rodents including guinea pigs (Andersson and Grundstrom, 1987; Canning and Fischer, 2001; Pan et al., 2010).

In the postnatal lung, NANC innervation is more important in submucosal mucus gland regulation (Wine, 2007), and cholinergic innervation in ASM regulation (Myers, 2001). Further examination of intrinsic neurons during development could reveal whether and how these different intrinsic ganglia subtypes innervate specific targets.

8.7 Lung smooth muscle activity and intrinsic neuron function

When culturing mouse and chick lungs in organotypic culture, lung peristaltic contractions were observed occurring at intervals ranging from 10 seconds to 5 minutes and these spontaneous contractions were used to confirm that lung tissue was surviving in culture (chapter 5). Lung peristalsis is thought to be involved in lung growth during development (Sparrow et al., 1999) and defects in lung peristalsis are a possible cause of the lung hypoplasia seen in the nitrofen-treated rat model of CDH (Martínez et al., 2004), which has neural crest-related defects. Now that the *Sox10Dom* mutant mouse has been shown to have an absence of intrinsic lung neurons, it could be useful to culture *Sox10Dom* mutant embryo lungs at E12.5 to determine the effect of absent intrinsic neurons on lung peristaltic contractions. Preliminary experiments were carried out using the sodium channel-blocking neurotoxin TTX to block neuronal firing and then observe the effects on lung peristalsis, but these studies were inconclusive (results not shown). Further investigation and refinement of such physiological experiments would be needed to study lung peristalsis in culture and further elucidate the role of lung innervation in lung peristalsis.

In an alternative approach investigating intrinsic neuron function in human disease, a protocol has been developed to analyse innervation in archived human lung tissue, laying the foundations for a larger study of lung innervation in Sudden Unexpected Death In Infancy (SUDI) cases (chapter 7).

8.8 Summary

In this thesis NCC migration into the mouse lungs and the formation of neural crest-derived intrinsic lung ganglia has been characterised using a transgenic NCC marker line. Investigation of NCC prespecification in the lung and gut was carried out in chick embryos using a recently developed transgenic chicken intraspecies grafting method. The roles of several genes, including possible signalling cues, were investigated in the mouse lung using three-dimensional imaging technology to characterise the morphology of lung innervation. Analysis of mouse mutant embryo lungs identified several possible mechanisms of NCC guidance into the developing lung. I have identified a number of avenues for future research into intrinsic ganglia function and formation that could increase understanding of broader lung developmental processes.

Acknowledgements

Thanks to my supervisor Dr Alan Burns for his help and mentorship and my secondary supervisor Dr Andy Stoker for his support. Thanks to my examiners, Dr Clare baker and Professor Roberto Mayor for their comments. Thanks to Dr David Tannahill, Dr Hideki Enomoto, Dr Wood-Yee Chan, Dr Elyanne Ratcliffe, Professor Helen Sang, Dr Vassilis Pachnis, Dr Peter Scambler and Dr Amelie Calmont, for providing experimental material or equipment access. And most importantly, thanks to my dear family and friends for providing proofreading, meals and sympathetic ears.

References

Abercrombie, M. and Heaysman, J. E. M. (1953). Observations on the social behaviour of cells in tissue culture : I. Speed of movement of chick heart fibroblasts in relation to their mutual contacts. *Experimental Cell Research* **5**, 111-131.

Abler, L. M., SL. and Sun, X. (2009). Conditional gene inactivation reveals roles for Fgf10 and Fgfr2 in establishing a normal pattern of epithelial branching in the mouse lung. *Developmental Dynamics* **238**, 1999-2013.

Acosta, J. M., Thibaud, B., Castillo, C., Mailleux, A., Tefft, D., Wuenschell, C., Anderson, K. D., Bourbon, J., Thiery, J.-P., Bellusci, S. et al. (2001). Novel mechanisms in murine nitrofen-induced pulmonary hypoplasia: FGF-10 rescue in culture. *American Journal of Physiology - Lung Cellular and Molecular Physiology* **281**, L250-L257.

Adriaensen, D. and Scheuermann, D. W. (1993). Neuroendocrine cells and nerves of the lung. *The Anatomical Record* **236**, 70-86.

Affolter, M., Zeller, R. and Caussinus, E. (2009). Tissue remodelling through branching morphogenesis. *Nat Rev Mol Cell Biol* **10**, 831-842.

Agrawal, M. and Brauer, P. R. (1996). Urokinase-type plasminogen activator regulates cranial neural crest cell migration in vitro. *Developmental Dynamics* **207**, 281-290.

Airaksinen, M. S. and Saarma, M. (2002). The GDNF family: signalling, biological functions and therapeutic value. *Nat Rev Neurosci* **3**, 383-94.

Airaksinen, M. S., Titievsky, A. and Saarma, M. (1999). GDNF family neurotrophic factor signaling: four masters, one servant? *Mol Cell Neurosci* **13**, 313-25.

Amiel, J., Laudier, B., Attie-Bitach, T., Trang, H., de Pontual, L., Gener, B., Trochet, D., Etchevers, H., Ray, P., Simonneau, M. et al. (2003). Polyalanine expansion and frameshift mutations of the paired-like homeobox gene PHOX2B in congenital central hypoventilation syndrome. *Nat Genet* **33**, 459-61.

Amiel, J., Salomon, R., Attie, T., Pelet, A., Trang, H., Mokhtari, M., Gaultier, C., Munnich, A. and Lyonnet, S. (1998). Mutations of the RET-GDNF signaling pathway in Ondine's curse. *Am J Hum Genet* **62**, 715-7.

Amiel, J., Sproat-Emison, E., Garcia-Barcelo, M., Lantieri, F., Burzynski, G., Borrego, S., Pelet, A., Arnold, S., Miao, X., Griseri, P. et al. (2008). Hirschsprung disease, associated syndromes and genetics: a review. *Journal of Medical Genetics* **45**, 1-14.

Anderson, R. B., Bergner, A. J., Taniguchi, M., Fujisawa, H., Forrai, A., Robb, L. and Young, H. M. (2007). Effects of different regions of the developing gut on the migration of enteric neural crest-derived cells: a role for Sema3A, but not Sema3F. *Developmental Biology* **305**, 287-99.

Anderson, R. B., Newgreen, D. F. and Young, H. M. (2006a). Neural crest and the development of the enteric nervous system. *Adv Exp Med Biol* **589**, 181-96.

Anderson, R. B., Turner, K. N., Nikonenko, A. G., Hemperly, J., Schachner, M. and Young, H. M. (2006b). The cell adhesion molecule l1 is required for chain migration of neural crest cells in the developing mouse gut. *Gastroenterology* **130**, 1221-32.

Andersson, R. G. G. and Grundstrom, N. (1987). Innervation of airway smooth muscle. Efferent mechanisms. *Pharmacology & Therapeutics* **32**, 107-130.

Andrew, D. J. and Ewald, A. J. (2010). Morphogenesis of epithelial tubes: Insights into tube formation, elongation, and elaboration. *Developmental Biology* **341,** 34-55.

Angrist, M., Jing, S., Bolk, S., Bentley, K., Nallasamy, S., Halushka, M., Fox, G. M. and Chakravarti, A. (1998). Human GFRA1: Cloning, Mapping, Genomic

Structure, and Evaluation as a Candidate Gene for Hirschsprung Disease Susceptibility. *Genomics* **48**, 354-362.

Ayer-Le Lievre, C. S. and Le Douarin, N. M. (1982). The early development of cranial sensory ganglia and the potentialities of their component cells studied in quail-chick chimeras. *Developmental Biology* **94**, 291-310.

Bai, Y., Zhang, M. and Sanderson, M. J. (2007). Contractility and Ca2+ Signaling of Smooth Muscle Cells in Different Generations of Mouse Airways. *Am J Respir Cell Mol Biol* **36**, 122-130.

Bajpai, R., Chen, D. A., Rada-Iglesias, A., Zhang, J., Xiong, Y., Helms, J., Chang, C.-P., Zhao, Y., Swigut, T. and Wysocka, J. (2010). CHD7 cooperates with PBAF to control multipotent neural crest formation. *Nature* **463**, 958-962.

Baker, C. V. H. (2008). The evolution and elaboration of vertebrate neural crest cells. *Current Opinion in Genetics & Development* **18**, 536-543.

Baker, C. V. H. and Bronner-Fraser, M. (2001). Vertebrate Cranial Placodes I. Embryonic Induction. *Developmental Biology* **232**, 1-61.

Barembaum, M. and Bronner-Fraser, M. (2005). Early steps in neural crest specification. *Semin Cell Developmental Biology* **16**, 642-6.

Barlow, A. J., Wallace, A. S., Thapar, N. and Burns, A. J. (2008). Critical numbers of neural crest cells are required in the pathways from the neural tube to the foregut to ensure complete enteric nervous system formation. *Development* **135**, 1681-91.

Barnes, P. J. (1988). Neuropeptides and airway smooth muscle. *Pharmacology & Therapeutics* **36**, 119-129.

Barnes, P. J. (2011). Pathophysiology of allergic inflammation. *Immunological Reviews* **242**, 31-50.

Barraud, P., Seferiadis, A. A., Tyson, L. D., Zwart, M. F., Szabo-Rogers, H. L., Ruhrberg, C., Liu, K. J. and Baker, C. V. H. (2010). Neural crest origin of olfactory ensheathing glia. *Proceedings of the National Academy of Sciences* **107**, 21040-21045.

Basch, M. and Bronner-Fraser, M. (2006). Neural Crest Inducing Signals
Neural Crest Induction and Differentiation, vol. 589 (ed. J.-P. Saint-Jeannet), pp. 24-31: Springer US.

Basch, M. L., Bronner-Fraser, M. and Garcia-Castro, M. I. (2006). Specification of the neural crest occurs during gastrulation and requires Pax7. *Nature* **441**, 218-222.

Bayha, E., Jorgensen, M. C., Serup, P. and Grapin-Botton, A. (2009). Retinoic Acid Signaling Organizes Endodermal Organ Specification along the Entire Antero-Posterior Axis. *PLoS ONE* **4**, e5845.

Becker, L. E., Zhang, W. and Pereyra, P. M. (1993). Delayed maturation of the vagus nerve in sudden infant death syndrome. *Acta Neuropathologica* **86**, 617-622.

Bellusci, S., Furuta, Y., Rush, M. G., Henderson, R., Winnier, G. and Hogan, B. L. (1997a). Involvement of Sonic hedgehog (Shh) in mouse embryonic lung growth and morphogenesis. *Development* **124**, 53-63.

Bellusci, S., Grindley, J., Emoto, H., Itoh, N. and Hogan, B. L. (1997b). Fibroblast growth factor 10 (FGF10) and branching morphogenesis in the embryonic mouse lung. *Development* **124**, 4867-4878.

Bellusci, S., Henderson, R., Winnier, G., Oikawa, T. and Hogan, B. L. (1996). Evidence from normal expression and targeted misexpression that bone morphogenetic protein (Bmp-4) plays a role in mouse embryonic lung morphogenesis. *Development* **122**, 1693-1702.

Belmonte, K. E. (2005). Cholinergic Pathways in the Lungs and Anticholinergic Therapy for Chronic Obstructive Pulmonary Disease. *Proc Am Thorac Soc* **2**, 297-304.

Belvisi, M. G. (2002). Overview of the innervation of the lung. *Current Opinion in Pharmacology* **2**, 211-215.

Belvisi, M. G. (2003). Sensory nerves and airway inflammation: role of A[delta] and C-fibres. *Pulmonary Pharmacology & Therapeutics* **16**, 1-7.

Berridge, M. J. (2008). Smooth muscle cell calcium activation mechanisms. *The Journal of Physiology* **586**, 5047-5061.

Berry-Kravis, E. M., Zhou, L., Rand, C. M. and Weese-Mayer, D. E. (2006). Congenital central hypoventilation syndrome: PHOX2B mutations and phenotype. *Am J Respir Crit Care Med* **174**, 1139-44.

Bevan, S. and Szolcsinyi, J. (1990). Sensory neuron-specific actions of capsaicin: mechanisms and applications. *Trends in Pharmacological Sciences* **11**, 331-333.

Bogni, S., Trainor, P., Natarajan, D., Krumlauf, R. and Pachnis, V. (2008). Non-cell-autonomous effects of Ret deletion in early enteric neurogenesis. *Development* **135**, 3007-3011.

Bogue, C., Lou, L., Vasavada, H., Wilson, C. and Jacobs, H. (1996). Expression of Hoxb genes in the developing mouse foregut and lung. *Am J Respir Cell Mol Biol* **15**, 163-171.

Bolande, R. P. (1997). NEUROCRISTOPATHY: Its Growth and Development in 20 Years. *Pediatric Pathology & Laboratory Medicine* **17**, 1-26.

Bondurand, N., Natarajan, D., Barlow, A., Thapar, N. and Pachnis, V. (2006). Maintenance of mammalian enteric nervous system progenitors by SOX10 and endothelin 3 signalling. *Development* **133**, 2075-86.

Branchek, T. A. and Gershon, M. D. (1989). Time course of expression of neuropeptide Y, calcitonin gene-related peptide, and NADPH diaphorase activity in neurons of the developing murine bowel and the appearance of 5-hydroxytryptamine in mucosal enterochromaffin cells. *J Comp Neurol* **285**, 262-73.

Breau, M. A., Pietri, T., Eder, O., Blanche, M., Brakebusch, C., F√§ssler, R., Thiery, J. P. and Dufour, S. (2006). Lack of Beta integrins in enteric neural crest cells leads to a Hirschsprung-like phenotype. *Development* **133**, 1725-1734.

Britsch, S., Goerich, D. E., Riethmacher, D., Peirano, R. I., Rossner, M., Nave, K. A., Birchmeier, C. and Wegner, M. (2001). The transcription factor Sox10 is a key regulator of peripheral glial development. *Genes Dev* **15**, 66-78.

Bronner-Fraser, M. (1993). Neural crest cell migration in the developing embryo. *Trends in Cell Biology* **3**, 392-397.

Brouns, I., Oztay, F., Pintelon, I., De Proost, I., Lembrechts, R., Timmermans, J.-P. and Adriaensen, D. (2009). Neurochemical pattern of the complex innervation of neuroepithelial bodies in mouse lungs. *Histochemistry and Cell Biology* **131**, 55-74.

Brouns, I., Pintelon, I., De Proost, I., Alewaters, R., Timmermans, J. P. and Adriaensen, D. (2006). Neurochemical characterisation of sensory receptors in airway smooth muscle: comparison with pulmonary neuroepithelial bodies. *Histochem Cell Biol* **125**, 351-67.

Brouns, I., Van Genechten, J., Hayashi, H., Gajda, M., Gomi, T., Burnstock, G., Timmermans, J. P. and Adriaensen, D. (2003). Dual sensory innervation of pulmonary neuroepithelial bodies. *Am J Respir Cell Mol Biol* **28**, 275-85.

Burns, A. J. and Delalande, J. M. (2005). Neural crest cell origin for intrinsic ganglia of the developing chicken lung. *Developmental Biology* **277**, 63-79.

Burns, A. J., Delalande, J. M. and Le Douarin, N. M. (2002). In ovo transplantation of enteric nervous system precursors from vagal to sacral neural crest results in extensive hindgut colonisation. *Development* **129**, 2785-96.

Burns, A. J. and Thapar, N. (2006). Advances in ontogeny of the enteric nervous system. *Neurogastroenterol Motil* **18**, 876-87.

Burns, A. J., Thapar, N. and Barlow, A. J. (2008). Development of the neural crest-derived intrinsic innervation of the human lung. *Am J Respir Cell Mol Biol* **38**, 269-75.

Burton, M. D., Kawashima, A., Brayer, J. A., Kazemi, H., Shannon, D. C., Schuchardt, A., Costantini, F., Pachnis, V. and Kinane, T. B. (1997). RET proto-oncogene is important for the development of respiratory CO2 sensitivity. *J Auton Nerv Syst* **63**, 137-43.

Calmont, A., Thapar, N., Scambler, P. J. and Burns, A. J. (2011). Absence of the vagus nerve in the stomach of Tbx1−/− mutant mice. *Neurogastroenterology & Motility* **23**, 125-130.

Calmont, A. l., Ivins, S., Van Bueren, K. L., Papangeli, I., Kyriakopoulou, V., Andrews, W. D., Martin, J. F., Moon, A. M., Illingworth, E. A., Basson, M. A. et al. (2009). Tbx1 controls cardiac neural crest cell migration during arch artery development by regulating Gbx2 expression in the pharyngeal ectoderm. *Development* **136**, 3173-3183.

Campanale, R. P. and Rowland, R. H. (1955). Hypoplasia of the Lung Associated with Congenital Diaphragmatic Hernia *Ann. Surg.* **142**, 176–189.

Canning, B. J. and Fischer, A. (2001). Neural regulation of airway smooth muscle tone. *Respiration Physiology* **125**, 113-127.

Canning, B. J. and Spina, D. (2009). Sensory Nerves and Airway Irritability. In *Sensory Nerves*, pp. 139-183.

Cardoso, W. V. and Lu, J. (2006). Regulation of early lung morphogenesis: questions, facts and controversies. *Development* **133**, 1611-1624.

Carmeliet, P. (2003). Blood vessels and nerves: common signals, pathways and diseases. *Nat Rev Genet* **4**, 710-720.

Carmona-Fontaine, C., Matthews, H. K., Kuriyama, S., Moreno, M., Dunn, G. A., Parsons, M., Stern, C. D. and Mayor, R. (2008). Contact inhibition of locomotion in vivo controls neural crest directional migration. *Nature* **456**, 957-961.

Cassiman, D., Barlow, A., Vander Borght, S., Libbrecht, L. and Pachnis, V. (2006). Hepatic stellate cells do not derive from the neural crest. *J Hepatol* **44**, 1098-104.

Chang, H. Y., Mashimo, H. and Goyal, R. K. (2003). IV. Current concepts of vagal efferent projections to the gut. *American Journal of Physiology - Gastrointestinal and Liver Physiology* **284**, G357-G366.

Chapman, D. L., Garvey, N., Sarah, H., Maria, A., Sergei, I. A., Jeremy, J. G.-B., Judith, C.-T., Roni, J. B., Lee, M. S. and Papaioannou, V. E. (1996). Expression of the T-box family genes, Tbx1-Tbx5, during early mouse development. *Developmental Dynamics* **206**, 379-390.

Coleman, C., Zhao, J., Gupta, M., Buckley, S., Tefft, J. D., Wuenschell, C. W., Minoo, P., Anderson, K. D. and Warburton, D. (1998). Inhibition of vascular and epithelial differentiation in murine nitrofen-induced diaphragmatic hernia. *American Journal of Physiology - Lung Cellular and Molecular Physiology* **274**, L636-L646.

Coppola, E., Rallu, M., Richard, J., Dufour, S., Riethmacher, D., Guillemot, F., Goridis, C. and Brunet, J.-F. (2010). Epibranchial ganglia orchestrate the development of the cranial neurogenic crest. *Proceedings of the National Academy of Sciences* **107**, 2066-2071.

Cornell, R. A. and Eisen, J. S. (2005). Notch in the pathway: The roles of Notch signaling in neural crest development. *Seminars in Cell and Developmental Biology* **16**, 663-672.

Cossais, F., Wahlbuhl, M., Kriesch, J. and Wegner, M. (2010). SOX10 structure-function analysis in the chicken neural tube reveals important insights into its role in human neurocristopathies. *Hum Mol Genet* **19**, 2409-2420.

Costa, R. H., Kalinichenko, V. V. and Lim, L. (2001). Transcription factors in mouse lung development and function. *American Journal of Physiology - Lung Cellular and Molecular Physiology* **280**, L823-L838.

Cutz, E. and Jackson, A. (1999). Neuroepithelial bodies as airway oxygen sensors. *Respir Physiol* **115**, 201-14.

Cutz, E., Perrin, D. G., Pan, J., Haas, E. A. and Krous, H. F. (2007a). Pulmonary Neuroendocrine Cells and Neuroepithelial Bodies in Sudden Infant Death Syndrome: Potential Markers of Airway Chemoreceptor Dysfunction. *Pediatric and Developmental Pathology* **10**, 106-116.

Cutz, E., Perrin, D. G., Pan, J., Haas, E. A. and Krous, H. F. (2007b). Pulmonary neuroendocrine cells and neuroepithelial bodies in sudden infant death syndrome: potential markers of airway chemoreceptor dysfunction. *Pediatr Dev Pathol* **10**, 106-16.

Dalvin, S., Anselmo, M. A., Prodhan, P., Komatsuzaki, K., Schnitzer, J. J. and Kinane, T. B. (2003). Expression of Netrin-1 and its two receptors DCC and UNC5H2 in the developing mouse lung. *Gene Expression Patterns* **3**, 279-283.

Danielian, P. S., Muccino, D., Rowitch, D. H., Michael, S. K. and McMahon, A. P. (1998). Modification of gene activity in mouse embryos in utero by a tamoxifen-inducible form of Cre recombinase. *Current Biology* **8**, 1323-S2.

Dauger, S., Pattyn, A., Lofaso, F., Gaultier, C., Goridis, C., Gallego, J. and Brunet, J. F. (2003). Phox2b controls the development of peripheral chemoreceptors and afferent visceral pathways. *Development* **130**, 6635-42.

de Bellard, E. M. and Bronner-Fraser, M. (2005). Neural crest migration methods in the chicken embryo. *Methods Mol Biol* **294**, 247-67.

De Calisto, J., Araya, C., Marchant, L., Riaz, C. F. and Mayor, R. (2005). Essential role of non-canonical Wnt signalling in neural crest migration. *Development* **132**, 2587-2597.

De Langhe, S. P., Sala, F. G., Del Moral, P.-M., Fairbanks, T. J., Yamada, K. M., Warburton, D., Burns, R. C. and Bellusci, S. (2005). Dickkopf-1 (DKK1) reveals that fibronectin is a major target of Wnt signaling in branching morphogenesis of the mouse embryonic lung. *Developmental Biology* **277**, 316-331.

de Pontual, L., Pelet, A., Trochet, D., Jaubert, F., Espinosa-Parrilla, Y., Munnich, A., Brunet, J. F., Goridis, C., Feingold, J., Lyonnet, S. et al. (2006). Mutations of the RET gene in isolated and syndromic Hirschsprung's disease in human disclose major and modifier alleles at a single locus. *J Med Genet* **43**, 419-23.

Debby-Brafman, A., Burstyn-Cohen, T., Klar, A. and Kalcheim, C. (1999). F-Spondin, Expressed in Somite Regions Avoided by Neural Crest Cells, Mediates Inhibition of Distinct Somite Domains to Neural Crest Migration. *Neuron* **22**, 475-488.

Dessimoz, J., Opoka, R., Kordich, J. J., Grapin-Botton, A. and Wells, J. M. (2006). FGF signaling is necessary for establishing gut tube domains alongthe anterior-posterior axis in vivo. *Mechanisms of Development* **123**, 42-55.

Dey, R. and Hung, K.-S. (1997). Development of innervation in the lung. In *Lung growth and development*, vol. 100 (ed. J. McDonald), pp. 244-265. New York: Dekker.

Dey, R. D., Shannon, W. A. and Said, S. I. (1981). Localization of VIP-immunoreactive nerves in airways and pulmonary vessels of dogs, cats, and human subjects. *Cell and Tissue Research* **220**, 231-238.

Doi, T. and Puri, P. (2009). Up-regulation of Wnt5a gene expression in the nitrofen-induced hypoplastic lung. *Journal of Pediatric Surgery* **44**, 2302-2306.

Duncker, H.-R. (1974). Structure of the avian respiratory tract. *Respiration Physiology* **22**, 1-19.

Duncker, H.-R. (2004). Vertebrate lungs: structure, topography and mechanics: A comparative perspective of the progressive integration of respiratory system, locomotor apparatus and ontogenetic development. *Respiratory Physiology & Neurobiology* **144**, 111-124.

Durbec, P. L., Larsson-Blomberg, L. B., Schuchardt, A., Costantini, F. and Pachnis, V. (1996). Common origin and developmental dependence on c-ret of subsets of enteric and sympathetic neuroblasts. *Development* **122**, 349-58.

Dutt, S., Kluber, M., Matasci, M., Sommer, L. and Zimmermann, D. R. (2006). Versican V0 and V1 Guide Migratory Neural Crest Cells. *Journal of Biological Chemistry* **281**, 12123-12131.

Echelard, Y., Vassileva, G. and McMahon, A. P. (1994). Cis-acting regulatory sequences governing Wnt-1 expression in the developing mouse CNS. *Development* **120**, 2213-2224.

Eketjall, S., Fainzilber, M., Murray-Rust, J. and Ibanez, C. F. (1999). Distinct structural elements in GDNF mediate binding to GFR[alpha]1 and activation of the GFR[alpha]1-c-Ret receptor complex. *EMBO J* **18**, 5901-5910.

Endo, Y., Osumi, N. and Wakamatsu, Y. (2002). Bimodal functions of Notch-mediated signaling are involved in neural crest formation during avian ectoderm development. *Development* **129**, 863-873.

Enomoto, H., Araki, T., Jackman, A., Heuckeroth, R. O., Snider, W. D., Johnson, E. M., Jr. and Milbrandt, J. (1998). GFR alpha1-deficient mice have deficits in the enteric nervous system and kidneys. *Neuron* **21**, 317-24.

Epstein, J. A. (2001). Developing models of DiGeorge syndrome. *Trends in Genetics* **17**, S13-S17.

Erickson, J. T., Conover, J. C., Borday, V., Champagnat, J., Barbacid, M., Yancopoulos, G. and Katz, D. M. (1996). Mice Lacking Brain-Derived Neurotrophic Factor Exhibit Visceral Sensory Neuron Losses Distinct from Mice Lacking NT4 and Display a Severe Developmental Deficit in Control of Breathing. *The Journal of Neuroscience* **16**, 5361-5371.

Fantin, A., Maden, C. H. and Ruhrberg, C. (2009). Neuropilin ligands in vascular and neuronal patterning. *Biochemical Society Transactions* **037**, 1228-1232.

Featherstone, N. C., Connell, M. G., Fernig, D. G., Wray, S., Burdyga, T. V., Losty, P. D. and Jesudason, E. C. (2006). Airway Smooth Muscle Dysfunction Precedes Teratogenic Congenital Diaphragmatic Hernia and May Contribute to Hypoplastic Lung Morphogenesis. *Am J Respir Cell Mol Biol* **35**, 571-578.

Featherstone, N. C., Jesudason, E. C., Connell, M. G., Fernig, D. G., Wray, S., Losty, P. D. and Burdyga, T. V. (2005). Spontaneous Propagating Calcium Waves Underpin Airway Peristalsis in Embryonic Rat Lung. *Am J Respir Cell Mol Biol* **33**, 153-160.

Fisher, M., Downie, H., Welten, M. C. M., Delgado, I., Bain, A., Planzer, T., Sherman, A., Sang, H. and Tickle, C. (2011). Comparative Analysis of 3D Expression Patterns of Transcription Factor Genes and Digit Fate Maps in the Developing Chick Wing. *PLoS ONE* **6**, e18661.

Fitzgerald, D. P., Seaman, C. and Cooper, H. M. (2006). Localization of Neogenin protein during morphogenesis in the mouse embryo. *Developmental Dynamics* **235**, 1720-1725.

Fontaine-Perus, J., Halgand, P., Cheraud, Y., Rouaud, T., Velasco, M. E., Cifuentes Diaz, C. and Rieger, F. (1997). Mouse-chick chimera: a developmental model of murine neurogenic cells. *Development* **124**, 3025-36.

Freem, L. J., Escot, S., Tannahill, D., Druckenbrod, N. R., Thapar, N. and Burns, A. J. (2010). The intrinsic innervation of the lung is derived from neural crest cells as shown by optical projection tomography in Wnt1-Cre;YFP reporter mice. *Journal of Anatomy* **217**, 651-664.

Freitag, A., Wessler, I. and Racké, K. (1996). Adrenoceptor- and cholinoceptor-mediated mechanisms in the regulation of 5-hydroxytryptamine release from isolated tracheae of newborn rabbits. *British Journal of Pharmacology* **119**, 91–98.

Fu, M., Vohra, B. P. S., Wind, D. and Heuckeroth, R. O. (2006). BMP signaling regulates murine enteric nervous system precursor migration, neurite fasciculation, and patterning via altered Ncam1 polysialic acid addition. *Developmental Biology* **299**, 137-150.

Gabella, G. (1987). Innervation of Airway Smooth Muscle: Fine Structure. *Annual Review of Physiology* **49**, 583-594.

Gammill, L. S., Gonzalez, C., Gu, C. and Bronner-Fraser, M. (2006). Guidance of trunk neural crest migration requires neuropilin 2/semaphorin 3F signaling. *Development* **133**, 99-106.

Gammill, L. S. and Roffers-Agarwal, J. (2010). Division of labor during trunk neural crest development. *Developmental Biology* **344**, 555-565.

Garcia-Castro, M. and Bronner-Fraser, M. (1999). Induction and differentiation of the neural crest. *Current Opinion in Cell Biology* **11**, 695-698.

Garcia-Castro, M., Marcelle, C. and Bronner-Fraser, M. (2002). Ectodermal Wnt Function as a Neural Crest Inducer. *Science* **297**, 848-851.

Garcia-Suarez, O., Perez-Pinera, P., Laura, R., Germana, A., Esteban, I., Cabo, R., Silos-Santiago, I., Cobo, J. L. and Vega, J. A. (2009). TrkB is necessary for the normal development of the lung. *Respiratory Physiology & Neurobiology* **167**, 281-291.

George, L., Chaverra, M., Todd, V., Lansford, R. and Lefcort, F. (2007). Nociceptive sensory neurons derive from contralaterally migrating, fate-restricted neural crest cells. *Nat Neurosci* **10**, 1287-1293.

Giangreco, A., Reynolds, S. D. and Stripp, B. R. (2002). Terminal Bronchioles Harbor a Unique Airway Stem Cell Population That Localizes to the Bronchoalveolar Duct Junction. *The American Journal of Pathology* **161**, 173-182.

Gianino, S., Grider, J. R., Cresswell, J., Enomoto, H. and Heuckeroth, R. O. (2003). GDNF availability determines enteric neuron number by controlling precursor proliferation. *Development* **130**, 2187-98.

Gillan, J. E., Curran, C., O'Reilly, E., Cahalane, S. F. and Unwin, A. R. (1989). Abnormal Patterns of Pulmonary Neuroendocrine Cells in Victims of Sudden Infant Death Syndrome. *Pediatrics* **84**, 828-834.

Goldstein, R. (2010). Transplantation of Mammalian Embryonic Stem Cells and Their Derivatives to Avian Embryos. *Stem Cell Reviews and Reports* **6**, 473-483.

Grapin-Botton, A. and Melton, D. A. (2000). Endoderm development: from patterning to organogenesis. *Trends Genet* **16**, 124-30.

Grindley, J. C., Bellusci, S., Perkins, D. and Hogan, B. L. M. (1997). Evidence for the Involvement of the Gli Gene Family in Embryonic Mouse Lung Development. *Developmental Biology* **188**, 337-348.

Gu, C., Rodriguez, E. R., Reimert, D. V., Shu, T., Fritzsch, B., Richards, L. J., Kolodkin, A. L. and Ginty, D. D. (2003). Neuropilin-1 Conveys Semaphorin and

VEGF Signaling during Neural and Cardiovascular Development. *Developmental Cell* **5**, 45-57.

Gu, Q., Lee, L. Y., Geoffrey, J. L. and Steven, D. S. (2006). NEUROPHYSIOLOGY | Neural Control of Airway Smooth Muscle. In *Encyclopedia of Respiratory Medicine*, pp. 138-145. Oxford: Academic Press.

Guembe, L. and Villaro, A. C. (1999). Histochemical demonstration of neuronal nitric oxide synthase during development of mouse respiratory tract. *Am J Respir Cell Mol Biol* **20**, 342-51.

Haddad, G., Mazza, N., R., D., Blanc, W., Driscoll, J., MAF., E., Epstein, R. and Mellins, R. (1978). Congenital Failure of Automatic Control of Ventilation, Gastrointestinal Motility and Heart Rate. *Medicine* **57**, 517-526.

Hakami, R. M., Hou, L., Baxter, L. L., Loftus, S. K., Southard-Smith, E. M., Incao, A., Cheng, J. and Pavan, W. J. (2006). Genetic evidence does not support direct regulation of EDNRB by SOX10 in migratory neural crest and the melanocyte lineage. *Mech Dev* **123**, 124-34.

Haldin, C. E. and LaBonne, C. (2010). SoxE factors as multifunctional neural crest regulatory factors. *The International Journal of Biochemistry & Cell Biology* **42**, 441-444.

Halfter, W., Chiquet-Ehrismann, R. and Tucker, R. P. (1989). The effect of tenascin and embryonic basal lamina on the behavior and morphology of neural crest cells in vitro. *Developmental Biology* **132**, 14-25.

Hall, A. (1998). Rho GTPases and the Actin Cytoskeleton. *Science* **279**, 509-514.

Harrison, T. A., Stadt, H. A., Kumiski, D. and Kirby, M. L. (1995). Compensatory responses and development of the nodose ganglion following ablation of placodal precursors in the embryonic chick (Gallus domesticus). *Cell and Tissue Research* **281**, 379-385.

Heard, D. J. (1997). Avian respiratory anatomy and physiology. *Seminars in Avian and Exotic Pet Medicine* **6**, 172-179.

Henderson, D. J. and Copp, A. J. (1997). Role of the extracellular matrix in neural crest cell migration. *Journal of Anatomy* **191**, 507-515.

Henderson, D. J., Ybot-Gonzalez, P. and Copp, A. J. (1997). Over-expression of the chondroitin sulphate proteoglycan versican is associated with defective neural crest migration in the Pax3 mutant mouse (splotch). *Mechanisms of Development* **69**, 39-51.

Herbarth, B., Pingault, V., Bondurand, N., Kuhlbrodt, K., Hermans-Borgmeyer, I., Puliti, A., Lemort, N., Goossens, M. and Wegner, M. (1998). Mutation of the Sry-related Sox10 gene in Dominant megacolon, a mouse model for human Hirschsprung disease. *Proc Natl Acad Sci U S A* **95**, 5161-5.

Hislop, A. A. (2002). Airway and blood vessel interaction during lung development. *Journal of Anatomy* **201**, 325-334.

Hong, C.-S. and Saint-Jeannet, J.-P. (2005). Sox proteins and neural crest development. *Seminars in Cell & Developmental Biology* **16**, 694-703.

Huang, R. Y. and Shapiro, N. L. (2000). Structural airway anomalies in patients with DiGeorge syndrome: A current review. *American Journal of Otolaryngology* **21**, 326-330.

Hueber, S. D. and Lohmann, I. (2008). Shaping segments: Hox gene function in the genomic age. *BioEssays* **30**, 965-979.

Ijpenberg, A., Perez-Pomares, J. M., Guadix, J. A., Carmona, R., Portillo-Sanchez, V., MacIas, D., Hohenstein, P., Miles, C. M., Hastie, N. D. and Muooz-Chapuli,

R. (2007). Wt1 and retinoic acid signaling are essential for stellate cell development and liver morphogenesis. *Developmental Biology* **312**, 157-170.

Inoue, K., Khajavi, M., Ohyama, T., Hirabayashi, S.-i., Wilson, J., Reggin, J. D., Mancias, P., Butler, I. J., Wilkinson, M. F., Wegner, M. et al. (2004). Molecular mechanism for distinct neurological phenotypes conveyed by allelic truncating mutations. *Nat Genet* **36**, 361-369.

Itasaki, N., Bel-Vialar, S. and Krumlauf, R. (1999). 'Shocking' developments in chick embryology: electroporation and in ovo gene expression. *Nat Cell Biol* **1**, E203-7.

Jerome, L. A. and Papaioannou, V. E. (2001). DiGeorge syndrome phenotype in mice mutant for the T-box gene, Tbx1. *Nat Genet* **27**, 286-291.

Jesudason, E. C. (2009). Airway smooth muscle: an architect of the lung? *Thorax* **64**, 541-545.

Jesudason, E. C., Smith, N. P., Connell, M. G., Spiller, D. G., White, M. R. H., Fernig, D. G. and Losty, P. D. (2006). Peristalsis of airway smooth muscle is developmentally regulated and uncoupled from hypoplastic lung growth. *Am J Physiol Lung Cell Mol Physiol* **291**, L559-565.

Jiang, X., Rowitch, D. H., Soriano, P., McMahon, A. P. and Sucov, H. M. (2000). Fate of the mammalian cardiac neural crest. *Development* **127**, 1607-1616.

Jiang, Y., Liu, M. T. and Gershon, M. D. (2003). Netrins and DCC in the guidance of migrating neural crest-derived cells in the developing bowel and pancreas. *Developmental Biology* **258**, 364-84.

Jing, S., Wen, D., Yu, Y., Holst, P. L., Luo, Y., Fang, M., Tamir, R., Antonio, L., Hu, Z., Cupples, R. et al. (1996). GDNF-Induced Activation of the Ret Protein Tyrosine Kinase Is Mediated by GDNFR-[alpha], a Novel Receptor for GDNF. *Cell* **85**, 1113-1124.

Kalcheim, C. and Le Douarin, N. M. (1999). The Neural Crest. Cambridge: Cambridge University Press.

Kapur, R. P. (1999). Early Death of Neural Crest Cells Is Responsible for Total Enteric Aganglionosis in Sox10 Dom / Sox10 Dom Mouse Embryos. *Pediatric and Developmental Pathology* **2**, 559-569.

Kasemeier-Kulesa, J. C., McLennan, R., Romine, M. H., Kulesa, P. M. and Lefcort, F. (2010). CXCR4 Controls Ventral Migration of Sympathetic Precursor Cells. *The Journal of Neuroscience* **30**, 13078-13088.

Kawasaki, T., Bekku, Y., Suto, F., Kitsukawa, T., Taniguchi, M., Nagatsu, I., Nagatsu, T., Itoh, K., Yagi, T. and Fujisawa, H. (2002). Requirement of neuropilin 1-mediated Sema3A signals in patterning of the sympathetic nervous system. *Development* **129**, 671-680.

Keith, I. M. (1991). Calcitonin gene-related peptide and its mRNA in pulmonary neuroendocrine cells and ganglia. *Histochemistry* **96**, 311-315.

Kelsh, R. N. (2006). Sorting out Sox10 functions in neural crest development. *BioEssays* **28**, 788-798.

Khadka, D. L., T. Sargent, TD. (2006). Msx1 and Msx2 have shared essential functions in neural crest but may be dispensable in epidermis and axis formation in Xenopus. *International Journal of Developmental Biology* **50**, 499-502.

Kim, J., Lo, L., Dormand, E. and Anderson, D. J. (2003). SOX10 maintains multipotency and inhibits neuronal differentiation of neural crest stem cells. *Neuron* **38**, 17-31.

Kirkby, N. S., Low, L., Seckl, J. R., Walker, B. R., Webb, D. J. and Hadoke, P. W. F. (2011). Quantitative 3-Dimensional Imaging of Murine Neointimal and Atherosclerotic Lesions by Optical Projection Tomography. *PLoS ONE* **6**, e16906.

Kitagawa, M., Hislop, A., Boyden, E. A. and Reid, L. (1971). Lung hypoplasia in congenital diaphragmatic hernia a quantitative study of airway, artery, and alveolar development. *British Journal of Surgery* **58**, 342-346.

Kliegman, R. and Nelson, W. E. (2007). Nelson textbook of pediatrics: Saunders.

Kochilas, L., Merscher-Gomez, S., Lu, M. M., Potluri, V., Liao, J., Kucherlapati, R., Morrow, B. and Epstein, J. A. (2002). The Role of Neural Crest during Cardiac Development in a Mouse Model of DiGeorge Syndrome. *Developmental Biology* **251**, 157-166.

Krull, C. E., Lansford, R., Gale, N. W., Collazo, A., Marcelle, C., Yancopoulos, G. D., Fraser, S. E. and Bronner-Fraser, M. (1997). Interactions of Eph-related receptors and ligands confer rostrocaudal pattern to trunk neural crest migration. *Curr Biol* **7**, 571-80.

Kuan, C. Y. K., Tannahill, D., Cook, G. M. W. and Keynes, R. J. (2004). Somite polarity and segmental patterning of the peripheral nervous system. *Mechanisms of Development* **121**, 1055-1068.

Kubota, Y., Morita, T., Kusakabe, M., Sakakura, T. and Ito, K. (1999). Spatial and temporal changes in chondroitin sulfate distribution in the sclerotome play an essential role in the formation of migration patterns of mouse neural crest cells. *Developmental Dynamics* **214**, 55-65.

Kulesa, P. M. and Gammill, L. S. (2010). Neural crest migration: Patterns, phases and signals. *Developmental Biology* **344**, 566-568.

Kulesa, P. M., Lefcort, F. and Kasemeier-Kulesa, J. C. (2009). The migration of autonomic precursor cells in the embryo. *Autonomic Neuroscience* **151**, 3-9.

Kumar, S. (2007). Caspase function in programmed cell death. *Cell Death Differ* **14**, 32-43.

Kumar, V. H., Lakshminrusimha, S., El Abiad, M. T., Chess, P. R. and Ryan, R. M. (2005). Growth Factors in Lung Development. In *Advances in Clinical Chemistry*, vol. Volume 40 (ed. S. M. Gregory), pp. 261-316: Elsevier.

Kummer, W., Fischer, A., Kurkowski, R. and Heym, C. (1992). The sensory and sympathetic innervation of guinea-pig lung and trachea as studied by retrograde neuronal tracing and double-labelling immunohistochemistry. *Neuroscience* **49**, 715-737.

Kuriyama, S. and Mayor, R. (2008). Molecular analysis of neural crest migration. *Philosophical Transactions of the Royal Society B: Biological Sciences* **363**, 1349-1362.

Kwong, K., Carr, M. J., Gibbard, A., Savage, T. J., Singh, K., Jing, J., Meeker, S. and Undem, B. J. (2008). Voltage-gated sodium channels in nociceptive versus non-nociceptive nodose vagal sensory neurons innervating guinea pig lungs. *The Journal of Physiology* **586**, 1321-1336.

LaBonne, C. and Bronner-Fraser, M. (1998). Neural crest induction in Xenopus: evidence for a two-signal model. *Development* **125**, 2403-2414.

Landolt, R. M., Vaughan, L., Winterhalter, K. H. and Zimmermann, D. R. (1995). Versican is selectively expressed in embryonic tissues that act as barriers to neural crest cell migration and axon outgrowth. *Development* **121**, 2303-2312.

Langsdorf, A., Radzikinas, K., Kroten, A., Jain, S. and Ai, X. (2011). Neural Crest Cell Origin and Signals for Intrinsic Neurogenesis in the Mammalian Respiratory Tract. *Am J Respir Cell Mol Biol* **44**, 293-301.

Larsell, O. (1922). The ganglia, plexuses, and nerve-terminations of the mammalian lung and pleura pulmonalis. *The Journal of Comparative Neurology* **35**, 97-132.

Lazarus, A., Del-Moral, P. M., Ilovich, O., Mishani, E., Warburton, D. and Keshet, E. (2011). A perfusion-independent role of blood vessels in determining branching stereotypy of lung airways. *Development* **138**, 2359-2368.

Le Douarin, N. M. (1993). Embryonic neural chimaeras in the study of brain development. *Trends in Neurosciences* **16**, 64-72.

Le Douarin, N. M., Creuzet, S., Couly, G. and Dupin, E. (2004). Neural crest cell plasticity and its limits. *Development* **131**, 4637-4650.

Le Douarin, N. M. and Kalcheim, C. (1999). The Neural Crest. Cambridge: Cambridge University Press.

Le Douarin, N. M. and Teillet, M. A. (1973). The migration of neural crest cells to the wall of the digestive tract in avian embryo. *J Embryol Exp Morphol* **30**, 31-48.

Le Lievre, C. S. and Le Douarin, N. M. (1975). Mesenchymal derivatives of the neural crest: analysis of chimaeric quail and chick embryos. *J Embryol Exp Morphol* **34**, 125-54.

Lee, M. K., Tuttle, J. B., Rebhun, L. I., Cleveland, D. W. and Frankfurter, A. (1990). The expression and posttranslational modification of a neuron-specific β-tubulin isotype during chick embryogenesis. *Cell Motility and the Cytoskeleton* **17**, 118-132.

Lefcort, F. and George, L. (2007). Neural Crest Cell Fate: To Be or Not To Be Prespecified. *Cell adhesion & migration* **1**, 199-201.

Lefcort, F., Venstrom, K., McDonald, J. A. and Reichardt, L. F. (1992). Regulation of expression of fibronectin and its receptor, alpha 5 beta 1, during development and regeneration of peripheral nerve. *Development* **116**, 767-782.

Leslie, K. O., Mitchell, J. J., Woodcock-Mitchell, J. L. and Low, R. B. (1990). Alpha smooth muscle actin expression in developing and adult human lung. *Differentiation* **44**, 143-149.

Liem, K. F., Tremml, G., Roelink, H. and Jessell, T. M. (1995). Dorsal differentiation of neural plate cells induced by BMP-mediated signals from epidermal ectoderm. *Cell* **82**, 969-979.

Lindsay, E. A., Vitelli, F., Su, H., Morishima, M., Huynh, T., Pramparo, T., Jurecic, V., Ogunrinu, G., Sutherland, H. F., Scambler, P. J. et al. (2001). Tbx1 haploinsufficiency in the DiGeorge syndrome region causes aortic arch defects in mice. *Nature* **410**, 97-101.

Litingtung, Y., Lei, L., Westphal, H. and Chiang, C. (1998). Sonic hedgehog is essential to foregut development. *Nat Genet* **20**, 58-61.

Liu, C., Shao, Z.-M., Zhang, L., Beatty, P., Sartippour, M., Lane, T., Livingston, E. and Nguyen, M. (2001). Human Endomucin Is an Endothelial Marker. *Biochemical and Biophysical Research Communications* **288**, 129-136.

Liu, J. P. and Jessell, T. M. (1998). A role for rhoB in the delamination of neural crest cells from the dorsal neural tube. *Development* **125**, 5055-5067.

Liu, Y., Stein, E., Oliver, T., Li, Y., Brunken, W. J., Koch, M., Tessier-Lavigne, M. and Hogan, B. L. M. (2004). Novel Role for Netrins in Regulating Epithelial Behavior during Lung Branching Morphogenesis. *Current Biology* **14**, 897-905.

Mailleux, A. A., Kelly, R., Veltmaat, J. M., De Langhe, S. P., Zaffran, S., Thiery, J. P. and Bellusci, S. (2005). Fgf10 expression identifies parabronchial smooth muscle cell progenitors and is required for their entry into the smooth muscle cell lineage. *Development* **132**, 2157-2166.

Mailleux, A. A., Tefft, D., Ndiaye, D., Itoh, N., Thiery, J. P., Warburton, D. and Bellusci, S. (2001). Evidence that SPROUTY2 functions as an inhibitor of mouse embryonic lung growth and morphogenesis. *Mechanisms of Development* **102**, 81-94.

Maina, J. N. (2003). A systematic study of the development of the airway (bronchial) system of the avian lung from days 3 to 26 of embryogenesis: a transmission electron microscopic study on the domestic fowl, Gallus gallus variant domesticus. *Tissue and Cell* **35**, 375-391.

Manie, S., Santoro, M., Fusco, A. and Billaud, M. (2001). The RET receptor: function in development and dysfunction in congenital malformation. *Trends Genet* **17**, 580-9.

Marchant, L., Linker, C., Ruiz, P., Guerrero, N. and Mayor, R. (1998). The Inductive Properties of Mesoderm Suggest That the Neural Crest Cells Are Specified by a BMP Gradient. *Developmental Biology* **198**, 319-329.

Martínez, L., González-Reyes, S., Burgos, E. and Tovar, J. A. (2004). The vagus and recurrent laryngeal nerves in experimental congenital diaphragmatic hernia. *Pediatric Surgery International* **20**, 253-257.

Martinez, L., Pederiva, F., Martinez-Calonge, W., Aras-Lopez, R. and Tovar, J. A. (2009). The Myenteric Plexus of the Esophagus is Abnormal in an Experimental Congenital Diaphragmatic Hernia Model. *Eur J Pediatr Surg* **19**, 163-167.

Maschhoff, K. L. and Baldwin, H. S. (2000). Molecular determinants of neural crest migration. *American Journal of Medical Genetics* **97**, 280-288.

Matthews, H. K., Marchant, L., Carmona-Fontaine, C., Kuriyama, S., Larrain, J., Holt, M. R., Parsons, M. and Mayor, R. (2008). Directional migration of neural crest cells in vivo is regulated by Syndecan-4/Rac1 and non-canonical Wnt signaling/RhoA. *Development* **135**, 1771-1780.

Mayor, R., Guerrero, N. and Martínez, C. (1997). Role of FGF and Noggin in Neural Crest Induction. *Developmental Biology* **189**, 1-12.

McGrew, M. J., Sherman, A., Ellard, F. M., Lillico, S. G., Gilhooley, H. J., Kingsman, A. J., Mitrophanous, K. A. and Sang, H. (2004). Efficient production of germline transgenic chickens using lentiviral vectors. *EMBO Rep* **5**, 728-33.

McGrew, M. J., Sherman, A., Lillico, S. G., Ellard, F. M., Radcliffe, P. A., Gilhooley, H. J., Mitrophanous, K. A., Cambray, N., Wilson, V. and Sang, H. (2008). Localised axial progenitor cell populations in the avian tail bud are not committed to a posterior Hox identity. *Development* **135**, 2289-2299.

McKeown, S. J., Newgreen, D. F. and Farlie, P. G. (2003). Temporal restriction of migratory and lineage potential in rhombomere 1 and 2 neural crest. *Developmental Biology* **255**, 62-76.

Merkus, P. J. F. M., Have-Opbroek, A. A. W. t. and Quanjer, P. H. (1996). Human lung growth: A review. *Pediatric Pulmonology* **21**, 383-397.

Metzger, R. J., Klein, O. D., Martin, G. R. and Krasnow, M. A. (2008). The branching programme of mouse lung development. *Nature* **453**, 745-750.

Metzger, R. J. and Krasnow, M. A. (1999). Genetic Control of Branching Morphogenesis. *Science* **284**, 1635-1639.

Mitzner, W. (2004). Airway Smooth Muscle: The Appendix of the Lung. *Am J Respir Crit Care Med* **169**, 787-790.

Moessinger, A. C., Harding, R., Adamson, T. M., Singh, M. and Kiu, G. T. (1990). Role of lung fluid volume in growth and maturation of the fetal sheep lung. *The Journal of Clinical Investigation* **86**, 1270-1277.

Mollaaghababa, R. and Pavan, W. J. (2003). The importance of having your SOX on: role of SOX10 in the development of neural crest-derived melanocytes and glia. *Oncogene* **22**, 3024-34.

Monier-Gavelle, F. and Duband, J.-L. (1997). Cross Talk between Adhesion Molecules: Control of N-cadherin Activity by Intracellular Signals Elicited by beta 1 and beta 3

Integrins in Migrating Neural Crest Cells. *The Journal of Cell Biology* **137**, 1663-1681.

Monkhouse, S. (2005). Cranial Nerves Functional Anatomy. *Cambridge University Press*.

Moore, S. W., Tessier-Lavigne, M. and Kennedy, T. E. (2007). Netrins and Their receptors. Axon Growth and Guidance, vol. 621 (ed. D. Bagnard), pp. 17-31: Springer New York.

Mosher, J. T., Yeager, K. J., Kruger, G. M., Joseph, N. M., Hutchin, M. E., Dlugosz, A. A. and Morrison, S. J. (2007). Intrinsic differences among spatially distinct neural crest stem cells in terms of migratory properties, fate determination, and ability to colonize the enteric nervous system. *Developmental Biology* **303**, 1-15.

Motoyama, J., Liu, J., Mo, R., Ding, Q., Post, M. and Hui, C. C. (1998). Essential function of Gli2 and Gli3 in the formation of lung, trachea and oesophagus. *Nat Genet* **20**, 54-7.

Murphy, M. C. and Fox, E. A. (2007). Anterograde tracing method using DiI to label vagal innervation of the embryonic and early postnatal mouse gastrointestinal tract. *Journal of Neuroscience Methods* **163**, 213-225.

Murphy, M. C. and Fox, E. A. (2010). Mice deficient in brain-derived neurotrophic factor have altered development of gastric vagal sensory innervation. *The Journal of Comparative Neurology* **518**, 2934-2951.

Myers, A., Undem, B. and Kummer, W. (1996). Anatomical and electrophysiological comparison of the sensory innervation of bronchial and tracheal parasympathetic ganglion neurons. *Journal of the Autonomic Nervous System* **61**, 162-168.

Myers, A. C. (2001). Transmission in autonomic ganglia. *Respiration Physiology* **125**, 99-111.

Nagy, N., Mwizerwa, O., Yaniv, K., Carmel, L., Pieretti-Vanmarcke, R., Weinstein, B. M. and Goldstein, A. M. (2009). Endothelial cells promote migration and proliferation of enteric neural crest cells via [beta]1 integrin signaling. *Developmental Biology* **330**, 263-272.

Nassenstein, C., Taylor-Clark, T. E., Myers, A. C., Ru, F., Nandigama, R., Bettner, W. and Undem, B. J. (2010). Phenotypic distinctions between neural crest and placodal derived vagal C-fibres in mouse lungs. *The Journal of Physiology* **588**, 4769-4783.

Natarajan, D., Marcos-Gutierrez, C., Pachnis, V. and de Graaff, E. (2002). Requirement of signalling by receptor tyrosine kinase RET for the directed migration of enteric nervous system progenitor cells during mammalian embryogenesis. *Development* **129**, 5151-60.

Newgreen, D. and Thiery, J. P. (1980). Fibronectin in early avian embryos: synthesis and distribution along the migration pathways of neural crest cells. *Cell Tissue Research* **211**, 269-91.

Newgreen, D. F. and Tan, S. S. (1993). Adhesion molecules in neural crest development. *Pharmacology & Therapeutics* **60**, 517-537.

Ogren, J. A., Macey, P. M., Kumar, R., Woo, M. A. and Harper, R. M. (2010). Central autonomic regulation in congenital central hypoventilation syndrome. *Neuroscience* **167**, 1249-1256.

Olesnicky Killian, E. C., Birkholz, D. A. and Artinger, K. B. (2009). A role for chemokine signaling in neural crest cell migration and craniofacial development. *Developmental Biology* **333**, 161-172.

Onimaru, H., Ikeda, K. and Kawakami, K. (2008). CO2-Sensitive Preinspiratory Neurons of the Parafacial Respiratory Group Express Phox2b in the Neonatal Rat. *The Journal of Neuroscience* **28**, 12845-12850.

Pan, J., Rhode, H. K., Undem, B. J. and Myers, A. C. (2010). Neurotransmitters in Airway Parasympathetic Neurons Altered by Neurotrophin-3 and Repeated Allergen Challenge. *Am J Respir Cell Mol Biol* **43**, 452-457.

Panganiban, G. and Rubenstein, J. L. R. (2002). Developmental functions of the Distal-less/Dlx homeobox genes. *Development* **129**, 4371-4386.

Paratcha, G. and Ledda, F. (2008). GDNF and GFR[alpha]: a versatile molecular complex for developing neurons. *Trends in Neurosciences* **31**, 384-391.

Paratcha, G., Ledda, F., Baars, L., Coulpier, M., Besset, V., Anders, J., Scott, R. and Ibanez, C. F. (2001). Released GFRalpha1 potentiates downstream signaling, neuronal survival, and differentiation via a novel mechanism of recruitment of c-Ret to lipid rafts. *Neuron* **29**, 171-84.

Paratore, C., Eichenberger, C., Suter, U. and Sommer, L. (2002). Sox10 haploinsufficiency affects maintenance of progenitor cells in a mouse model of Hirschsprung disease. *Hum Mol Genet* **11**, 3075-85.

Paratore, C., Goerich, D. E., Suter, U., Wegner, M. and Sommer, L. (2001). Survival and glial fate acquisition of neural crest cells are regulated by an interplay between the transcription factor Sox10 and extrinsic combinatorial signaling. *Development* **128**, 3949-61.

Parisi, M. A. and Kapur, R. P. (2000). Genetics of Hirschsprung disease. *Curr Opin Pediatr* **12**, 610-7.

Paterson, A. M. (1888). On Congenital Diaphragmatic Hernia. *British Medical Journal* **2**, 1207-1210.

Pattyn, A., Morin, X., Cremer, H., Goridis, C. and Brunet, J. F. (1997). Expression and interactions of the two closely related homeobox genes Phox2a and Phox2b during neurogenesis. *Development* **124**, 4065-4075.

Pattyn, A., Morin, X., Cremer, H., Goridis, C. and Brunet, J. F. (1999). The homeobox gene Phox2b is essential for the development of autonomic neural crest derivatives. *Nature* **399**, 366-70.

Pederiva, F., Aras Lopez, R., Martinez, L. and Tovar, J. (2008). Abnormal development of tracheal innervation in rats with experimental diaphragmatic hernia. *Pediatric Surgery International* **24**, 1341-1346.

Pera, E. M. and Kessel, M. (1998). Demarcation of ventral territories by the homeobox gene NKX2.1 during early chick development. *Development Genes and Evolution* **208**, 168-171.

Perissinotto, D., Iacopetti, P., Bellina, I., Doliana, R., Colombatti, A., Pettway, Z., Bronner-Fraser, M., Shinomura, T., Kimata, K., Morgelin, M. et al. (2000). Avian neural crest cell migration is diversely regulated by the two major hyaluronan-binding proteoglycans PG-M/versican and aggrecan. *Development* **127**, 2823-2842.

Perris, R., Brandenberger, R. and Chiquet, M. (1996). Differential neural crest cell attachment and migration on avian laminin isoforms. *International Journal of Developmental Neuroscience* **14**, 297-314.

Perris, R. and Perissinotto, D. (2000). Role of the extracellular matrix during neural crest cell migration. *Mechanisms of Development* **95**, 3-21.

Perris, R., Syfrig, J., Paulsson, M. and Bronner-Fraser, M. (1993). Molecular mechanisms of neural crest cell attachment and migration on types I and IV collagen. *Journal of Cell Science* **106**, 1357-1368.

Powley, T. L. and Phillips, R. J. (2002). I. Morphology and topography of vagal afferents innervating the GI tract. *American Journal of Physiology - Gastrointestinal and Liver Physiology* **283**, G1217-G1225.

Pozas, E. and Ibanez, C. F. (2005). GDNF and GFR[alpha]1 Promote Differentiation and Tangential Migration of Cortical GABAergic Neurons. *Neuron* **45**, 701-713.

Previtali, S. C., Feltri, M. L., Archelos, J. J., Quattrini, A., Wrabetz, L. and Hartung, H.-P. (2001). Role of integrins in the peripheral nervous system. *Progress in Neurobiology* **64**, 35-49.

Que, J., Wilm, B., Hasegawa, H., Wang, F., Bader, D. and Hogan, B. L. M. (2008). Mesothelium contributes to vascular smooth muscle and mesenchyme during lung development. *Proceedings of the National Academy of Sciences* **105**, 16626-16630.

Racke, K., Juergens, U. R. and Matthiesen, S. (2006). Control by cholinergic mechanisms. *European Journal of Pharmacology* **533**, 57-68.

Racke, K. and Matthiesen, S. (2004). The airway cholinergic system: physiology and pharmacology. *Pulmonary Pharmacology & Therapeutics* **17**, 181-198.

Randall, V., McCue, K., Roberts, C., Kyriakopoulou, V., Beddow, S., Barrett, A. N., Vitelli, F., Prescott, K., Shaw-Smith, C., Devriendt, K. et al. (2009). Great vessel development requires biallelic expression of Chd7 and Tbx1 in pharyngeal ectoderm in mice. *The Journal of Clinical Investigation* **119**, 3301-3310.

Ratcliffe, E. M. (2011). Molecular development of the extrinsic sensory innervation of the gastrointestinal tract. *Autonomic Neuroscience* **161**, 1-5.

Ratcliffe, E. M., D'Autréaux, F. and Gershon, M. D. (2008). Laminin terminates the Netrin/DCC mediated attraction of vagal sensory axons. *Developmental Neurobiology* **68**, 960-971.

Ratcliffe, E. M., Fan, L., Mohammed, T. J., Anderson, M., Chalazonitis, A. and Gershon, M. D. (2011). Enteric neurons synthesize netrins and are essential for the development of the vagal sensory innervation of the fetal gut. *Developmental Neurobiology* **71**, 362-373.

Rauch, U. and Schafer, K. H. (2003). The extracellular matrix and its role in cell migration and development of the enteric nervous system. *Eur J Pediatr Surg* **13**, 158-62.

Reynolds, S. D., Giangreco, A., Power, J. H. T. and Stripp, B. R. (2000). Neuroepithelial Bodies of Pulmonary Airways Serve as a Reservoir of Progenitor Cells Capable of Epithelial Regeneration. *The American Journal of Pathology* **156**, 269-278.

Rickmann, M., Fawcett, J. W. and Keynes, R. J. (1985). The migration of neural crest cells and the growth of motor axons through the rostral half of the chick somite. *Journal of Embryology and Experimental Morphology* **90**, 437-455.

Ring, C., Hassell, J. and Halfter, W. (1996). Expression Pattern of Collagen IX and Potential Role in the Segmentation of the Peripheral Nervous System. *Developmental Biology* **180**, 41-53.

Rothman, T. P., Le Douarin, N. M., Fontaine-Perus, J. C. and Gershon, M. D. (1990). Developmental potential of neural crest-derived cells migrating from segments of developing quail bowel back-grafted into younger chick host embryos. *Development* **109**, 411-23.

Rothman, T. P., Le Douarin, N. M., Fontaine-Perus, J. C. and Gershon, M. D. (1993). Colonization of the bowel by neural crest-derived cells re-migrating from foregut backtransplanted to vagal or sacral regions of host embryos. *Developmental Dynamics* **196**, 217-33.

Ruhrberg, C. and Schwarz, Q. (2010). In the beginning: Generating neural crest cell diversity. *Cell adhesion & migration* **4**, 622-630.

Saint-Jeannet, J.-P. and Duband, J.-L. (2006). Neural Crest Delamination and Migration. In *Neural Crest Induction and Differentiation*, vol. 589, pp. 45-77: Springer US.

Saint-Jeannet, J.-P., He, X., Varmus, H. E. and Dawid, I. B. (1997). Regulation of dorsal fate in the neuraxis by Wnt-1 and Wnt-3a. *Proceedings of the National Academy of Sciences* **94**, 13713-13718.

Sanderson, M. J., Delmotte, P., Bai, Y. and Perez-Zogbhi, J. F. (2008). Regulation of Airway Smooth Muscle Cell Contractility by Ca2+ Signaling and Sensitivity. *Proc Am Thorac Soc* **5**, 23-31.

Sato, H., Murphy, P., Giles, S., Bannigan, J., Takayasu, H. and Puri, P. (2008). Visualizing expression patterns of Shh and Foxf1 genes in the foregut and lung buds by optical projection tomography. *Pediatric Surgery International* **24**, 3-11.

Sato, H., Murphy, P., Hajduk, P., Takayasu, H., Kitagawa, H. and Puri, P. (2009). Sonic hedgehog gene expression in nitrofen induced hypoplastic lungs in mice. *Pediatric Surgery International* **25**, 967-971.

Sato, T., Sasai, N. and Sasai, Y. (2005). Neural crest determination by co-activation of Pax3 and Zic1 genes in Xenopus ectoderm. *Development* **132**, 2355-2363.

Sauka-Spengler, T. and Bronner-Fraser, M. (2008). A gene regulatory network orchestrates neural crest formation. *Nat Rev Mol Cell Biol* **9**, 557-68.

Schafer, K. H. and Mestres, P. (1999). The GDNF-induced neurite outgrowth and neuronal survival in dissociated myenteric plexus cultures of the rat small intestine decreases postnatally. *Exp Brain Res* **125**, 447-52.

Schittny, J. C., Miserocchi, G. and Sparrow, M. P. (2000). Spontaneous peristaltic airway contractions propel lung liquid through the bronchial tree of intact and fetal lung explants. *Am J Respir Cell Mol Biol* **23**, 11-8.

Schlosser, G. (2006). Induction and specification of cranial placodes. *Developmental Biology* **294**, 303-351.

Schlosser, G. (2010). Chapter Four - Making Senses: Development of Vertebrate Cranial Placodes. In *International Review of Cell and Molecular Biology*, vol. Volume 283 (ed. J. Kwang), pp. 129-234: Academic Press.

Schreiner, S., Cossais, F., Fischer, K., Scholz, S., Basl, M. R., Holtmann, B., Sendtner, M. and Wegner, M. (2007). Hypomorphic Sox10 alleles reveal novel protein functions and unravel developmental differences in glial lineages. *Development* **134**, 3271-3281.

Schuchardt, A., D'Agati, V., Larsson-Blomberg, L., Costantini, F. and Pachnis, V. (1994). Defects in the kidney and enteric nervous system of mice lacking the tyrosine kinase receptor Ret. *Nature* **367**, 380-3.

Schuller, H. M., Plummer, H. K. and Jull, B. A. (2003). Receptor-mediated effects of nicotine and its nitrosated derivative NNK on pulmonary neuroendocrine cells. *The Anatomical Record Part A: Discoveries in Molecular, Cellular, and Evolutionary Biology* **270A**, 51-58.

Schwarz, Q., Maden, C. H., Davidson, K. and Ruhrberg, C. (2009a). Neuropilin-mediated neural crest cell guidance is essential to organise sensory neurons into segmented dorsal root ganglia. *Development* **136**, 1785-1789.

Schwarz, Q., Maden, C. H., Vieira, J. M. and Ruhrberg, C. (2009b). Neuropilin 1 signaling guides neural crest cells to coordinate pathway choice with cell specification. *Proceedings of the National Academy of Sciences* **106**, 6164-6169.

Sela-Donenfeld, D. and Kalcheim, C. (1999). Regulation of the onset of neural crest migration by coordinated activity of BMP4 and Noggin in the dorsal neural tube. *Development* **126**, 4749-4762.

Serbedzija, G. N., Burgan, S., Fraser, S. E. and Bronner-Fraser, M. (1991). Vital dye labelling demonstrates a sacral neural crest contribution to the enteric nervous system of chick and mouse embryos. *Development* **111**, 857-66.

Serls, A. E., Doherty, S., Parvatiyar, P., Wells, J. M. and Deutsch, G. H. (2005). Different thresholds of fibroblast growth factors pattern the ventral foregut into liver and lung. *Development* **132**, 35-47.

Sharpe, J., Ahlgren, U., Perry, P., Hill, B., Ross, A., Hecksher-Sorensen, J., Baldock, R. and Davidson, D. (2002). Optical Projection Tomography as a Tool for 3D Microscopy and Gene Expression Studies. *Science* **296**, 541-545.

Sherwood, R. I., Chen, T.-Y. A. and Melton, D. A. (2009). Transcriptional dynamics of endodermal organ formation. *Developmental Dynamics* **238**, 29-42.

Short, K. M., Hodson, M. J. and Smyth, I. M. (2010). Tomographic quantification of branching morphogenesis and renal development. *Kidney Int* **77**, 1132-1139.

Sorokin, S. P., Hoyt, R. F., Jr. and Shaffer, M. J. (1997). Ontogeny of neuroepithelial bodies: correlations with mitogenesis and innervation. *Microsc Res Tech* **37**, 43-61.

Southard-Smith, E. M., Angrist, M., Ellison, J. S., Agarwala, R., Baxevanis, A. D., Chakravarti, A. and Pavan, W. J. (1999). The Sox10(Dom) mouse: modeling the genetic variation of Waardenburg-Shah (WS4) syndrome. *Genome Res* **9**, 215-25.

Southard-Smith, E. M., Kos, L. and Pavan, W. J. (1998). Sox10 mutation disrupts neural crest development in Dom Hirschsprung mouse model. *Nat Genet* **18**, 60-4.

Sparrow, M. P. and Lamb, J. P. (2003). Ontogeny of airway smooth muscle: structure, innervation, myogenesis and function in the fetal lung. *Respir Physiol Neurobiol* **137**, 361-72.

Sparrow, M. P., Warwick, S. P. and Everett, A. W. (1995). Innervation and function of the distal airways in the developing bronchial tree of fetal pig lung. *Am J Respir Cell Mol Biol* **13**, 518-25.

Sparrow, M. P., Warwick, S. P. and Mitchell, H. W. (1994). Foetal airway motor tone in prenatal lung development of the pig. *Eur Respir J* **7**, 1416-24.

Sparrow, M. P. and Weichselbaum, M. (1997). Structure and function of the adventitial and mucosal nerve plexuses of the bronchial tree in the developing lung. *Clinical and Experimental Pharmacology and Physiology* **24**, 261-268.

Sparrow, M. P., Weichselbaum, M. and McCray, P. B. (1999). Development of the innervation and airway smooth muscle in human fetal lung. *Am J Respir Cell Mol Biol* **20**, 550-60.

Srinivas, S., Watanabe, T., Lin, C.-S., William, C., Tanabe, Y., Jessell, T. and Costantini, F. (2001). Cre reporter strains produced by targeted insertion of EYFP and ECFP into the ROSA26 locus. *BMC Developmental Biology* **1**, 4.

Stanchina, L., Baral, V., Robert, F., Pingault, V., Lemort, N., Pachnis, V., Goossens, M. and Bondurand, N. (2006). Interactions between Sox10, Edn3 and Ednrb during enteric nervous system and melanocyte development. *Developmental Biology* **295**, 232-49.

Stefansson, K., Wollmann, R. L. and Moore, B. W. (1982). Distribution of S-100 protein outside the central nervous system. *Brain Research* **234**, 309-317.

Steventon, B., Carmona-Fontaine, C. and Mayor, R. (2005). Genetic network during neural crest induction: From cell specification to cell survival. *Seminars in Cell and Developmental Biology* **16**, 647-654.

Stewart, A. L., Young, H. M., Popoff, M. and Anderson, R. B. (2007). Effects of pharmacological inhibition of small GTPases on axon extension and migration of enteric neural crest-derived cells. *Developmental Biology*.

Stolt, C. C. and Wegner, M. (2010). SoxE function in vertebrate nervous system development. *The International Journal of Biochemistry & Cell Biology* **42**, 437-440.

Streit, A. (2007). The preplacodal region: an ectodermal domain with multipotential progenitors that contribute to sense organs and cranial sensory ganglia. *Inernational Journal of Developmental Biology* **51**, 447-461.

Stretton, D. (1991). Non-Adrenergic, Non-Cholinergic Neural Control of the Airways. *Clinical and Experimental Pharmacology and Physiology* **18**, 675-684.

Sun, K. L. W., Correia, J. P. and Kennedy, T. E. (2011). Netrins: versatile extracellular cues with diverse functions. *Development* **138**, 2153-2169.

Tallini, Y. N., Shui, B., Greene, K. S., Deng, K.-Y., Doran, R., Fisher, P. J., Zipfel, W. and Kotlikoff, M. I. (2006). BAC transgenic mice express enhanced green fluorescent protein in central and peripheral cholinergic neurons. *Physiol. Genomics* **27**, 391-397.

Taneyhill, L. A., Coles, E. G. and Bronner-Fraser, M. (2007). Snail2 directly represses cadherin6B during epithelial-to-mesenchymal transitions of the neural crest. *Development* **134**, 1481-1490.

Tansey, M. G., Baloh, R. H., Milbrandt, J. and Johnson Jr, E. M. (2000). GFR[alpha]-Mediated Localization of RET to Lipid Rafts Is Required for Effective Downstream Signaling, Differentiation, and Neuronal Survival. *Neuron* **25**, 611-623.

Taraviras, S., Marcos-Gutierrez, C. V., Durbec, P., Jani, H., Grigoriou, M., Sukumaran, M., Wang, L. C., Hynes, M., Raisman, G. and Pachnis, V. (1999). Signalling by the RET receptor tyrosine kinase and its role in the development of the mammalian enteric nervous system. *Development* **126**, 2785-97.

Taylor, K. M. and LaBonne, C. (2005). SoxE Factors Function Equivalently during Neural Crest and Inner Ear Development and Their Activity Is Regulated by SUMOylation. *Developmental Cell* **9**, 593-603.

Ten Have-Opbroek, A. A. W. (1991). Lung Development in the Mouse Embryo. *Experimental Lung Research* **17**, 111-130.

Teramoto, H., Yoneda, A. and Puri, P. (2003). Gene expression of fibroblast growth factors 10 and 7 is downregulated in the lung of nitrofen-induced diaphragmatic hernia in rats. *Journal of Pediatric Surgery* **38**, 1021-1024.

Theveneau, E., Marchant, L., Kuriyama, S., Gull, M., Moepps, B., Parsons, M. and Mayor, R. (2010). Collective Chemotaxis Requires Contact-Dependent Cell Polarity. *Developmental Cell* **19**, 39-53.

Thompson, H., Blentic, A., Watson, S., Begbie, J. and Graham, A. (2010). The formation of the superior and jugular ganglia: Insights into the generation of sensory neurons by the neural crest. *Developmental Dynamics* **239**, 439-445.

Tollet, J., Everett, A. W. and Sparrow, M. P. (2001). Spatial and temporal distribution of nerves, ganglia, and smooth muscle during the early pseudoglandular stage of fetal mouse lung development. *Developmental Dynamics* **221**, 48-60.

Tollet, J., Everett, A. W. and Sparrow, M. P. (2002). Development of neural tissue and airway smooth muscle in fetal mouse lung explants: a role for glial-derived neurotrophic factor in lung innervation. *Am J Respir Cell Mol Biol* **26**, 420-9.

Tovar, J. A. (2007). The neural crest in pediatric surgery. *Journal of Pediatric Surgery* **42**, 915-926.

Unbekandt, M., del Moral, P.-M., Sala, F. G., Bellusci, S., Warburton, D. and Fleury, V. (2008). Tracheal occlusion increases the rate of epithelial branching of embryonic mouse lung via the FGF10-FGFR2b-Sprouty2 pathway. *Mechanisms of Development* **125**, 314-324.

Undem, B. J. and Larry, R. S. (2009). Autonomic Nervous System: Respiratory Control. In *Encyclopedia of Neuroscience*, pp. 975-981. Oxford: Academic Press.

Vaccaro, R., Parisi Salvi, E. and Renda, T. (2006). Early development of chick embryo respiratory nervous system: an immunohistochemical study. *Anatomy and Embryology* **211**, 345-354.

van Bueren, K. L., Papangeli, I., Rochais, F., Pearce, K., Roberts, C., Calmont, A., Szumska, D., Kelly, R. G., Bhattacharya, S. and Scambler, P. J. (2010). Hes1 expression is reduced in Tbx1 null cells and is required for the development of structures affected in 22q11 deletion syndrome. *Developmental Biology* **340**, 369-380.

Van Lommel, A. (2001). Pulmonary neuroendocrine cells (PNEC) and neuroepithelial bodies (NEB): chemoreceptors and regulators of lung development. *Paediatric Respiratory Reviews* **2**, 171-176.

Vennemann, M., Bajanowski, T., Butterfass-Bahloul, T., Sauerland, C., Jorch, G., Brinkmann, B. and Mitchell, E. A. (2007). Do risk factors differ between explained sudden unexpected death in infancy and sudden infant death syndrome? *Archives of Disease in Childhood* **92**, 133-136.

Verhein, K., Fryer, A. and Jacoby, D. (2009). Neural control of airway inflammation. *Current Allergy and Asthma Reports* **9**, 484-490.

Verloes, A., Elmer, C., Lacombe, D., Heinrichs, C., Rebuffat, E., Demarquez, J. L., Moncla, A. and Adam, E. (1993). Ondine-Hirschsprung syndrome (Haddad syndrome). *European Journal of Pediatrics* **152**, 75-77.

Vitelli, F., Morishima, M., Taddei, I., Lindsay, E. A. and Baldini, A. (2002). Tbx1 mutation causes multiple cardiovascular defects and disrupts neural crest and cranial nerve migratory pathways. *Hum Mol Genet* **11**, 915-922.

Wallace, A. S. and Burns, A. J. (2005). Development of the enteric nervous system, smooth muscle and interstitial cells of Cajal in the human gastrointestinal tract. *Cell Tissue Research* **319**, 367-82.

Walls, J. R., Coultas, L., Rossant, J. and Henkelman, R. M. (2008). Three-Dimensional Analysis of Vascular Development in the Mouse Embryo. *PLoS ONE* **3**, e2853.

Walters, L. C., Cantrell, V. A., Weller, K. P., Mosher, J. T. and Southard-Smith, E. M. (2010). Genetic background impacts developmental potential of enteric neural crest-derived progenitors in the Sox10Dom model of Hirschsprung disease. *Hum Mol Genet* **19**, 4353-4372.

Warburton, D., Bellusci, S., De Langhe, S., Del Moral, P.-M., Fleury, V., Mailleux, A., Tefft, D., Unbekandt, M., Wang, K. and Shi, W. E. I. (2005). Molecular Mechanisms of Early Lung Specification and Branching Morphogenesis. *Pediatric Research* **57**, 26R-37R.

Warburton, D., Bellusci, S., Del Moral, P.-M., Kaartinen, V., Lee, M., Tefft, D. and Shi, W. (2003). Growth factor signaling in lung morphogenetic centers: automaticity, stereotypy and symmetry. *Respiratory Research* **4**, 5.

Watson, N., Maclagan, J. and Barnes, P. J. (1993). Vagal control of guinea pig tracheal smooth muscle: lack of involvement of VIP or nitric oxide. *Journal of Applied Physiology* **74**, 1964-1971.

Weaver, M., Batts, L. and Hogan, B. L. M. (2003). Tissue interactions pattern the mesenchyme of the embryonic mouse lung. *Developmental Biology* **258**, 169-184.

Weaver, M., Yingling, J. M., Dunn, N. R., Bellusci, S. and Hogan, B. L. (1999). Bmp signaling regulates proximal-distal differentiation of endoderm in mouse lung development. *Development* **126**, 4005-4015.

Weese-Mayer, D. E., Rand, C. M., Berry-Kravis, E. M., Jennings, L. J., Loghmanee, D. A., Patwari, P. P. and Ceccherini, I. (2009). Congenital central hypoventilation syndrome from past to future: Model for translational and transitional autonomic medicine. *Pediatric Pulmonology* **44**, 521-535.

Weichselbaum, M., Everett, A. W. and Sparrow, M. P. (1996). Mapping the innervation of the bronchial tree in fetal and postnatal pig lung using antibodies to PGP 9.5 and SV2. *Am J Respir Cell Mol Biol* **15**, 703-10.

Weichselbaum, M. and Sparrow, M. P. (1999). A confocal microscopic study of the formation of ganglia in the airways of fetal pig lung. *Am J Respir Cell Mol Biol* **21**, 607-20.

Wessler, I., Kirkpatrick, C. and Racké, K. (1999). The cholinergic 'pitfall': Acetylcholine, a universal cell molecule in biological systems, including humans. . *Clinical and Experimental Pharmacology and Physiology* **26**, 198-205.

Wessler, I. K. and Kirkpatrick, C. J. (2001). The Non-neuronal Cholinergic System: an Emerging Drug Target in the Airways. *Pulmonary Pharmacology & Therapeutics* **14**, 423-434.

West, J. B. (2008). Respiratory Physiology: The Essentials: Lippincott Williams & Wilkins.

White, P. M. and Anderson, D. J. (1999). In vivo transplantation of mammalian neural crest cells into chick hosts reveals a new autonomic sublineage restriction. *Development* **126**, 4351-63.

Widdicombe, J. (2001). Airway receptors. *Respiration Physiology* **125**, 3-15.

Widdicombe, J. G. (1998). Autonomic Regulation . i-NANC/e-NANC. *Am J Respir Crit Care Med* **158**, S171-175.

Wine, J. J. (2007). Parasympathetic control of airway submucosal glands: Central reflexes and the airway intrinsic nervous system. *Autonomic Neuroscience* **133**, 35-54.

Yan, H., Bergner, A. J., Enomoto, H., Milbrandt, J., Newgreen, D. F. and Young, H. M. (2004). Neural cells in the esophagus respond to glial cell line-derived neurotrophic factor and neurturin, and are RET-dependent. *Developmental Biology* **272**, 118-133.

Yazdani, U. and Terman, J. (2006). The semaphorins. *Genome Biology* **7**, 211.

Yin, Y., Wang, F. and Ornitz, D. M. (2011). Mesothelial- and epithelial-derived FGF9 have distinct functions in the regulation of lung development. *Development* **138**, 3169-3177.

Young, H. M., Anderson, R. B. and Anderson, C. R. (2004). Guidance cues involved in the development of the peripheral autonomic nervous system. *Autonomic Neuroscience* **112**, 1-14.

Young, H. M., Bergner, A. J. and Muller, T. (2003). Acquisition of neuronal and glial markers by neural crest-derived cells in the mouse intestine. *Journal of Comparative Neurology* **456**, 1-11.

Young, H. M., Hearn, C. J., Farlie, P. G., Canty, A. J., Thomas, P. Q. and Newgreen, D. F. (2001). GDNF is a chemoattractant for enteric neural cells. *Developmental Biology* **229**, 503-16.

Yu, J., Gonzalez, S., Rodriguez, J. I., Diez-Pardo, J. A. and Tovar, J. A. (2001). Neural crest-derived defects in experimental congenital diaphragmatic hernia. *Pediatric Surgery International* **17**, 294-298.

Zhou, L., Dey, C. R., Wert, S. E. and Whitsett, J. A. (1996). Arrested Lung Morphogenesis in Transgenic Mice Bearing an SP-C-TGF-[beta]1 Chimeric Gene. *Developmental Biology* **175**, 227-238.